UNIVERSITY OF BIRMINGHAM

Catalytic Upgrading of Bio-oil via the Hydrodeoxygenation of Short Chain Carboxylic Acids

By
AHMED MASHI LAWAL

A thesis submitted to
The University of Birmingham
for the degree of
DOCTOR OF PHILOSOPHY

School of Chemical Engineering
College of Engineering and Physical Science
University of Birmingham
August 2019

Abstract

Petroleum is non-renewable and contributes to environmental pollution, thus bio-oil can be substituted as a potential alternative. However, bio-oil in its crude form cannot be used directly as fuel since it contains a high proportion of oxygenated, acidic and reactive compounds such as carboxylic acids. These are known to cause corrosion of vessels and pipework, instability and phase separation. The oxygen content of bio-oil can be reduced through hydrodeoxygenation of oxygenated compounds. In this study, the hydrogenation of short chain (C_2-C_4) carboxylic acids typical of model compounds present in bio-oil was investigated using commercial Pt supported on Al_2O_3, SiO_2, carbon and graphite, and prepared Pt and Pt-Re on TiO_2 catalysts. This study reports the preparation of 4% Pt/TiO_2 and 4% Pt-4%Re/TiO_2 catalysts for alcohol production, which were screened against their commercial counterparts, the reaction space explored in the following ranges temperature 80-200 °C, pressure 10-40 bar, time 1-4 h, catalyst 0.1-0.4 g and stirring speed 400-1000 min^{-1} using 4%Pt/TiO_2, and kinetic modelling of acetic acid hydrogenation.

The catalysts were characterized using Brunauer–Emmett–Teller (BET), X-ray diffraction (XRD), Scanning electron microscopy (SEM), H_2-Temperature Programmed Reduction (H_2-TPR) and NH_3-Temperature Programmed Desorption (NH_3-TPD) techniques. BET analysis showed features of Type IV isotherm with Type 3 hysteresis for 4% Pt/TiO_2, 4% Pt-4%Re/TiO_2, 4% Pt/SiO_2 and 5% Pt/graphite; in contrast, 5% Pt/C and 5% Pt/Al_2O_3 exhibited Type 2 hysteresis. Further, both commercial and synthesized catalysts are mesoporous. The XRD peaks present in 4% Pt/TiO_2 and 4% Pt-4%Re/TiO_2 were found to be rutile and anatase phases of TiO_2 only. The incorporation of Pt and Re into TiO_2 occupied more rutile than anatase phases. Catalyst morphology of spent 4% Pt/TiO_2 and 4% Pt-4%Re/TiO_2 showed the formation of compact mass and agglomerates after three reuse cycles. NH_3-TPD analysis showed that 4%

Pt/TiO_2 had the highest acidity (0.48 mmol g^{-1}) which favoured esterification reaction. Catalyst screening showed that 4% Pt/TiO_2 and 4% Pt-4%Re/TiO_2 outperformed the commercial catalysts, and favoured the production of ethyl acetate and ethanol respectively. Consequently, the production of alcohol over 4% Pt-4%Re/TiO_2 increased with increasing Re loading from 1 to 4%. The achieved optimum conditions were 200 °C, 40 bar, 4 h, 0.4 g and 1000 min^{-1} for acetic acid conversion, and 160 c, 40 bar, 4 h, 0.4 g and 1000 min^{-1} for ethanol production.

The hydrogenation of C_2-C_4 acids over 4% Pt/TiO_2 and 4% Pt-4%Re/TiO_2 as single acid feed showed that an increase in the molecular weight of the carboxylic acid from acetic to butanoic acid enhanced the selectivity towards the respective alcohol which can be summarized: butanol > propanol > ethanol. Conversely, ester selectivity is as follows: ethyl acetate > propyl propionate > butyl butyrate. The selectivity to alcohol decreased as the reaction temperature increases from 145 to 200 °C. Higher alcohol selectivities were achieved over 4% Pt-4%Re/TiO_2 in all cases. The investigation of acids in a mixed acid feed system over 4% Pt/TiO_2 showed that higher alcohol selectivity was attained compared to the single feed system. On the other hand, the conversion of propanoic and butanoic acids in the mixture containing acetic acid dropped from 94 to 77% and 88.2 to 70% respectively. The presence of acetic acid in the mixed feed inhibited the other acids due to competitive effect but favoured higher alcohol selectivity.

Reaction kinetics of acetic acid hydrogenation was investigated using catalyst particle sizes < 65 μm and a stirring speed of 1000 min^{-1} at which negligible internal and external mass transfer resistances were experienced. The reaction order with respect to acetic acid and hydrogen were found to be 0.78 and 0.35 respectively, which indicated fractional order kinetics. Hence, the experimental data was fitted with a Langmuir-Hinshelwood model for dissociative H_2 adsorption. The activation energy and pre-exponential factor were found to be 80.6 kJ mol^{-1} and 4.6 $\times 10^{-7}$ $kmol.kgcat^{-1}.min^{-1}$ respectively.

Finally, 4% Pt/TiO_2 catalyst favours the production of esters and alcohols from the hydrogenation of short chain carboxylic acids (C_2-C_4) in single and multiple feed systems. However, the addition of Re to form bimetallic catalyst (4% Pt-4%Re/TiO_2) further increased the selectivity towards alcohols while maintaining a high acid conversion. Furthermore, the reaction kinetics of acetic acid using 4% Pt/TiO_2 catalyst was adequately described using a model that assumes a dissociative adsorption of hydrogen.

Dedication

This thesis is proudly dedicated to my beloved parents who offered unconditional support and love throughout my life.

To my late father:

May Allah (SWT) grant you the highest of ranks in Jannah.

Acknowledgement

I would like to express gratitude to Almighty Allah for successful completion of this work. I would also like to thank Petroleum Technology Development Fund (PTDF), Nigeria for the financial support.

My sincere appreciation goes to my supervisor Prof Joe Wood for his patience, guidance and efforts in helping me throughout my research. I would also like to extend my appreciation to Prof Christopher Hardacre and Dr Helen Daly from the University of Manchester for their collaboration and help with catalyst preparation. Special thanks to Dr Abarasi Hart for his immense support, guidance and contributions.

I am forever indebted to my parents, Late Alhaji Lawal Mashi and Hajiya Fatima Lawal Mashi, for investing heavily on me. Thank you for your prayers, financial and moral support. I would like to deeply appreciate the support and prayers of my entire family. You have been extremely supportive of me through the good and difficult moments. A special mention goes to my amazing wife for her patience, love and motivation. To my children Fatima and Mohammed, you cannot be forgotten for always been a source of happiness.

My sincere thanks to friends, colleagues and staff of the University of Birmingham who have helped towards the success of this work. I cannot forget to mention Ms Lynn Draper for her administrative support and care throughout my stay in the university. Thanks to Mr Dave Boylin for his technical help.

Lastly, thanks to my friends for their encouragement and understanding.

Table of Contents

List of Figures

List of Tables

Nomenclature

a	Gas-liquid interfacial area, m^2
a_s	catalyst particle, m^2
A	Pre-exponential factor, dimensionless
C_A	Initial reactant concentration, $mol.cm^{-3}$
C_{GB}	Concentration of gas G in the bulk liquid, $mol.cm^{-3}$
C_{GI}	Concentration of gas bubbles in the bulk gas region, $mol.cm^{-3}$
C_{GIG}	Concentration of gas in the gas region of the gas-liquid interface, $mol.cm^{-3}$
C_{GS}	Concentration of gas at the catalyst surface, $mol.cm^{-3}$
C_I	Reactant concentration, $mol.cm^{-3}$
D	Diameter, m
$D_{e,H2}$	Effective diffusivity of hydrogen in hexane, $m^2.s^{-1}$
$D_{e,acetic}$	Effective diffusivity of acetic acid in hexane, $m^2.s^{-1}$
d_I	Stirrer diameter, cm
D_p	Particle diameter, m
d_I	Reactor diameter, cm
E_a	Activation energy, $kJ.mol^{-1}$
g	Gravity constant, $m.s^2$
H	Henry's constant, $pa.cm^3.mol^{-1}$
L	Catalyst particle size,
k	Rate constant, $kmol.kgcat^{-1}.min^{-1}$
K_{AA}	Equilibrium constant for acetic acid, $m^3.mol^{-1}$
K_{H2}	Equilibrium constant for hydrogen, $m^3.mol^{-1}$
k_{int}	Specific reaction rate with internal mass transfer, $dm^3.gcat^{-1}.s^{-1}$
k_{GL}	Gas film mass transfer coefficient, $cm^2.s^{-1}$
k_La	volumetric liquid-side mass transfer coefficient, $cm^2.s^{-1}$

ks	Liquid-solid mass transfer coefficient, $cm^2.s^{-1}$
M_w	Wagner-Weisz-Wheeler modulus
Na	Avogadro's number
N_m	Minimum agitation speed, min^{-1}
P_{H2}	Hydrogen partial pressure, pa
R_A	Resistance of mass transfet into the liquid phase though gas-liquid interface, $gcat.s.dm^{-3}$
R_B	Rate of mass transfer onto the catalyst through liquid-solid interface, $gcat.s.dm^{-3}$
R_C	Rate of internal diffusion, $gcat.s.dm^{-3}$
Rr	Liquid-solid mass transfer resistance, $gcat.s.dm^{-3}$
r_G	Rate of gaseous transfer from bulk gaseous phase, $mol.g^{-1}.s^{-1}$
r_v	Observed reaction rate, $mol.g^{-1}.s^{-1}$
T	Temperature, K
TPR	Temperature Programmed Reduction
w'	Percentage catalyst loading, $g(catalyst).100g(solution)^{-1}$
w	Catalyst loading, $dm^3.g$

Greek Symbols

φ	Thiele modulus
μ	Viscosity, $kg.s^{-1}.m^{-1}$
η	Effectiveness factor
α,β	Parameter
ρ	Density, $kg.m^{-3}$

Chapter 1. **Introduction**

1.1 Background and Motivation

Due to the rise in human population and their activities, the demand for energy has grown and will even become larger in the future (Gollakorta et al., 2018; Mortensen et al., 2011). Most commonly among the human activities is the increase in use of transportation fuel which accounts about 20% of the total energy (van Ruijven and van Vuuren, 2009). In addition, petroleum-based transportation fuels account for most of the world transportation energy consumption which has recently increased at an annual average rate of 1.4%, and this growth is expected to continue through to 2040 (EIA, 2017). A large portion of liquid transportation fuels are obtained from petroleum reserves, which are believed to have peaked, and are now in decline. According to IEA (2008), the transportation sector accounts for approximately 50% of global oil consumption and generates about 25% of greenhouse gas emissions such as CO_2, resulting in global warming and climate change (Eisentraut, 2010). In addition, legislative and environmental challenges associated with petroleum based fuels make bio-oil a renewable alternative to resolve these challenges (Hart et al., 2013). In order to cut down the emissions contributed from the combustion of petroleum fuels for transportation, bio-oil has shown potential for the production of alternative transportation fuels and other valuable chemicals (Wang et al., 2013).

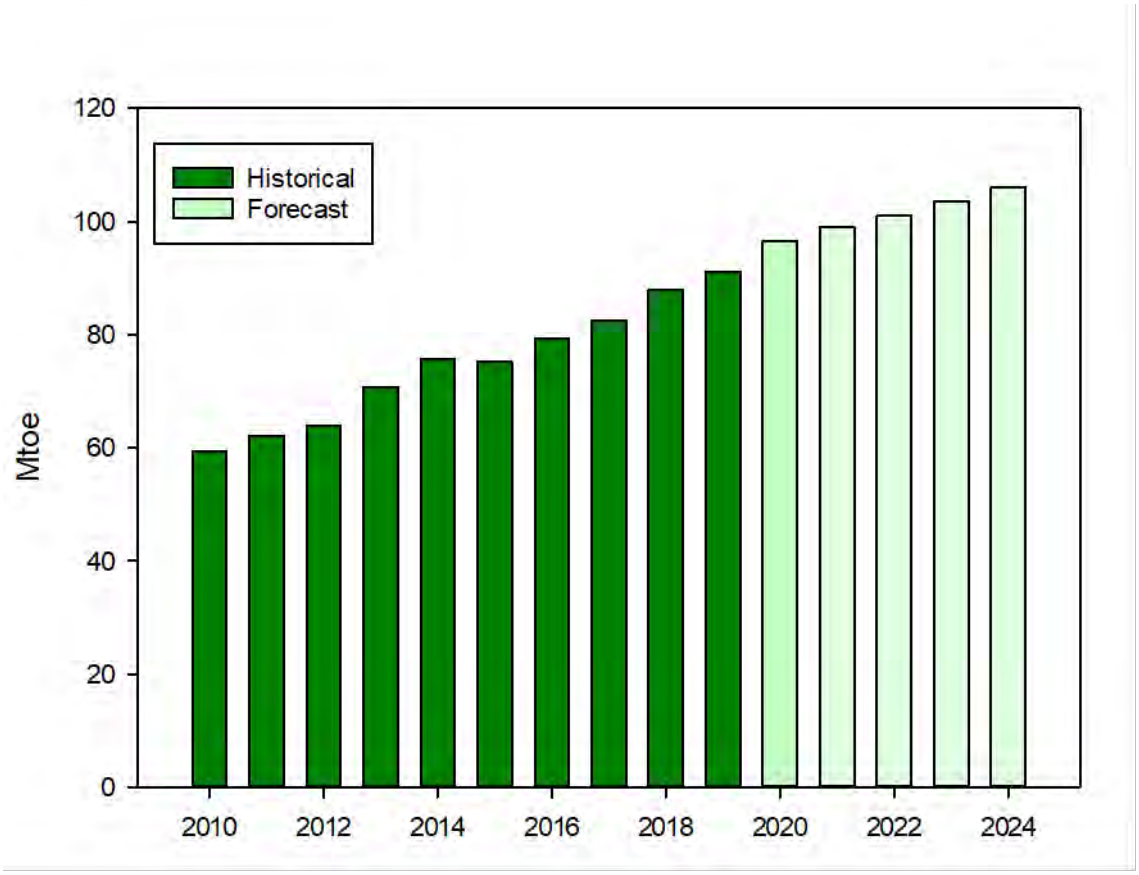

Figure 1.1: *Projected growth of biofuels (IEA, 2019).*

Biomass, which is a cheap and abundant carbon-based renewable source, has appeared to be a potential alternative feedstock to fossil fuels for the production of fuel grade hydrocarbons (Wang et al., 2011). Bio-oil is produced from fast pyrolysis and hydrothermal liquefaction of biomass (Wang et al., 2017; Shakya et al., 2018; Zhang et al, 2019), making it a potential alternative for fossil fuels with lower emissions of nitrogen oxides (NOx) and sulphur dioxide (SO_2), and carbon neutrality. However, unprocessed bio-oil has limited use as fuel due to high oxygen and aqueous phase content resulting to detrimental properties such as high acidity, low heating value, high viscosity and poor miscibility with fossil fuels (Mortensen et al., 2011; Ruddy et al., 2014). In this regard, upgrading has become a necessity to improve its fuel properties. Catalytic hydrodeoxygenation and zeolite cracking are the most common techniques in bio-oil upgrading. Hydrodeoxygenation (HDO) appears to be the preferred

upgrading technique in recent years because it produces higher quality fuels in comparison with zeolite cracking (Wang et al., 2013). It involves the conversion or removal of oxygenates in the bio-oil in the presence of suitable catalyst, hydrogen pressure, and temperature to produce hydrocarbon products. However, hydrodeoxygenation has not yet fulfilled its potential due to issues associated with catalyst deactivation, uneconomical process costs and insufficient understanding of kinetics (Ruddy et al., 2014; Wang et al., 2013). Another limitation is that industrial hydrotreating prefers continuous flow but comparison of data between continuous flow and batch reactors has been uncertain.

Typically, bio-oil is composed of approximately 15% carboxylic acid, mainly acetic and formic acids (Mullen and Boateng, 2008; Oasmaa et al., 2005). This makes it highly acidic in nature and self-catalysing with a pH range of 2-4, resulting in continuous degradation and alteration of bio-oil properties. Bio-oils usually contain a large water content (typically 15-30%) (Elliott, 2007; Mortensen et al., 2011). The complexity of bio-oil makes it difficult to understand the upgrading chemistry and reaction pathways due to the numerous compounds it contains. Hence, model compound studies have been adopted and reported in the literature for a range of classes of compounds found in bio-oil such as carboxylic acids, ketones, aromatics, aldehydes etc. However, most studies on hydrogenation of carboxylic acids have mainly focused on high molecular weight acids such as fatty acids with less emphasis on low molecular weight acids such as acetic, propanoic and butanoic acids.

The catalytic HDO of carboxylic acids to their corresponding alcohols and other valuable hydrocarbons is an effective route for bio-oil utilization. The generation of these products depends on the type of catalyst and reaction mechanism. Hydrogenolysis and ketonization are the predominant pathways that describe the generation of alcohols and other products such as esters. In contrast to the hydrogenation of amides (Rasu et al., 2017; M. L.

Yuan et al., 2016), and esters (Chakraborty et al., 2014; Saudan, 2007), which are straightforward and effective synthetic methods to generate alcohols and other fine chemicals, carboxylic acids are difficult to hydrogenate because they are thermodynamically and kinetically stable which results from the low electrophilicity of carbonyl carbon and its interaction with the catalyst (He et al., 1995; Lu et al., 2018; Pritchard et al., 2015). In continued efforts to address these challenges, several studies have been performed using heterogeneous and homogenous catalysts. However, the reaction requires harsh operating conditions in the range of 200-300 °C and hydrogen pressure of 140-300 bar, thereby favouring side reactions (Pritchard et al., 2015), and a low yield of targeted products may be achieved.

Hydrogenation of long chain carboxylic acids using heterogeneous catalysts have mainly proceeded via hydrogenation-dehydration-hydrogenation reaction pathway to yield alcohols and alkanes. For example, Manyar et al., (2010) have studied the hydrogenation of fatty acids using titania supported Pt catalysts to generate alcohols and alkanes. Similarly, Ullrich and Breit, (2018) reported the same reaction pathway for the hydrogenation of long chain carboxylic acids using Pd-Re/C. From various studies on hydrogenation of carboxylic acids, the mechanism that favors production of alcohols and alkanes on further hydrogenation appears to be more generic for long chain acids. However, most of these processes require harsh operating conditions which results in the degradation of reactants and formation of side products (Pritchard et al., 2015; Rase, 2016). Due to the complexities associated with carboxylic acids toward hydrogenation, the selective hydrogenation of carboxylic acids into alcohols and other bulk platform chemicals could offer great potential in the utilization of bio-oil model compounds, especially when deactivation resistant catalysts are used to improve the process in terms of selectivity and reusability. The production of ethanol fuel accounts for two-thirds of biofuels growth between 2018 and 2023 (IEA, 2019), thus, making the production of

deoxygenated products from bio-oil model compounds an attractive process. However, the investigation of acetic acid hydrogenation over different catalysts has shown higher selectivity of gaseous products with lower ethanol selectivity (He and Wang, 2013; Rachmady and Vannice, 2000; Wan et al., 2013). Subsequently, the formation of ethyl acetate is observed as a dominant side product due to esterification reaction occurring in the solution phase.

An understanding on the reaction pathways and kinetics is anticipated to be beneficial in modelling and process design. Several studies have reported the kinetic modelling for the hydrogenation of acetic acid over various catalysts (Joshi and Lawal, 2012; Lawal et al., 2019; Rachmady and Vannice, 2000; Zhou et al., 2017a). Chen et al., (2007) studied the HDO of different organic acids and their mixtures, and have reported the kinetics of the system taking into account competitive adsorption of reactants and product inhibition. These studies have mainly considered Langmuir-Hinshelwood models that assumed the incorporation of dissociative hydrogen adsorption. Other models that assumed non-competitive adsorption of molecular hydrogen such as Eley-Rideal model, were less applicable in bi-molecular kinetics system.

Most studies on the hydrogenation of carboxylic acids had been investigated for longer chain acids mainly fatty acids, towards the production of alcohols and other deoxygenated products. There is a need to understand how acetic acid and other short chain acids behave under suitable reaction conditions, and develop a promoted catalyst for this reaction. Furthermore, the investigation of the acids in a mixed feed system is required to describe how each acid influences the reaction system. The reaction kinetics of the hydrogenation of acetic acid will also be described.

1.2 Objectives of study

The aim of this work is to study catalytic systems to reduce oxygen content of bio-oil through hydrogenation of oxygenated compounds. However, the focus of the study is on short chain carboxylic acids typical of model compounds found in bio-oil. Therefore, the specific objectives of interest are to:

- Formulate and prepare titania supported platinum catalysts for the production of alcohols.
    - To investigate the catalytic performance of the prepared catalysts against commercial platinum catalysts towards the hydrogenation of acetic acid.
- Optimize the process parameters and their influence towards the maximization of acetic acid conversion and ethanol yield over 4% Pt/TiO_2.
- Evaluate the hydrogenation reactions of short chain carboxylic acids over 4% Pt/TiO_2 and 4% $Pt\text{-}4\%Re/TiO_2$ catalysts in single and mixed feed systems.
- Investigate the kinetics of acetic acid hydrogenation over 4% Pt/TiO_2 using optimum conditions, specifically to:
    - Investigate the internal and external mass transfer in acetic acid hydrogenation.
    - Investigate the influence of reaction conditions and interpret their kinetic parameters.
    - Correlate the reaction results by fitting a Langmuir-Hinshelwood expression to the experimental data.

1.3 Thesis organization

The layout of the current thesis is presented in seven (7) chapters based on the objectives outlined above.

Chapter 1 provides background information and motivation to the current study. It also identifies the importance of upgrading bio-oil properties through the removal of oxygen in carboxylic acids. The drawbacks from previous studies, mainly covering long chain carboxylic acids were highlighted.

Chapter 2 provides a literature review on upgrading of bio-oil and the various reaction routes involved in the hydrodeoxygenation of carboxylic acids. The role of noble metals as well as catalyst supports and promoters are described. Methods of catalyst formulation and preparation are discussed. This chapter also gives a description of slurry reactors and mass transfer in a three phase system.

Chapter 3 provides a detailed description of materials, methods and analytical equipment used in this study. The procedures for catalyst characterization techniques are discussed. In addition, design of experiment using the Taguchi method is described.

Chapter 4 presents the properties of commercial and titania supported Pt/Pt-Re catalysts used in this study based on different characterization techniques. The optimization of reaction factors towards the conversion of acetic acid and ethanol yield in hydrogenation of acetic acid is discussed.

Chapter 5 presents the hydrogenation of short chain carboxylic acids specifically acetic, propanoic and butanoic acids as individual and multiple feeds, using 4% Pt/TiO_2 and 4% Pt-4%Re/TiO_2 catalysts.

Chapter 6 presents the hydrogenation of acetic acid under the regime of kinetics using 4% Pt/TiO_2 catalyst and optimum reaction conditions from Chapter four.

Chapter 7 provides the conclusion to this study and recommendation for future work.

Chapter 2. **Literature Survey**

2.1 Chapter Overview

This chapter opens with an overview of bio-oil and its properties in Section 2.2. Typical bio-oil upgrading techniques such as hydrodeoxygenation (HDO) and zeolite cracking are discussed with emphasis on HDO in this study (Section 2.2.1). Due to the complexity of bio-oil, the HDO of carboxylic acids as typical bio-oil model compounds and their possible reaction routes are reviewed (Section 2.3). The selective hydrogenation of short chain carboxylic acids to alcohols with the aim of suppressing side products is reviewed (Section 2.3.2). Thereafter, the reaction mechanism describing the hydrogenation of acetic acid via hydrogenation and esterification pathways is described (Section 2.3.3).

Typical heterogeneous catalysts used in the hydrogenation process consist of an active metal, secondary metal (promoter or co-catalyst) and support. The application of HDO catalysts and noble metals as the active metal required for the hydrogenation reaction to take place are reviewed in Section 2.4 and 2.41 respectively. Despite the high activity associated with noble metal catalysts, Pt-based catalysts are prone to deactivation as described in Section 2.4.2.

Thereafter, the role of rhenium metal as a promoter on noble metal catalysts with specific focus on Pt-based catalysts is explained in Section 2.5. Consequently, the function of catalyst supports and their interaction with active metals in hydrogenation reactions is described in Section 2.6. The methods involved in catalyst preparation and formulation specific to this study are reviewed in Section 2.7. A three-phase slurry reactor is chosen for the current study as presented in Section 2.8, with emphasis on mixing requirements and mass transfer considerations. At the end of this chapter, the conclusions and rationale for the current study is presented in Section 2.9.

2.2 Bio-oil

Bio-oil, widely known as pyrolysis oil, is a dark liquid produced from biomass feedstock via the process of pyrolysis (Bridgwater, 2012; Mercader et al., 2010). Typically, bio-oil contains a mixture of complex oxygenated compounds with a high water content of about 15-30 wt% derived from both vapour in the feedstock and dehydration step during pyrolysis (Jacobson et al., 2013; Venderbosch et al., 2010). The occurrence of water during the pyrolysis process lowers bio-oil viscosity and improves the fluidity, however, reduces the heating value and calorific value of the bio-oil. Bio-oils from different raw materials possess varying physical properties because of the composition of original biomass, which is distinct from crude oil. It was revealed by several studies that bio-oil is composed of over 300 organic compounds and is comprised of about 38 wt% oxygen (Bridgwater, 2010; He and Wang, 2012; Jacobson et al., 2013). Organic compounds present in bio-oils mainly include acids, alcohols, aldehydes, esters, furans, ketones and phenols (Basagiannis and Verykios, 2008). Owing to the relatively high contents of carboxylic acids commonly formed during hemicellulose pyrolysis, bio-oil exhibits acidity in the pH range 2-4, resulting in problems associated with the utilization of downstream operations towards the production of petrol (Zhang et al., 2007). Other limitations of utilizing raw bio-oil as a combustive fuel in automobile engines comprises of: (i) Thermal and chemical instability, (ii) high polarity, (iii) high viscosity, and (iv) low heating value. As shown in Table 2.1, the presence of high oxygen content to about 50% is the distinguishable property between bio-oil and conventional fuels. Due to the high oxygen content, the resulting heating value of bio-oil is significantly lower than that of hydrocarbon fuel by approximately 50%. In addition, the heating value of bio-oil from lignocellulosic biomass is about 20 MJ/kg as compared to 45 MJ/kg in fossil fuels (Si et al., 2017).

Table 2.1: *Comparison of bio-oil and crude oil properties.*

Oil Characteristics	Bio-oil[a]	Bio-oil[b]	Crude-oil
Water (wt.%)	15-30	5.1	0.1
pH	2.8-3.8	-	-
ρ (Kg/l)	1.05-1.25	-	0.86
μ at 50 °C (cP)	40-100	15000	180
HHV (MJ/kg)	16-19	12	44
C (wt.%)	55-65	73	83-86
O (wt.%)	28-40	26.3	<1
H (wt.%)	5-7	3.7-8	11-14
S (wt.%)	<0.05	0.7	<4
N (wt.%)	<0.4	2.4	<1
Ash (wt.%)	<0.2	24.2	0.1
H/C	0.9-1.5	-	1.5-2.0
O/C	0.3-0.5	-	~0

[Adapted from (Gollakota et al., 2018; Venderbosch et al., 2010; Zhang et al., 2007)]. [a]Bio-oil produced from pyrolysis. [b]Bio-oil produced from hydrothermal liquefaction.

As a blending component, bio-oil is highly immiscible with hydrocarbon fuels which is caused by the high oxygen content. The ash content in bio-oil could result in catalyst poisoning during the upgrading process and potential problems in automobile engines such as corrosion, deposition and abrasion. As a result of these challenges, the necessity of improving the properties of bio-oil via catalytic upgrading becomes significant, before it can potentially substitute or compliment petro-fuel for combustion purposes (Bridgwater, 2010; Jacobson et al., 2013; Ruddy et al., 2014).

2.2.1 Bio-oil Upgrading

The presence of oxygen and other undesirable properties in bio-oil shows that it requires post-production upgrading. Several reports have identified different upgrading techniques such as chemical, physical and catalytic methods (Bridgwater, 2012; Chiaramonti et al., 2003; Czernik and Bridgwater, 2004; Ikura et al., 2003; Zhang et al., 2007). The chemical methods are mainly esterification, mild cracking and aqueous phase processing (Si et al., 2017). Production of petro-fuels requires total deoxygenation of bio-oil. However, partially deoxygenated products from bio-oil upgrading are compatible with existing infrastructure and thus offer an economic benefit (Bridgwater, 2011). Furthermore, the advantages of high heating value that can be utilised in combustion engines is realised via compounds that contain chemically bonded oxygen, thus strengthening the relevance of partially deoxygenated products. For example, the content of gasoline in the US is composed of about 10-15 wt% blended ethanol with 3.5-5.2 wt% oxygen (Jacobson et al., 2013; Ruddy et al., 2014). Detailed reviews on the different bio-oil upgrading techniques have been widely reported elsewhere (Mortensen et al., 2011; Ruddy et al., 2014; Si et al., 2017). Hydrodeoxygenation (HDO) and zeolite cracking (ZC) are the most popular techniques employed in catalytic upgrading of bio-oil to liquid fuel with fully or partially deoxygenated hydrocarbons depending on the product of interest. The reaction stages for both HDO and ZC are similar as shown in Figure 2.1.

Cracking:

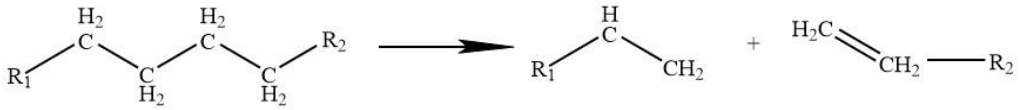

Decarbonylation:

Decarbonylation:

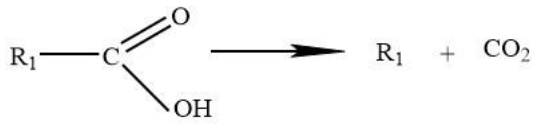

Hydrocracking:

Hydrodeoxygenation:

Hydrogenation:

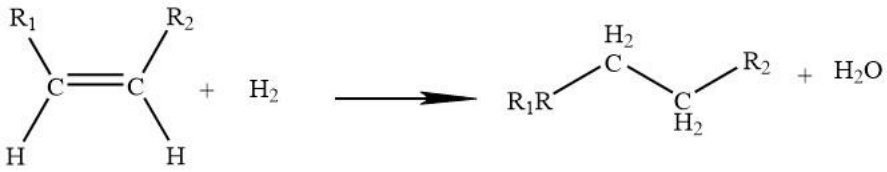

Figure 2.1: *Reactions involved in bio-oil upgrading (Mortensen et al., 2011; Wildschut et al., 2009).*

Upgrading via ZC involves the use of zeolite catalysts at elevated temperatures and atmospheric pressure above 400 °C to eliminate oxygen in the form of CO and CO2 (Bridgwater, 2010; Zacher et al., 2014; Zhu et al., 2011). This method is very similar to the fluid catalytic cracking process in petroleum refineries. The reactions involved in ZC mainly favour C-C bond cleavage, decarbonylation, dehydration, methyl transfer, isomerization and decarboxylation. Even though the efficient removal of oxygen from bio-oil is possible using ZC, the production of high grade fuels is not feasible due to the loss of carbon (approximately

0.6 molar ratio of H/C and O/C) (Huber et al., 2006; Mortensen et al., 2011). The high temperature required in achieving proper deoxygenation suggests an increase in C-C cracking and production of undesirable hydrocarbon gases (Ruddy et al., 2014; Zacher et al., 2014). Furthermore, zeolite catalysts are prone to coke formation and subsequent catalyst deactivation. This study will focus on the hydrodeoxygenation technique of carboxylic acids contained in bio-oil.

2.2.2 Hydrodeoxygenation

Hydrodeoxygenation (HDO) technique is a process similar to hydrodesulphurization (HDS) process used in refineries for sulphur removal from organic hydrocarbons. It involves the consumption of hydrogen at high pressure of 70-200 bar and temperatures of 250-450 °C in the presence of catalyst. The elimination of oxygen occurs in the form of water as a by-product and the production of high-grade fuel with a high H/C molar ratio. The process involves the saturation of C=O, C=C and cyclic ring bonds present in the bio-oil mixture, followed by cleavage of heteroatoms. During the HDO process, a combination of cracking, hydrocracking, hydrogenation, dealkylation, direct deoxygenation, decarbonylation and decarboxylation reactions take place with carbon formation as a significant side reaction (Wang et al., 2013). Due to the complex reaction network in HDO, it is highly significant to identify an effective catalyst with bi-functional acidic and metallic sites as both hydrogenation and dehydration reactions are required.

Early studies have reported the utilization of conventional HDS catalysts (sulfided $NiMo/Al_2O_3$ and $CoMo/Al_2O_3$) and operating conditions for HDO processes. However, a steady re-sulfurization is required to maintain the catalyst activity, which, in turn contaminates the end products. Furthermore, the susceptibility of Al_2O_3 support in the presence of water contained in bio-oil adversely affects the catalyst lifetime. HDO offers better advantages over

ZC due to its compatibility with existing HDS refining units and the production of high-quality grade fuels. Hence, this makes the HDO a more attractive process in the upgrading of bio-oil. Table 2.2 compares the upgraded properties of bio-oil from HDO and ZC.

In comparison with ZC, HDO produces higher quality fuel as the process is compatible with existing HDS refining infrastructure. ZC appears to be efficient for oxygen removal in the presence of zeolite catalyst at high temperatures but the fuel quality is affected by carbon loss during the process (Mortensen et al., 2011; Ruddy et al., 2014; Zacher et al., 2014).

Table 2.2: *Properties of crude oil, raw bio-oil and catalytically upgraded bio-oil (Mortensen et al., 2011)*

	Bio-oil	**ZC**	**HDO**	**Crude oil**
Upgraded bio-oil (wt.%)				
Y_{oil}	100	12-28	21-65	-
$Y_{water\ phase}$	-	24-28	13-49	-
Y_{gas}	-	6-13	3-15	-
Y_{carbon}	-	26-39	4-26	-
Oil Characteristics				
Water (wt.%)	15-30	-	1.5	0.1
pH	2.8-3.8	-	5.8	-
P (Kg/l)	1.05-1.25	-	1.2	0.86
μ at 50 °C (cP)	40-100	-	1-5	180
HHV (MJ/kg)	16-19	21-36	42-45	44
C (wt.%)	55-65	61-79	85-89	83-86
O (wt.%)	28-40	13-24	< 5	< 1
H (wt.%)	5-7	2-8	10-14	11-14
S (wt.%)	< 0.05	-	<	< 4
N (wt.%)	< 0.4	-		< 1

Ash (wt.%)	< 0.2	-		0.1
H/C	0.9-1.5	0.3-1.8		1.5-2.0
O/C	0.3-0.5	0.1-0.3		~0

In spite of the advantage of quality fuel obtained via HDO, the requirement of excess hydrogen makes it economically unattractive. According to Bridgwater (1996), about 700L of H_2 is required to deoxygenate 1kg of bio-oil, combined with H_2 in the excess of about 100-200% needed for the process to be kept at high partial pressure. Thus, the main drawback faced by researchers on the application of HDO is formulating effective catalysts that can cope under low pressure near H_2 stoichiometry. In order to overcome this challenge, an understanding of the fundamental reaction mechanisms of bio-oil model compounds is required.

2.3 HDO of Bio-oil Model Compounds

Due to the complexity of bio-oil and simultaneous reactions during upgrading, the reaction routes of bio-oil remain unclear. This makes the development of an effective catalyst for the HDO reaction more challenging. Instead of using crude pyrolysis oil at lab-scale, the alternative study of bio-oil model compounds provides a better understanding of the HDO reaction networks and mechanism (Si et al., 2017). In addition, experiments on model compounds contribute to screening, designing and developing catalysts (Shafaghat et al., 2015). Currently, model compounds are chosen based on their significant activity towards the bio-oil instability, which is mainly due to the presence of chemically-bound oxygen in the bio-oil. These compounds contain different functional groups that allow the investigation of their respective activities and selectivity of several reactions which includes decarboxylation, hydrogenation, hydrocracking etc. It is interesting to note that even HDO of same model compound proceeds through various reaction pathways when different catalysts are used,

resulting in the formation of different products. In order to produce desired fuels and chemicals, it is very essential to understand the reaction mechanism of the different model compounds for better selectivity of target products (He and Wang, 2012; Wang et al., 2013). The HDO of real bio-oil is not replicated as other reactions may occur due to its complexity. Thus, the HDO of model compounds can address the drawback from HDO of real bio-oil.

Reaction pathways of HDO of model compounds have been widely investigated but kinetic study and catalyst active site requirements have gained little attention. In addition, the use of batch and continuous-flow reactors have been reported for the study of HDO of model compounds. In the industrial scale of bio-oil hydrotreatment, the continuous flow reactor is preferred but the challenge in comparing process data between batch and continuous-flow reactors is apparent. Therefore, it is desirable to compare kinetic data between both reactors using model compound studies.

2.3.1 HDO of Carboxylic acids

The presence of carboxylic acids in bio-oil contributes to its low pH of 2-4 and high acidity, making bio-oil highly corrosive in nature and it even degrades at higher temperatures (Sipilaè and Kuoppala, 1998; Zhang et al., 2007). Low molecular weight carboxylic acids such as acetic, propanoic and butanoic acids are classified as the least reactive components contained in bio-oil (Bergem et al., 2017), which makes them more difficult to hydrogenate when compared with ketones and aldehydes (Manyar et al., 2010; Ponec, 1997). Several studies have investigated the hydrogenation of these acids using aqueous phase conditions and catalysts suitable for the production of gaseous phase products such as CO, CO_2, CH_4, C_2H_6 (Chen et al., 2011; He and Wang, 2013; Wan et al., 2013). However, the production of liquid phase products that can be used as drop-in fuels and fine chemicals have gained less attention. Since carboxylic acids are typically considered as corrosion causing components in bio-oil, the conversion of

these acids is important. Therefore, the selective hydrogenation of carboxylic acids can be of great interest in the production of alternative drop-in fuels. Many researchers have reported the catalysts, mechanisms and reaction conditions for the hydrogenation of carboxylic acids aimed at achieving the desired product selectivity. Accordingly, the HDO of carboxylic acids could proceed through different reaction routes as shown in Figure 2.2, which is based on the type of catalyst and reaction conditions selected; (Chen et al., 2011; He and Wang, 2012; Wan et al., 2013).

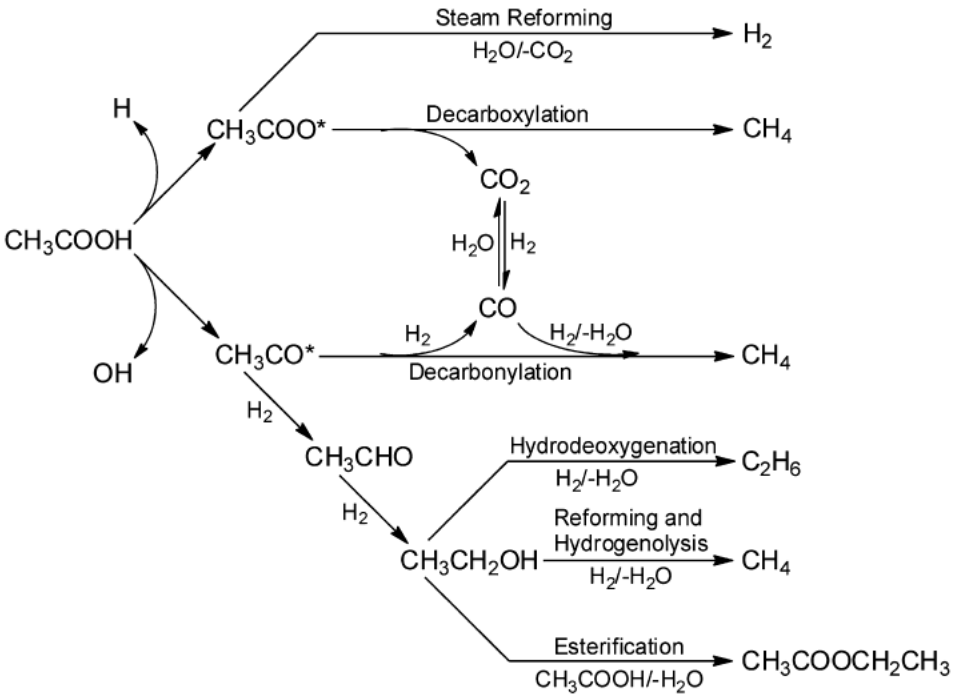

Figure 2.2: *Major reaction pathways of HDO of carboxylic acids (Wan et al., 2013).*

The production of alcohols mainly proceeds via different reaction routes. Ketonization mainly involves the generation of ketones by C-O bond cleavage and further hydrogenation to produce alcohols. While ketones can be produced as intermediate products in alcohol production, similarly, aldehyde is formed as an alternative intermediate via C-O bond cleavage, and further hydrogenated to produce alcohol. Sequentially, the dehydration and hydrogenation of alcohol can result in alkane formation. An alternative route to the formation of alkanes from

alcohols is the reaction between the alcohols and unreacted carboxylic acids to form esters via esterification reaction. Other alternative routes are the decarboxylation and decarbonylation routes which involve the production of carbon-less alkanes, CO and CO_2. Further hydrogenation results in methane. This reaction route is typical of aqueous phase hydrogenation and low molecular weight acids (Chen et al., 2011; Wan et al., 2013)

Early studies on HDO of acetic acid have focused on the use of oxide catalysts (titania, iron oxide, chromium oxide) for the conversion of acetic acid to acetaldehyde (Pestman et al., 1997; Rachmady and Vannice, 2002a; Rachmady and Vannice, 2002b). Better selectivity and activity is evident after the addition of platinum. Further studies showed that the reaction mechanism and kinetics are influenced by the hydrogenation of acetic acid on the oxide-supported platinum catalyst which is initiated through reactions involving adsorbed H_2 atoms on the platinum active sites and an acyl group on the oxide support. This route appears to be the major pathway for the production of acetaldehyde and ethanol as a product of further hydrogenation.

Haruo et al., (2016) studied the HDO of acetic acid over Pt/TiO_2 and Pt/C catalysts at temperatures between 130-225 °C and hydrogen pressure of 60-150 bar in a batch reactor. Ethanol was formed as the major product of acetic acid HDO on Pt/TiO_2 at 130 °C, with a reasonable formation of ethyl acetate as a secondary product. Further hydrogenation led to an improved ethanol yield with a moderate yield of ethyl acetate.

According to Joshi and Lawal, (2012), the HDO of acetic acid over sulfided $NiMo/Al_2O_3$ catalyst at <300 °C and 20.6 bar proceeded via the hydrogenolysis pathway. Similarly, (Xu et al., 2009) investigated the HDO of acetic acid over sulfided $NiMo/Al_2O_3$ catalyst at 200 °C and 30 bar which proceeded through the same route. However, sulphur

containing intermediates are likely to be formed which are attributed to continuous sulfur leaching from the catalyst. In contrast to the HDO of acetic acid over sulfided catalysts, Elliot and Hart (2009) reported that HDO of acetic acid over Pd/C and Ru/C noble metal catalysts showed a significant selectivity and activity at reduced temperatures but followed the same reaction route. Higher catalytic activities exhibited by noble metal catalysts can be attributed to their potential in activating H_2 under mild conditions.

2.3.2 Selective hydrogenation of carboxylic acids to alcohols

Hydrogenation of carboxylic acids to produce alcohols is a significant synthetic transformation for biomass utilization and chemical industries (Gunanathan and Milstein, 2014; Magano and Dunetz, 2012; Pritchard et al., 2015; Toyao et al., 2017). This reaction was conventionally carried out using stoichiometric methods which involves the use of metal hydrides as reductants, such as lithium aluminium hydride and sodium hydride (Cha and Brown, 1993; Jaita et al., 2014; Nagendra et al., 2012). From an environmental and economic perspective, this method became less attractive in comparison to catalytic processes because it results in large amount of waste and poor atom efficiency. Therefore, hydrogenation of carboxylic acid using molecular hydrogen as a reducing agent gained attention as it offers better atom efficiency up to 100% (Pritchard et al., 2015).

Nevertheless, carboxylic acids are difficult to hydrogenate because they are thermodynamically and kinetically stable which results from the low electrophilicity of carbonyl carbon and its interaction with the catalyst (He et al., 1995; Toyao et al., 2017). Additional difficulty results from the low polarizability of carbonyl group present in carboxylic acids which makes them less reactive towards reduction (Figure 2.3). In contrast to the hydrogenation of amides (Chakraborty et al., 2014; Spasyuk et al., 2012), esters (Rasu et al., 2017; Yuan et al., 2016) and other carbonyl compounds which is a straightforward and effective

synthetic method to generate alcohols and other fine chemicals, hydrogenation of carboxylic acids has gained less attention and lags behind (vom Stein et al., 2014; Wienhöfer et al., 2013).

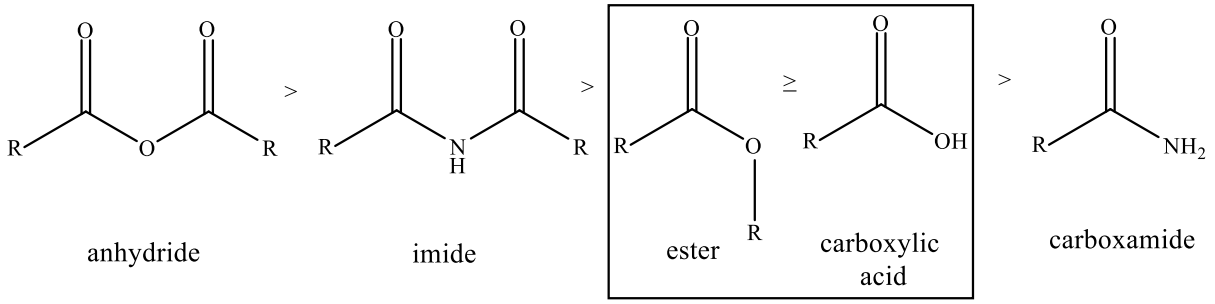

Figure 2.3: *Decreasing order of carbonyl group polarizability.*

Carboxylic acids like esters and lactones, are associated with issues of interconversion under applied reaction conditions. The extent of the interconversion of carboxylic acids could possibly affect the degree of catalytic hydrogenation in terms of product distribution. Due to the complexities associated with carboxylic acids towards hydrogenation, the formulation of an efficiently robust catalyst becomes inevitable. In a continued efforts to address these challenges, several studies have been performed using heterogeneous and homogenous catalysts. However, the reaction requires harsh operating conditions in the range 200-300 °C and hydrogen pressures of 140-300 bar (Pritchard et al., 2015), thereby favouring side reactions and degradation of reaction substrates. Although, a low yield of targeted products may be achieved which necessitates the need to improve catalyst performance. For example, Manyar et al., (2010) have studied the hydrogenation of fatty acids using titania supported Pt catalysts to generate alcohols and alkanes. However, the proposed mechanism for hydrogenation of fatty acids lacks generality as it is not analogous to short chain carboxylic acids. This study will be aimed at investigating the hydrogenation of low molecular weight acids which includes acetic, propanoic and butanoic acids, in order to selectively generate their corresponding alcohols and other

valuable chemicals. Until now, a generic mechanism that describes the reaction pathways for these acids have received little attention. Thus, an outlook describing a unified mechanism will be proposed for these acids using bi-functional Pt/TiO_2 and $Pt\text{-}Re/TiO_2$ catalysts under optimized reaction conditions.

2.3.3 Reaction Mechanism for the Hydrogenation of Acetic Acid

Hydrogenation of acetic acid proceeds via different reaction routes according to different proposed reaction mechanisms. This involves the dissociative adsorption of acetic acid to form acetyl surface species, acetyl species or intermediates (Pallassana and Neurock, 2002; Rachmady and Vannice, 2002b; Zhou et al., 2017a). Subsequently, hydrogen is activated on the metallic sites which react with the carbonyl component of acetic acid via spillover mechanism. As shown in Figure 2.2, acetic acid proceeds first to acetaldehyde and subsequently to ethanol and other products. The formation of acetaldehyde takes place via four probable routes as either a product or intermediate (Liu et al., 2017). The reaction routes include:

a) The breaking of O-H in acetic acid to form acetate species which undergo C-O bond scission followed by H_2 attack on the carbon of acetyl to form acetaldehyde (Equations 2.3, 2.6 and 2.8)

b) The formation of acetate species via O-H breaking and H_2 atom attack of the carbon of the acetate to form dioxethylidene and further C-O scission to form acetaldehyde (Equations 2.3, 2.7 and 2.10).

c) The direct dissociation of acetic acid C-OH to form acetyl and hydroxyl species, and subsequent acetyl hydrogenation to form acetaldehyde (Equations 2.4 and 2.8).

d) Formation of hydroxyalkyl intermediate of ethane-1,1-diol followed by scission pf C-OH bond to form acetaldehyde (Equations 2.5 and 2.9).

$$H_{2_{(g)}} + 2^* \leftrightarrow 2H^* \quad (2.1)$$

$$2H^* + {}^{**} \leftrightarrow 2H^{**} + * \quad (2.2)$$

$$CH_3COOH^{**} + {}^{**} \rightarrow CH_3COO^{**} + H^{**} \quad (2.3)$$

$$CH_3COOH^{**} + {}^{**} \rightarrow CH_3CO^{**} + OH^{**} \quad (2.4)$$

$$CH_3COOH^{**} + H^{**} \rightarrow CH_3CH(OH)O^{**} + {}^{**} \quad (2.5)$$

$$CH_3COO^{**} + {}^{**} \rightarrow CH_3CO^{**} + O^{**} \quad (2.6)$$

$$CH_3COO^{**} + H^{**} \rightarrow CH_3CHOO^{**} + {}^{**} \quad (2.7)$$

$$CH_3CO^{**} + H^{**} \rightarrow CH_3CHO^{**} + {}^{**} \quad (2.8)$$

$$CH_3CH(OH)O^{**} + {}^{**} \rightarrow CH_3CHO^{**} + OH^{**} \quad (2.9)$$

$$CH_3CHOO^{**} + {}^{**} \rightarrow CH_3CHO^{**} + O^{**} \quad (2.10)$$

The adsorbed molecules of acetaldehyde are either desorbed as a product or further hydrogenated as an intermediate into ethanol (Zhou et al., 2017a). Subsequently, acetyl species are considered to have reacted extremely fast as free radicals with hydrogen species, when the formation of acetaldehyde is not evident in the production of ethanol. Thus, the first hydrogenation step involved in surface reaction can be considered as the rate limiting step.

The two probable pathways for the production of ethanol include:

The formation of C-H in acetaldehyde followed by O-H formation to form ethanol (Equations 2.11-2.12) or, the formation of O-H in acetaldehyde then C-H formation to form ethanol (Equations 2.13-2.14).

$$CH_3CHO^{**} + H^{**} \rightarrow CH_3CH_2O^{**} + {}^{**} \quad 2.11$$

$$CH_3CH_2O^{**} + H^{**} \rightarrow CH_3CH_2OH^{**} + {}^{**} \quad 2.12$$

$$CH_3CHO^{**} + H^{**} \rightarrow CH_3CHOH^{**} + {}^{**} \quad 2.13$$

$$CH_3CHOH^{**} + H^{**} \rightarrow CH_3CH_2OH^{**} + {}^{**} \quad 2.14$$

Conversely, acetic acid adsorbs associatively on a proton donating catalyst with Brönsted acid sites to form di-hydroxyl radical (Equation 2.15), which subsequently reacts with ethanol to form ethyl acetate (Equations 2.16-2.17). Thus, the concentration of the proton donating support (**) and concentration of hydrogen metallic sites (H^{**}) strongly influences acetic acid conversion to ethanol, and further reaction with ethanol to form ethyl acetate via esterification. This also results in the elimination of water molecule (Equation 2.16).

$$CH_3COOH + H^{**} \leftrightarrow CH_3C(OH)_2{}^{**} \quad 2.15$$

$$CH_3C(OH)_2{}^{**} + CH_3CH_2OH \leftrightarrow CH_3C(\mathrm{OH})C_2H_5{}^{**} + H_2O \quad 2.16$$

$$CH_3C(\mathrm{OH})C_2H_5{}^{**} \leftrightarrow CH_3COOC_2H_5 + H^{**} \quad 2.17$$

Because most of the reaction mechanisms for carboxylic acids HDO do not follow the Power law model; therefore, Langmuir-Hinshelwood (L-H) Kinetic Models are mostly used to describe complex rate reactions. Table 2.3 shows typical L-H models used to describe kinetic data of hydrogenation of carboxylic acid model compounds commonly found in bio-oil. The value of their characteristics constants and activation energy are also presented.

Table 2.3: *Langmuir-Hinshelwood models used in the hydrogenation of carboxylic acids.*

S/No	Rate model	Acid	Characteristic	Parameters	Reference
1	$\frac{kC_{LA}P_{H_2}}{(1+K_{LA}C_{LA}+K_{OH}C_{OH})(1+\sqrt{K_{H_2}P_{H_2}})^2}$	Lactic	Competitive adsorption, dissociative adsorption of H_2	E_a = 54 kJ/mol K_{LA} = 1.75 m^3/kmol K_{H2} = 0.215 M/Pa R^2 = 0.990	(Chen et al., 2007)
2	$\frac{kC_{AA}C_{H_2}^{1/2}}{\left(1+K_{AA}C_{AA}+K_{H_2}C_{H_2}^{1/2}\right)^2}$	Acetic	Competitive adsorption, dissociative adsorption of H_2	E_a = 80.6 kJ/mol, K_{AA} = 3.94 m^3/kmol, K_{H2} = 0.8 M/Pa R^2 = 0.992	(Lawal et al., 2019)
3	$\frac{kC_{PA}P_{H_2}}{(1+K_{PA}C_{PA}+K_{OH}C_{OH})(1+\sqrt{K_{H_2}P_{H_2}})^2}$	Palmitic	Competitive adsorption, dissociative adsorption of H_2	E_a = 92.9 kJ/mol, K_{PA} = 0.00106 m^3/kmol, K_{H2} = 0.0377 M/Pa R^2 = 0.999	(Zhou and Lawal, 2017)
4	$\frac{kC_{PA}P_{H_2}}{(1+K_{A}C_{A}+K_{OH}C_{OH})(1+\sqrt{K_{H_2}P_{H_2}})^2}$	Propanoic	Competitive adsorption, dissociative adsorption of H_2	E_a = 68 kJ/mol K_{PA} = 1.36 m^3/kmol K_{H2} = 0.215 M/Pa R^2 = 0.990	(Chen et al., 2007)
5	$\frac{kC_{LA}P_{H_2}}{\left(1+K_{LA}C_{LA}+K_{H_2}P_{H_2}\right)^2}$	Lactic	Competitive adsorption, molecular adsorption of H_2	E_a = 138 kJ/mol, K_{LA} = 0.55 m^3/kmol, K_{H2} = 0.0037 M/Pa R^2 = 0.86	(Zhang et al., 2002)

2.4 HDO Catalysts

Catalyst activity and stability are vital during the HDO process. The different types of catalyst used for HDO act as active phases for HDO of model compounds and tend to have different reaction mechanisms. Different catalysts have been studied for HDO processes such as Mo-based sulfides, noble metals, base metals and metal phosphides (Ruddy et al., 2014; Si et al., 2017).

Molybdenum sulfide typically supported on porous support (e.g., Al_2O_3) and promoted by cobalt or nickel (Ni/Co-MoS_2) has been popularly reported as a catalyst used in modern hydrotreating processes such as HDS and HDN. The reaction network and mechanism of HDS and HDN processes using Ni/Co-MoS_2 catalysts have been widely investigated and broadly understood (Wang et al., 2013). The similarities of the HDS and HDN processes to HDO make the Ni/Co-MoS_2 catalysts applicable for HDO and, thus, are normally used for hydrotreating of bio-oil (Elliott, 2007). It was further reported that significant removal of oxygen from 45% to < 1% was achieved over the molybdenum sulphide catalyst. Despite a good understanding of the reaction mechanism, further research on the catalyst's active site is still necessary (Furimsky, 2000). To maintain the active form of the catalyst and avoid catalyst deactivation during the HDO reaction, an addition of H_2S to the system becomes significant which deprives bio-oil of its low sulphur advantage (Baskar et al., 2012).

Similar to molybdenum sulfide catalyst, other metals (e.g., Ni, Cu and P) have been investigated for HDO of phenolics. HDO of guaiacol has witnessed an improved conversion using metal phosphide catalysts compared to the commercial Co-MoS_2 (Zhao et al., 2011). However, metal phosphide catalysts are prone to deactivation in the presence of water as a result

of phosphates formation, which might cover the active sites. In addition to this limitation, metal phosphide catalysts have been commonly reported for the HDO of phenolic compounds.

Further studies have identified supported noble metal catalysts as effective non-sulfide based hydrotreating catalysts. The application of these catalysts have gained interest in response to issues associated with deactivation and degradation of transition metal sulfided (TMS) catalysts and other HDO catalysts.

2.4.1 Noble Metal Catalyst

The application of TMS catalysts in the HDO process have been widely reported in the literature. However, the susceptibility of these catalysts to aqueous media and subsequent catalyst deactivation due to boemite formation has resulted into the search for substitute catalysts (Bui et al., 2011; Kubička and Horáček, 2011). In addition, the economy of resulfiding the catalyst for the HDO process and catalyst instability makes it less attractive. Over the years, noble metal catalysts have gained attention because sulphur is not required during HDO and subsequently, product contamination is not evident (Honkela et al., 2010; Ruddy et al., 2014). Therefore, more activity could be anticipated on noble metal catalysts and better stability on supports other than alumina (He and Wang, 2012; Honkela et al., 2010).

Noble metals are quite effective in activating and splitting molecular hydrogen on the metal surface under mild operating conditions, making it readily reactive with other reactants (Ruddy et al., 2014). During HDO, the active metal site provides the platform for H_2 adsorption and activation. On the other hand, the metal sites and metal support provide the platform for adsorption and activation of oxy-compounds respectively, and subsequent H_2 spill over during hydrogenation thereby leading to C-O bond cleavage and formation of deoxygenated products. The reaction requires both hydrogenation and acidic sites which normally proceeds via a

sequence of hydrogenation-dehydration-hydrogenation (Boffa, 1993; Lee et al., 2012); Lin et al., 2011; Mendes et al., 2001; Pestman et al., 1997). According to literature reports, Pt (Li and Huber, 2010; Wang et al., 2011), Pd (Sitthisa et al., 2011; Zhao et al., 2011), Rh (Lee et al., 2012; Lin et al., 2011; Zhao et al., 2011), Ru (Centeno et al., 1999; Chen et al., 2011; Lee et al., 2012; C. Zhao et al., 2011), or any two of them in bimetallic form, have been studied in the HDO process with promising results (Ardiyanti et al., 2011; Gutierrez et al., 2009). As shown in Figure 2.4, the reaction mechanism over these catalysts is proposed in accordance with the literature (Mendes et al., 2001; Pestman et al., 1997a).

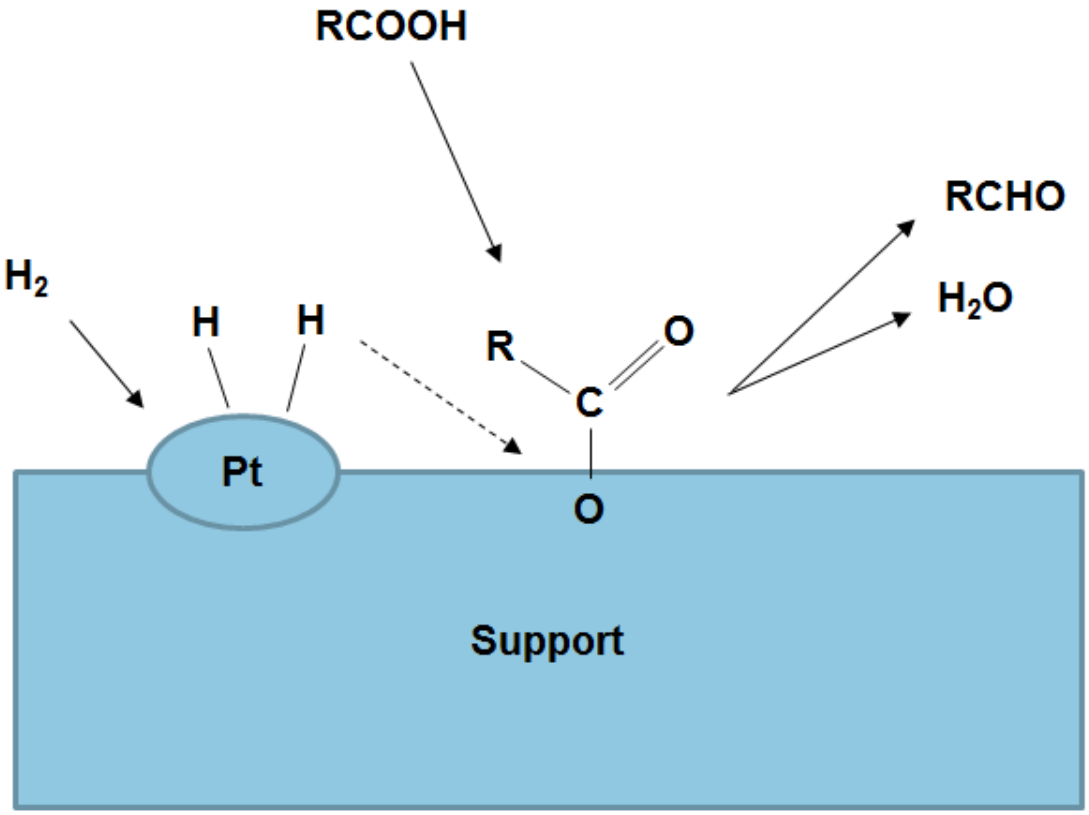

Figure 2.4: *HDO of carboxylic acid over noble metal supported catalysts.*

For HDO reactions involving the use of reducible metal oxides as supports, suitable metal-oxygen bond strength is required to remove oxygen from oxygenated compounds (Moberg et al., 2010). Accordingly, a very strong metal-oxygen bond makes it difficult to create

surface vacant sites that allow adsorption of oxygenated compounds, whereas a very weak metal-oxygen bond makes it difficult for the catalysts to remove oxygen from the oxygenated compounds. This follows the Sabatier rule which states that metal oxide supports with an intermediate metal-oxide bond strength are the best (Cheng and Hu, 2008). According to Pestman et al., (1997), the order of metal-oxygen bond strength is as follows;

Mg>Al>Zr>Ti>W>Cr>Zn>V>Sn>Fe>Ge>Mn>Ni>Bi>Cu>Pb 2.18

Recent reports on noble metal catalysts have focused on the HDO of model compounds with a few reports addressing the HDO of actual bio-oil (Ardiyanti et al., 2011; Wildschut et al., 2010, 2009). Two similar studies that compared noble metal catalysts over HDO of bio-oil (Ardiyanti et al., 2011) and guaiacol (Gutierrez et al., 2009) at 100 °C and 8 MPa was reported. Though the trend of catalyst activity for these studies follows different reaction pathways due to different temperature and pressure, noble metals appear to be more efficient with respect to hydrocarbon yield and deoxygenation level compared to Co/Ni-MoS catalysts in both studies. Sanna et al., (2015) studied the HDO of the aqueous fraction of bio-oil with Ru/C and Pt/C catalysts. Additionally, acetic acid being one of the most difficult compounds to be hydrogenated, has seen a successful increase in conversion from 17% to 59%-75% over the two-step hydrogenation process using Ru/C and Pt/C catalysts. However, the HDO process over these catalysts requires extreme reaction temperature and high pressure to achieve significant conversion. Moreover, the production of liquid hydrocarbons is mainly influenced by elevated hydrogen pressure in the range 52-100 bar. Pt/C further showed retention of about 70% and 80% of carbon in the liquid phase at 220 °C and 250 °C respectively. Olcay et al., (2010) investigated the activity of carbon-supported noble metals in aqueous phase hydrogenation of acetic acid at 110-410 °C and 52 bar of H_2. The activity and selectivity of the tested metals in terms of hydrogenation of acetic acid to ethanol was determined to be significantly different.

In order to better utilize noble metal catalysts and understand the reaction routes, it is necessary to understand the synergistic effects from metal, support, promoters, operating conditions and acidity in promoting deoxygenation using bio-oil model compounds. Table 2.4 presents an overview of recent literature in HDO study over noble metal catalysts including reactor type, operating conditions and primary products.

Table 2.4: *Overview result obtained for HDO of model compounds.*

Substrate	Reactor	Catalyst (s)	Time (h)	Pressure (MPa)	Temperature (°C)	Stirring Speed (rpm)	Main Product (s)	Reference
Acetic Acid	Fixed Bed	Pt/TiO_2, Pt/C, Pt/ZrO_2, Pt/CeO_2	-	4	300	-	Ethane, ethanol, ethyl acetate, acetone, CO_2	(He and Wang, 2013)
Acetic Acid and Furfural	Batch	$Ni/Al_2(SiO_3)_3$	3	6.7-8.0	260	300	Ethanol, Ethyl acetate, acetaldehyde, Furan,2-methyl,1,1-diethoxy, Pentanoic acid	(Wang et al., 2011)
Acetic Acid and Furfural	Batch	Pt/HZSM-5, Pd/HZSM-5, Ru/HZSM-5	3	7-7.5	260	500	Ethyl acetate, Ethanol, Acetaldehyde, 2-furanmethanol	(Chen et al., 2013)
Acetic Acid	Packed Bed Micro	NiMo/ Al_2O_3	-	2.06	<300	-	Ethanol, Ethyl Acetate, Acetaldehyde	(Joshi and Lawal, 2012)
Acetic Acid	fixed bed	Pt-Sn	-	3	255	-	Ethanol, Ethyl Acetate, Acetaldehyde	(Zhang et al., 2014)
Acetic Acid	Batch	$NiMo/Al_2O_3$	2	3	200	-	Ethanol, Ethyl Acetate, Acetaldehyde	(Xu et al., 2009)
Propanoic Acid	Plug flow	Pd/SiO_2, Pd/TiO_2, Pd/C	-	0.1	200–400	-	Ethane, propionaldehyde	(Lugo-José et al., 2014)

Acetic acid	Trickle bed	Ru/C, Ru/Al_2O_3, Ru/ZrO_2	1	6.4	150-190	-	Ethanol, methane, ethane	(Chen et al., 2011)
Propanoic	Trickle bed	Ru/C, Ru/Al_2O_3, Ru/ZrO_2	1	6.4	130-210	-	Propanol, methane, ethane, propane	(Chen et al., 2011)
Butanoic acid	Trickle bed	Ru/C, Ru/Al_2O_3, Ru/ZrO_2	1	6.4	150-210	-	Butanol, methane, ethane, propane, butane	(Chen et al., 2011)
Butanoic acid	Fixed bed	Ru/ZrO, 1Ru-2Sn/ZrO	0.9	2.5	265	-	Butanol, butylbutanoate	(Lee et al., 2014)

2.4.2 Deactivation

Catalyst deactivation in the HDO process has been associated with several mechanisms due to coking, sintering and chemical transformations that can result in inactive phases and deactivate the catalyst (Bartholomew, 2001; Furimsky and Massoth, 1999). The extent of remaining catalyst activity is linked to these phenomena. Coke formation is mainly influenced by polymerization and poly-condensation reactions due to the difference between the average molecular weight of coke in the system and those present in the feeds. Thus, the strength of the reactant adsorption on the catalyst surface strongly contributes to the degree of carbon deposition. Furimsky, (2000) have reported that phenols and furans present in bio-oil were considered to be the major coke precursors due to their strong interaction with the catalyst surface. Furthermore, single-oxygen compounds were reported to be less vulnerable to coke formation than double-oxygen compounds such as carboxylic acids (Popov et al., 2010). Though noble metal catalysts are not prone to aqueous media containing water and acids like Co/Ni-MoS catalysts, carbon deposition is still regarded to be the major cause of catalyst deactivation. In the study of hydrogenation of stearic acid over 4% Pt/TiO_2 and 4% Pt-4%Re/TiO_2 catalysts, Manyar et al., (2010) reported the reusability of these catalysts over two cycles after recovery and subsequent regeneration via catalyst reduction. Even though both catalysts showed good reusability in terms of alcohol selectivity, 4% Pt/TiO_2 still maintained a significant hydrogenation rate while 4% Pt-4%Re/TiO_2 showed a sequential drop over the reusability cycles, which was linked to the adsorption of carbonaceous residue on the catalyst and loss in Pt-Re interaction. Apart from the reactant structure, the acidic property of the catalyst also contributes towards coke formation. For example, Bui et al., (2011) reported that the acidity of Al_2O_3 support in CoMoS catalyst gave rise to the formation of heavier HDO products which causes catalyst deactivation, while less acidic supports such as ZrO_2 and TiO_2

favour lighter by-products. Meanwhile, coke precursors are formed as carbocations due to the interaction between the adsorbed reactant species on the Lewis acid sites and proton supply from the Brönsted acid sites (Furimsky and Massoth, 1999). As confirmed by Zanuttini et al., (2014), Pt/SiO_2 showed a higher carbon deposition compared to Pt/Al_2O_3 during the hydrogenation of m-cresol as a result of both Brönsted and Lewis acid sites in SiO_2, while Al_2O_3 only contained Lewis acid sites. However, it still remains unclear how both Lewis and Brönsted acids contribute to coke formation. Other factors such as reaction temperature, H_2 pressure and reaction time contribute to coke formation during the HDO process. In addition, low reaction temperature and hydrogen pressure were reported to enhance coke formation instead of hydrogenation reaction (Si et al., 2017). Moreover, it has been reported by Li et al., (2015) that high temperature resulted in severe coke formation in spite of improved HDO.

2.5 Catalyst Promoters

The development of heterogeneous catalysts to upgrade bio-oil components to produce desired chemicals has received increased attention in industrial processes (Si et al., 2017). Bio-oil upgrading requires a catalyst that tends to promote the product selectivity by enhancing the catalyst activity and lifetime. A range of catalyst modifications are carried out by adding another metal in order to promote the catalyst performance towards a targeted product. This includes geometric rearrangements through selective blockage of specific surface sites, suppression of undesired gas phase reactions and electronic effects through enhanced adsorption-desorption on the metal surface (Ertl et al., 2008a; Hutchings, 2001). The resulting bimetallic surface could possess different chemical and catalytic properties compared to the surfaces of the active metal (Dimitratos et al., 2006; Ertl et al., 2008b). The overall catalytic activity of the bimetallic catalysts is not uniquely dependent on the electronic and geometric modification of the metal species, but is also influenced by the reaction conditions and catalyst

support (Prati et al., 2007). The improved selectivity and activity of the promoted catalyst can be described by the synergy of all the promotional effects involved.

The role of promoters in enhancing catalyst selectivity towards targeted products have been investigated using gold, cobalt oxide, and ferric oxide-containing catalysts (Corma and Serna, 2006; Wang et al., 2016; Westerhaus et al., 2013). However, these catalysts have been faced with the drawback of low activities, high reaction temperatures and long reaction times. Early studies involving the use of transition metal catalysts were carried out by Fuchikami and co-workers (1995), which laid the foundation for further development of bimetallic catalysts in the hydrogenation of carboxylic acids. The bimetallic catalysts reportedly outperformed their monometallic counterparts in the hydrogenation of pentadecanoic acid in terms of alcohol selectivity and catalyst activity under relatively mild temperature. Consequently, the preferential hydrogenation towards pentadecanol in excess yield was associated with the combination of $Ru(acac)_2/Rh/Al_2O_3$ metal complexes with $Re_2(CO)_{10}$ or $Mo(CO)_6$. In this section, the function of rhenium addition upon supported platinum catalyst is considered and described, towards the hydrogenation of carboxylic acids.

2.5.1 Rhenium-promoted catalysts

The potential of rhenium-promoted catalysts was first discovered in the 1960s (Broadbent et al., 1959; Broadbent and Whittle, 1959), and later in the early 1980s, further studies were carried out which revealed the tendency of rhenium heptoxide to form synergistic combinations with Pt, Pd, Rh and Ru metals (He et al., 1995). The application of the Re-promoted catalysts for the hydrogenation of carboxylic acids gained attention in the 2000s, with the first study being carried out on fumaric acid. This study pointed out the problems associated with product distribution, where products such as succinic acid, butyrolactone and tetrahydrofuran can inhibit the reduction of the acids into diols (Bockrath et al., 1999; Campos

et al., 2003). For example, kinetic studies involving the hydrogenation of fumaric acid using Ru-Re catalyst at 250-270 °C resulted in the formation of butyrolactone and tetrahydrofuran with succinic acid intermediate. The analysis of kinetic parameters suggested that further hydrogenation reactions are limited to the abundant formation of succinic acid as an intermediate and decreased amount of fumaric acid.

Promoters greatly influence the selectivity routes for HDO reactions. For example, Ly et al., (2012) studied the HDO of succinic acid over Pd/TiO_2 at 160 °C and was found to be highly selective for butyrolactone. Addition of Re to Pd/TiO_2 switched the selectivity to about 80% towards 1,4-butanediol with a complete conversion of succinic acid and butyrolactone in a shorter period. Similarly, the addition of Re on carbon supported Pt/Ru catalysts improved succinic acid conversion, with increased yield and selectivity of 1,4-butanediol (62-66%) under batch conditions 160 – 180 °C and 150 bar (Minh et al., 2010). In addition, catalyst reuse showed an insignificant drop in catalyst performance after recycling. The method of impregnation or surface reduction techniques were mainly used to prepare $Pd\text{-}Re/TiO_2$ catalyst and subsequently reduced by passing hydrogen over it at 450 °C. However, characterization studies have revealed the difficulty in reducing Re-promoted catalysts that are prepared by surface redox reaction to their complete metallic state (Betizeau et al., 1976; Ciftci et al., 2014b, 2014a). This suggests that Re exists as ReO_x next to metallic Pd on titania. Furthermore, the minimum addition of 3.5% Re to $Pd\text{-}TiO_2$ using the impregnation method was required to induce the desired Pd-Re, which is equivalent to 0.6-0.8% Re loading required when using the surface redox reaction. This indicates that the synergy of Re with active metal can be influenced by the method of catalyst preparation. Even though a lower loading is required for catalyst preparation using the surface redox technique, the impregnation method appears to be more attractive considering the complete reduction of ReO_x to Re that could be achieved.

The versatility of Re promoted catalysts for the hydrogenation of fatty acids (C_6-C_{18}) cannot be over emphasized, as the selectivity towards hydrogenated products such as alcohols and alkanes is significant (Manyar et al., 2010; Sá et al., 2011; Takeda et al., 2012). According to Takeda et al., (2012), the hydrogenation of fatty acids using ReO_x-Pd/SiO_2 catalyst in a Pd:Re of 1:8 molar, was highly selective for fatty alcohols in excess of 92% yield. Shorter chain fatty acids such as hexanoic and octanoic acid demonstrate higher alcohol yields in excess of 98% with trace amounts of alkanes as by-products. However, this selective trend contrasted the findings of Manyar et al., (2010) who studied the hydrogenation of stearic acid and observed an alcohol selectivity of 93% and 60-80% selectivity over Pt/TiO_2 and Pt-Re/TiO_2 respectively. The addition of Re to Pt/TiO_2 facilitated the hydrogenation reaction which reduced stearyl alcohol selectivity and gave rise to heptadecane as the major by-product. Furthermore, the increase in Re loading up to 4wt% resulted in increased activity but did not correlate with stearyl alcohol selectivity. Mendes et al., (2001) investigated the hydrogenation of oleic acid and proposed a reaction mechanism over Pt and Pt-Re/TiO_2 for product selectivities in the hydrogenation of carboxylic acid (Figure 2.5). For the monometallic Pt/TiO_2 catalyst, the presence of oxygen vacant/defect sites (Ti^{n+}) provides the platform for the carbonyl group of the acid to adsorb while hydrogen is activated on Pt. Subsequently, the hydrogenation reaction is facilitated by the interaction between the hydrogen spill-over and adsorbed carbonyl species. For the Re promoted Pt/TiO_2 catalyst, the availability of oxophilic Re centres facilitates the hydrogenation of carboxylic acids towards the formation of alcohols and alkanes through several mechanisms, as a result of the interaction between the oxygen of the carbonyl species and Re as shown in Figure 2.5.

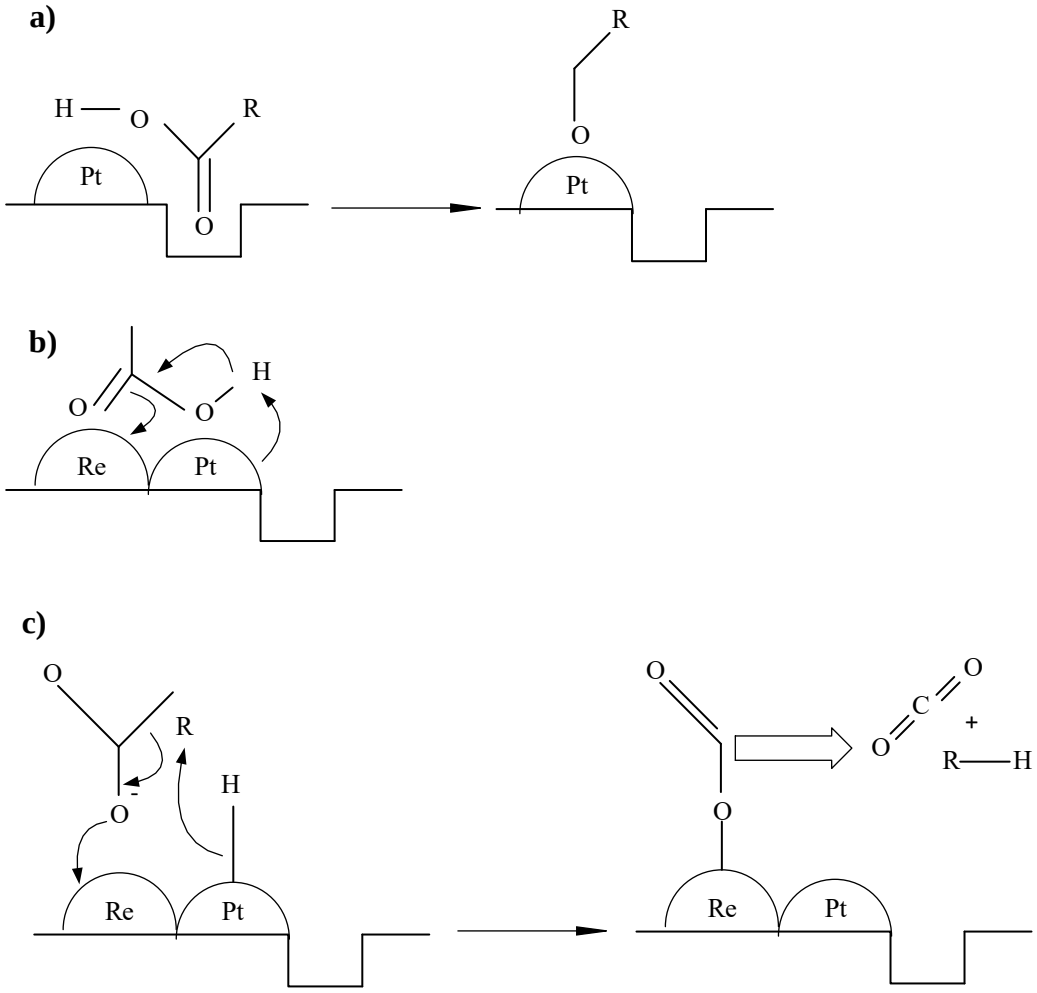

Figure 2.5: *Proposed HDO mechanism over titania supported Pt/Pt-Re catalysts for the hydrogenation of carboxylic acids for a) the interaction of the oxygen atoms of the carbonyl specie with oxygen vacant sites created by H_2 spillover facilitated by Pt, b) the interaction between the carbonyl specie and Pt/Re, and c) the decarboxylation of carboxylic acid specie over Pt-Re/TiO_2 facilitated by Re.*

The choice of support (TiO_2 and Al_2O_3) was observed to have a significant influence on the reduction of Pt/Re metals (Manyar et al., 2010). In addition, TiO_2 provided a more efficient reduction of the Pt and Re metals. However, the Pt-Re/TiO_2 catalyst loses its catalyst activity upon recycle which is attributed to the formation of surface carbonaceous deposit. Furthermore, the propensity of metal leaching was insignificant towards the drop in catalyst activity, and the original activity of the catalysts could be regenerated by calcination and subsequent reduction. The extent of restoration of the catalyst activity also depends on the hydrogenation reaction on

the synergy of Pt-Re. Overall, Re promoted catalysts are highly attractive due to the presence of oxophilic centres in Re, which facilitates the hydrogenation of carboxylic acids, giving rise to alcohols and alkanes through different mechanisms. In this study, supported Pt-Re catalysts have been prepared by wetness impregnation method and applied in the hydrogenation of C_2-C_4 carboxylic acids.

2.6 Catalyst Support

The role of active phases and promoters in catalytic hydrogenation reactions is very important. Supports are very significant in dispersing and stabilizing active phases during HDO activity. Some supports exhibit Brönsted acid character, interacting with supported active phases in the presence of Lewis acid sites on the surface of the catalyst (He and Wang, 2012). The Brönsted acid sites function as proton donors to the adsorbed compounds while Lewis sites provides the binding of species to the catalyst surface (Furimsky and Massoth, 1999; Rakshit et al., 2018). The choice of support depends on two basic functions: (i) Low affinity for carbon formation, (ii) Propensity for activation of oxy compounds (Mortensen et al., 2011).

2.6.1 Alumina

The use of Alumina (Al_2O_3) has been linked to the early years of hydrodesulfurization (HDS) and hydrodenitrogenation (HDN) reactions (He and Wang, 2012; Vissers et al., 1987). It is characterized by a large surface area and presence of Lewis acid sites, making it proffer excellent crushing strength and sustainable activity. In addition, this initially made Al_2O_3 appear to be an excellent choice of catalyst support. However, the formation of a single slab monolayer due to the strong interaction between Al_2O_3 and MoS_2 and electronic exchange through Mo-O-Al bonds results in low activity of alumina supported catalysts (He and Wang, 2012). Furthermore, the formation of coke is likely to occur which reacts with the acidic Al_2O_3 support

from both oxygenated reactants and intermediates, and consequently causes loss of activity and catalyst deactivation (Laurent and Delmon, 1994; Popov et al., 2010). In the presence of a large volume of water, Al_2O_3 support converts into boehmite and oxidizes the active metal to its oxide form, resulting in the blockage of active sites and subsequent deactivation (Bu et al., 2012; Honkela et al., 2010; Furimsky, 2000). Therefore, the applicability of Al_2O_3 support for hydrogenation reactions becomes limited to the presence of water and oxygen-containing compounds with two or more oxygen atoms. Due to these reasons, efforts in developing new catalysts have been made by replacing Al_2O_3 support with SBA mesoporous support (Duan et al., 2012), neutral supports like silica and activated carbon (Centeno et al., 1995; Puente et al., 1999; Ferrari et al., 2002), oxide supports such as ZrO_2 (Ardiyanti et al., 2011; Bui et al., 2011) TiO_2 (Ardiyanti et al., 2011) or MgO basic support (Yang et al., 2009).

2.6.2 Silica

Silica (SiO_2) exists as inert support due to its weak interaction with the sulfide phase in $CoMo/SiO_2$ catalyst (He and Wang, 2012). For example, Centeno et al., (1995) reported that the activity of sulfided $CoMo/SiO_2$ is less than that of sulfided $CoMo/Al_2O_3$. Although these catalysts are not as active as Al_2O_3–based catalysts, the formation of strong interaction between silica (SiO_2) and the oxygen-containing reactants and products is averted by the inert nature of silica (Centeno et al., 1995). SiO_2-based catalysts offer better catalyst performance compared to Al_2O_3–based catalysts due to the weaker metal support interaction that exists on the former (Jasik et al., 2005; Olcese et al., 2012). During the hydrodeoxygenation of phenolic compounds, phenates are weakly adsorbed and only the OH group interacts with H_2 bonds from SiO_2 (Popov et al., 2010), while they are strongly adsorbed to Al_2O_3 with the phenate species found on Al_2O_3 (Popov et al., 2011). Furthermore, SiO_2 has a moderately low affinity for carbon formation and

its interaction with water is weak in comparison to Al_2O_3, hence, making it a suitable option for use as catalyst support for HDO processes.

2.6.3 Activated Carbon

Activated carbon (AC) support exhibits less tendency for coke formation and weak acidity, in addition to its low cost and neutral nature. AC supported catalysts have been identified to be more active than both SiO_2 and Al_2O_3 based catalysts (Ardiyanti et al., 2011; Duchet et al., 1983). AC also possesses a high surface area which provides higher dispersion and complete sulfidation of the oxide species present in Mo-based catalyst. However, higher metal loading results in agglomeration, weak interaction with the supported phases and blockage of micropores, which in turn favours sintering. The microporosity of carbon supports is a drawback in hydrotreating processes because some active metals present in the micropores are lost during catalytic reactions involving large hydrocarbon molecules (He and Wang, 2012). Other challenges associated with AC are poor crushing strengths and low bulk density. For example, hydrogenation of acetic acid was investigated in a batch system using noble metals (Pd, Pt and Ru) supported on carbon (Kawamoto et al., 2016; Wan et al., 2013). The mechanism describing reaction over these catalysts showed that the high dispersion possessed by carbon supported catalysts is not sufficient to provide the desired selectivity and activity for acetic acid hydrogenation.

2.6.4 Metal Oxide

Other metal oxide supports have been reported as alternative catalyst supports in recent times which include CeO_2, ZrO_2 and TiO_2 (Ruddy et al., 2014; Wang et al., 2013). Early progress on these supports proposed both ZrO_2 and TiO_2 to be popular in HDS, which has been attributed to their reducibility and favourable morphology (Zhang et al., 2013). ZrO_2 is less susceptible to coke formation due to its amphoteric property (Bui et al., 2011; Zhang et al.,

2013). In addition, ZrO_2 also favours the activation of oxygenated compounds on CoMoS catalysts and shows less carbon deposition on the surface than that of the sulfided $CoMo/Al_2O_3$ catalyst. Metal oxide supports exhibit features of both Lewis and Brönsted acid sites (Furimsky and Massoth, 1999), which are required in the mechanism of HDO (Mortensen et al., 2011; Rakshit et al., 2018). Subsequently, Lewis acid sites allow the adsorption of oxy-compounds on the catalyst surface, which is further attacked by hydrogen atoms as a result of proton donating Brönsted sites. However, higher catalyst acidity increases the tendency of coking. Bui et al., (2011a) reported that TiO_2 and ZrO_2 exhibit sufficient acidity to improve HDO activity and are intolerant to coke formation. The oxide supports follow this order of acidity: Al_2O_3 > TiO_2 > ZrO_2 > CeO_2 (Bui et al., 2011; He & Wang, 2012). However, the susceptibility of coke formation in Al_2O_3 results in catalyst deactivation over time. This suggests that the acidity requires a proper metal-oxygen bond strength in the oxide support to achieve the desired activity and selectivity (He and Wang, 2013). For example, He and Wang (2014) studied the HDO of guaiacol over Pt/TiO_2 and Pt/Al_2O_3 catalysts and revealed that Pt/TiO_2 showed better catalyst stability while Pt/Al_2O_3 deactivates over time due to coke formation. In a different study on Pt supported on ZrO_2, TiO_2 and CeO_2 supports, the presence of weak acidity and improper metal-oxygen bond strength in Pt/ZrO_2 and Pt/CeO_2 favours the production of ethylacetate and ethane, while Pt/TiO_2 favours ethane production due to strong acidity and proper metal-oxygen bond strength (He and Wang, 2013). Even though metal oxide supports exhibits a microporous surface area that allows less dispersion, the metal-oxide interface, acidity and enhanced oxygen vacancy regeneration makes them suitable catalysts. Furthermore, the design of these catalysts with noble metal active phases other than CoMoS/NiMoS is beneficial in HDO processes.

2.7 Catalyst Preparation and Formulation

The preparation of supported catalysts involves the deposition of active phases on a carrier as shown in Figure 2.6 (Perego and Villa, 1997; Richardson, 1989). A good support offers high dispersion, with a high degree of thermal stability of the active component. In other words, deposition of active phase precursors in dispersed form onto the powdered support, followed by converting it into the final component is highly desirable (Ertl et al., 2008c). For catalyst preparations consisting of one or more precious metal(s), the most popular methods employed in depositing the active component are mainly ion exchange and impregnation (Bamwenda et al., 1997; Campanati et al., 2003; Ertl et al., 2008c). During impregnation, a certain amount of the solution containing the metal precursor occupies the pores of the support, which subsequently, is dried to eliminate the adsorbed solvent. These active metals can be deposited consecutively or simultaneously when multiple active metals are required for the preparation of supported bimetallic catalysts (Ertl et al., 2008c). With precious metals such as platinum on activated carbon, the impregnation method is more attractive since waste is eliminated (Deutschmann et al., 2009; Ertl et al., 2008d).

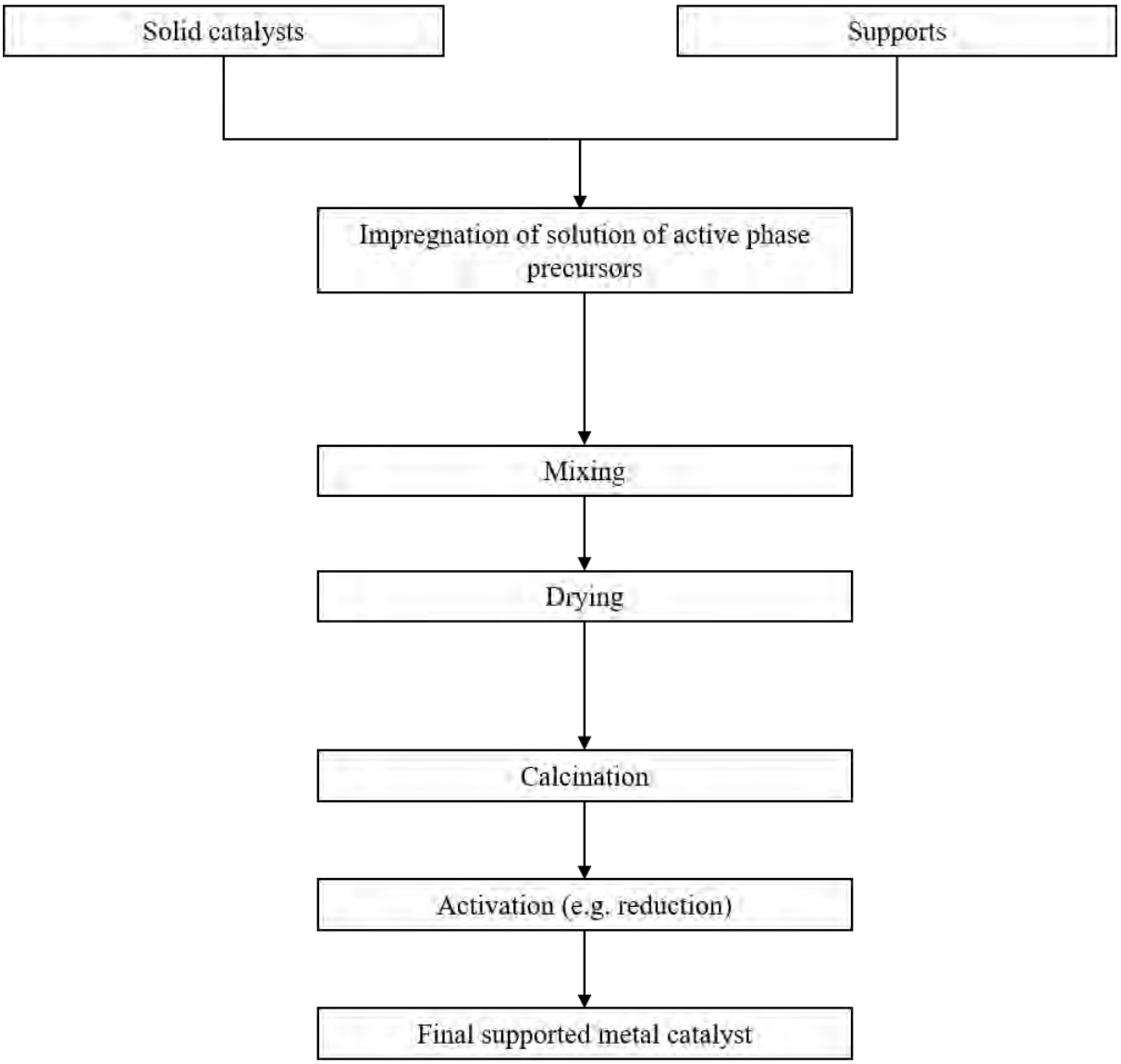

Figure 2.6: *Stages involved in catalyst preparation and formulation by impregnation method.*

After the impregnation, the degree of distribution of active species is affected by the rate of drying which requires careful control, some active species can redistribute, as the liquid fronts occupy the pore structure thereby creating concentration gradients (Campanati et al., 2003; Regalbuto, 2007). Subsequently, this results in catalyst profiles such as uniform, egg-shell, egg-white and egg-york, which exhibit different features in terms of pore diffusion and lifetime in heterogeneous reactor systems. After drying, calcination is required to eliminate

surface impurities while reduction is needed to transform the metal oxide form of the catalyst into an active phase. In this study, mono and bi-metallic titania-supported platinum catalysts are formulated which is reported in the following section.

2.8 Three-Phase Catalytic Reactor

Most heterogeneous reactions that involve catalytic hydrogenation and oxidation are characterized by mass transfer, good heat transfer, temperature control and catalyst utilization (Ramachandran and Chaudhari, 1983). A three-phase reactor is mainly employed for this kind of reaction system. Three-phase catalytic reactors that are popularly used in industries are summarized in Figure 2.7 as follows:

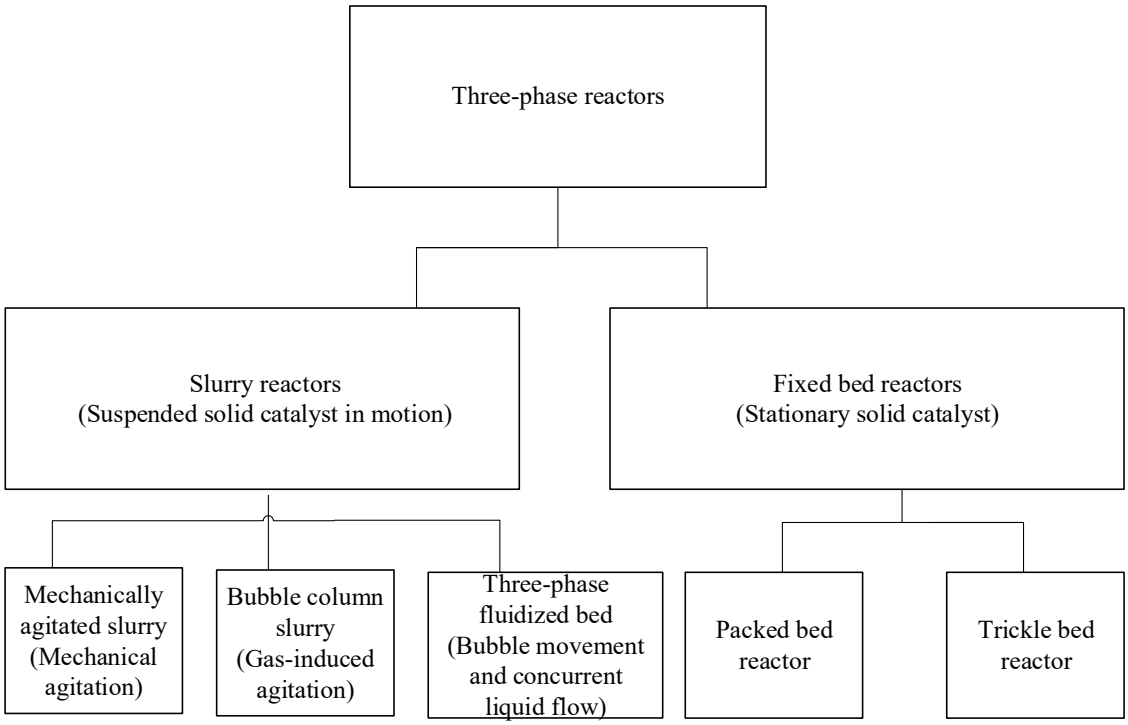

Figure 2.7: *Types of three-phase catalytic reactors (Deutschmann et al., 2009; Ramachandran and Chaudhari, 1983).*

The choice of a reactor is crucial and depends on information from the reaction kinetics, heat and mass transfer, thermodynamics and characteristics of the reaction mixture (Sheldon

and Bekkum, 2008). In addition, the criteria for selection of lab-scale and industrial scale reactors for catalyst testing are quite different. The laboratory scale reactors are mainly small-scale reactors. To scale down a reactor as much as possible is beneficial due to cost associated with equipment, material, waste formation, utility requirements and intrinsic safety. However, the utilization of a small-scale reactor to its optimum capacity requires accurate experimentation in the presence of representative catalyst samples.

For the investigation of reaction kinetics, composed of a three-phased system, the most suitable type of laboratory scale reactor is widely regarded to be the mechanically agitated slurry reactor (Ramachandran and Chaudhari, 1983; Sheldon and Bekkum, 2008), if after rigorous investigations in eliminating mass transfer limitations has been carried out. In addition, highly active catalysts with catalyst effectiveness factor approaching unity can be used, and the ease of equipment design and scale up is attainable.

2.8.1 Mechanically Stirred Slurry Reactor

The mechanically stirred reactors are dead-end autoclaves that operate as either a batch or semi-continuous system. They are mainly encompassed with a gas entrainment impeller that allows the feed of the reactant gas by maintaining a constant pressure (Kapteijn and Moulijn, 2008). The reactor vessels are also incorporated with alternative stirrers to ensure a homogenous suspension of catalyst particles in the liquid phase, which is subsequently extracted from the vessel and isolated from the product mixture.

For a surface reaction to occur during a three-phase catalytic reaction, several mass transfer steps are involved, which includes the dissolution of the gaseous reactant into the liquid phase and subsequent adsorption of both reactants on the catalyst surface. It becomes insignificant to increase the amount of catalyst loading when the overall reaction rate is

influenced by the extent of mass transfer. Therefore, in the selection and design of a three-phase reactor, the characteristics of mass transfer must be incorporated in order to promote mixing and minimise mass transfer resistance (Sheldon and Bekkum, 2008).

2.8.2 Mixing and Particle Suspension

To achieve the intrinsic rate kinetics from experimental data without the assumption of heat and mass transfer limitations, there are several conditions that must be fulfilled. These conditions include the intimacy between the catalyst and reactants, as well as effective catalyst suspension, and the proper description of reactor characteristics under isothermal conditions (Kapteijn and Moulijn, 2008).

2.8.2.1 Particle Suspension

Proper mixing is required in ensuring effective contact between the reactant phases (Jafari et al., 2012; Sheldon and Bekkum, 2008). In the reaction medium, the catalyst particles need to be maintained in a uniformly dispersed manner. This subsequently allows for adequate utilization of the catalyst activity, i.e. the total catalyst particles are thoroughly distributed above the bottom of the vessel. The extent of agitation is required to achieve a thoroughly mixed system which depends on the reactor geometry (internal diameter of reactor d_T, stirrer diameter d_I, catalyst properties (catalyst density ρ_P, catalyst loading w', catalyst particle average diameter d_P) and properties of the solvent medium (density ρ_L, viscosity μ_P). The Zweitering equation (Equation 2.19) is widely applied in calculating the minimal agitation conditions required to achieve absolute suspension of catalyst particles in a stirred vessel which aids in selecting the appropriate conditions (Ibrahim et al., 2012; Zwietering, 1958);

$$N_m = \frac{\beta d_p^{0.2} \mu_L^{0.1} g^{0.45} (\rho_p - \rho_L)^{0.45} \omega'^{0.13}}{\rho_L^{0.55} d_I^{0.85}} \qquad 2.19$$

where β is a dimensionless value for a stated reactor geometry. According to Nienow (1975, 1968), an approximate value of β can be calculated by:

$$\beta = 2\left(\frac{d_T}{d_I}\right)^{1.33} \qquad 2.20$$

2.8.3 External Mass Transfer

For a three phase solid-catalysed reaction involving gaseous and liquid reactants to occur, it is pivotal that the reactants are transported through the layers of the boundary, and onto the surface of the catalyst. This mode of transport means that hydrogen diffusion has to occur from the gaseous phase to the liquid phase and subsequently onto the catalyst surface, while the diffusion of liquid substrate has to occur through the liquid catalyst boundary layer (Doraiswamy and Sharma, 1984). For this mode of transport to occur, it is implicated that there is the need for hydrogen diffusion from the gaseous phase onto the liquid phase, and sequentially onto the surface of the catalyst to occur, whereas the liquid substrate diffuses through the boundary layer of the liquid catalyst. The interface diffusion stages can be regarded as limitations, which may reduce the substrate concentration thereby affecting the rate of reaction as the substrate travels through different phases, which is dependent on the superficial contact area and mass transfer coefficients (Fogler, 2010; Forni, 1999). Figure 2.8 illustrates the stages of material transport through different phases and boundary layers of gas-liquid-solid mass transfer and intra -particle diffusion, followed by chemical reaction in the active sites.

The mass transfer resistances involved in the transport of gaseous reactants from the bulk gas phase to the surface of the catalyst are grouped as the region of external mass transfer (See Figure 2.8).

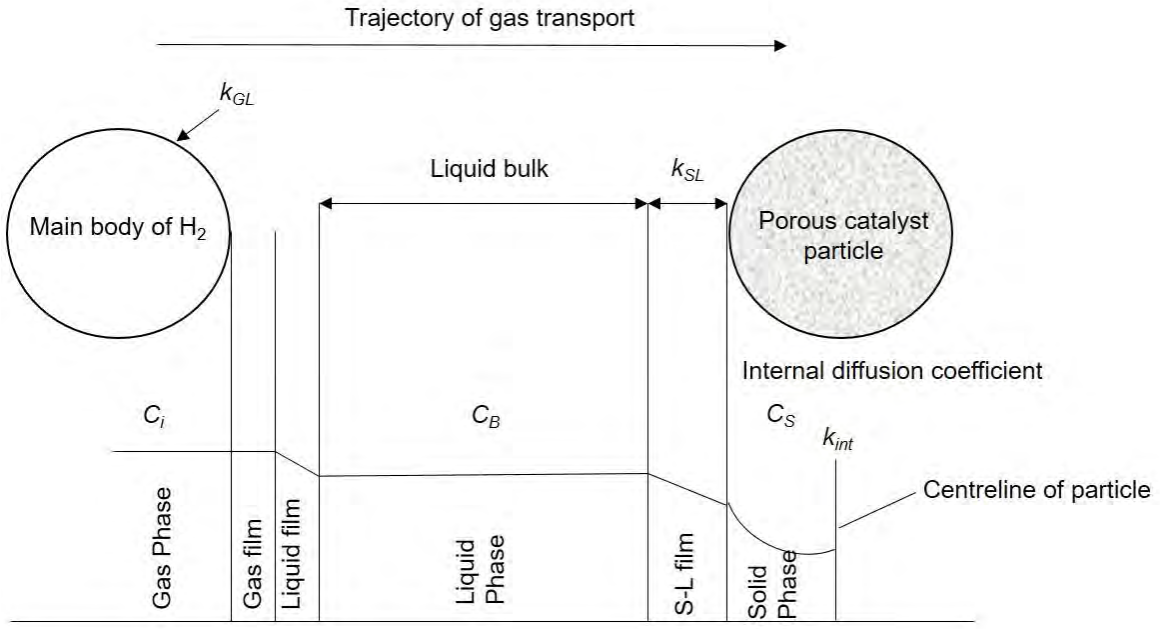

Figure 2.8: *Gas concentration profile and mass transfer in a multiphase system.*

The gaseous reactant (G) exists as gas bubbles in the bulk gas phase. The rate of diffusion of the gas bubbles (G) in the gas phase is resoluted by the gas-film mass transfer coefficient (k_{GL}), gas-liquid interfacial area (a), and the difference in concentration between the gas bubbles (C_{Gi}) and gas-region of the gas-liquid interface (C_{GiG}). This can be expressed as follows:

$$r_G = k_{GL}a(C_{Gi} - C_{GiG}) \qquad 2.21$$

This region of diffusional resistance is insignificant for gases that are slightly soluble such as pure gas feeds and hydrogen (Santacesaria et al., 1994)

The rate of mass transfer in the gas-liquid interface is dependent on the volumetric liquid-side mass-transfer coefficient (k_La) and the difference in concentration between the gaseous reactant in liquid-region of the gas-liquid interface and bulk liquid (C_{GiL}-C_{GB}).

$$R_A = k_L a(C_{GiL} - C_{GB}). \quad 2.22$$

The concentration of gas bubbles on the liquid region of the interface can be determined using Henry's law, assuming interfacial equilibrium exists between the phases.

$$C_{GiL} = C_{GiG}/H \quad 2.23$$

In an agitated slurry vessel, the characteristics of the reactor and reaction variables such as agitation speed, operating temperature, properties of the solvent medium (density ρ_L, viscosity μ_P) and diameter of the reactor and stirrer respectively (d_T and d_I), may affect the k_La (Fillion et al., 2002). Several literature articles have reported values of gas-liquid mass transfer coefficient for agitated slurry vessels at different conditions (Rawase et al., 1997).

A poor gas-liquid mass transfer usually results in a low rate of reaction but is not fundamentally considered as the limiting step in a heterogeneous catalytic reaction (Kapteijn and Moulijn, 2008). Because improper mixing may result in low reaction rate, the effect of agitation can be used to examine the existence of interface gradient across the gas-liquid interface, at which the extent of mass transfer resistance can be reduced by sufficient agitation (Froment et al., 2010). Furthermore, it can be assumed that the diffusive resistance of gaseous reactant *G* in the bulk liquid phase is insignificant considering a thorough mixing takes place at a stirring speed above the calculated minimum stirring speed (N_m).

As shown in Figure 2.8, the final step of external mass transfer is the transport of gaseous reactant *G* through the liquid-solid film then onto the catalyst surface. The rate of mass transfer can be governed by the liquid-solid mass transfer coefficient (k_S), the difference between reactant concentration in the liquid-bulk and catalyst surface (C_{GB}-C_{GS}), specific

external surface area of the catalyst particles (a_s) and the catalyst loading w, which can be expressed as:

$$R_B = k_s a_s w(C_{GB} - C_{GS}) \quad 2.24$$

Ramachandran and Chaudhari, (1983) have reported several techniques that can be used to calculate $k_S a_S$ in addition to semi-empirical correlations which are based on Reynolds and Schmidt number (Gutierrez-Ortiz et al., 1994; Kluytmans et al., 2000; Kushalkar and Pangarkar, 1995). An enhanced mass transfer at the liquid-solid interface can be achieved by improving the relative particle velocity for a three-phase catalytic reaction (Fernández et al., 2007).

The final stage involves the rate of internal diffusion which is dependent on the reactant concentration on the catalyst surface C_{GS}, specific reaction rate k_{int}, the catalyst loading w and the internal effectiveness factor. Therefore, the surface reaction rate is described as:

$$R_C = k_{int}\eta C_{GS} w \quad 2.25$$

At steady state, the different rates of mass transfer are equivalent, as presented in equation 2.26. Upon rearrangement, the different mass transfer equations become:

$$R_A = R_B = R_C \quad 2.26$$

$$\frac{C_i}{R_A} = \frac{1}{k_{GL}a} + \frac{1}{w}\left(\frac{1}{k_{SL}a} + \frac{1}{k\eta}\right) \quad 2.27$$

By plotting $\frac{C_i}{R_A}$ against $\frac{1}{w}$ from experimental data, the mass transfer coefficients for the different boundary layers can be established from the following resistances for a pseudo-first order reaction as shown in Figure 2.9.

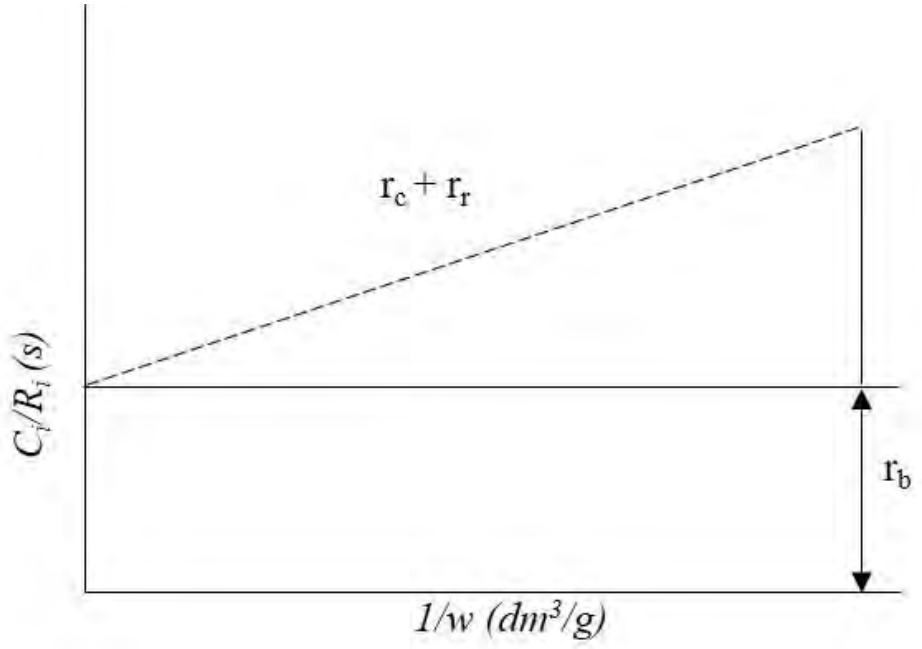

Figure 2.9: *A plot of mass transfer resistances.*

Resistance to gas adsorption: $Intercept = r_B = \frac{1}{k_{GL}a_B}$ 2.28

Liquid-solid mass transfer resistance and internal diffusion with surface reaction respectively:

$Slope = r_c + r_r = \frac{1}{k_{SL}a_P} + \frac{1}{k\eta}$ 2.29

To ensure a reaction is under kinetic control, the degree of liquid phase and liquid-solid mass transfer resistances can be determined by the extent of liquid phase agitation. It is suggested that reaction rate is not dependent upon the mass transfer coefficients k_L and k_{SL}, and subsequently should be independent of the agitation speed (Zhang et al., 2002). Several studies have experimentally investigated this effect by altering the stirring speed over different ranges and establishing the minimum speed when no practical change in reaction rates is observed (Bindwal et al., 2013, Lain et al., 2015).

2.8.4 Internal Mass Transfer

Most solid catalysts contain pores that provide increased surface area for adsorption and desorption to occur during reactions. The concentration gradient of reactants in the pores can be affected by internal mass transfer resistance if the catalyst support used provided the platform for active metal distribution (Klaewkla et al., 2011). Since the reactant has to be transported into the catalytically active sites located in the pore network, it becomes crucial to ensure the internal diffusion of the reactant molecules is not limiting the reaction rate. This is expected when the reactant concentration remains constant throughout the catalyst particle, alluding to negligible mass transfer. The reaction rates and selectivities are both affected when diffusion inside the catalyst pores becomes the rate-limiting step (Diepen and Moulijn, 2008). Liquid and gas reactants are transferred into the catalyst pores via molecular and Knudsen diffusion respectively (Forni, 1999).

Equation 2.30 shows the internal diffusion and reaction rate where w is catalyst loading, k_{int} is intrinsic reaction rate, C_{GS} is surface reactant concentration and η is the effectiveness factor.

$$R = wk_{int}C_{GS}\eta_c \qquad 2.30$$

To investigate the outcome of internal mass transfer on the reaction rates, it is important to determine the effectiveness factor and Thiele Modulus which explains the Weisz and Prater criterion ($\eta\varphi^2$) (Singh and Vannice, 2001).

$$\text{Thiele modulus, } \varphi^2 = \frac{surface\ reaction\ rate}{diffusion\ rate} \qquad 2.31$$

$$\text{Effectiveness Factor, } \eta = \frac{actual\ mean\ reation\ rate}{reaction\ rate\ if\ all\ active\ sites\ were\ on\ the\ surface} \qquad 2.32$$

$$(\eta\varphi^2) = \frac{Observed\ reaction\ rate}{diffusion\ rate} \quad 2.33$$

For a diffusion-free regime; $\eta\varphi^2 = \frac{rwL^2}{C_A D_{eff}} < 0.15$ 2.34

For a diffusion-limited regime; $\eta\varphi^2 = \frac{rwL^2}{C_A D_{eff}} > 0.4$ 2.35

where L represents the catalyst particle size, r_v represents the observed reaction rate, C_A represents the initial reactants concentration, w represents catalyst loading and D_{eff} represents the effective diffusivity.

Equations 2.34 and 2.35 are used to measure whether internal diffusion is rate limiting for an nth order reaction. It is also suggested that particle size influences the rate of intra-particle diffusion (Klaewkla et al., 2011; McManus et al., 2015; Tike and Mahajani, 2007). Subsequently, catalysts with small particles exhibit higher diffusivity and have a Thiele modulus close to zero which results in a reaction that is intrinsically limited. Several studies have reported the effect of catalyst particle size on reaction rates in mechanically stirred reactors (Akpa et al., 2012; Singh and Vannice, 2001). According to Akpa et al., (2012), rate of reaction increases with decreasing particle sizes in sieve fractions, over a particle size range of 0-250 μm. Subsequently, the particle size range of 0-45 μm revealed the highest reaction rate of 0.0195 mol min^{-1} g^{-1} while 150-250 μm particle sizes gave 0.003 mol min^{-1} g^{-1}, which suggests a mass transfer free system.

2.9 Chapter Summary

In this chapter, upgrading of bio-oil and hydrogenation of carboxylic acids were reviewed. The application of heterogeneous catalysts with emphasis on noble metals towards hydrodeoxygenation was described. The influence of supports and promoters towards the

hydrogenation of carboxylic acids were also discussed. The choice of a three-phase reactor and its benefit in this study was established. A detailed mass transfer explanation was presented as a preliminary stage towards the investigation of kinetics. Overall, this chapter provides the fundamentals and reference sources for the subsequent chapters of this study.

Chapter 3. **Experimental and Analytical Methods**

3.1 Overview

This chapter presents detailed methods and materials used to carry out this study. In addition, the method of catalyst preparation and characterization techniques used are explained in detail, along with the experimental laboratory setup and procedures used to perform hydrogenation reactions are reported. Furthermore, quantitative and qualitative analytical methods used to identify and quantify the products formed are explained in detail. This chapter also covers the design of experiment using the Taguchi method to establish an orthogonal array of experiments and determine the optimum reaction conditions for the conversion of acetic acid and yield of ethanol during the hydrogenation of acetic acid.

3.2 Materials

The list of chemicals required for this study were purchased from different suppliers as presented in Table 3.1.

Table 3.1: *List of Materials.*

Material	**Supplier**	**Specification**
Chemical reagents		
Acetic acid	Sigma-Aldrich	≥ 99.5%
Propanoic acid	Sigma-Aldrich	≥ 99.5%
Butanoic acid	Alfa aesar	99%
Ethanol	Fischer Scientific	99.99%
Propanol	Alfa aesar	99%
Butanol	Acros Organics	99%
Ethyl acetate	Fischer Scientific	Pure

Propyl acetate	VWR International	Pure
Butyl acetate	Fisher Scientific	Lab grade reagent
Ethyl propionate	Sigma Aldrich	99%
Propyl propionate	Acros organics	98+%
Butyl propionate	Sigma-Aldrich	99%
Ethyl butyrate	Sigma-Aldrich	99%
Propyl butyrate	Sigma-Aldrich	99%
Butyl butyrate	Acros organics	98%
Platinum (IV) nitrate	Alfa aesar	Pt 15% w/w soln.
Perrhenic acid	Alfa aesar	75-80% aq. soln.
Methanol	Acros Organics	99.99%
Hexane	Fischer Scientific	99%
Commercial Catalysts		
5% Pt/C	Sigma Aldrich	
5% Pt/graphite	John Matthey	
5% Pt/SiO_2	John Matthey	
0.5% Pt/Al_2O_3	John Matthey	
Gases		
Hydrogen	BOC	99.9%
Helium	BOC	99.9%
Nitrogen	BOC	99.9%
Others		
Titanium dioxide (P90)	Evonik	

3.3 Catalyst Preparation

3.3.1 Synthesis of 4%Pt/TiO_2

4% Pt/TiO_2 was prepared by incipient wetness impregnation method from titanium dioxide, TiO_2 (P90) and platinum (IV) nitrate, Pt $(NO_3)_4$ (15% w/w) as Pt precursor. 2.93 g of platinum (IV) nitrate was added dropwise to 9.6g of titania TiO_2 (P90) to make up 10g of 4%Pt/TiO_2. Subsequently, 100ml of methanol was added to the mixture and stirred overnight using a magnetic stirrer to ensure homogeneity of the mixture. The resulting suspension was filtered and the solid residue was oven dried for 3 hours at 80 °C. After oven drying, the solid was ground to powder form using pestle and mortar, and calcined at 500 °C under air flow for 6 hours at 10 °C/min ramp rate using an elite thermal system furnace.

3.3.2 Synthesis of Pt-Re/TiO_2

2g of Pt-Re/TiO_2 were prepared at different metal loadings by incipient wetness impregnation method from TiO_2 (P90), platinum (IV) nitrate solution Pt $(NO_3)_4$ (15% w/w) as Pt precursor and perrhenic acid, $HReO_4$ (75-80 wt%, aqueous) as Re precursor. For the different Pt-Re/TiO_2 catalysts synthesized, an appropriate amount of Pt $(NO_3)_4$ and $HReO_4$ were added dropwise to titania TiO_2 (P90) as presented in Table 3.2. Subsequently, methanol solvent was added to the mixture in a solvent to catalyst mass ratio of 10 ml:1 g and stirred overnight to ensure the solution was homogenous. The resulting suspension was filtered and the solid was oven dried for 3 hours at 80 °C. The dried solid was ground to powder form using pestle and mortar, and calcined at 500 °C under air flow for 6 hours at 10 °C/min ramp rate.

Table 3.2: *Summary of precursor masses for different Pt:Re catalysts.*

Metal loadings	Pt (g)	Re (g)	TiO_2 (g)
1%Pt - 2.5%Re	0.167	0.112	2.413
2.5%Pt - 1%Re	0.417	0.045	2.413
1%Pt - 4%Re	0.167	0.179	2.375
4%Pt - 1%Re	0.667	0.045	2.375

3.4 Catalyst Characterization

The performance of catalyst in terms of product selectivity and reaction mechanism is driven by the properties of the catalyst such as surface morphology, pore size, surface area, bulk structure and particle size. This section outlines the various techniques used to characterize both the prepared and commercial catalysts used in this study.

3.4.1 The Brunauer–Emmett–Teller (BET) and Barrett-Joyner-Halenda model (BJH)

The Brunauer–Emmett–Teller (BET) method was used to investigate the microstructural properties of the prepared and commercial catalysts such as catalyst isotherm, specific surface area and hysterisis. The BET method uses the adsorption-desorption of nitrogen molecules on the catalyst surface to determine the microstructural properties by fitting an equation to the data. The analysis was conducted at a temperature of 77K, using a Micrometrics Analytical Instrument ASAP*, to establish an adsorption isotherm. Before each analysis, approximately 1.05g of the catalysts were degassed at increased temperature before the analysis to eliminate contaminants. The BET model as shown in equation 3.1 describes the relationship between adsorption of nitrogen at monolayer surface coverage with respect to partial pressure. The resulting monolayer of adsorbed nitrogen on the catalyst surface is used to calculate the actual surface area, while the principle of capillary condensation of the nitrogen gas is used to

estimate the pore size, pore volume and size distribution in accordance with the Barrett-Joyner-Halenda model (BJH). The BJH model characterizes the catalyst particles as microporous, mesoporous or macroporous (Condon, 2006; Joyner et al., 1951). Nitrogen is mainly used because it is available in high purity, cost-effective, inert and its well-established molecular size.

$$\frac{P}{V(P_o - P)} = \frac{1}{V_m C} + \frac{(C-1)P}{V_m C P_o} \qquad 3.1$$

where P is partial pressure, P_o s saturation pressure, V is volume adsorbed at P, V_m is volume adsorbed at monolayer surface and C is a constant. Equation 3.2 was used to calculate the BET surface area based on V_m established from the BET plot.

$$S_{BET} = \frac{v_m n_a a_m}{m_v} \qquad 3.2$$

where a_m is the cross-sectional area occupied by each molecule of nitrogen adsorbate (0.162 nm^2), n_a is Avogadro's number (6.022 x 10^{23} mol^{-1}) and m_v is the gram-molecule volume (22400 cm^3).

3.4.2 X-ray Diffraction

X-ray Diffraction (XRD) is a non-destructive analytical technique that provides information about crystalline materials based on constructive interference of monochromatic X-rays and the crystalline sample. The diffraction pattern can be used for phase identification and can provide information on unit cell dimensions. For the identification of unknown components, the XRD pattern is compared with known standards as contained in the ICSD and JCPDS databases (Barbara and Christine, 2019).

The principle of XRD consists of emitted X-rays by a cathode ray tube which is filtered to produce monochromatic radiation in a parallel pattern and directed towards the sample. This interaction is described by Bragg's Law ($n\lambda=2d\sin\theta$) which relates the wavelength of electromagnetic radiation to the diffraction angle and the lattice spacing in a crystalline sample. The resulting diffracted rays and constructive interference are further detected, processed and counted. All possible diffraction directions of the crystal lattice are generated through a range of 2θ due to the random orientation of the powdered material. The diffraction peaks are converted to a set of d-spacings which are unique to individual minerals.

The XRD analysis was performed using a BRUKER D8 X-ray diffractometer equipped with copper Kα radiation (1.5406 Å). Prior to placing the sample holder in the diffractometer for every analysis, finely ground samples were placed on a sample holder and smoothened with a glass slide. The data were recorded using a scan time of 30 mins, sample stage revolution of 15 min^{-1} and a step size of 0.02 in the 2θ ranges of 20-70 °C. The XRD patterns obtained were identified by matching them against XRD patterns from literature and ICSD standard reference patterns.

3.4.3 Scanning Electron Microscopy (SEM)

The surface morphology and textural properties of the fresh and spent 4% Pt/TiO_2 and 4% $Pt\text{-}4\%Re/TiO_2$ catalysts were studied using a scanning electron microscope. A Hitachi Scanning Electron Microscope (SEM Hitachi TM3030 Plus) equipped with a high-sensitivity detector and 4-subdivision backscattered electron detector was used because it provides information on the distribution of regions of distinct composition in addition to surface roughness. In addition, the catalyst samples do not require any preparation or modification prior to analysis. It can also produce clear images on the reflecting surface even at a low accelerating

voltage of 5 kV. This technique uses a high-energy beam of secondary electrons to scan a sample surface which allows interaction with atoms within various depths of the sample. The resulting images are generated by signals obtained from secondary electrons (SE), reflected electrons or backscattered electrons (BSE). The SEM photomicrographs were obtained by manual focusing on a selected region of about 30 μm width at 2500× magnification.

The SEM Hitachi TM3030 Plus is incorporated with Energy-Dispersive X-ray spectroscopy (EDX) which is a chemical microanalysis technique used to characterize the elemental composition present in a catalyst sample. This technique relies on the interaction between electrons from an excited X-ray source and the sample surface. Electron vacancies are created by the bombardment of SEM electron beam on the catalyst surface which results in the release of electrons from the sample surface, which are captured and characterized into different elemental composition. The vacancies will require electrons from a higher energy state, and x-ray is emitted to balance the energy difference between the electrons released from the sample surface and the electrons.

In this study, the powdered catalyst samples were placed on a microscope stub, then analysed using the SEM Hitachi TM3030 Plus equipped with a Bruker Quantax 70 energy dispersive X-ray spectroscopy (EDX) system, under an accelerated voltage of 15 kV.

3.4.4 Temperature Programmed Reduction (H_2-TPR)

H_2-Temperature-Programmed reduction (H_2-TPR) is a commonly used characterization technique to provide the most efficient reduction conditions for metal oxides, metal oxides on support and mixed metal oxides. The H_2-TPR technique provides quantitative information on the number of reducible species present on the surface of a catalyst and the resulting temperatures which the reduction of each species occurs. Typically, H_2-TPR analysis does not

require the sample to possess any specific property except the presence of reducible metals (Knözinger, 2008; Reiche et al., 2000).

The powdered sample is filled into a quartz U-tube vessel and positioned in the furnace with a temperature control equipment and a thermocouple. The H_2-TPR analysis is initiated by passing about 5% of hydrogen gas in an inert carrier gas (mainly helium or nitrogen) through the sample at room temperature. As the sample temperature increases with time while gas is flowing, the amount of hydrogen uptake is monitored using the thermal conductivity detector (TCD) by the difference in the concentration of the gas mixture downstream. Accordingly, the peak maxima observed in the H_2-TPR profile represents the degree of reducibility of the metal oxide phase in the sample (Gervasini, 2013; Reiche et al., 2000)

In this study, a Quantachrom ChemBet Pulsar TPR equipped with a thermal conductivity detector (TCD) was used for temperature programmed reduction (TPR) measurements of 4% Pt/TiO_2 and 4% Pt-4%Re/TiO_2 catalysts. For each analysis, approximately 20 mg of catalyst was loaded into a quartz U-tube and was purged with quartz wool. The sample was pre-treated under 10% O_2/He at 300 °C for 60 min at a total flow of 40 $cm^3 \cdot min^{-1}$ to eliminate any volatile component. Subsequently, the H_2-TPR was initiated by decreasing the temperature to -50 °C, where 5% H_2/Ar was introduced by maintaining the total flow rate. The temperature was then increased from -50 °C to 800 °C at 5 $°C \cdot min^{-1}$.

3.4.5 NH_3-Temperature Programmed Desorption (NH_3-TPD)

The NH_3-TPD is an important technique used for characterizing the acidity and adsorption sites present on the catalyst surface. The degree of acidity and number of acid sites provides information on the catalyst performance. The NH_3-TPD is equipped with a built-in thermal conductivity detector (TCD). The analysis commences by pulsing NH_3 (typically 5-

20% NH_3 in helium) into the sample, either by loop or continuous flow in order to saturate the sample. While helium is flowing during the analysis, the temperature of the sample increases with time and the TCD monitors the amount of NH_3 adsorbed.

In this study, a ThermoFinnigan TPDRO 1100 series equipped with a TCD was used to carry out the NH_3-TPD analysis of the catalysts. For each analysis, 100 mg of catalyst sample was placed in a TPDRO cell and dried at 300 °C under helium gas and held for 2 h. The sample temperature was subsequently reduced to room temperature by flowing helium. After cooling, the temperature was held at 50 °C and the samples were saturated by a continuous flow of 5% NH_3/He at a rate of 20 ml/min for 1h. Consequently, the weakly physisorbed NH_3 molecules were eliminated by purging the system under the flow of 100% helium for 1h. The resulting TCD profiles show the extent of chemisorbed NH_3, which were attained by keeping the helium flow constant and increasing the system temperature from 50 °C to 800 °C at a rate of 10 °C/min.

3.5 Reactor Set-up

A 100 ml Parr autoclave stirred reactor manufactured by Parr Instruments Company, Illinois, US was used to carry out the hydrogenation reactions throughout this project (See Figure 3.1). The reactor is fabricated from stainless steel and has a flat-bottomed cylindrical shape with inner dimensions of 10 cm × 15 cm. It has a maximum operating capacity of 350 °C and 180 bar for temperature and pressure respectively. The reactor is equipped with a mechanical stirrer, a thermocouple, a pressure gauge and a controller system for temperature, and stirring rate. Also the reactor is equipped with a rupture disk, inlet and outlet gas ports and a retrofitted liquid sampling port.

The autoclave is fitted with a gas entrainment impeller connected to a hollow stirring shaft to provide efficient gas dispersion into the liquid mixture. The impeller is primarily designed with four blades of 2.06 cm diameter to allow a constant recirculation of the gas contained in the gas phase into the liquid phase. The transport of gas reaches the dispersion port at the impeller tips through the openings situated at the top of the shaft with a possibility of creating vacuum at the tip of the impeller due to the speed of the stirrer. In the Parr autoclave, increasing the stirring speed produces a higher vacuum and increased energy resulting in effective gas dispersion system.

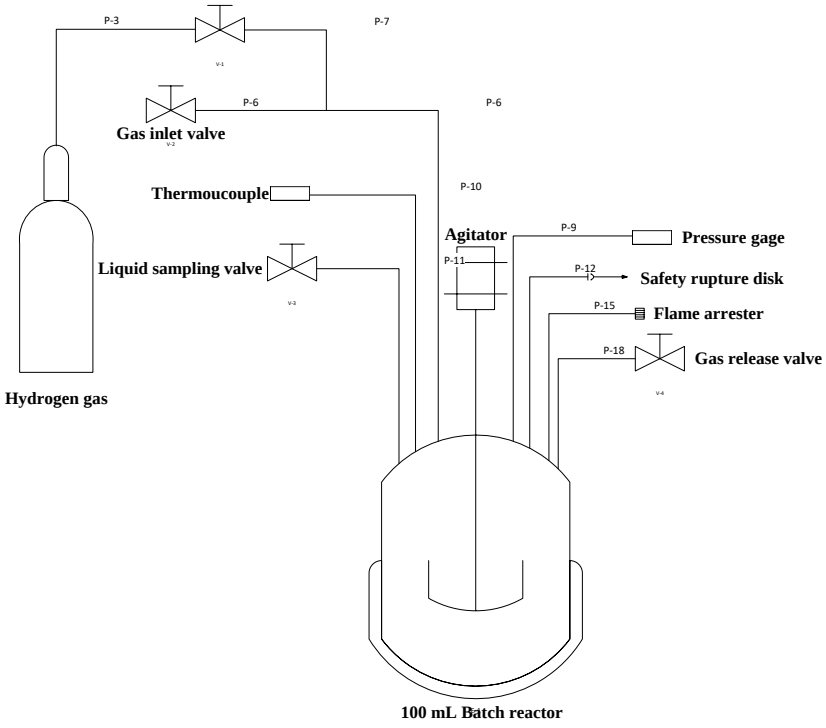

Figure 3.1: *Experimental Setup.*

3.5.1 Experimental Procedure

For each experiment, the desired amount of reactant solution was charged into the reactor with a required amount of powdered solid catalyst. The reactor was sealed and

pressurized to 10 bar of hydrogen gas to purge other gases out of the system three times to ensure an inert atmosphere. Subsequently, the reactor was pressurized to 50 bar and allowed to stabilize for five minutes to ensure a leak-proof system. Thereafter, hydrogen gas was released through the gas outlet port leaving the desired amount of hydrogen gas for the reaction. The gas lines and gas bottle regulator were shut down prior to heating the reactor. The reactor content was stirred at the desired agitation speed and heating commenced afterwards. The reaction start time was considered when the desired temperature is attained, which usually takes around 8-10 mins. About 1 mL of liquid samples were collected through the liquid sampling port at time intervals when necessary. After each experiment, the reactor was submerged in a bucket of water for rapid cooling. For reactions involving the use of titania supported catalyst, catalyst activation was carried out in-situ by introducing 20 bar of hydrogen gas at 200 °C and for 65 minutes. The mixture was cooled and subsequently charged with the amount of reactant required. All experiments were repeated and reproduced within an error of less than 1.5%.

3.6 Analytical Methods

3.6.1 Gas Chromatography (Mass Spectrometer)

The gas chromatography-mass spectrometry (GC-MS) method combines the principles of gas chromatography and mass spectrometry to predict the components present in liquid mixtures. The detection of components depends on the interaction between the molecules and the stationary phase of the column. The column retains the molecules as they travel through the length of the column and subsequently come off at different retention times which allows capture, ionization, acceleration, deflection and detection of ionized molecules separately. The liquid product mixtures from this study were analysed using an Agilent 7890A GC and Waters GCT Premier time of flight mass spectrometer (GC-TOFMS) equipped with a ZB-Wax

capillary column (30 m ×0.25 mm × 0.25 μm). The electron energy and source temperatures were 70 eV and 250 °C respectively.

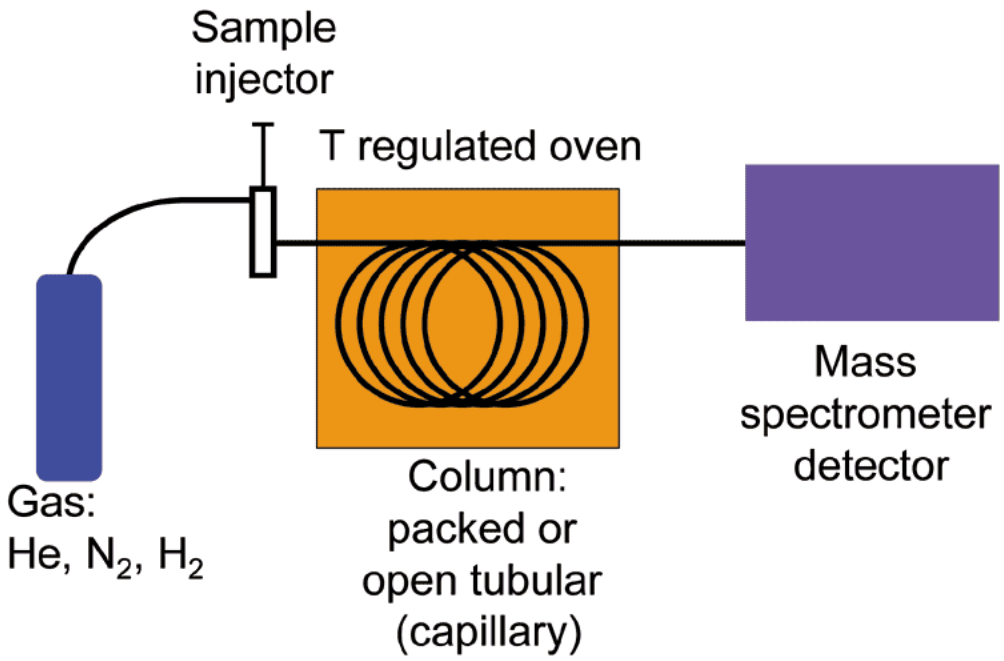

Figure 3.2: *A schematic of a gas chromatography-mass spectrometry setup (Wikipedia images).*

3.6.2 Gas Chromatography (Flame Ionization Detector)

Liquid sample mixtures from experiments were quantified using a Trace GC Ultra gas chromatography equipped with a Flame Ionization Detector (FID) and 30 m × 0.25 mm × 0.25 μm ZB-Wax capillary column. This analysis uses helium (He) as a carrier gas, while hydrogen and air provide a flame for the FID to burn off hydrocarbons. The FID is mass sensitive and thus, detects the ionic sub-components based on the amount of signal obtained for individual components at different retention times with respect to the amount of hydrocarbons injected into the GC. Figure 3.3 shows the different components of a GC-FID.

The choice of a capillary column is highly significant for effective separation of components, and should be based on the following factors:

- Column I.D (depending on the size of the molecules).
- Stationary Phase (strongly depending on the sample polarity).
- Film Thickness (depending on the sample volatility).
- Column Length.

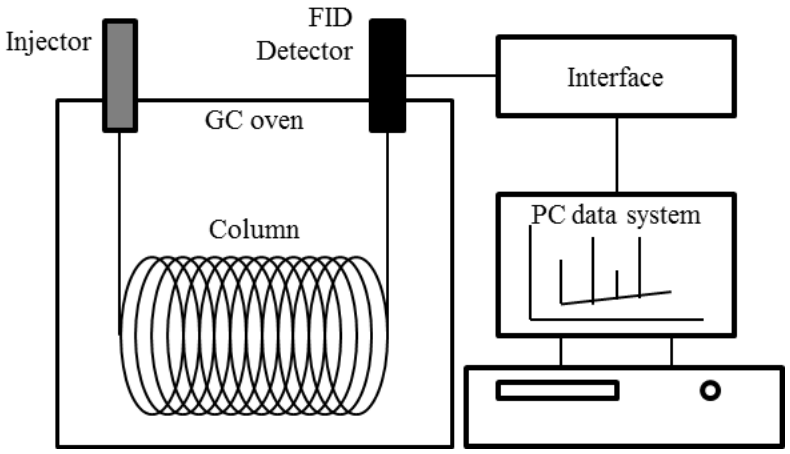

Figure 3.3: *Schematic diagram of the gas chromatography-FID system (Zhu, 2014).*

A suitable GC oven method was developed to ensure the column was operated within the temperature limits that would allow sufficient interaction of components with the column, and enhance separation from each other to result in sharp peaks within a reasonable time. The retention times that represent each compound are established by injecting known chemical standards into the GC which are used to identify the corresponding compounds from reaction mixtures by matching their retention times. The procedure for the sample amount and injection are developed for the auto sampler. Standard calibration plots were developed for the substrate and potential products as established from GC-MS analysis, which would allow the quantifications of analyte concentrations in the product mixture. An internal standard calibration method was used which involves spiking different known concentrations of the analyte of interest with a constant concentration of internal standard in a ratio of 10:1 to obtain standard curves (Appendix A). The calibration curves were developed by plotting the ratios of

the analyte to internal standard peak area versus analyte to internal standard concentration. Calibration standards were mainly prepared at different concentrations in the range of 0.02 – 0.60 M for all the components. Also, the reaction mixtures from experiments were prepared and analysed by adding the same constant concentration of internal standard prior to injection into the GC. Butanol was used as a standard for experiments involving the hydrogenation of acetic and/or propanoic acids while propanol was used when acetic and/or butanoic acid was involved.

In addition, the internal standard method was used because it is more accurate and precise, and can compensate for errors due to instrumental and sample preparation. In this study, alcohols and esters formed during the hydrogenation of carboxylic acids (C_2-C_4) were analysed by the Trace GC Ultra (GC-FID). The GC equipment was operated under a constant pressure mode with a split flow of 181. The injection volume was 1 µl, both injector and detector temperatures were 250 °C, inlet pressure was 75 KPa, and the flow rate for helium (He) carrier gas was 1 mL/min. The GC oven temperature was held at 40 °C for 5 minutes and then subsequently heated up to 215 °C at a ramp rate of 20 °C/min. Further heating to 220 °C was carried out with a ramping of 5 °C/min and held at 220 °C for 5 minutes.

3.6.3 Calculation of carboxylic acid conversion, alcohol yield, alcohol selectivity and ester selectivity

The experimental results investigated from the hydrogenation of carboxylic acids were obtained and presented in terms of conversion, alcohol yield, and alcohol and ester selectivities. It should be noted that most of the reactants/products of interest are liquid so not usually of variable volume, apart from samples removed and insignificant amount converted to gas.

$$\text{Conversion (\%)} = \frac{(\text{Initial moles of acid} - \text{Final moles of acid}}{\text{Initial moles of acid}} \times 100 \quad 3.3$$

$$\text{Selectivity (\%)} = \frac{\text{Moles of desired product}}{\text{Total moles of products formed}} \times 100 \quad 3.4$$

$$\text{Alcohol Yield (\%)} = \text{Conversion (starting material)} \times \text{Selectivity (desired product)} \times 100 \quad 3.5$$

3.6.4. Mass Balance

Gaseous products are formed as a result of hydrogenation and decarboxylation reactions involving carboxylic acids. The mass balance showing the amount of gaseous and liquid products was obtained from the respective masses of the reactant and product mixtures. Therefore, the total mass of gases formed was calculated by subtracting the mass of liquid products from the initial mass of the reactant mixture. The mass of catalyst at the start and end of reactions was assumed to be the same because coke deposit was not observed on the impeller after completion of reactions. The mass balance of liquid and gas products was calculated as the percentage of the mass of reactant mixture fed into the reactor using equations 3.6 and 3.7:

$$\text{Liquid (wt.\%)} = \frac{m_f}{m_i} \times 100 \quad 3.6$$

$$\text{Gas (wt.\%)} = 100 - \text{liquid yield (wt.\%)} \quad 3.7$$

where m_f is mass of product mixture and m_i is the mass of reactant mixture.

3.7 Process Optimization

Bio-oil upgrading via hydrogenation has been associated with high process cost and insufficient understanding of kinetics. It has been reported in the literature that the complex composition of bio-oil owing to the presence of a large number of hydrocarbons makes it

difficult to carry out kinetic studies (Mortensen et al., 2011; Sheu et al., 1988). However, understanding the contributing reaction routes involving individual bio-oil model compounds would provide details of the overall reaction network. In this study, one-factor-at-a-time (OFAT) and design of experiment (DOE) were considered in order to investigate the optimized factors and their contributions towards the hydrogenation of acetic acid. The application of OFAT by engineers and scientists was considered less effective due to reasons such as time consumption and more experiments, which results in fewer interactions between factors and susceptibility to bias due to time index in experimental errors (Frey et al., 2003). Therefore, this makes the DOE more attractive as it offers a predictive knowledge of complex and multi-variable processes with a few experimental trials. The application of the different approaches in DOE such as full factorial design, surface response methodology and Taguchi method are relatively similar. However, the Taguchi method is a simpler, cost effective, systematic and comprehensive approach which uses fewer experiments to provide an optimisation of complex and multi variable process. Optimisation in a Taguchi designed experiment involves reducing the variation in the process by minimizing the effects of uncontrollable factors (noise factors) and keeping the response mean value (Kowalczyk, 2014). In this study, the Taguchi method was used to optimize the controllable reaction factors affecting the hydrogenation of acetic acid. The major advantages of the Taguchi method are principle of orthogonal array and signal-to-noise ratio (S/N). The orthogonal array was designed to simultaneously study the effect of multiple process variables with respect to the mean response under lesser number of experiments (Table 3.3). The principle of Signal-Noise ratio (S/N) ensures that the optimum conditions are stable and kept under minimum process variation under different noise conditions (Mukherjee and Kumar, 2006).

Table 3.3: *Selected Controllable factors and their levels.*

Factors	**Level 1**	**Level 2**	**Level 3**	**Level 4**
Temperature (ºC)	80	120	160	200
Initial Pressure (bar)	10	20	30	40
Catalyst Loading (g)	0.1	0.2	0.3	0.4
Agitation Speed (min^{-1})	400	600	800	1000
Reaction Time (h)	1	2	3	4

3.7.1. Orthogonal Array

The Taguchi method uses a special experimental matrix called the orthogonal array. These experiments are generated based on the number of controllable factors and their levels in order to simultaneously examine the effect of different controllable factors with respect to mean response (Athreya and Venkatesh, 2012; Kowalczyk, 2014). In order to generate the right orthogonal array for this study, an array that consists of five controllable factors at four different levels was chosen. The reaction factors considered include reaction temperature, initial hydrogen pressure, catalyst loading, reaction time and stirring speed (Table 3.3). An orthogonal array of sixteen experimental runs (L_{16}) was generated using design expert software as shown in Table 3.4. The array comprises of five columns that represents the control factors and their respective levels. Furthermore, the rows represent the sixteen (16) experiments that should be carried out at the given level of each control factor.

Table 3.4: *Orthogonal array for optimization of process variables.*

Experiment No.	A Temperature (ºC)	B Pressure (bar)	C Time (h)	D Stirring (min^{-1})	E Catalyst (g)
1	80	10	400	0.1	1
2	80	20	600	0.2	2
3	80	30	800	0.3	3
4	80	40	1000	0.4	4
5	120	10	1000	0.3	2
6	120	20	800	0.4	1
7	120	30	600	0.1	4
8	120	40	400	0.2	3
9	160	10	600	0.4	3
10	160	20	400	0.3	4
11	160	30	1000	0.2	1
12	160	40	800	0.1	2
13	200	10	800	0.2	4
14	200	20	1000	0.1	3
15	200	30	400	0.4	2
16	200	40	600	0.3	1

3.7.2 Signal-to-noise ratio

The Taguchi method proposes the signal-to-noise ratio (S/N) function as a suitable approach in selecting optimum conditions with respect to response variables. Typically, the signal-to-noise ratio is a measure of the desired output signal to the background noise of a response variable (Tansel et al., 2011). It also measures the extent of deviation from a desired variable output and should always be kept minimum in order to ensure the response variable approaches optimum conditions (Ghani et al., 2004; Kowalczyk, 2014). There are three different S/N functions suggested by the Taguchi method which are employed based on the

desired optimization objective. Table 3.5 shows the types of S/N, their functions and applications.

Table 3.5: *Types of signal-to-noise ratio and their application.*

Objective	Application	Formula
Smaller the better	Minimum response variable	$\left(\frac{S}{N}\right) = -10log\left(\frac{1}{n}\sum_{i=1}^{n} y_i^2\right)$
Larger the better	Maximum response variable	$\left(\frac{S}{N}\right) = -10log\left(\frac{1}{n}\sum_{i=1}^{n} \frac{1}{y_i^2}\right)$
Nominal the best		$\left(\frac{S}{N}\right) = -10log\left(\frac{1}{n}\sum_{i=1}^{n} \frac{1}{\boldsymbol{y_i^2}}\right)$

where n, is the number of measured value, y_i is the measured response value, y_i^2 mean square of measure response value. The Larger-the-better type of control function was used for this study which is applicable for a maximum variable response function.

3.7.3. Analysis of Variance

ANalysis Of VAriance (ANOVA) is a statistical model that is used to evaluate the mean response value of each factor at different levels in the array of experiment. The influence of each factor with respect to the hydrogenation of acetic acid was determined by calculating the F-value and P-value using the one-way ANOVA (Athreya and Venkatesh, 2012). The one-way ANOVA was carried out by determining the sum of squares, degree of freedom, mean variance and factor contribution. The main property of ANOVA is that the total sum of squares is equal to the sum of the squares of deviations for all the factors and the error components. The following equations were used for the ANOVA:

$$SS_{Total} = \sum \left(X - \frac{G}{N}\right)^2 \quad 3.8$$

$$SS_{within} = \sum (X - \bar{X}_1) \quad 3.9$$

$$SS_{between} = SS_{Total} - SS_{within} \quad 3.10$$

$$DOF_{within} = N - M \quad 3.11$$

$$DOF_{between} = M - 1 \quad 3.12$$

$$DOF_{Total} = DOF_{between} + DOF_{within} \quad 3.13$$

$$\mu s_{between} = \frac{SS_{between}}{DOF_{between}} \quad 3.14$$

$$\mu s_{within} = \frac{SS_{within}}{DOF_{within}} \quad 3.15$$

$$\text{Percentage contribution (\%)} = \frac{\mathrm{SS_{within}}}{\mathrm{SS_{Total}}} \quad 3.16$$

where N is the total number of response values, M is the number of levels, G is the sum of all responses at all levels, X is response value and $\bar{X}_1$ is the mean of all responses at a particular level.

Chapter 4. **Catalyst Characterization, Catalyst Screening and Process Optimization**

4.1 Chapter Overview

This chapter presents the properties of prepared titania supported Pt/Pt-Re catalysts and commercial Pt-based catalysts using a range of characterization techniques, followed by screening of the prepared catalysts against their commercial counterparts, and optimization of operation conditions towards the maximization of alcohol yield in hydrodeoxygenation of carboxylic acids. Nitrogen sorption-desorption experiments followed by Brunauer-Emmett-Teller (BET) analysis was used to determine the catalyst surface area and Barett-Joyner-Halenda (BJH) method was used to estimate the pore size distribution. To investigate the crystal phases present in the catalysts, X-Ray diffraction (XRD) powder analysis was carried out. Scanning electron microscopy (SEM) was used to investigate the surface morphology, and the elemental composition was confirmed by Energy Dispersive X-ray spectroscopy (EDX). The minimum temperature required to activate the prepared catalysts was investigated using the H_2-temperature programmed reduction (H_2-TPR) measurement. In order to examine the number of acid sites and their strength, NH_3-temperature programmed desorption (NH_3-TPD) analysis was performed. Both H_2-TPR and NH_3-TPD analysis were carried out at the University of Manchester. Subsequently, prepared catalysts were screened against their commercial counterparts in a hydrogenation reaction test in a batch reactor under identical reaction conditions. Furthermore, the Taguchi method of design of experiment (DOE) was used to optimize the reaction factors towards the conversion of acetic acid and ethanol selectivity using an L16 orthogonal array and 4% Pt/TiO_2 catalyst.

4.2 Surface Area, Pore Volume and Pore Size Distribution

The textural properties of the prepared titania-supported catalysts and commercial catalysts were characterized using the BET model and nitrogen adsorption-desorption isotherms. The monolayer coverages for the catalysts in the range of low relative pressures ($\frac{P}{P_O}$ = 0.054-0.272) were estimated in accordance with equation 3.1, which is regarded as the linear region where pore condensation is unlikely to occur. Similarly, the BJH model was used to estimate the pore size and pore volume by using the branches of desorption isotherm at P/P_o = 0.99. The nitrogen adsorption-desorption isotherms for the prepared and commercial catalysts are shown in Figure 4.1 while the pore size distribution and porosimetry properties are shown in Figure 4.2 and Table 4.1 respectively.

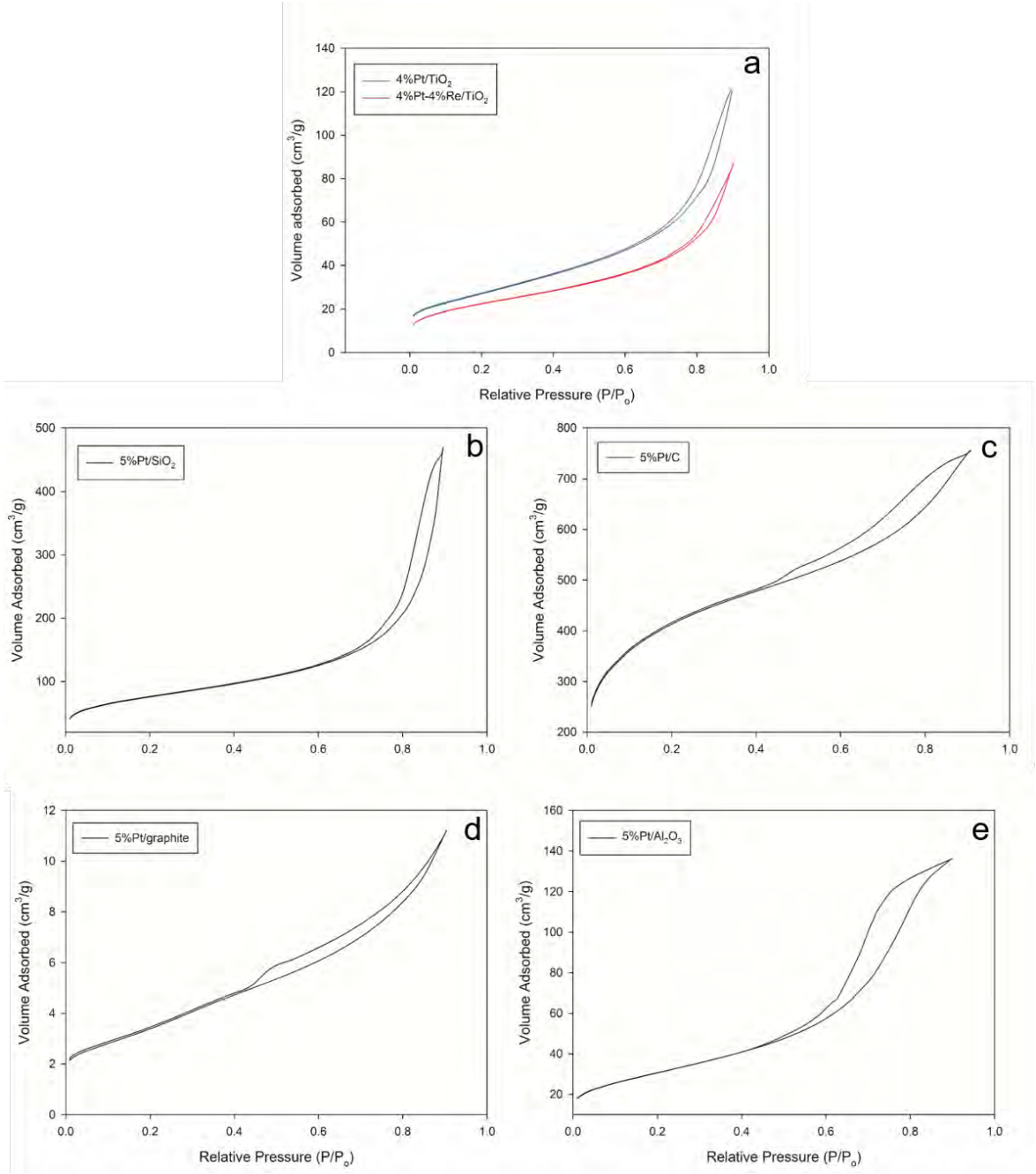

Figure 4.1: *Nitrogen adsorption-desorption isotherm for (a) 4% Pt/TiO_2 and 4% Pt-4% Re/TiO_2 (b) 5% Pt/SiO_2 (c) 5% Pt/C (d) 5% Pt/graphite (e) 5% Pt/Al_2O_3.*

As shown in Figure 4.1a, the nitrogen adsorption-desorption isotherm for the prepared 4% Pt/TiO_2 and 4% Pt-4%Re/TiO_2 catalysts exhibited a Type IV isotherm with Type H3 hysteresis loop (Condon, 2006; Cychosz and Thommes, 2018; Thommes et al., 2015). This type of isotherm exhibits features of monolayer-multilayer adsorption in the initial region of low

relative pressure between 0 and 0.6, followed by capillary condensation which depends on the size of the mesopores. The observed hysteresis in the multilayer region is mainly associated with capillary condensation due to larger mesopores (> 4 nm) and the adsorption mechanism (Cychosz and Thommes, 2018; Thommes et al., 2015). Consequently, the Type H3 hysteresis consists of aggregates of plate like particles which result in slit-shaped pores (Abida et al., 2011). Even though both 4% Pt/TiO_2 and 4% Pt-4%Re/TiO_2 catalysts exhibited the same type of isotherm, it is evident that the extent of nitrogen adsorption and capillary condensation within the pores of 4% Pt/TiO_2 is higher than 4% Pt-4%Re/TiO_2. This can be linked to the higher surface area associated with 4% Pt/TiO_2 (98 m^2/g) compared to 4% Pt-4%Re/TiO_2 (80 m^2/g). The observed decrease in surface area for 4% Pt-4%Re/TiO_2 can also be linked to the incorporation of 4% Re into 4% Pt/TiO_2 which occupies some pore sites, which in turn limits the accessibility of nitrogen adsorption.

Figures 4.1b and 4.1d present the isotherm for 5% Pt/SiO_2 and 5% Pt/graphite respectively. Similar to 4% Pt/TiO_2 and 4% Pt-4%Re/TiO_2 catalysts, 5% Pt/SiO_2 and 5% Pt/graphite both exhibited a Type IV isotherm with Type 3 hysteresis, though, the mesopores are broader for 5% Pt/SiO_2. This observation can be ascribed to the steep increase in nitrogen uptake from 100 to 470 cm^3/g through capillary condensation giving rise to higher surface area of 268 m^2/g. Furthermore, the observed hysteresis loop exhibited by catalysts can be correlated with the textural properties such as surface area (Cychosz and Thommes, 2018; Thommes and Cychosz, 2014). However, 5% Pt/SiO_2 exhibited a much higher surface area of 268 m^2/g which can be ascribed to the steep increase in nitrogen uptake from 100 to 470 cm^3/g through capillary condensation.

In contrast to 4% Pt/TiO_2, 4% Pt-4%Re/TiO_2, 5% Pt/SiO_2 and 5% Pt/graphite catalysts, 5% Pt/C and 5% Pt/Al_2O_3 exhibited a H2 type hysteresis loop (Cychosz and Thommes, 2018;

Park et al., 2016), as shown in Figures 4.1c and 4.1e. This hysteresis indicates a steep desorption step towards lower relative pressure in the isotherm as a result of pore blocking effects and cavitation mechanism (Cychosz and Thommes, 2018). The behavior of Type H2 hysteresis is typical for ink bottle-shaped pores which indicates delayed condensation and absence of pore evaporation via equilibrium from an open pore (Park et al., 2016). Notably, the steepest region of the desorption branch resulting to the lower closure points occurred at $P/P_o = 0.45$.

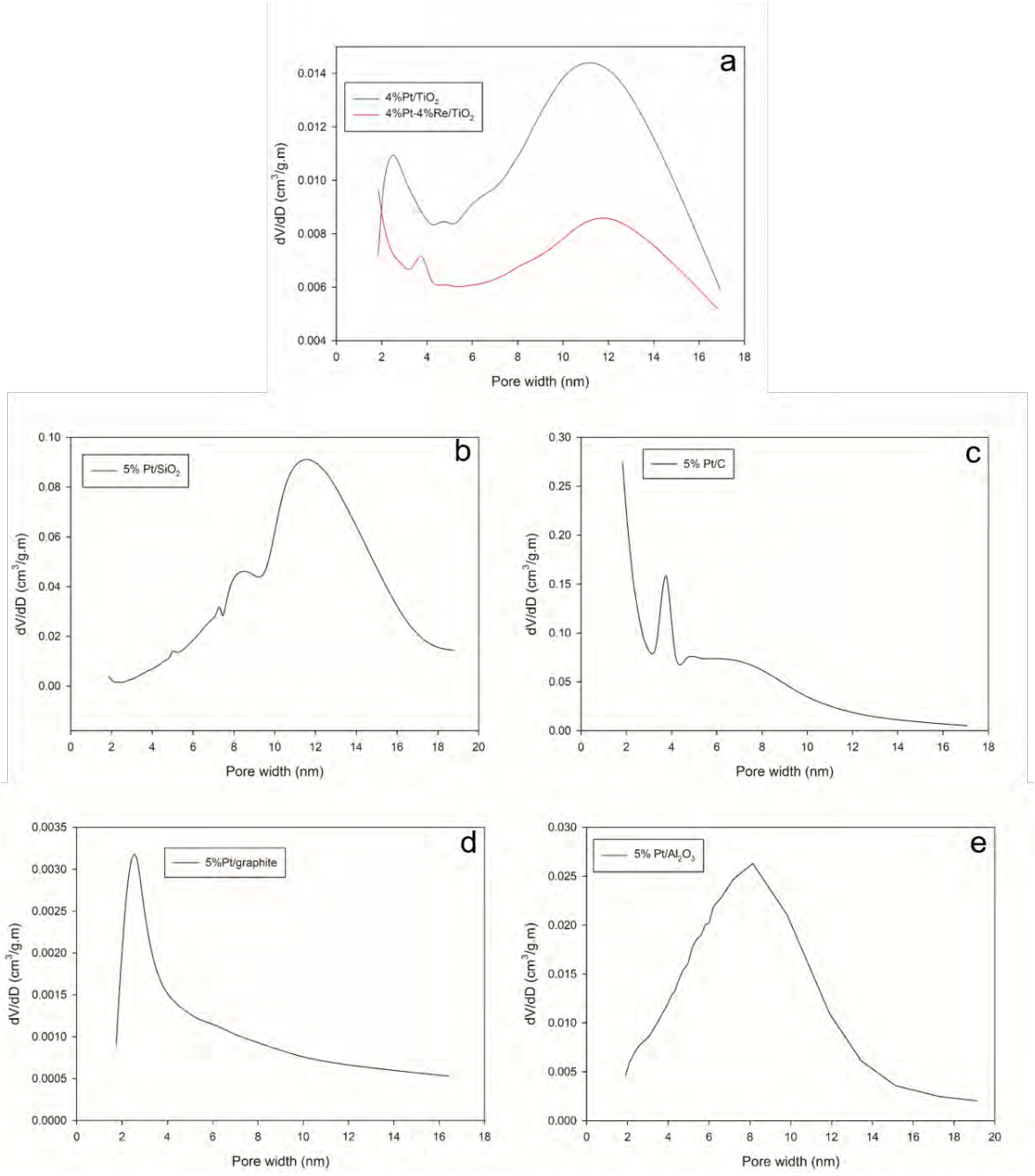

Figure 4.2: *Pore size distribution for (a) 4% Pt/TiO_2 and 4% Pt-4%Re/TiO_2 (b) 5% Pt/SiO_2 (c) 5% Pt/C (d) 5% Pt/graphite (e) 5% Pt/Al_2O_3.*

Figure 4.2a shows the pore size distribution of 4% Pt/TiO_2 and 4% Pt-4%Re/TiO_2. Both catalysts exhibited a bimodal pore distribution with a small and broad peak, though 4% Pt/TiO_2 has broader peaks compared to 4% Pt-4%Re/TiO_2. The small peaks for 4% Pt/TiO_2 and 4% Pt-4%Re/TiO_2 are within a pore width range of 2-4 nm and 3-4 nm respectively, whereas the broad

peaks are within the same range of 6-17 nm. The observed peaks for both catalysts fall within the range of small mesopores (2-20 nm). For bimodal pore size distribution, the small pores correspond to pores present in the individual particles while the bigger pores represents the vacancy generated due to the aggregation of particles (Tao et al., 2011). Subsequently, bimodal pores within the same range of pore size could be formed due to the extent of mixing during impregnation, and further calcination in the catalyst preparation. The difference in peak size for both catalysts reaffirms the alteration evidenced from the incorporation of Re within the pores of 4% Pt/TiO_2 in addition to the decreased surface area.

As shown in Figure 4.2b, the pore size distribution of 5% Pt/SiO_2 exhibits a broad peak between 3 and 17 nm with a centroid at 11 nm and shoulder peak around 8.5 nm centroid. In contrast to the pore size distribution for 5% Pt/C, 5% Pt/graphite and 5% Pt/Al_2O_3 as shown in Figures 4.2c-e, a unimodal pore size distribution was observed in the region of 3 to 20 nm. Both 5% Pt/C and 5% Pt/graphite exhibited an obvious centred peak at 3.5 nm, while 5% Pt/Al_2O_3 revealed a centroid of 9 nm. The presence of unimodal pore structure observed confirms the availability of uniform pores typical of small nanoparticles.

Table 4.1: *Textural Properties of Catalysts.*

Catalyst	S_{BET}[a] (m^2/g)	S_{ext}[b] (m^2/g)	S_{mic}[c] (m^2/g)	V_{tot}[d] (cm^3/g)	V_{meso}[e] (cm^3/g)	V_{mic}[d] (cm^3/g)
4% Pt/TiO_2	97.78	95.55	2.23	0.184	0.183	0.001
4% Pt-4%Re/TiO_2	79.94	75.4	4.54	0.125	0.124	0.001
5% Pt/C	720	406.58	313.42	0.84	0.675	0.165
5% Pt/SiO_2	267.56	249.85	17.71	0.71	0.7024	0.0076
5% Pt/Al_2O_3	111.91	103.56	8.35	0.215	0.2107	0.0043
5% Pt/graphite	12.84	11.72	1.12	0.018	0.0176	0.0004

[a]Surface area by the BET model. [b]$S_{ext} = S_{BET} - S_{mic}$. [c]Obtained from the t-plot method. [d]Total pore volumes are obtained at the maxima of the isotherm.

Table 4.1 shows the textural properties of the prepared catalysts and commercial catalysts. The obtained results show that 5% Pt/C has the highest surface area (720m^2/g) and high pore volume (0.84 cm^3/g) while 5% Pt/graphite has the lowest surface area (12.84 m^2/g) and small pore volume (0.018 cm^3/g). The high surface area exhibited by 5% Pt/C can be associated with the higher surface area of carbon support. It is important to note that carbon support offers greater dispersion of platinum metals on the 5% Pt/C catalyst, which is known to be beneficial in allowing efficient accessibility of reactants into catalyst active sites and subsequent product diffusion into the bulk fluid. However, these catalysts require a moderate pore volume in order to achieve an efficient catalyst activity during hydrogenation reactions. On the other hand, catalysts with a low surface area such as 5% Pt/graphite are known to exhibit lower concentration of active sites which limits the activation of reactant species during reactions. Thus, catalyst characteristics other than surface area could be the reason to explain catalyst activity.

The surface areas of 4% Pt/TiO_2 and 4% Pt-4%Re/TiO_2 are shown in Table 4.1. In comparison to 4% Pt/TiO_2, the surface area of 4% Pt-4%Re/TiO_2 (79.9 m^2/g) decreased by approximately 18% as a result of the incorporation of 4% Re into 4% Pt/TiO_2. The decreased surface area is evidence that the incorporated Re^{4+} occupied some of the Ti^{4+} lattice to form 4% Pt-4%Re/ TiO_2. In addition, the incorporation of Re decreased the pore volume of 4% Pt/TiO_2 and can be linked to the shrinkage of pore sizes, which results in decreased bimodal pore size distribution (Figure 4.2a).

4.3 XRD Powder Analysis

The crystal phase arrangement of the prepared titania-supported catalysts was studied using the XRD powder method. Figure 4.3 shows the XRD pattern of titania support and the

corresponding titania supported catalysts. It is clear that TiO_2, 4% Pt/TiO_2, 4% Re/TiO_2 and 4% Pt-4%Re/TiO_2 have the same crystal phase arrangement which suggests that the crystal pattern of TiO_2 remains unchanged after the addition of Pt and Re. The most distinct peak at 2θ = 25 º and others at 38 º, 48 º, 55 º and 63 º corresponds to Miller indices (101), (004), (200), (211), and (002) diffraction peaks.

Two different phases of TiO_2 were identified as shown in Figure 4.3. All the observed reflections could be attributed to either anatase or rutile phases in accordance with the ICSD database (He and Wang, 2014; Zhang et al., 2006). It can also be observed that Re/TiO_2 has the most symmetrical anatase peaks compared to TiO_2 and the other TiO_2 supported catalysts, due to the incorporation of Re into TiO_2. On the other hand, the incorporation of Pt into TiO_2 slightly increased the intensity of the rutile phases which mainly occur as shoulder peaks close to the anatase peaks, while the anatase phase remained unaltered. When Pt was added to Re/TiO_2, the asymmetry of the anatase phases decreased significantly which resulted in anatase phases with similar peak intensities to TiO_2 and Pt/TiO_2 peaks. The observed phasic differences can be associated with the affinity of Pt and Re for the crystal phases present in TiO_2. In addition, this can be linked to the unit cell volume, Ti-O interaction and density of the anatase/rutile unit cell. However, the composition of the different phases would provide a better interpretation of the differences in symmetry and broadness of the crystal phases. From the ICSD database, the diffraction peaks related to Pt and Re scattering were not annexed due to apparent amorphous nature of the metals.

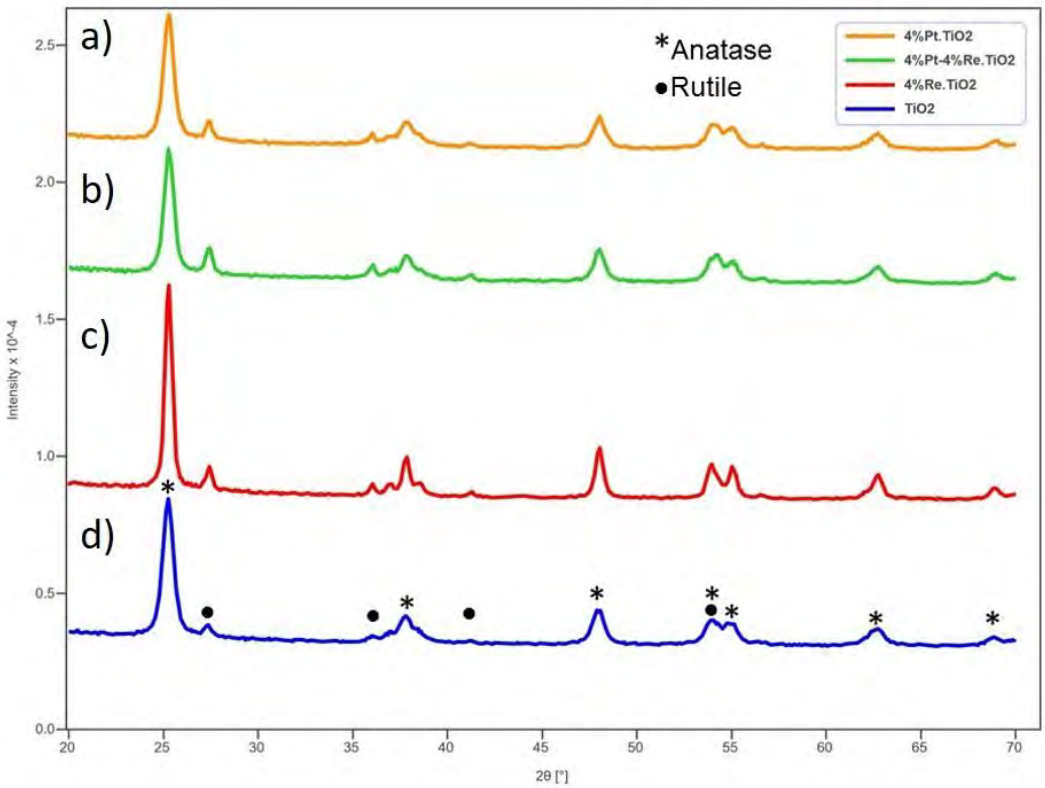

Figure 4.3: *X-Ray Powder Diffraction Patterns for TiO_2 and TiO_2 supported catalysts.*

Figure 4.4 shows the unit cell diagram of anatase and rutile phases present in TiO_2 and TiO_2 supported catalysts. The unit cell of the anatase phase has a tetragonal symmetry that exhibits an elongated c-axis which conforms to space group I 41/a m d s. The dimension of the c-axis is about three times the dimension of a/b-axis. Similarly, the rutile phase has a tetragonal symmetry albeit with elongated b-axis belonging to space group P 42/m n m. The elongated b-axis is twice the dimension of a/c-axis. For detailed structural studies, GSAS II refinement software was used to obtain unit cell parameters, cell volume, phase fractions and theoretical density (Table 4.2).

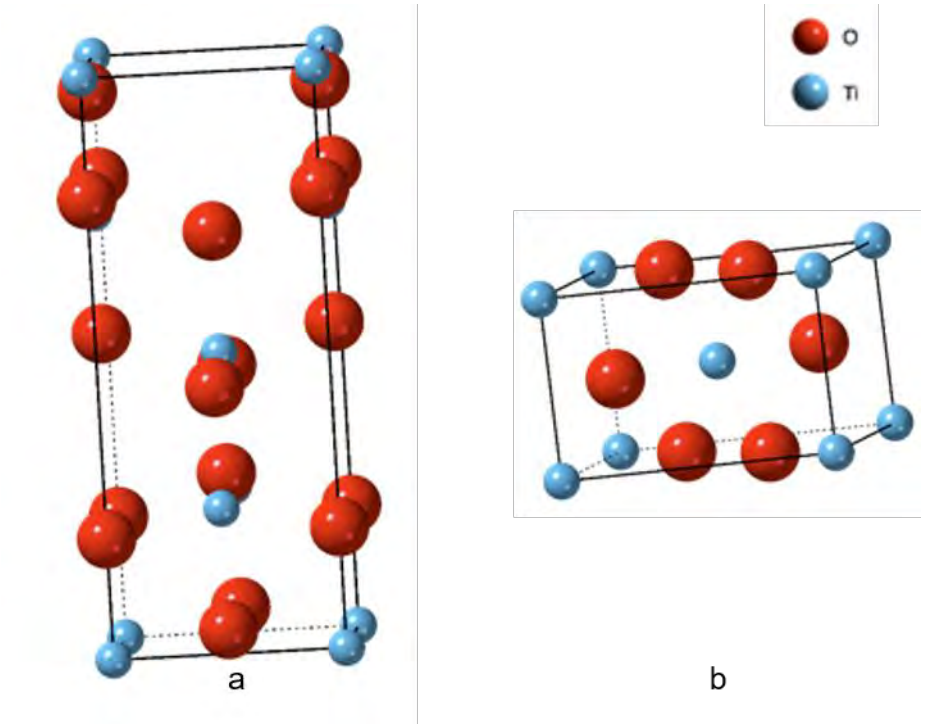

Figure 4.4: *Unit Cell diagram for the (a) anatase phase and (b) rutile phase present in TiO_2.*

Table 4.2: *Data obtained from GSAS refinement of powder XRD data.*

Catalyst/Support	**Anatase**		**Rutile**		**Refinement**
	Density ($g.cm^{-3}$)	Unit Cell Volume ($Å^{-3}$)	Density ($g.cm^{-3}$)	Unit Cell Volume ($Å^{-3}$)	GoF
TiO_2	8.99	135	4.33	62.37	6.78
4% Re/TiO_2	8.03	135.3	4.29	62.40	6.52
4% Pt/TiO_2	7.83	135.6	4.25	62.43	4.91
4% Pt-4%Re/TiO_2	7.8	136	4.24	62.58	5.02

GoF: Goodness of fit

The phase distribution of pure TiO_2 was found to be 81% anatase to 19% rutile (Figure 4.5). When Pt and Re were incorporated into TiO_2, a drastic change in the relative phase distribution was observed. In particular, a trend emerged in which the incorporation of Pt and/or Re into TiO_2 favours the transformation of some anatase phases into rutile phases (Figure 4.5

and Table 4.2). This observation is expected considering the relatively larger atoms of Pt (0.80 Å) and Re (0.63 Å) that were incorporated into the unit cell with Ti (0.60 Å). The refinement results also suggested that Pt and Re atoms occupy Ti site, with the rutile Ti phase more preferred to the anatase Ti phase. This resulted in the observed increase in phase fraction of rutile phase upon Pt/Re/Pt-Re incorporation into TiO_2.

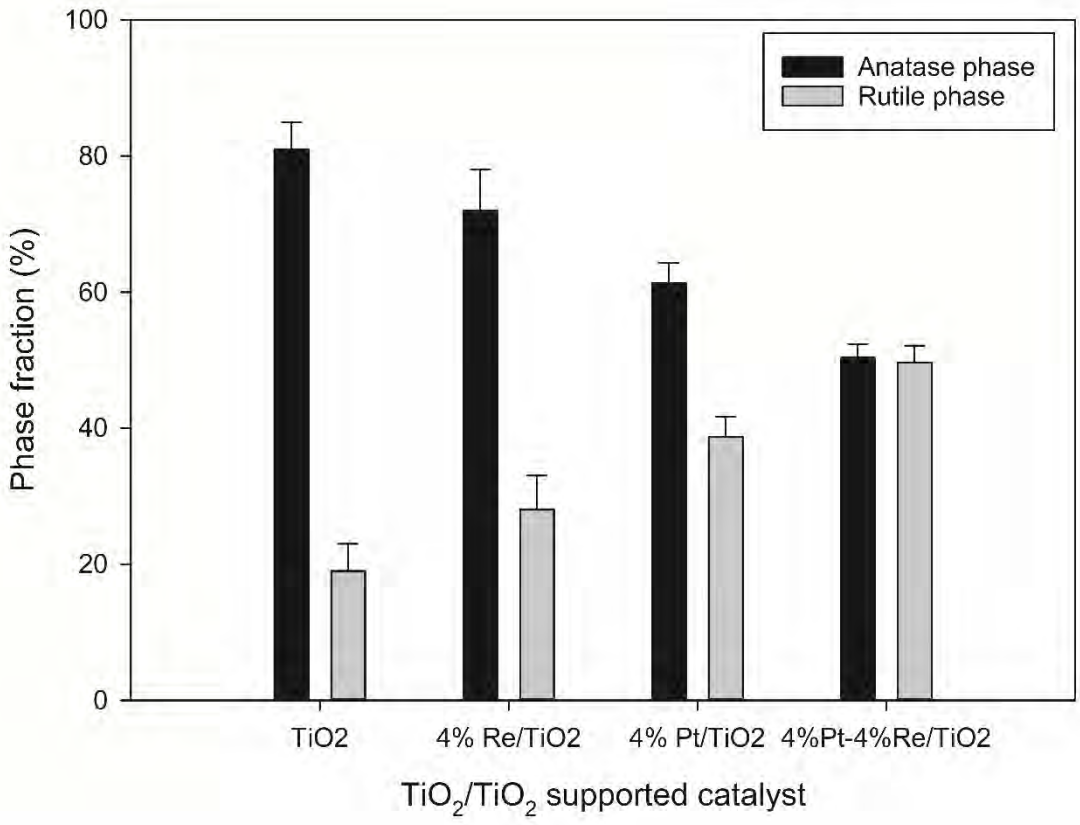

Figure 4.5: *Phase fractions present in TiO_2 and TiO_2 supported catalysts.*

In a previous study (Panpranot et al., 2006), the influence of the composition of anatase and rutile crystalline phases on the hydrogenation function of Pd/TiO_2 in terms of acetylene conversion and selectivity was elucidated. Optimum anatase to rutile phase composition was achieved for the titania support with rutile phase content of 44%, which resulted in 93% selectivity of ethylene. In addition, rutile titania is more thermodynamically and structurally

stable than anatase titania (Li et al., 2004). Based on the proposed mechanism for the hydrogenation of carboxylic acids over Pt and Pt–Re/TiO_2 (Manyar et al., 2010), the adsorption of the carbonyl group on TiO_2 would occupy either the rutile and anatase phases of TiO_2, which in turn could promote the catalytic activity.

4.4 Catalyst Morphology and Composition

Scanning electron microscopy (SEM) was used to reveal the morphological properties of the prepared catalysts under the principle of electron microscopy. The prepared catalysts are Pt/Pt-Re on titania support. More SEM images of 4% Pt/TiO_2 and 4% Pt-4%Re/TiO_2 powder were collected which show particular features as shown in Figure 4.6 and 4.7 respectively.

It can be observed from Figure 4.6a that the fresh 4% Pt/TiO_2 contains dispersed particles of TiO_2 granules in the range of 1-2.5 μm, with nano size platinum particles (≤ 4nm) impregated on titania which is necessary for slurry reactions (Zhang et al., 2006). This suggests that proper deposition of Pt precursor and thorough dispersion were achieved during the impregnation step of 4% Pt/TiO_2 catalyst preparation. In addition, the formation of agglomerates is not evident. Figures 4.6c-f reveals the EDX elemental mapping image of 4% Pt/TiO_2 which further confirms the extent of Pt dispersion on the TiO_2 support. Consequently, the availability of the metal active sites is mainly dependent on the degree of dispersion on the catalyst support. On the other hand, Figure 4.6b shows the SEM image for the spent 4% Pt/TiO_2. It is apparent that the fresh and spent catalysts are different; for the spent catalyst the TiO_2 particulate sizes range from 2-7 μm. This observation can be linked to the formation of agglomerates as a result of deposits of granules after surface reaction. It can also be observed on the morphology of the spent catalyst, features of compact ground mass and holes which are absent in the fresh counterpart, which can be attributed to the loss of some impregnated Pt

grains during reaction or liquid bridging after the reaction. The presence of agglomerates on the spent catalyst may result in partial or complete loss of catalyst activity. However, catalyst activity on spent catalyst could be regenerated depending on post reaction catalyst recovery, washing, reactivation via calcination and subsequent reduction.

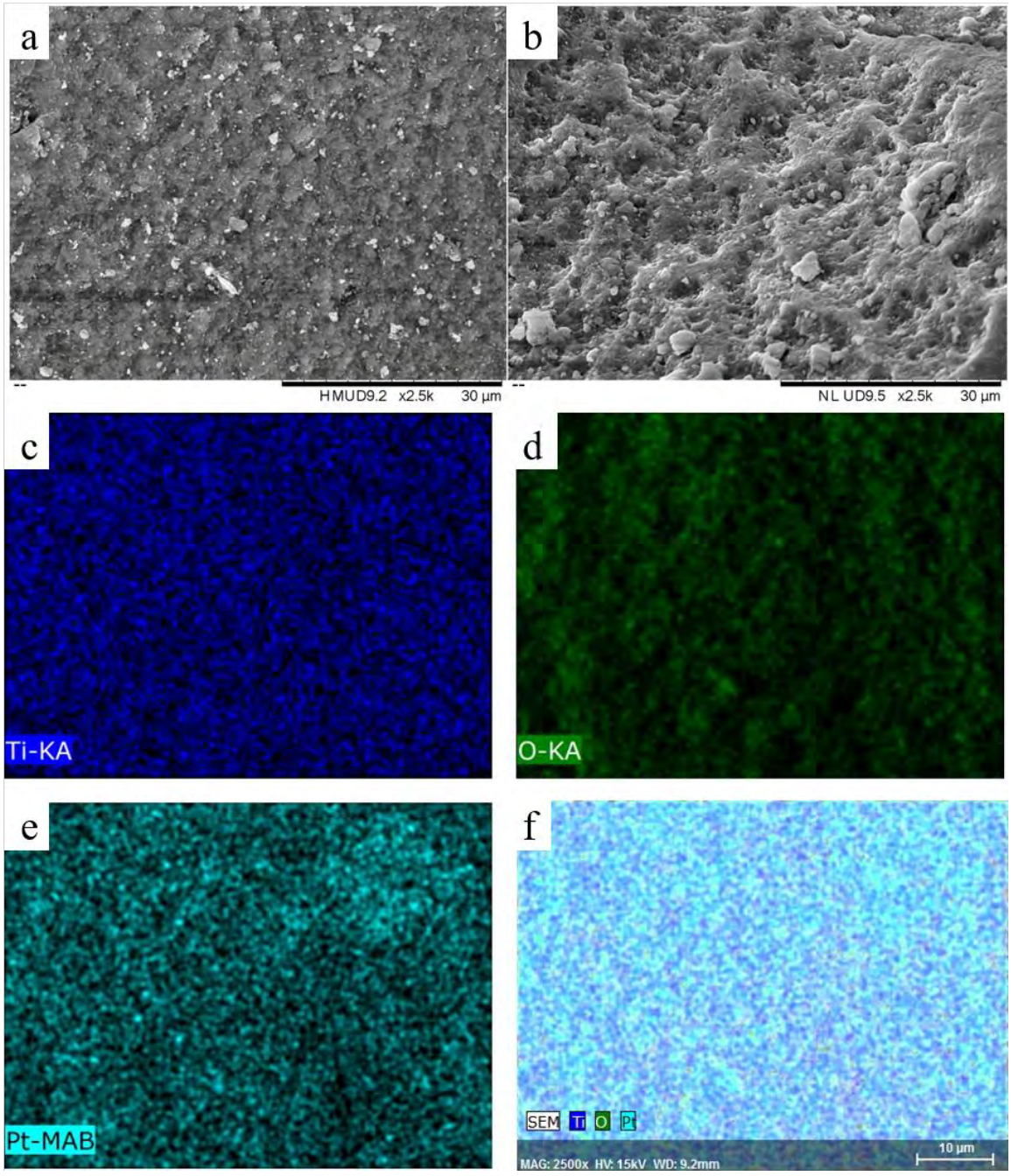

Figure 4.6: *SEM images for the **a**) fresh and **b**) spent 4%Pt/TiO_2 catalyst; EDX elemental mapping of **c**) titania, **d**) oxygen, **e**) platinum and **f**) 4%Pt/TiO_2 for fresh 4%Pt/TiO_2.*

Figures 4.7a-b shows the SEM image for the fresh and spent 4% Pt-4% Re/TiO_2 catalyst. In comparison to 4% Pt/TiO_2, the morphology of fresh 4% Pt-4%Re/TiO_2 is somewhat similar. However, the particles of TiO_2 granules was found to be 1-6 μm due to the presence of impregnated Pt and Re nano particles. As shown in Figures 4.7c-g, EDX mapping shows that Pt and Re are well dispersed in TiO_2, which means increased size of TiO_2 granules compared to 4% Pt/TiO_2 cannot be linked to the aggregation of particles due to Re incorporation. After reaction, the particles mostly agglomerated into a lump of mass with bigger particle size range of 2-8 μm.

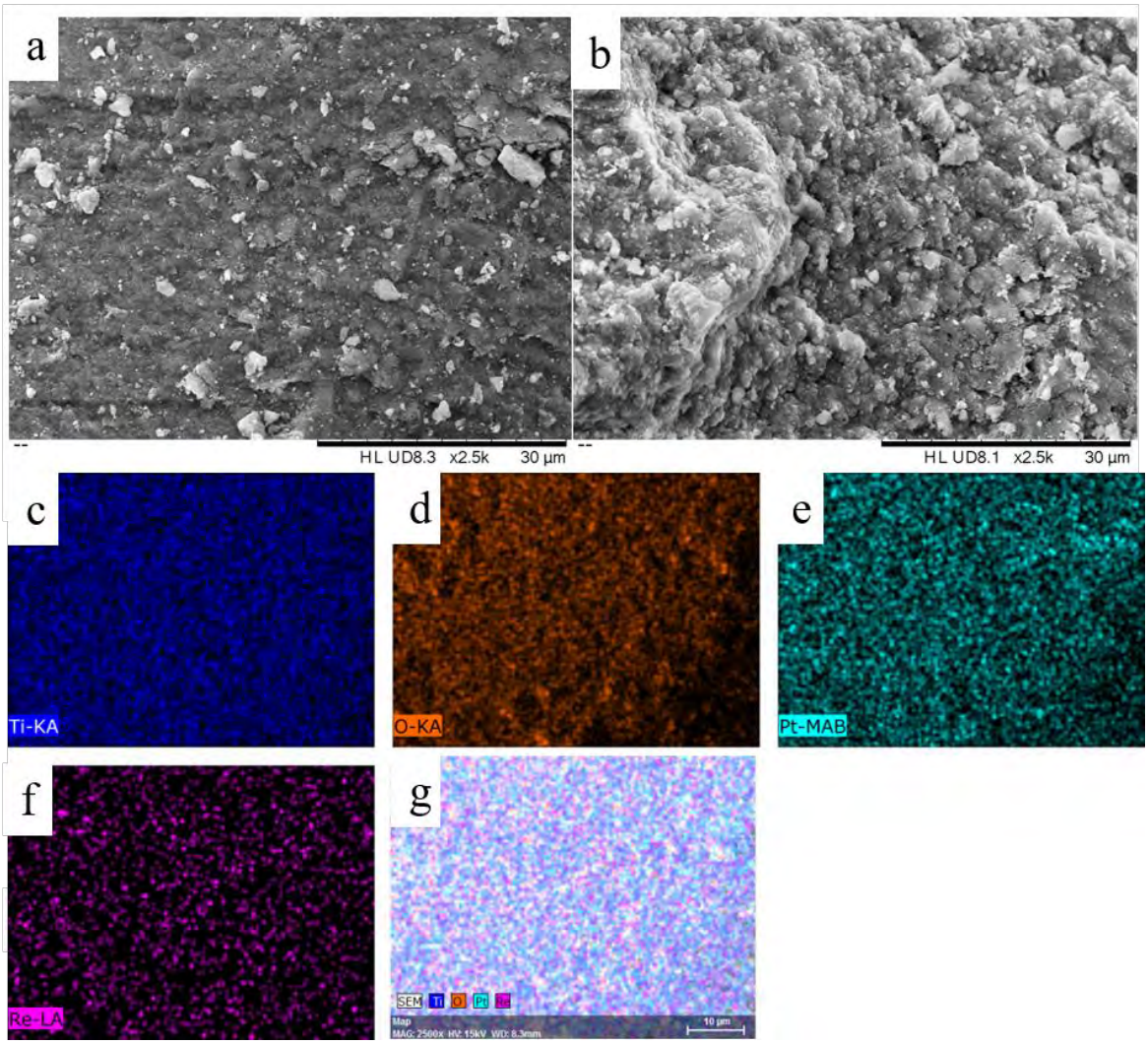

Figure 4.7: *SEM images for the* ***a****) fresh and* ***b****) spent 4% Pt-4%Re/TiO_2 catalyst; EDX elemental mapping of* ***c****) titania,* ***d****) oxygen,* ***e****) platinum and* ***f****) 4% Pt-4%Re/TiO_2 for fresh 4% Pt-4%Re/TiO_2.*

4.5 H_2-TPR

All the TiO_2 based catalysts in this study were prepared with the primary target of evaluating their activity in the HDO of carboxylic acids. As previously mentioned in Section 2.1.2, hydrogenation reaction catalysed by noble metals is considered to be one of the main reactions that take place during HDO. A known rule of thumb is that the complete activity of transition metal catalysts is achieved at zero state of oxidation for hydrogenation reaction (Resende et al., 1999; Zhang et al., 2006). Subsequently, the reduction of PtO_2 to Pt metal (i.e.

Pt^{4+} and Re^{7+} are reduced to Pt^0 and Re^0) is highly significant. H_2-TPR technique provides information on the minimum temperature required for the activation of the prepared catalysts and the extent of catalyst reducibility. Furthermore, H_2-TPR reveals information on the dispersion of Pt/Re on the TiO_2 support and their interaction.

Figure 4.8 shows the H_2-TPR profiles of 4% Pt/TiO_2 and 4% Pt-4%Re/TiO_2 catalysts. 4% Pt/TiO_2 showed two distinct H_2 consumption peaks in the range of 6 – 140 °C and 430 – 650 °C, and centroids at 42 °C and 560 °C, respectively. The low temperature peak corresponds to reduction of Pt^{4+} (PtO_2) impregnated into the 4% Pt/TiO_2 to Pt^0 in the presence of hydrogen gas. It is worth noting that the reduction of bulk oxygen of TiO_2 occurs at temperatures higher than 600 °C (Resende et al., 1999; Xiaoyuan et al., 2004; Zhang et al., 2006). Thus, the broad peak between 300 °C and 600 °C can be ascribed to partial or complete reduction of the oxygen on the TiO_2 (Xiaoyuan et al., 2004), which means TiO_2 reduction was very tough. Pritchard et al., (2017) performed X-ray Photoelectron Spectroscopy (XPS) on Pt/TiO_2 and Pt-Re/TiO_2 catalysts which are the same as those used in this study, and found that the addition of Re to 4% Pt/TiO_2 marginally increased the binding energy from 71 to 71.7 eV, which suggest a good contact between Re and Pt and a strong interaction with the support. In addition, PtO_2 is highly dispersed inside the pores of TiO_2 which is confirmed by the absence of Pt peaks in the XRD profile and EDX mapping of 4% Pt/TiO_2 (See Sections 4.3 and 4.6).

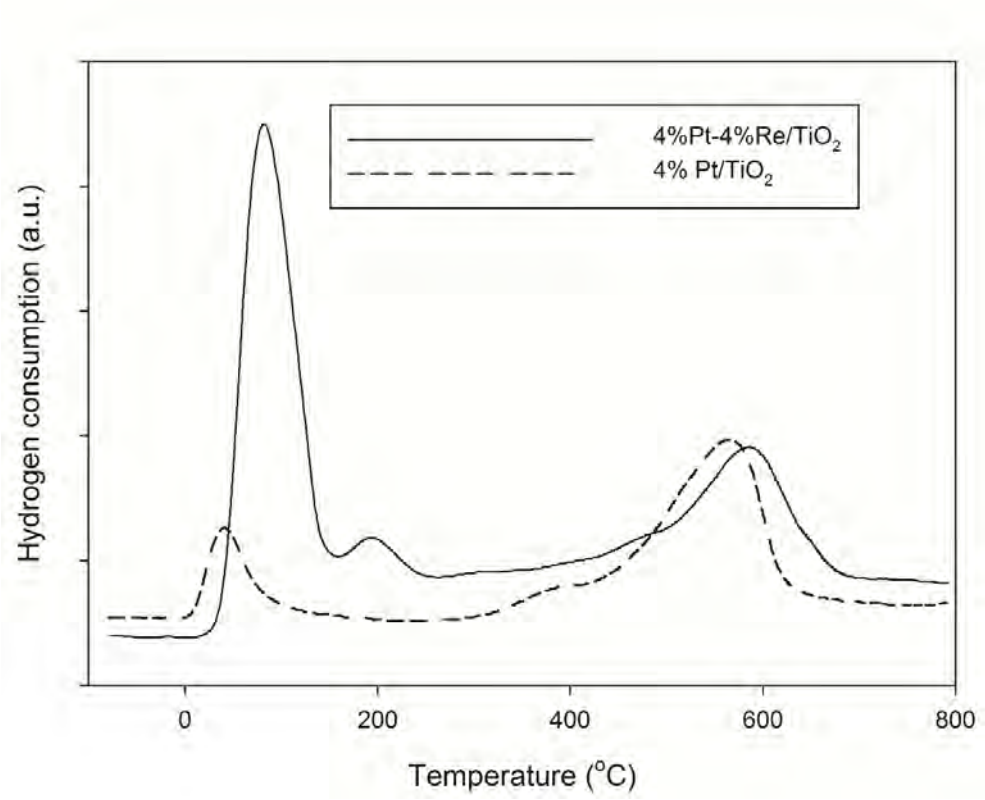

Figure 4.8: *TPR profiles of 4% Pt/TiO_2 and 4% Pt - 4%Re/TiO_2 catalysts.*

For the 4% Pt-4%Re/TiO_2 catalyst, TPR showed three peaks in different ranges of reduction temperature. The H_2 consumption peaks show that Pt^{4+} and Re^{7+} are reduced to Pt^0 and Re^0, which corresponds to the peaks at 20 – 160 °C and 170 – 260 °C, respectively. It is evident that the addition of 4% Re resulted in a change of the peak shapes and a slight drift in the reduction centroids of the Pt and TiO_2 reduction peaks towards the higher temperatures, which in turn increases the intensity of the Pt reduction peak (Murata et al., 2014; Simonetti et al., 2007). In this study, a temperature of 200 °C was used for H_2 reduction of 4% Pt/TiO_2 and 4% Pt-4% Re/TiO_2 catalysts in-situ, for the hydrogenation of carboxylic acids.

4.6 NH_3-TPD

The acidic property of a catalyst is an integral aspect in the choice of catalyst and support for HDO reactions (He and Wang, 2012; Mortensen et al., 2011). The hydrogenation of carboxylic acids mainly require Lewis acid/base interaction for the absorption of the carbonyl group while Brönsted acid provides the hydrogen spill-over to attack the adsorbed carbonyl compound which results in the formation of deoxygenated products (He and Wang, 2013). Therefore, it is significant to consider the influence of catalyst acidity from the Pt-based catalysts. NH_3-TPD technique is useful in providing information on the acidic strength and number of acidic sites exhibited by a catalyst. The temperature range at which ammonia is desorbed corresponds to the extent of catalyst acidic strength while the total amount of the desorbed ammonia provides the total number of acidic sites. In general, the acidic sites of catalysts are categorized into weak, moderate and strong, which corresponds to temperature ranges ≤ 200 °C, 200-350 °C and ≥ 350 °C respectively (Sundaramurthy et al., 2008). Figures 4.9-4.11 show the NH_3-TPD profiles of the prepared and commercial Pt-based catalysts while Table 4.3 shows their total number of acidic sites.

Table 4.3: *Summary of catalyst acidic sites.*

Catalyst	Weak acidic sites (mmol g^{-1})	Moderate acidic sites (mmol g^{-1})	Strong acidic sites (mmol g^{-1})	Total acidic sites (mmol g^{-1})
5% Pt/SiO_2	0.271	-	0.184	0.46
5% Pt/Al_2O_3	0.046	0.125	0.112	0.28
4% Pt/TiO_2	0.044	0.350	0.089	0.48
4%Pt-4%Re/TiO_2	0.079	0.242	0.096	0.42
5% Pt/graphite	0.004	0.005	0.049	0.06
5% Pt/C	0.020	0.050	0.110	0.18

The NH_3-TPD profile for 4% Pt/TiO_2 and 4% Pt-4%Re/TiO_2 catalysts is shown in Figure 4.9. Both catalysts show a similar profile with four desorption peaks in different regions of acidic strength. For 4% Pt/TiO_2, four desorption peaks correspond to temperatures of 140 °C, 290 °C, 330 °C and 616 °C. Similarly, the four peaks for 4% Pt-4%Re/TiO_2 corresponds to 140 °C, 300 °C, 340 °C and 646 °C. For 4% Pt/TiO_2 and 4% Pt-4%Re/TiO_2, the first peak corresponds to NH_3 adsorbed on the weak acid sites. Subsequently, the second and third peaks are classified as moderate acidic sites while the last peak is an indication of strong acidic sites (He and Wang, 2013; Sundaramurthy et al., 2008). For 4% Pt-4%Re/TiO_2, the peak maxima for moderate acidic sites slightly drifted towards higher temperature with increased intensity. This shows that the incorporation of 4% Re to 4% Pt/TiO_2 strengthens the moderate acidic sites and decreases the number of acid sites (Table 4.3). In addition, an increase in intensity of moderate acidic sites does not correlate with increase in number of acidic sites.

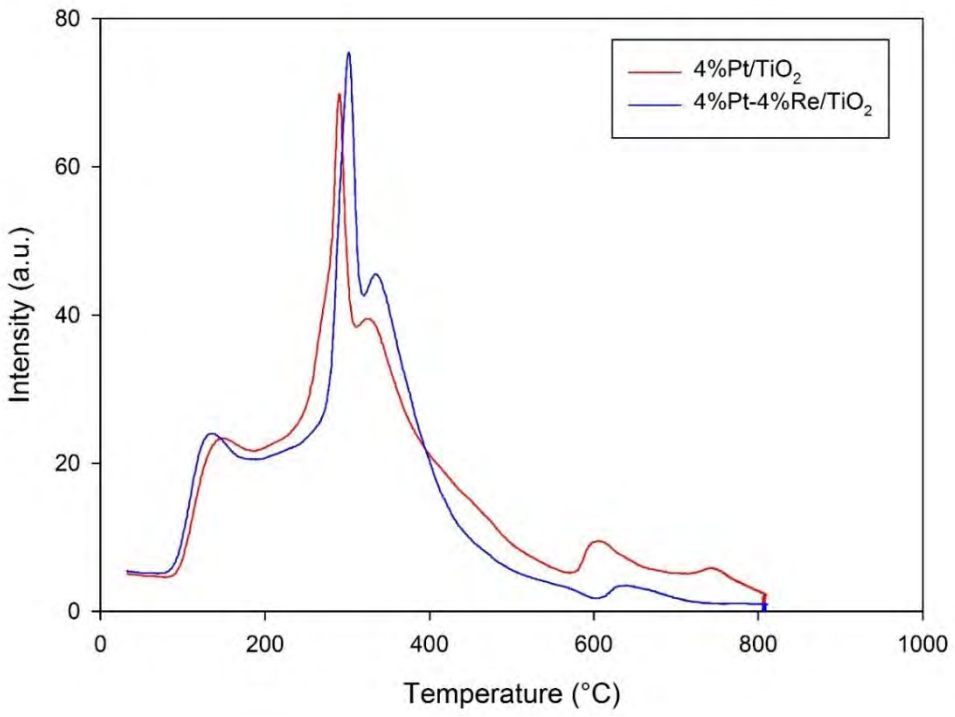

Figure 4.9: *NH_3-TPD over 4% Pt/TiO_2 and 4% Pt-4%Re/TiO_2.*

As evident from Figure 4.10, two desorption peaks were observed for 5% Pt/SiO_2 and 5% Pt/Al_2O_3. Similarly, the first peak maxima for both catalysts indicate NH_3 adsorption in the weak acidic region (140 °C and 147 °C for 5% Pt/SiO_2 and 5% Pt/Al_2O_3 respectively) while the second peak maxima corresponds to strong acidic sites (550 °C and 500 °C for 5% Pt/SiO_2 and 5% Pt/Al_2O_3 respectively). In addition, the temperature at which NH_3 desorbs from the catalyst is similar, although, the total acidic sites vary significantly (Table 4.3).

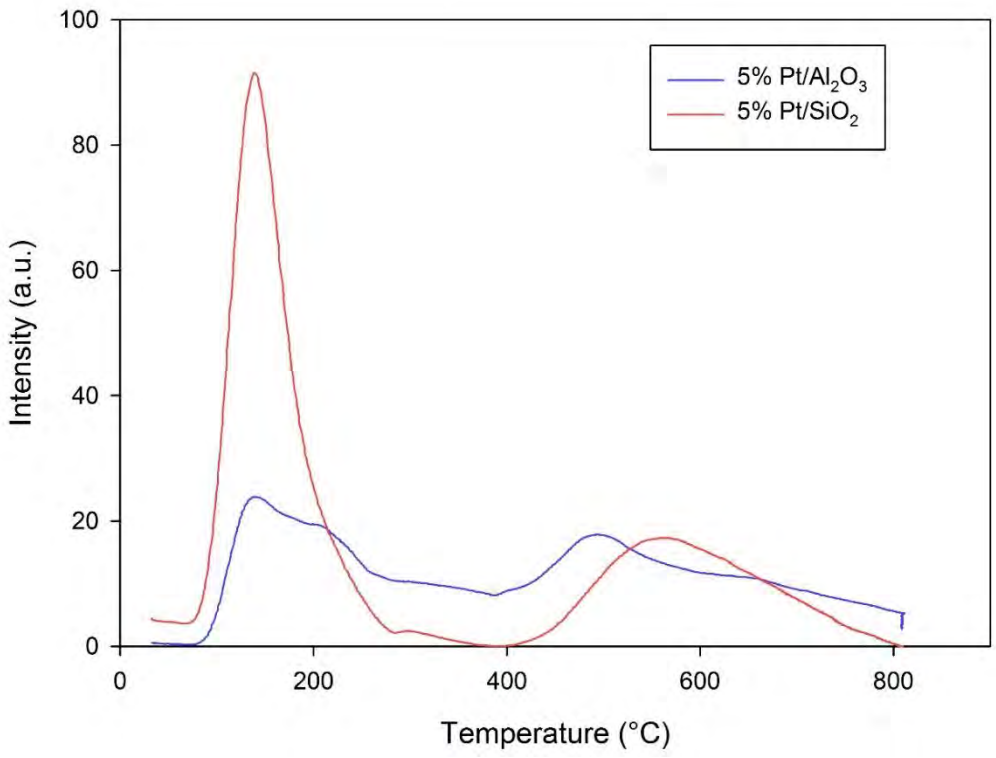

Figure 4.10: *NH_3-TPD over 5% Pt/Al_2O_3 and 5% Pt/SiO_2.*

Three desorption peaks were observed for 5% Pt/graphite as shown in Figure 4.11. However, the intensity of these peaks are very weak, which to a large extent is correlated to the small number of acidic sites (Table 4.3). The first peak corresponds to the weak acidic sites while the second and third are assigned to strong acidic sites. Apart from the single desorption peak in the weak acidic region for 5% Pt/C (Figure 4.11), the presence of two intense peaks

corresponding to strong acidic sites at much higher temperatures indicates the adsorption capacity of carbonyl component on the catalyst surface, which is highly detrimental to HDO reaction (He and Wang, 2013).

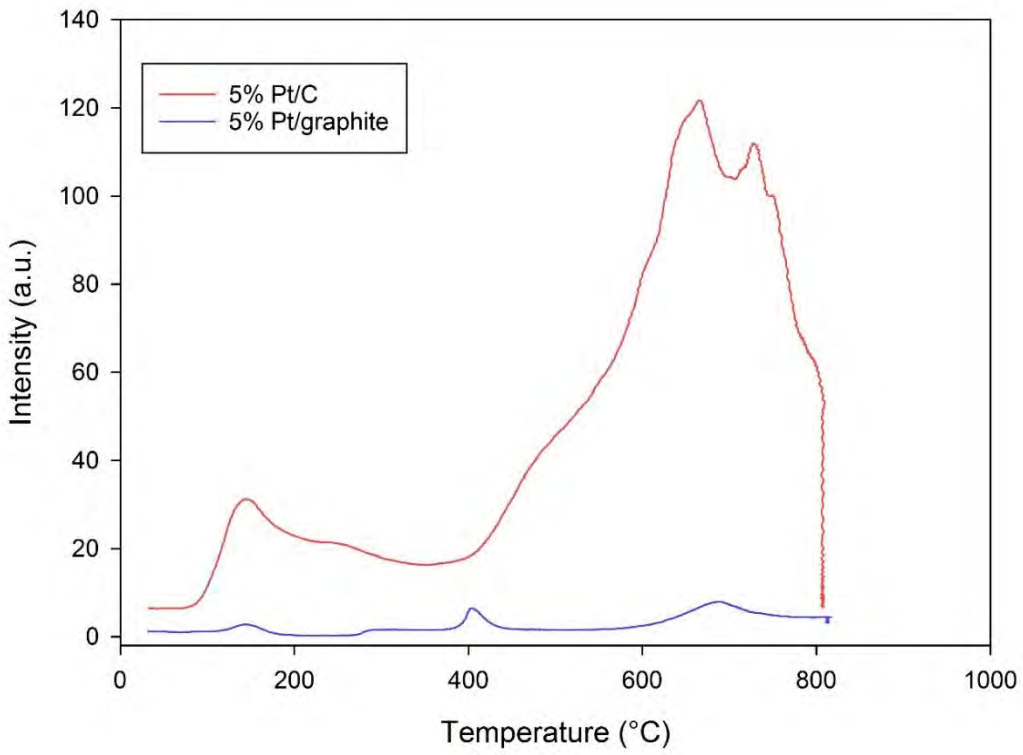

Figure 4.11: *NH_3-TPD over 5% Pt/C and 5% Pt/graphite.*

As shown in Table 4.3, 4% Pt/TiO_2 catalyst was found to have the highest number of acidic sites, and is anticipated to influence performance in the HDO of carboxylic acids to produce deoxygenated compounds using 4% Pt/TiO_2 (Pan et al., 2018). In addition, the extent of adsorption of carbonyl specie was mainly influenced by the Lewis acid/base while donation of hydrogen by the platinum metal specie was mainly due to Brönsted acid (He and Wang, 2012; Mortensen et al., 2011). The availability of moderate acidic sites influences the HDO performance which suggests that the presence of only weak acidic sites is insufficient to provide

the desired catalyst performance. Therefore, 4% Pt/TiO_2 and 4% $Pt\text{-}4\%Re/TiO_2$ can potentially have a much beneficial effect in HDO reactions.

4.7 Catalyst Screening

The effects of different Pt based catalysts supported on SiO_2, Al_2O_3, carbon, graphite and TiO_2 were investigated under identical reaction conditions of 40 bar, 200 °C, 4 hours, 0.3 g catalyst and 1000 min^{-1}, with the resulting conversion of acetic acid and selectivities toward ethanol and ethyl acetate shown in Figure 4.12. During liquid phase hydrogenation, the rate of reaction can be affected by solvent adsorption on the catalyst support and active metal which could influence the adsorption equilibria of reactants and hydrogen solubility (Beamson et al., 2011; Cheng et al., 2009; McManus et al., 2015). For example, alcohol solvents such as methanol exhibit a strong polarity and can react with the acid reagent shifting the reaction equilibrium towards production of methyl esters during hydrogenation of carboxylic acids lowering the selectivity to the desired hydrogenation products (Demirbas, 2008; Li et al., 2011). Several publications have reported the use of alkane solvents for the study of hydrogenation of bio-oil model compounds (Haruo Kawamoto et al., 2016; McManus et al., 2015). Pritchard et al., (2015) studied the hydrogenation of esters to alcohols and reported that hexane was the optimal solvent from solvent screening. Herein, the use of hexane as a solvent is reported.

The hydrogenation of acetic acid mainly proceeds via three reaction routes; Ketonization, hydrogenolysis, decomposition (See Figure 2.2). The desired products in this study are ethanol and ethyl acetate which are mainly generated via the hydrogenolysis reaction route. This involves the C-O bond cleavage of acetic acid to produce acetaldehyde as an intermediate, followed by further hydrogenation to form ethanol (See equation 4.1). Subsequently, ethanol undergoes either dehydration-hydrogenation to yield ethane or

esterification with acetic acid to form ethyl acetate (See equations 4.2-4.3). Other undesirable gaseous products such as CO_2 and methane are mainly produced via decomposition reactions.

$$CH_3COOH + 2H_2 \rightarrow C_2H_5OH + H_2O \quad 4.1$$

$$C_2H_5OH + H_2 \rightarrow C_2H_6 + H_2O \quad 4.2$$

$$C_2H_5OH + CH_3COOH \rightarrow CH_3COOC_2H_5 + H_2O \quad 4.3$$

As shown in Figure 4.12, Pt/SiO_2 and Pt/Al_2O_3 showed the lowest conversion with little or no formation of the desired product (ethanol and ethyl acetate). Decarboxylation and decarbonylation reactions mainly dominated on Pt/SiO_2 and Pt/Al_2O_3 with carbon loss to produce CO which was further hydrogenated to produce CH_4 (Alcala et al., 2005). Mass balance analysis revealed that about 1.5% of gaseous products was formed which corresponds to the low acetic acid conversion of 2% and 4% over Pt/SiO_2 and Pt/Al_2O_3 respectively. In a similar study, low conversion of acetic acid over Pt/SiO_2 and Pt/Al_2O_3 was reported at 265 °C with formation of CO and CH_4 gaseous products as the major products (Wan et al., 2013). Furthermore, Alcala et al., (2005) and Gursahani et al., (2001) have demonstrated that CO and CH_4 are primarily produced over Pt/SiO_2 which can be associated to the gaseous products formed in this study. Elsewhere, Manyar et al., (2010) studied the hydrogenation of stearic acid and found that the conversion over Pt/SiO_2 and Pt/Al_2O_3 was $\leq$ 2% even after 24 h. It is imperative to note that blank experiment carried out in the absence of catalyst showed a minimal conversion of 2% due to thermal reaction.

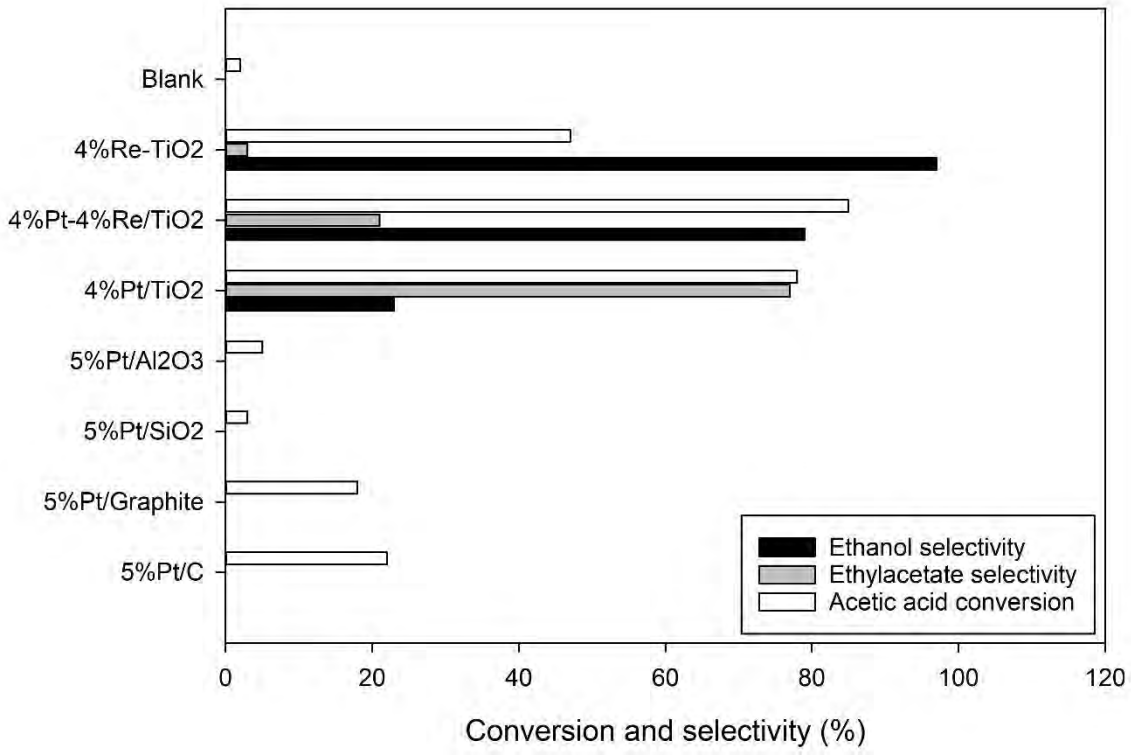

Figure 4.12: *Conversion and selectivity of different catalysts (Reaction conditions: catalyst 0.3 g, temperature 200 °C, initial concentration 0.521 M, reaction time 4 h, pressure 40 bar; Standard deviation: Pt/C, ± 0.08; Pt/graphite, ± 0.002; Pt/SiO_2, ± 0.0008; Pt/Al_2O_3, ± 0.006; Pt/TiO_2, ± 0.001; Pt-Re/TiO_2, ± 0.008).*

As presented in Figure 4.12, Pt/C and Pt/graphite showed conversions of 22% and 18%, respectively. In spite of the improved conversion of acetic acid compared to Pt/SiO_2 and Pt/Al_2O_3, there was no observed formation of desired liquid products. This observation suggests that undesirable gaseous products were formed as evident from mass balance (97% gases). This is further supported by Wan et al., (2013) where the formation of methane, CO_2 and ethane were reported as the main products for the hydrogenation of acetic acid over Pt/C. Due to the neutral nature of carbon and graphite supports in Pt/C and Pt/graphite, hydrogenation of acetic acid is limited by platinum metal sites as the only platform for both hydrogen activation and acetic acid adsorption (He and Wang, 2013; Vargas et al., 2008, 2004).

He and Wang, (2013) reported that Pt/TiO_2 favours ethane and acetaldehyde formation while Pt/C favours ethanol using a fixed bed reactor despite the strength of Pt and support interaction being approximately the same for both carbon and TiO_2. However, in this study, it can be observed that the use of TiO_2 as a support for Pt is more effective for the conversion of acetic acid and the production of ethanol and ethyl acetate when compared to other supports such as carbon, alumina and silica (Figure 4.12). Pritchard et al., (2017) demonstrated that the strength of acid sites on TiO_2 and its interaction with the impregnated Pt/Pt-Re species enhanced the HDO performance which can be linked to findings in this study. Consequently, the adsorption of carbonyl species was primarily through interaction with the Ti^{n+} cations (Lewis acid sites) and/or oxygen vacancies created in the reducible oxide after the reduction at 200 °C, these sites can activate the acid carbonyl group for hydrogenation. With Pt providing dissociated hydrogen and the adsorption sites on TiO_2 activating the carbonyl group, Pt/TiO_2 promotes the hydrogenation reaction to the formation of ethanol (He and Wang, 2012; Mortensen et al., 2011). In contrast, the absence of oxygen vacancies and the neutrality of the Pt/C and Pt/graphite could alter the adsorption of acetic acid favouring decomposition reactions over hydrogenation with activation of both hydrogen and the acids occurring on the Pt sites (Vargas et al., 2008, 2004).

In contrast with the carbon, graphite, silica and alumina supports, the formulated 4% Pt/TiO_2 and 4% Pt-4%Re/TiO_2 catalysts showed significant conversions of 78% and 83%, respectively, in addition to the formation of ethanol and ethylacetate (see Figure 4.12). However, while 4% Pt/TiO_2 is more selective towards ethyl acetate, the selectivity towards ethanol was more favoured by 4% Pt-4%Re/TiO_2. The higher selectivity of ethyl acetate over 4% Pt/TiO_2 compared to 4% Pt-4%Re/TiO_2 can be associated to the higher number of acidic sites in 4% Pt/TiO_2 (0.48 mmol g^{-1}) as shown in Table 4.3. Due to the high acidity in 4%Pt/TiO_2,

the Brönsted acid sites on TiO_2 becomes highly concentrated and cannot undergo further hydrogenation (Rakshit et al., 2018). Accordingly, acetic acid adsorbs associatively on the concentrated sites resulting in the formation of protonated acetic acid molecules, which undergo further esterification and subsequently increases ethyl acetate selectivity and reduces ethanol selectivity. From Figure 4.2, it can be deduced that the presence of broad peaks in the bimodal pore size distribution of TiO_2 enhanced efficient transfer of reactants into the active sites of 4% Pt/TiO_2 and 4% Pt-4%Re/TiO_2 (Zhang et al., 2004), which can be linked to catalyst activity. It is worth noting that no reaction occurred over titania without Pt or Re metal impregnated. The impregnation of Re only (4% Re/TiO_2) strongly favoured the selectivity to ethanol compared to ethyl acetate. It is clear, therefore, that the presence of Re magnified the route to ethanol production while suppressing that leading to ethyl acetate formation. This is confirmed from the results of the use of Pt, Re and Pt-Re shown in Figure 4.12. Although, the selectivity to ethanol is high with 4% Re/TiO_2, the conversion of acetic acid is low at 47% compared to 4% Pt/TiO_2 and 4% Pt-4%Re/TiO_2. Hence, addition of Re influences the catalyst activity and performance. As shown in Figure 4.12, the opposite trend in product selectivity over 4%Pt/TiO_2 and 4% Pt-4%Re/TiO_2 catalysts can be distinguished by the presence of highly oxophillic Re centres present in 4% Pt-4%Re/TiO_2 which makes them highly potent to C=O reduction of the acetic acid (Pritchard et al., 2015). When compared to the observation with 4% Pt/TiO_2, the synergistic effect of Pt and Re showed that Pt facilitates the hydrogenation activity of the catalyst likely through dissociation of H_2 while Re acts as a promoter, activating the C=O group. However, for stearic acid it has been reported that the addition of Re to Pt/TiO_2 enhanced the hydrogenation activity but reduced alcohol selectivity resulting in more alkane products (Manyar et al., 2010). In the same study, it was observed that further increase in the Re loading to 4wt% enhanced the reaction rate but did not correlate with alcohol selectivity.

4.8 Optimization of Process Factors

The effect of reaction factors on the conversion of acetic acid and yield of ethanol over 4%Pt/TiO_2 was evaluated and their relative contributions quantified. An orthogonal array of sixteen (16) experiments and the corresponding S/N ratios obtained are shown in Table 4.4. For each factor at a particular level, the total S/N ratio was calculated by summing the individual S/N ratios for the respective experiments. For example, the total S/N ratio for H_2 pressure at level 3 was obtained by adding the individual S/N ratio for experiment numbers 3, 7, 11, 15 (Table 4.4). The effect of reaction factors with respect to each level is graphically presented in Figure 4.13. The upper end of the range of reaction temperature was chosen based on preliminary experiments which shows that at higher temperatures above 200 °C, the conversion of acetic acid remained approximately the same with minimal formation of liquid products. The profile depicts that temperature reached its maximum at 200 °C and has a profound effect with respect to the conversion of acetic acid. It can be observed that the total S/N ratios for each factor increased with each increase in level, thereby attaining the maximum at level 4. Even though C-O bond cleavage is catalytically driven and possesses high activation energy, it is evident that higher temperatures enhance the hydrogenolysis of C-O bonds towards aldehyde formation as an intermediate species, followed by the subsequent formation of ethanol and ethyl acetate.

Table 4.4: *Experimental design for L16 array and corresponding S/N ratio for reactions over* Pt/TiO_2.

Experiment No.	A Temp. (ºC)	B Pressure (bar)	C Time (h)	D Stirring (min^{-1})	E Catalyst (g)	Acetic acid Conversion (%)	S/N Conversion	Ethanol Yield (%)	S/N Yield
1	80	10	1	400	0.1	0.30	-10.46	0.05	-25.35
2	80	20	2	600	0.2	1.37	2.73	0.41	-7.72
3	80	30	3	800	0.3	3.79	11.57	2.08	6.38
4	80	40	4	1000	0.4	7.50	17.50	6.00	15.56
5	120	10	2	1000	0.3	29.11	29.28	16.01	24.09
6	120	20	1	800	0.4	17.61	24.92	13.91	22.87
7	120	30	4	600	0.1	36.45	31.23	25.52	28.14
8	120	40	3	400	0.2	35.14	30.91	29.86	29.50
9	160	10	3	600	0.4	65.07	36.27	33.19	30.42
10	160	20	4	400	0.3	70.68	36.99	37.46	31.47
11	160	30	1	1000	0.2	50.00	33.98	32.50	30.24
12	160	40	2	800	0.1	52.26	34.36	31.88	30.07
13	200	10	4	800	0.2	83.44	38.43	25.03	27.97
14	200	20	3	1000	0.1	81.95	38.27	28.68	29.15
15	200	30	2	400	0.4	79.30	37.99	38.06	31.61
16	200	40	1	600	0.3	68.19	36.67	13.64	22.69

The total S/N ratio of factor B increased linearly with pressure and reached an optimum at 40 bar. At prevailing conditions, the extent of hydrogen solubility in the reaction mixture improves hydrogen adsorption on the catalyst surface which in turn promotes hydrogen spill over to react with the adsorbed carbonyl species (Zaera, 2017).

It was also observed that increased reaction time strongly favours conversion of acetic acid. Subsequently, the S/N ratio increased with reaction time which validates the maximum

conversion achieved at a reaction time of 4 h, thus confirming the optimal reaction time to be level 4. The longer time required to achieve maximum conversion is associated with the difficulty in polarizing the carbonyl group of acetic acid and resistance to hydrogenation (Pritchard et al., 2015). The S/N ratio for factor D increases with stirring speed and attained maximum at level 4 which represents the highest level. From Figure 4.13, the increase in S/N ratio for stirring speed from level 2 to 4 was less significant which suggests that the extent of external mass transfer limitation is negligible. This observation conforms to findings from mass transfer investigations (Section 6) which suggested that a stirring speed of 1000 min^{-1} is sufficient to overcome limitations due to external mass transfer. The effect of Factor E on S/N ratio revealed that increased catalyst loading increased the conversion of acetic acid. The improved activity of the catalyst upon increase in loading in the reactor is attributed to the increase in the number of active sites which provides an efficient platform for adsorption of carbonyl carbon and hydrogen attack as activated on platinum. Based on the results obtained in Figure 4.13 and Table 4.5, the optimum reaction factors can be reported as thus: A_4, B_4, C_4, D_4, E_4 i.e., temperature 200 °C, initial hydrogen pressure 40 bar, reaction time 4 h, catalyst loading 0.4 g and stirring speed 1000 min^{-1} respectively. To validate the optimization results, it is essential to carry out a confirmation experiment using the optimum reaction factors from the Taguchi method, considering the fact that the optimum conditions did not form a set of experiments in the orthogonal array. The confirmation experiment was performed in duplicate (Table 4.5) and revealed that the conversion of acetic acid and corresponding S/N ratio was higher than the highest S/N ratio obtained in Experiment 13 of Table 4.4, thus confirming the applicability of the Taguchi method for optimizing the conversion of acetic acid using 4% Pt/TiO_2.

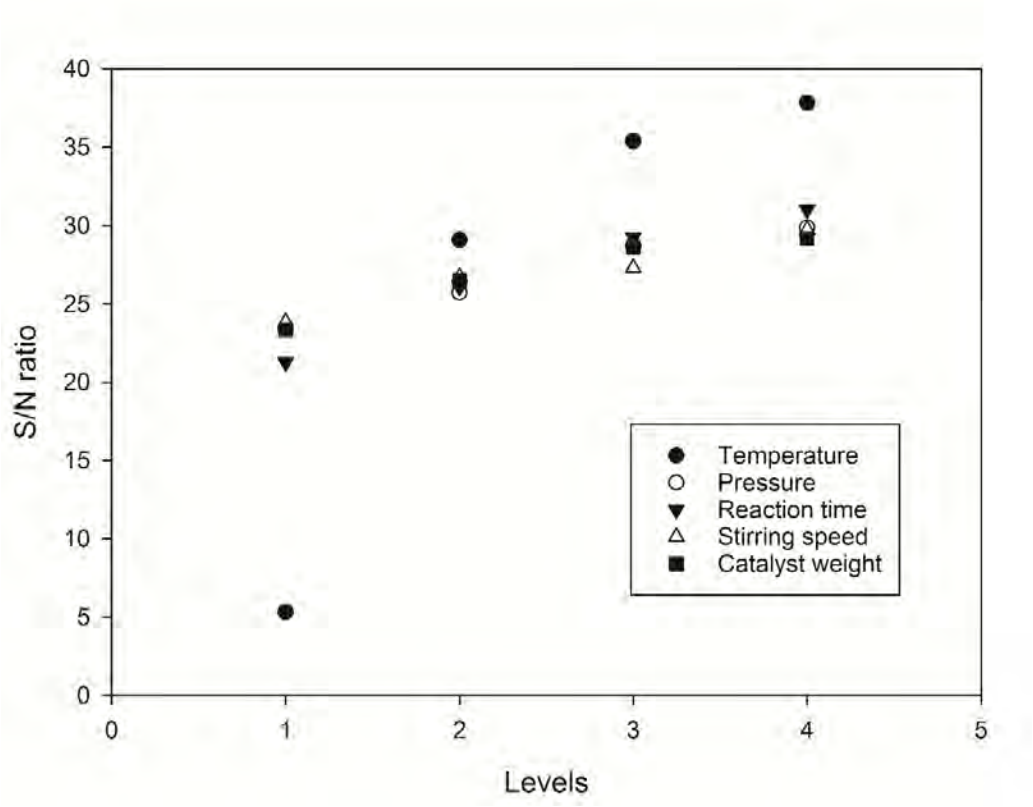

Figure 4.13: *Effect of process factors at each level for conversion of acetic acid.*

Table 4.5: *Confirmation experiment under reaction space explored for conversion of acetic acid.*

Experiment	Levels					Conversion (%)	S/N ratio
	A	B	C	D	E		
Exp. No. 13	4	1	4	3	2	83.44	38.43
Confirmation Exp.	4	4	4	4	4	94	39.46

In order to examine the contributory effect of each reaction factor with respect to conversion of acetic acid, ANOVA was carried out. Table 4.6 presents the ANOVA result where the contribution of each factor was estimated by comparison of individual mean variance (V). Based on the mean variances obtained, temperature exerted the highest impact on acetic acid conversion while stirring speed was the least influential controllable factor. However, the

variance provides only qualitative information in estimating the most significant parameter (Srivastava et al., 2018; Yildiz, 2008). The percentage contribution of each controllable factor based on the ANOVA results can be summarized as thus: Temperature > reaction time > initial H_2 pressure > catalyst loading > stirring speed.

Table 4.6: *Analysis of variance (ANOVA) for conversion of acetic acid.*

Parameter	DOF	Sum of Squares	Variance	% Contribution
Temperature	3	2646.49	882.16	84.70
Pressure	3	103.06	34.35	3.30
Stirrer Speed	3	70.54	23.51	2.30
Reaction time	3	219.74	73.25	7.00
Catalyst Weight	3	83.43	27.81	2.70
Error	1	0.00	0.000	
Total	16	3123.25		100

In order to maximise the yield of ethanol, the S/N ratio was calculated by considering the larger the better function (equation 1). The mean ethanol yield was calculated as shown in Table 4.4. As seen in Figure 4.14, the maximum S/N ratio for each factor was attained at level 4 with the exception of temperature at level 3 (160 °C). Unlike the acetic acid conversion in which 200 °C (level 4) was the optimum, for ethanol production the temperature dropped to 160 °C which means beyond 160 °C there is a side reaction that favours ethyl acetate formation. It is worth noting that high pressure and high catalyst weight favours the selective hydrogenation of acetic acid to ethanol. Table 4.8 shows the confirmatory test experiment [160 °C (level 3), 40 bar (level 4), 4 h (level 4), 0.4 g (level 4) and 1000 min^{-1} (level 4)]. This is compared to the highest ethanol yield reported in Table 2 which corresponds to experiment 15 as shown in Table 4.7. It is clear the ethanol yield and the S/N ratio under the best reaction

condition explored is marginally higher than the best found in Table 4.4 (experiment 15). Table 4.8 shows the ANOVA analysis result for the yield of ethanol. Similar to the conversion of acetic acid, the ANOVA results with respect to ethanol yield is summarized as follows Temperature > reaction time > initial H_2 pressure > catalyst loading > stirring speed. This ranking order is consistent with that of the acetic acid conversion.

Table 4.7: *Confirmation experiment under reaction space explored for yield of ethanol.*

Experiment	Levels					Yield (%)	S/N ratio
	A	B	C	D	E		
Exp. No. 15	4	3	2	1	4	38.06	31.61
Confirmation Exp.	3	4	4	4	4	38.92	31.80

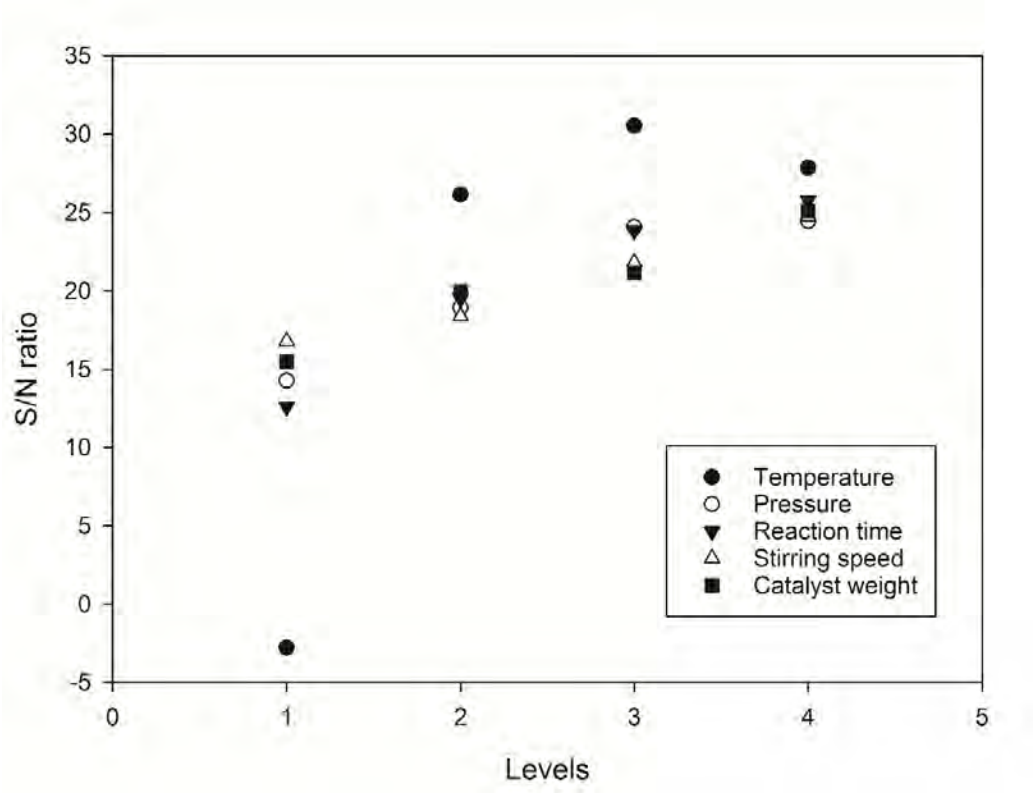

Figure 4.14: *Effect of process factors at each level for yield of ethanol.*

Table 4.8: *Analysis of variance (ANOVA) for yield of ethanol.*

Parameter	DOF	Sum of Squares	Variance	% Contribution
Temperature	3	2916.47	972.16	73.90
Pressure	3	278.58	92.86	7.10
Stirrer Speed	3	152.01	50.67	3.90
Reaction time	3	409.74	136.58	10.40
Catalyst Weight	3	187.81	62.60	4.80
Error	1	0.00	0.00	0.00
Total	16	10631.34	1314.87	100

4.9 Conclusions

This chapter revealed the characterization properties of prepared and commercial catalysts used in this study. Further, investigation on catalyst screening between the prepared and commercial catalysts was reported. Results from Taguchi method of DOE was reported for the optimization of reaction conditions towards the maximization of acetic acid conversion and ethanol yield. BET results revealed that 5% Pt/C exhibited the highest surface area (1389.5 m^2/g) while 5% Pt/graphite (12.8 m^2/g) had the least. BJH pore size distribution for all the catalysts showed a bimodal distribution with peaks mainly found in the mesoporous range. The crystal phases present in TiO_2 and other titania supported catalysts as investigated using XRD showed that rutile and anatase phases were the only peaks observed. The crystal phase arrangement remained unaltered even after the addition of Pt and Re into TiO_2. The rutile phases were favored over the anatase phases due to Pt and Re addition as evidenced from the phase fraction obtained using GSAS refinement. SEM analysis for 4% Pt/TiO_2 and 4% Pt-4% Re/TiO_2 showed a distinct morphology for the fresh and spent catalyst which was linked to agglomeration and liquid bridging. EDX analysis also confirmed the uniformity of elemental dispersion in the catalysts. The reduction temperature for both 4% Pt/TiO_2 and 4% Pt-4%

Re/TiO_2 were investigated using H_2-TPR analysis, which revealed a small and large peak corresponding to Pt and TiO_2 respectively. The reduction temperature for both catalysts was found to be 200 °C. 4% Pt/TiO_2 exhibited the highest number of acidic sites as investigated using the NH_3-TPD analysis. Catalyst screening investigation showed that prepared 4% Pt/TiO_2 and 4% Pt-4%Re/TiO_2 outperformed the commercial catalysts for acetic acid hydrogenation and were found to favor ethyl acetate and ethanol respectively. Taguchi method of optimization revealed that 200 °C, 40 bar H_2, 0.4 g catalyst loading, 1000 min^{-1}, and 4 h were the optimum conditions for acetic acid conversion, while 160 °C, 40 bar H_2, 0.4 g catalyst loading, 1000 min^{-1}, and 4 h were the optimum conditions for ethanol yield.

Chapter 5. Catalytic Hydrogenation of Short Chain Carboxylic Acids Typical of Model Compound Found In Bio-Oils

5.1. Chapter Overview

This chapter describes the hydrogenation of short chain carboxylic acids specifically acetic, propanoic and butanoic acids as individual feed component and multi-feed components. The conversion of carboxylic acids and selectivity of alcohols and esters were studied for individual acids, to compare them and see if the presence of more than one acid in a multi-feed system led to higher alcohol selectivity or not. The study was carried out over 4% Pt/TiO_2 and 4% $Pt\text{-}4\%Re/TiO_2$ catalysts using reaction conditions as established from chapter 4 of this study. The investigation of catalyst reusability for 4% Pt/TiO_2 and 4% $Pt\text{-}4\%Re/TiO_2$ was carried out to reveal the extent of catalyst stability over several reaction cycles. The effect of Re as a promoter towards the conversion of acetic acid and selectivity of ethanol and ethyl acetate was investigated.

5.2. Effect of temperature on the Hydrogenation of C_2-C_4 carboxylic acids over 4% Pt/TiO_2 and 4% $Pt\text{-}4\%Re/TiO_2$

The effect of temperature in the range of 145-200 °C was investigated in terms of catalyst activity and product selectivity for the hydrogenation of acetic, propanoic and butanoic acids over 4% Pt/TiO_2 and 4% $Pt\text{-}4\%Re/TiO_2$ at 2 h. Figures 5.1-5.3 shows the respective conversions of acetic, propanoic and butanoic acids and their selectivity towards alcohol and ester. It was observed that the production of liquid products was found to be ≥ 98% which were mainly alcohols and esters corresponding to each acid. Typical gaseous products such as CO, CO_2 and C_1 - C_4 alkanes were anticipated based on the negligible gas formations from mass

balance (< 2%). The formation of coke was not evident in all reaction cases. It is clear that the conversion of the short chain carboxylic acids and their respective esters selectivity increased as the reaction temperature increased for the 4% Pt/TiO_2 catalyst. Under the same reaction temperature, the conversion of the carboxylic acid decreased as the carbon number increased from C_2 to C_4 while the selectivity of their respective alcohols increased as the carbon number within the carboxylic acid increased (Figures 5.1-5.3). The observed conversion trend can be ascribed to decreased volatility and increased boiling point (Averill and Eldredge, 2007; Wang et al., 2016). In addition, increased molecular weight as well as increased carbon number results in decreased diffusion of reactants into the catalyst particles. Conversely, alcohol selectivity increases with increasing carbon number of the corresponding carboxylic acid and decreasing polarity of the carbonyl (C=O) group. It can also be observed in Figures 5.1-5.3 that alcohol selectivity decreased as reaction temperature increased for 4%Pt/TiO_2 catalyst. This shows that lower temperatures favour the production of alcohols which is facilitated by the hydrogenation of the carbonyl C=O bond and the suppression of esterification reaction. Another possible reaction route due to further hydrogenation of alcohol to produce alkanes was not observed. Even though the cleavage of C-O bond is facilitated at high temperatures resulting to higher conversion of carboxylic acids (Chen et al., 2011), the selectivity of C_1-C_4 alkanes and other gases was found to be ≤2% which suggests that esterification was favoured via a reaction of produced alcohols and unreacted carboxylic acids to produce esters. It was also observed that the solubility of acids in hexane solvent becomes stronger with decreasing polarity of the carboxylic acid as a result of non-polar interaction between them, which improves the hydrogenation of acids (Smith, 1977).

At 145 °C, 53% of acetic acid was converted into ethanol (52% selectivity) and ethyl acetate (48% selectivity) as the sole products (Figure 5.1). The significant production of ethyl

acetate even at low temperature may be attributed to stronger adsorption of formed ethanol on the catalyst surface which is evident from adsorption study (See Appendix B). Even at 200 °C, the selectivity to liquid products was ≥ 99% which suggests that 4% Pt/TiO_2 does not favour further hydrogenation and decarboxylation reactions. The other trace products were thought to be gases as evident from product mass balance which was reported in earlier studies, such as ethane, methane and CO_2 (He and Wang, 2013; Wan et al., 2013).

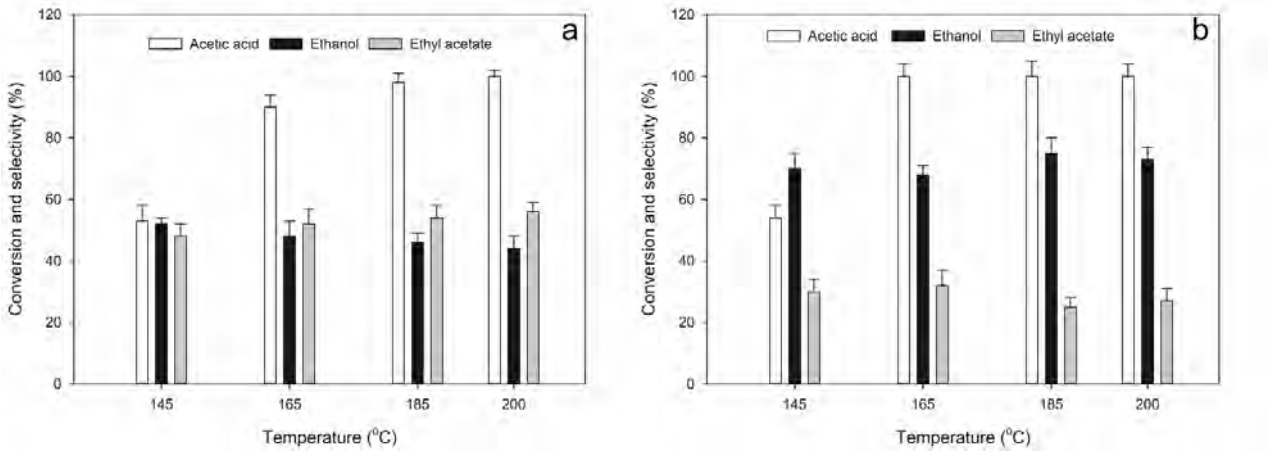

Figure 5.1: *Effect of temperature on the hydrogenation of acetic acid over a) 4% Pt/TiO_2, b) 4%Pt-4%Re/TiO. Reaction conditions: 0.3 g of 4%Pt/TiO_2/4% Pt-4%Re/TiO_2, 0.2 M initial concentration, H_2 pressure of 40 bar, 50 ml of hexane and batch reaction time of 2 h.*

As shown in Figure 5.2, the conversion of propanoic acid at 145 °C was found to be 46.5%, and two liquid products were mainly observed under all temperatures: propanol (73% selectivity) and propyl propionate (27% selectivity). An increase in temperature from 145 – 165 °C significantly increased the conversion to 90% while alcohol selectivity decreased to 62%. Conversely, the selectivity to propyl propionate increased from 27% to 39% over the temperature range of 145-165°C. Further increase to 200 °C shows that temperature has a profound effect on product formation which was evident in the decreased selectivity of propanol

from 73 to 45 % and increased selectivity to propyl propionate from 27 to 55%. The resulting gaseous products from mass balance were insignificant and neglected as traces (≤1%).

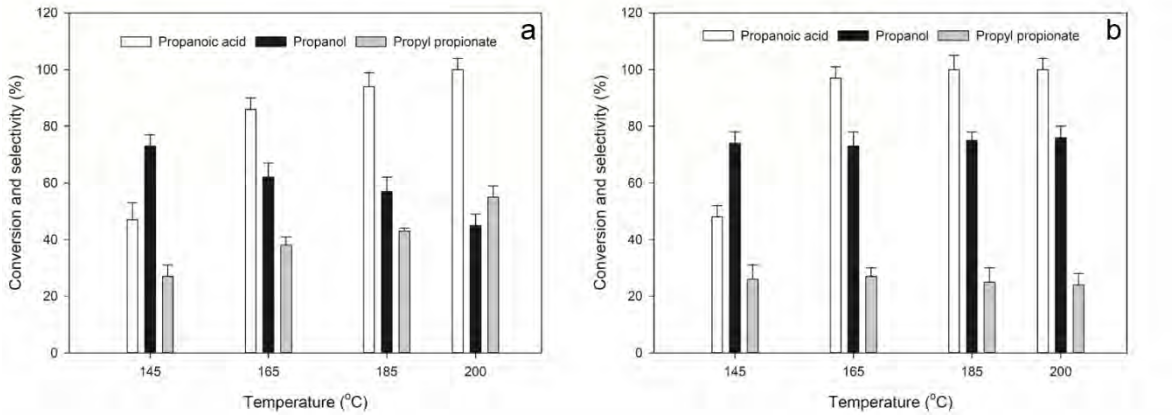

Figure 5.2: *Effect of temperature on the hydrogenation of propanoic acid over a) 4% Pt/TiO_2, b) 4% Pt-4%Re/TiO_2. Reaction conditions: 0.3 g of 4%Pt/TiO_2/4% Pt-4%Re/TiO_2, 0.2 M initial concentration, H_2 pressure of 40 bar, 50 ml of hexane and batch reaction time of 2 h.*

The hydrogenation of butanoic acid mainly resulted in butanol and butyl butyrate as primary products as presented in Figure 5.3. As reaction temperature increases from 145 to 200 °C, butanoic acid conversion increased from 48.2 to 90.1%. Under these conditions, butanoic acid was highly selective to butanol with selectivity between 77 and 99%. The observed slower conversion of butanoic acid was mainly influenced by the hydrogenation pathway to butanol in comparison with acetic and propanoic acids, which were strongly favoured by the esterification pathway.

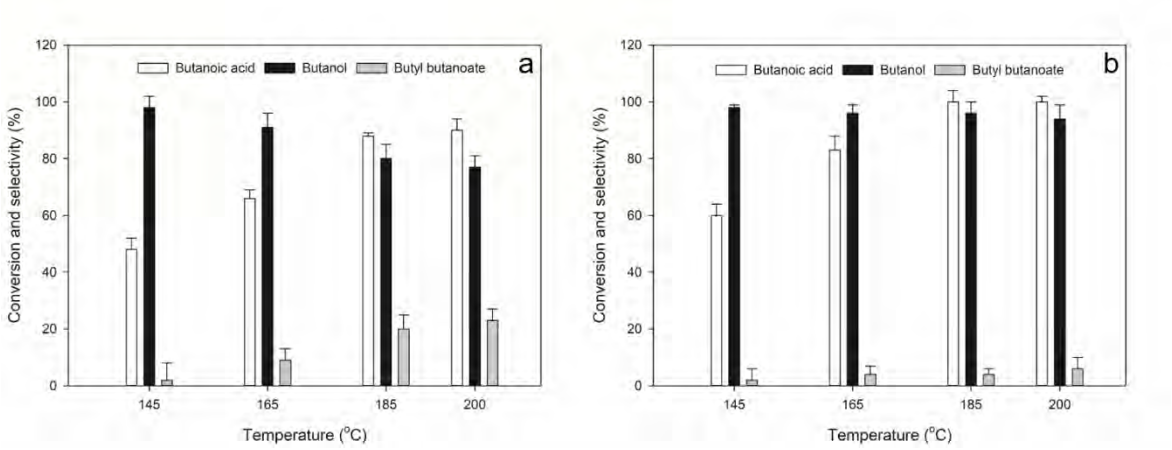

Figure 5.3: *Effect of temperature on the hydrogenation of butanoic acid over a) 4% Pt/TiO_2, b) 4% Pt-4%Re/TiO_2. Reaction conditions: 0.3 g of 4% Pt/TiO_2/4% Pt-4%Re/TiO_2, 0.2 M initial concentration, H_2 pressure of 40 bar, 50 ml of hexane and batch reaction time of 2 h.*

The hydrogenation of acetic, propanoic and butanoic acids was carried out using 4% Pt-4%Re/TiO_2 under the same conditions as shown in Figures 5.1-5.3. The reactions reached completion at 185 °C in all cases at 2 h. Even though the products remain the same as that of 4% Pt/TiO_2 for C_2-C_4 carboxylic acids, the addition of Re promoted the catalytic activity and alcohol selectivity over ester in all cases. A lack of clear trend between the alcohol selectivity and Re content over Pt-Re/TiO_2 catalysts was reported by Manyar et al., (2010) in the hydrogenation of stearic acid. Elsewhere, Pritchard et al., (2017) acknowledged that while increasing the Re content in Pt-Re/TiO_2 increases the conversion of methyl esters, the selectivity towards alcohol was not clear. The effect of Re in Pt-Re/TiO_2 catalysts was probed using the hydrogenation of acetic acid as reported in section 5.6 of this study.

While acetic acid was completely converted at 165 °C, the selectivity to ethanol is 67.5% and selectivity to ethyl acetate is 32.5% for Pt-Re/TiO_2 (Figure 5.1). The selectivity of ethanol linearly increased to 73% with an increase in temperature to 200 °C. It has been observed that Pt-Re/TiO_2 converts fatty acids into alkanes via alcohol (Manyar et al., 2010;

Pritchard et al., 2015); however, for short chain carboxylic acids such as acetic acid, the resulting synergy of Pt-Re on TiO_2 suppresses the dehydration-hydrogenation of ethanol into ethane, which, in turn, minimizes the interaction of oxygen atom in ethanol by enhancing desorption. As shown in Figure 5.2, catalyst performance for the hydrogenation of propanoic acid clearly shows that, at 185 °C, complete conversion was achieved, with a dominant selectivity of 74.9% towards propanol. At 200 °C, propyl propionate splits up into propanol and propanoic acid, which improves propanol selectivity to 76.4%.

In comparison with acetic and propanoic acids, hydrogenation of butanoic acid over 4% Pt-4%Re/TiO_2 showed improved catalyst activity in terms of butanol selectivity (Figure 5.3). Butanol selectivity was 98% at 145 °C, decreasing by only 3.7% as temperature increased to 200 °C. This observation is similar to findings for the hydrogenation of butanoic acid at 265 °C over Ru/Ru-Sn/ZnO and 25 bar of hydrogen, where 99% butanol selectivity was achieved (Lee et al., 2014). This implies that the promotion of Pt/TiO_2 with Re in this study can be used to achieve high alcohol selectivities under milder reaction conditions. In general, the observed higher selectivity of butanol over ethanol and propanol even at higher temperatures could be associated with the lower adsorption strength of butanol on the catalyst surface (Appendix B). This results in enhanced desorption of butanol and reduced possibility of esterification reaction. This study shows that liquid phase hydrogenation of carboxylic acid (C_2-C_4) can be achieved with high conversion and significant selectivity towards alcohols ($\geq$ 70 %) under mild reaction conditions.

5.3 Effect of time on the hydrogenation of C_2-C_4 carboxylic acids over 4% Pt/TiO_2 and 4% Pt-4%Re/TiO_2

The effect of reaction time on conversion and product selectivity was investigated on the hydrogenation of C_2-C_4 carboxylic acids using 4% Pt/TiO_2 at 185 °C and the results are shown in Figure 5.4-5.6. Under these conditions, alcohols and esters were observed as the primary products and 100 % conversion was achieved in 3 h in all cases. It was also evident that de-esterification reaction occurred after the complete conversion of short chain carboxylic acids which gave rise to increased alcohol selectivity. The ester hydrolyses by splitting up into alcohol and acid as a result of equilibrium. It was also observed that further dehydration-hydrogenation reactions of alcohol to yield alkane products did not occur. With 4% Pt-4%Re/TiO_2 catalyst, the respective selectivity toward alcohol production increases from 59 to 75% (acetic acid), 67 to 78% (propanoic acid) and 95 to 98% (butanoic acid) as the reaction increases from 1 to 4 h. It is clear that as the molecular weight of the carboxylic acid increases the selectivity towards alcohol production increases, in this case butanoic > propanoic > acetic acid. However, with 4% Pt/TiO_2 catalyst for acetic acid the selectivity towards ethanol decreased as the reaction time increased from 1 to 2 h and increased as the reaction increased from 2 to 4 h (Figure 5.4). A similar observation can be noted for butanol selectivity with butanoic acid, except for propanoic acid in which propanol selectivity dropped as the reaction increased from 1 to 3 h and thereafter increased as the reaction time increased from 3 to 4 h (Figures 5.4 and 5.5). Overall, the alcohol selectivity decreases and subsequently increases as the reaction time increases from 1 to 4 h.

As seen in Figure 5.4, the hydrogenation of acetic acid required 1 h to achieve 89.6 % conversion over 4% Pt/TiO_2. The production of ethanol diminished between 1 to 2 h and began

to increase afterwards until 4 h. Further hydrogenation of ethanol after complete conversion of acetic acid did not occur even after 4 h. The binding interaction between oxygen atom in ethanol and oxygen defect sites (Ti^{3+}) on titania support is likely too strong for further reaction to take place (Bahruji et al., 2013).

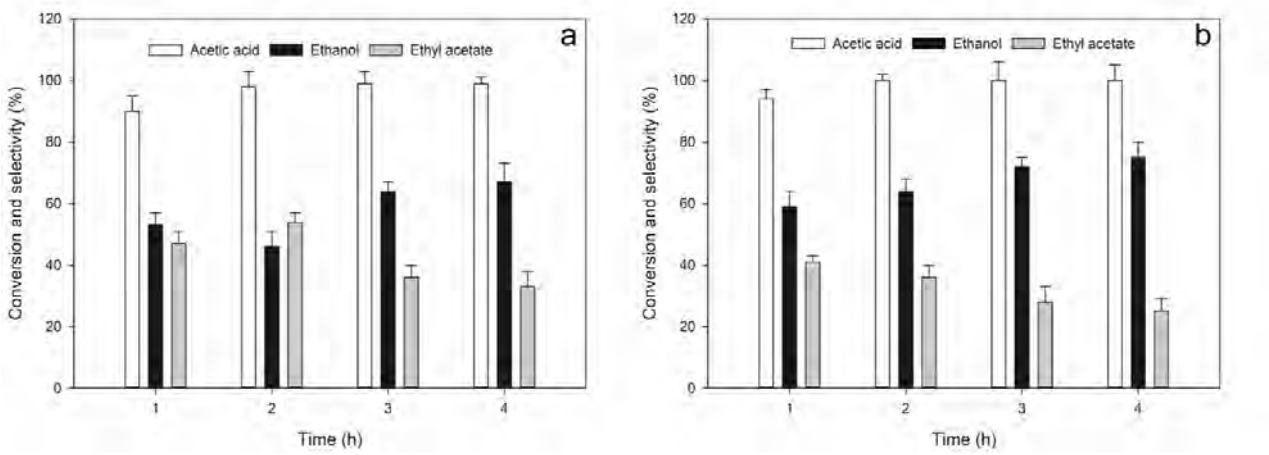

Figure 5.4: *Effect of reaction time on the hydrogenation of acetic acid over a) 4% Pt/TiO_2, b) 4% Pt-4%Re/TiO_2. Reaction conditions: 0.3 g of 4% Pt/TiO_2/4% Pt-4%Re/TiO_2, 0.2 M initial concentration, H_2 pressure of 40 bar, 50 ml of hexane and batch reaction time of 2 h.*

During the hydrogenation of propionic acid, the selectivity towards propanol decreased from 73% to 52% while propyl propionate increased from 27% to 48% over a period of 1 h to 3 h (Figure 5.5). After the complete conversion of propanoic acid, the selectivity of propanol slightly improved to within 2% as a result of hydrolysis of propyl propionate.

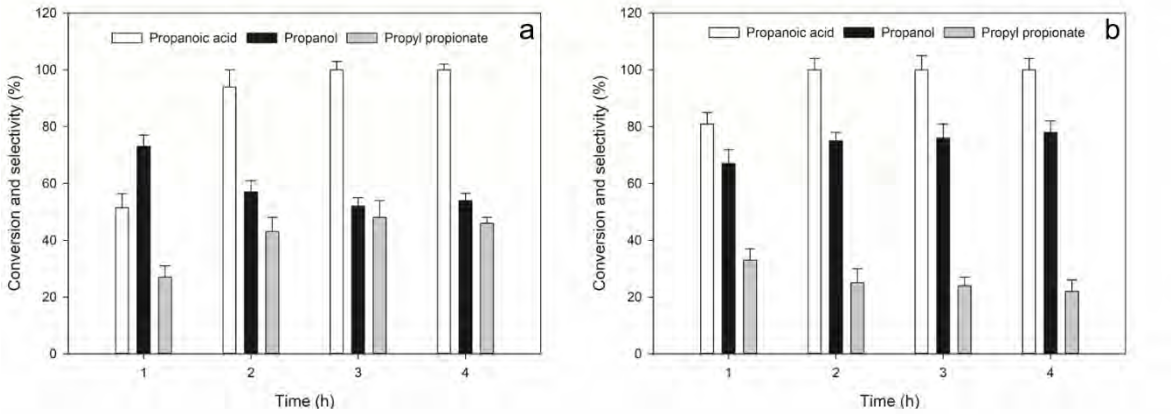

Figure 5.5: *Effect of reaction time on the hydrogenation of propanoic acid over a) 4% Pt/TiO_2, b) 4% Pt-4%Re/TiO_2. Reaction conditions: 0.3 g of 4% Pt/TiO_2/4% Pt-4%Re/TiO_2, 0.2 M initial concentration, H_2 pressure of 40 bar, 50 ml of hexane and batch reaction time of 2 h.*

Butanoic acid conversion increases from 55% to 100% in the range of 1-4 h (Figure 5.6). At the beginning of the reaction, the selectivity of butanol was 87.5% and butyl butyrate was 12.5%. However, as the reaction proceeds from 1-2 h, the selectivity of butanol gradually decreased to 80.4% and subsequently increased to 84.2% from 2-4 h.

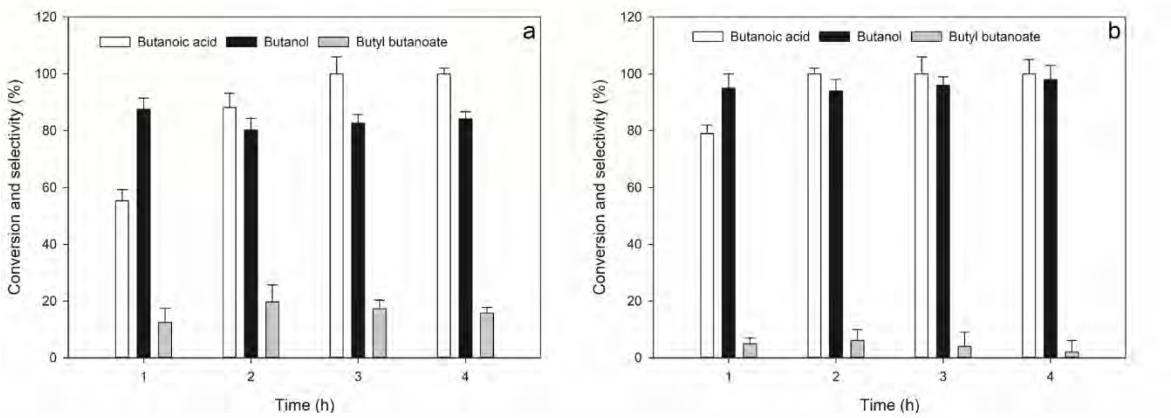

Figure 5.6: *Effect of reaction time on the hydrogenation of butanoic acid over a) 4% Pt/TiO_2, b) 4% Pt-4%Re/TiO_2. Reaction conditions: 0.3 g of 4% Pt/TiO_2/4% Pt-4%Re/TiO_2, 0.2 M initial concentration, H_2 pressure of 40 bar, 50 ml of hexane and batch reaction time of 2 h.*

The effect of reaction time on the hydrogenation of C_2-C_4 carboxylic acids was investigated using 4% Pt-4%Re/TiO_2 as shown in Figures 5.4-5.6. Interestingly, the reactions at different times showed improved conversion of carboxylic acid and alcohol selectivity in all cases compared to 4% Pt/TiO_2, with only 2 h required for reactions to reach completion. It was also observed that the selectivity towards alcohol linearly increases with time due to presence of highly oxophilic Re centers in 4% Pt-4%Re/TiO_2, which was described as essential for enhancing hydrogenation of carboxylic acids and interaction of carbonyl oxygen atom with oxygen vacant sites (Pritchard et al., 2015). Butanoic acid showed the highest alcohol selectivity of ≥ 95% under the different reaction times. In addition, the observed production of butyl butyrate (≤ 5%) can be utilized as an additive in blended fuels towards enhancing ignition properties as also demonstrated by Ali et al., (2011) and Sjöblom et al., (2016). Thus, the utilization of butyl butyrate makes the hydrogenation of butanoic acid more attractive compared to acetic and propanoic acids, towards the upgrading process. Overall, the conversion and selectivity observed over 4% Pt/TiO_2 and 4% Pt-4%Re/TiO_2 could be attributed to sustained oxygen vacancy over time due to the availability of acid sites as presented in Table 4.3.

5.4 Hydrogenation of multi-acid feed

Hydrogenation of multi-acid feed components with 4% Pt/TiO_2 catalyst was carried out to investigate the various reaction pathways for short chain carboxylic acids present in real bio-oil and the mutual interaction they impose on their respective reactivity. Reaction conditions identical to those employed for the hydrogenation of single acids earlier reported was adopted for comparison with the mixed acids.

Figure 5.7 shows the conversions of acetic and propanoic acids in a multiple feed system and their respective product distribution in terms of selectivity. The complete conversion of

both acids was achieved and the formation of their corresponding alcohol and esters was observed. In comparison to the single feed system, the improved conversion of acetic acid and propanoic acid from 98% to 100% and 94% to 100% respectively, suggests enhanced hydrogenation activity in the mixed system. On the other hand, the selectivity towards ethanol and propanol dropped from 46% and 57% to 35% and 37% respectively. Despite the observed drop in alcohol selectivity, an overall improvement in alcohol selectivity (72% selectivity for both ethanol and propanol) was achieved. While ethyl acetate and propyl propionate were formed in a single feed system as the corresponding esters of acetic and propanoic acids respectively, there was additional esterification pathways identified in the mixed system as a result of reactions involving ethanol and propanoic acid, and propanol and acetic acid. This resulted in the formation of ethyl propionate and propyl acetate. In addition, esters of acetic acid such as ethyl acetate (11%) and propyl acetate (8.5%) were found to have a higher ester selectivity compared to their propanoic acid counterparts, such as ethyl propionate (5%) and propyl propionate (3.5%). The order of ester selectivity can be summarized accordingly: ethyl acetate > propyl acetate > ethyl propionate > propyl propionate. One possible explanation to this trend is that acetic acid forms protonated molecules due to the high acidity on 4% Pt/TiO_2 surface, and the inhibitory effect is linked to stronger extent for esterification. Even though more products of ester were formed, the selectivity towards alcohol (72%) was significantly higher than that of esters (28%). This could be attributed to the formation of protonated acetic acid molecules due to the acidic sites present in 4% Pt/TiO_2 which favours esterification products.

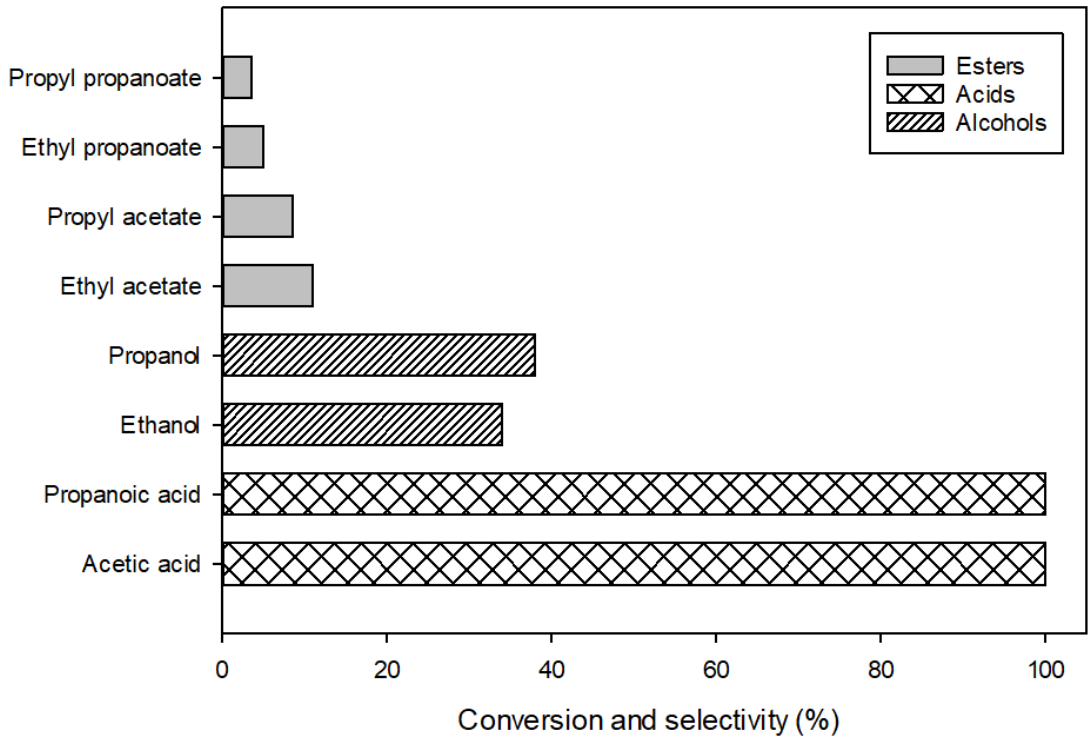

Figure 5.7: *Mixed feed Hydrogenation of acetic acid and propanoic acid. Reaction conditions: 0.3 g of 4% Pt/TiO_2, 0.2 M initial concentration, H_2 pressure of 40 bar, 50 ml of hexane and batch reaction time of 185 °C.*

Mix feed hydrogenation of acetic acid and butanoic acid resulted in complete conversion of acetic acid, whereas butanoic acid conversion slightly improved from 87% to 89% when compared to the single feed (Figure 5.8). In terms of product distribution, butanol (44%) was the major product observed with minimal amount of esters formed. Similar to the mixed feed of acetic acid and propanoic acid, the formation of multiple esters was evident due to additional esterification pathways. Apart from ethyl acetate (11%) and butyl butyrate (3.5%) formed similar to the single feed, ethyl butyrate (6.5%) and butyl acetate (7%) were also formed. Interestingly, the overall selectivity towards the esters was found to be 16% compared to 84% alcohol. Regardless of the increased esterification pathways, the decreased ester selectivity indicates that the hydrogenation pathway was the predominant reaction route.

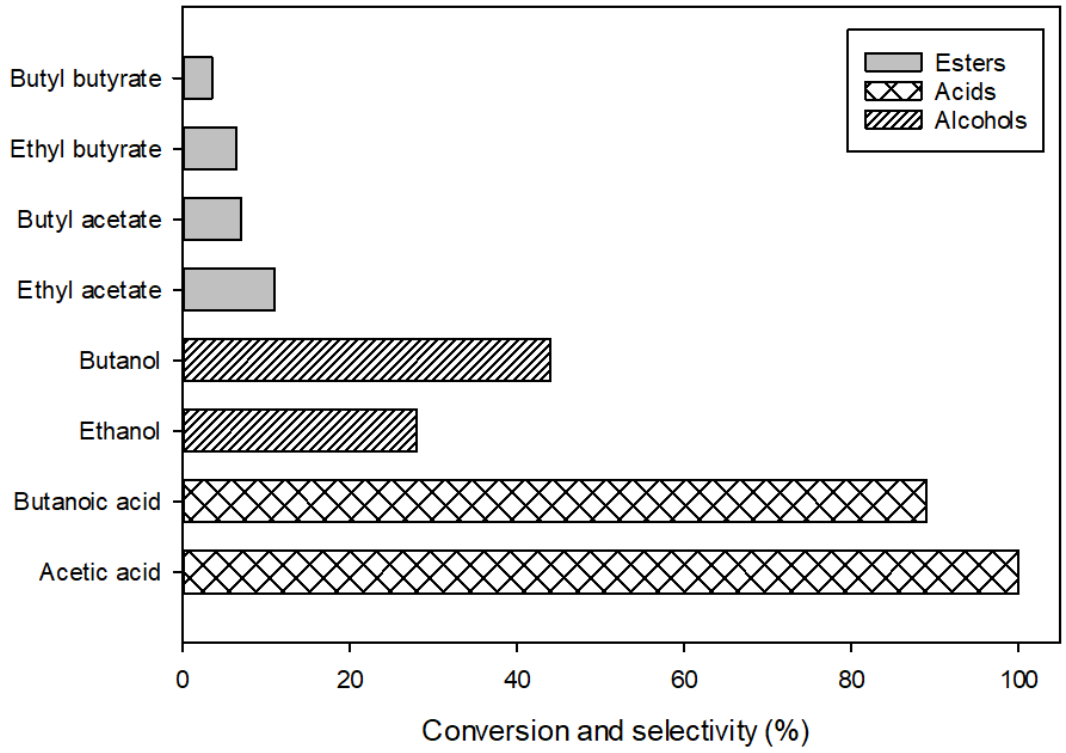

Figure 5.8: *Mixed feed Hydrogenation of acetic acid and butanoic acid. Reaction conditions: 0.3 g of 4% Pt/TiO_2, 0.2 M initial concentration, H_2 pressure of 40 bar, 50 ml of hexane and batch reaction time of 185 °C.*

Figure 5.9 shows the conversion and product distribution for the hydrogenation of propanoic acid and butanoic acid. In contrast to the single feeds, a sharp drop in conversion of acids (78% Propanoic acid and 72% butanoic acid) was observed in the mixed feed. On the other hand, the selectivity towards propanol and butanol were found to be 44% and 51% respectively, which means the overall ester selectivity is 5%. The summary of the esters is as follows: propyl propionate (2%), butyl propionate (1.4%), propyl butyrate (1.1%), butyl butyrate (0.5%). In comparison to other mix feeds which show improved conversions when compared to their single feed, the decreased conversion trend observed for propanoic and butanoic acid mix feed can be linked to suppressed esterification pathway which suggests

dominant hydrogenation pathway to alcohol. This is due to weakly adsorbed propanol and butanol on the catalyst surface (Appendix B), which does not favour consecutive reaction between adsorbed alcohol and unreacted acids. In general, further observation showed that ester selectivity decreases with increasing molecular weight of ester. For the different mix feeds investigated, the mixture of propanoic acid and butanoic acid favoured the most alcohol production (95% selectivity). Furthermore, higher selectivity of butanol over propanol and ethanol was observed in all cases, which is consistent with findings obtained for the single feed.

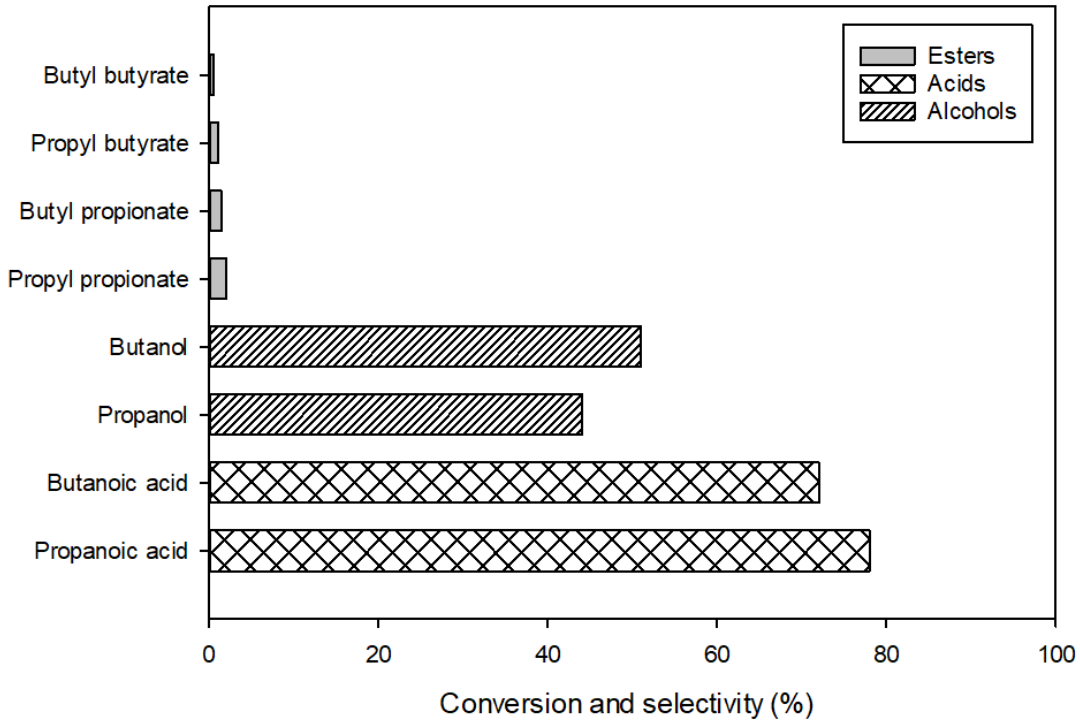

Figure 5.9: *Mixed feed Hydrogenation of propanoic acid and butanoic acid. Reaction conditions: 0.3 g of 4% Pt/TiO_2, 0.2 M initial concentration, H_2 pressure of 40 bar, 50 ml of hexane and batch reaction time of 185 °C.*

The hydrogenation of acetic, propanoic and butanoic acids was investigated as shown in Figure 5.10. It is clear that acetic acid reached 100% conversion while propanoic and

butanoic acids were found to be 77% and 70% respectively. In terms of product selectivity, the three acid feed system favours the significant production of alcohol (96% selectivity) with butanol (50%) observed to be the most dominant alcohol. This observation is supported by the absence of potential esters of butanoic acid such as propyl butyrate and butyl butyrate, though, only ethyl butyrate (0.3%) is formed in negligible quantity. In addition, the weak adsorption strength exhibited by butanol strengthens the trend of alcohol selectivity observed. An overall trend for three acid feed system shows that increasing the length of the alkyl chain decreases the acid conversion whereas the corresponding alcohol selectivity increases. This pattern can be summarized as acetic acid > propanoic acid > butanoic acid, and ethanol < propanol < butanol for acids and alcohols respectively.

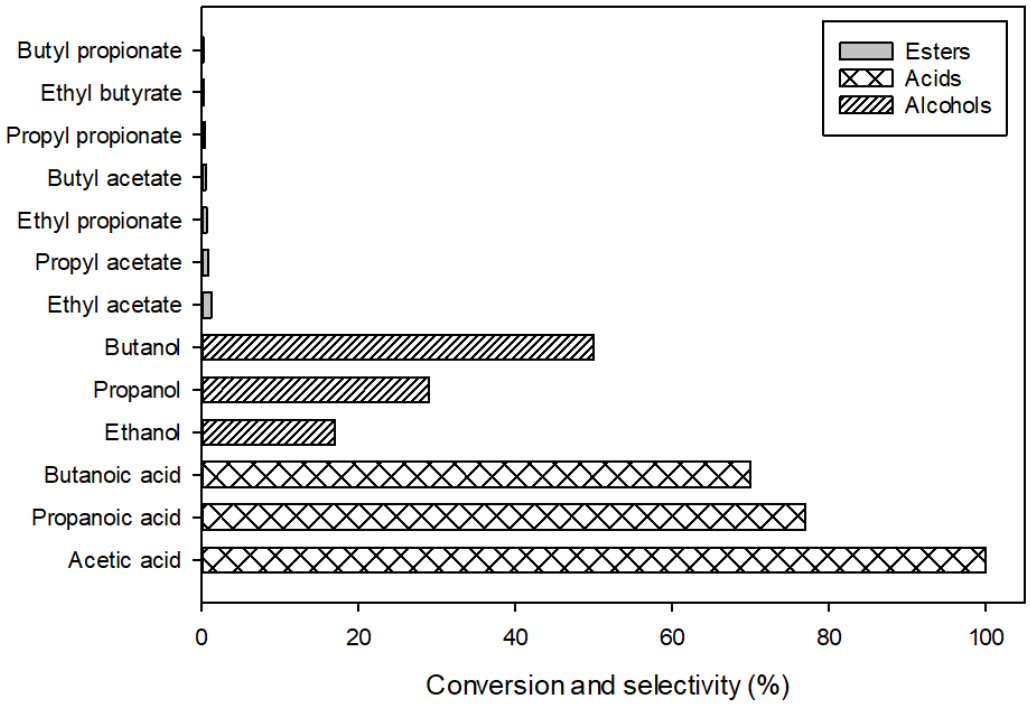

Figure 5.10: *Mixed feed Hydrogenation of acetic acid, propanoic acid and butanoic acid. Reaction conditions: 0.3 g of 4% Pt/TiO_2, 0.2 M initial concentration, H_2 pressure of 40 bar, 50 ml of hexane and batch reaction time of 185 °C.*

Overall, the mixed feed system offers improved acid conversion and alcohol selectivity when compared with single feed system. Most notably, the dominant selectivity of alcohols (≥ 95%) over esters in all cases implies that partial deoxygenation of bio-oil can be achieved via the hydrogenation of C_2-C_4 carboxylic acids. In addition, the presence of partially deoxygenated products such as ethanol (10-15 wt.%) in blended fuel can improve its combustion characteristics and decrease the formation of soot (Ruddy et al., 2014).

5.5. Catalyst Reusability Test

The reusability of 4% Pt/TiO_2 catalyst was investigated by recovering the fresh and 1st reused catalysts at the end of hydrogenation of acetic acid. The recovered catalysts were regenerated for reuse by washing with acetone and drying at 120 °C for 2 h, then subsequent pre-reduction under hydrogen atmosphere for 65 mins. The reusability of the 4% Pt/TiO_2 as function of time is shown in Figure 5.11. The acetic acid conversion and ethanol selectivity followed a similar trend for the fresh, first and second reuse tests carried out. The conversion of acetic acid decreased from fresh to second reuse, likewise, the selectivity towards ethanol production. This slight drop in acetic acid conversion and ethanol selectivity after successive reaction and regeneration can be attributed to the presence of strongly adsorbed carbonaceous deposits as shown in Figure 4.7. In addition, metal leaching could probably result in observed performance drop, as also suggested by Manyar et al., (2010). It can be observed that this drop is very narrow.

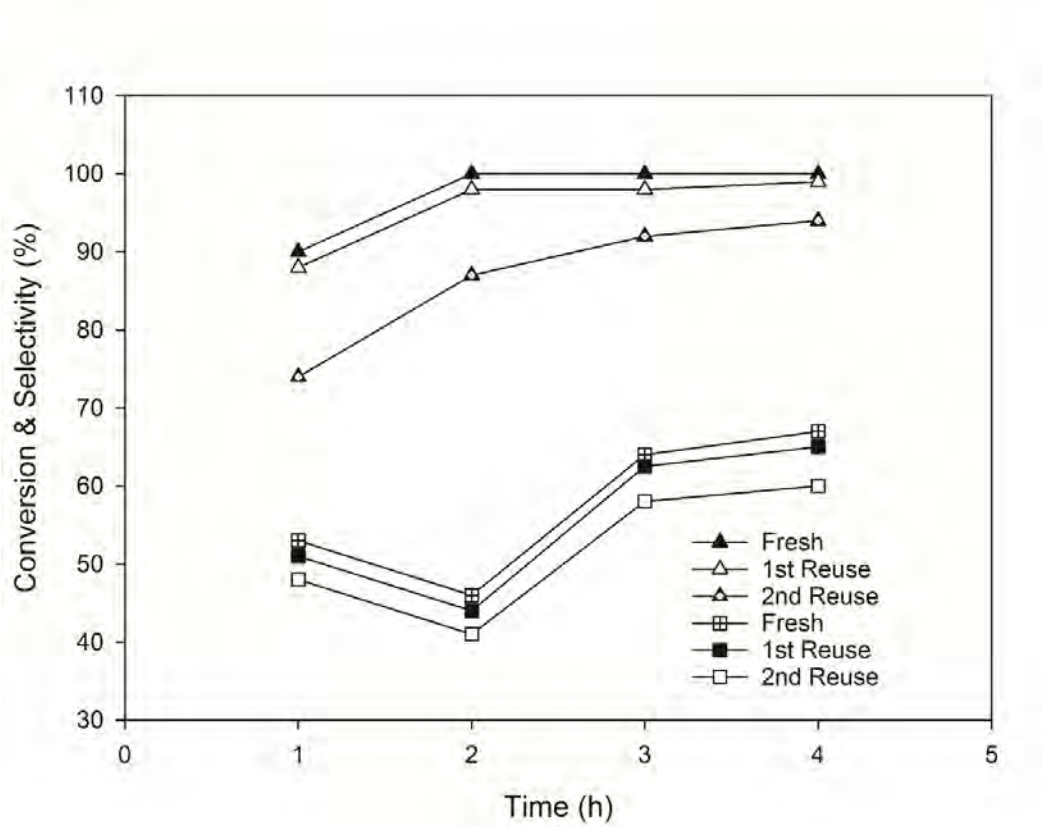

Figure 5.11: *Reusability of monometallic 4% Pt/TiO_2 catalyst is shown by the hydrogenation activity in terms of acetic acid conversion and ethanol selectivity with respect to time. Legend: Triangle, Conversion of acetic acid; Square, Selectivity of ethanol. Reaction conditions: catalyst 0.3 g, initial concentration 0.2 M, temperature 185 °C, pressure 40 bar and hexane 50 ml.*

In all cases, the ethanol selectivity decreased as the reaction time increased from 1 to 2 h and, thereafter, increased as the reaction time increased from 2 to 4 h. The fresh and the two cycles of reuse followed the same pattern with little decrease in the catalyst performance for both conversion and selectivity between the fresh and the first reuse test for 4 h experiment. However, further drop in the catalyst performance was observed for second reuse test for 4 h experiment compared to the fresh catalyst, which suggests minimal 4% Pt/TiO_2 catalyst deactivation attributed to material deposit leading to decreased strength of the active sites.

The reusability of 4% Pt-4%Re/TiO_2 was investigated over the fresh catalyst and two cycles of catalyst reuse (Figure 5.12). In each cycle, both ethanol selectivity and acetic acid conversion increased linearly with time, except for the fresh catalyst which reached complete conversion at the different reaction times. However, catalyst reuse over the two cycles showed a slight decrease in both conversion and selectivity. Most notably is the marginal drop in ethanol selectivity from 86% to 83% and acetic acid conversion from 100% to 94% after 4 h of reaction over the fresh catalyst and second reuse. This suggests that only 3.4% decrease in selectivity and 6% decrease in conversion was observed between the fresh catalyst and second reuse. The minimal drop in activity could be associated to the formation of aggregates on the catalyst surface as shown in Figure 4.9. In comparison between 4% Pt/TiO_2 and 4% Pt-4%Re/TiO_2, it is evident that 4% Pt-4%Re/TiO_2 offers better catalyst stability upon reuse, in terms of both hydrogenation activity and ethanol selectivity, which can be linked to the presence of highly oxophilic Re centres (Mendes et al., 2001; Pritchard et al., 2015). The synergy between Pt and Re enhances the interaction of the carbonyl oxygen atom with the titania support which in turn promotes the hydrogenation activity to produce ethanol.

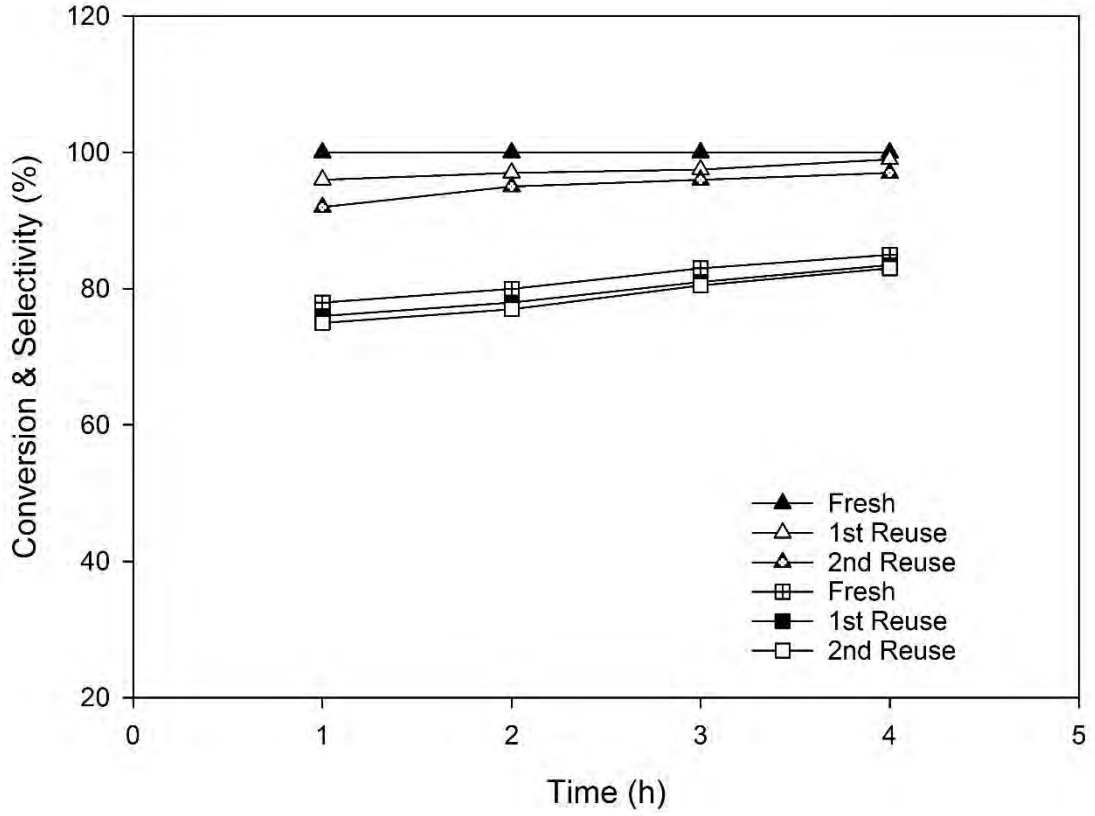

Figure 5.12: *Reusability of monometallic 4% Pt-4%Re/TiO_2 catalyst is shown by the hydrogenation activity in terms of acetic acid conversion and ethanol selectivity with respect to time. Legend: Triangle, Conversion of acetic acid; Square, Selectivity of ethanol. Reaction conditions: catalyst 0.3 g, initial concentration 0.2 M, temperature 185 °C, pressure 40 bar and hexane 50 ml.*

5.6 Effect of Rhenium (Re) loading in Hydrogenation of carboxylic acids

Figure 5.13 shows the conversion and the respective selectivity of ethanol and ethyl acetate for the hydrogenation of acetic acid as a function of the ratio of Pt to Re on a TiO_2 support. The conversion of acetic acid increases as the loading of Re increases from 0 to 4% when the loading of Pt on TiO_2 was held constant (4%). It was reported that higher metal loadings above 4% may cause agglomeration which could be detrimental to catalyst activity (Ma'amor and Hamid, 2006). While the selectivity of ethanol increases as the loading of Re on

the 4% Pt/TiO_2 increases from 0 to 4%, the selectivity of ethyl acetate decreases in a similar manner. This further reinforces the notion that the presence of Re magnifies the hydrogenation reaction towards ethanol production while at the same time suppressing esterification and ethyl acetate formation. This observation is true for the C_2-C_4 carboxylic acids investigated (Figures 5.1-5.6).

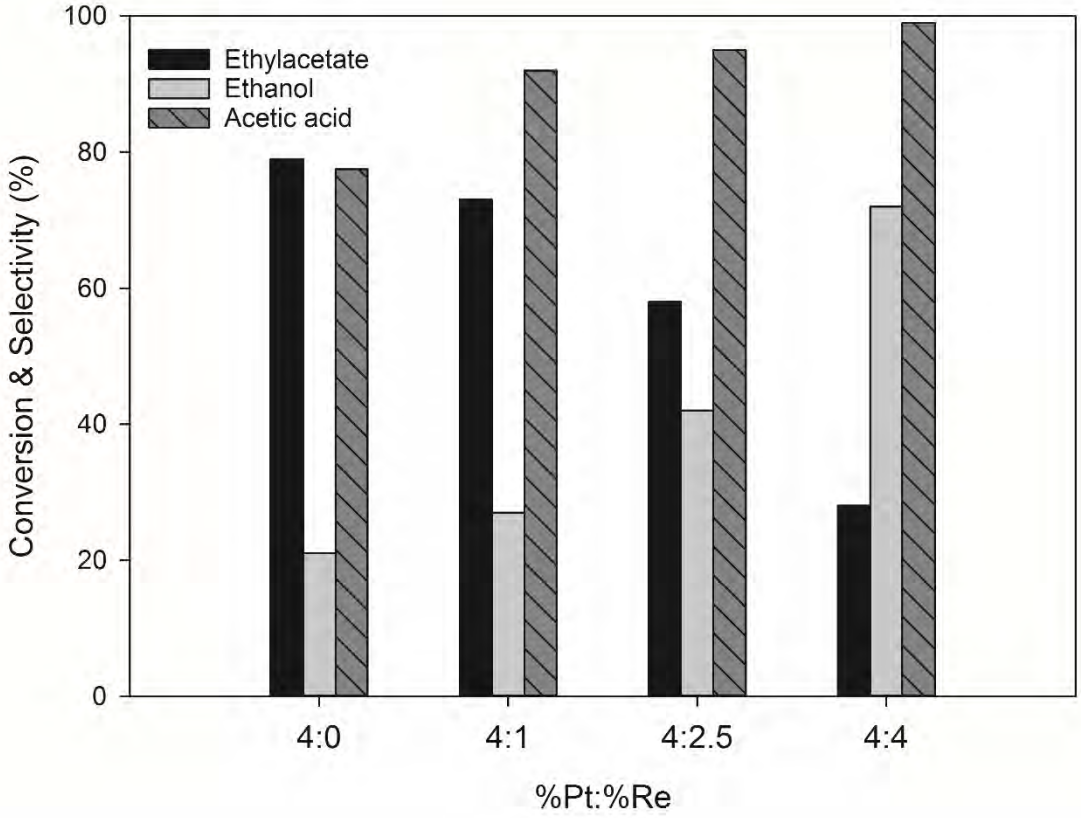

Figure 5.13. *Evaluation of Pt-Re (x:y)/TiO_2 catalysts in the hydrogenation of acetic acid. (Reaction conditions: catalyst 0.3g, initial concentration 0.2 M, reaction time 4h, pressure 40 bar, temperature 200 °C).*

Specifically, as the Re loaded on the 4% Pt/TiO_2 increased from 0 to 4%, the ethanol selectivity increased from around 20 to 74% representing an approximately 73% increase by adding 4% Re to 4% Pt/TiO_2.. A similar effect on acetic acid conversion gives a 22% increase

and for ethyl acetate selectivity there is a 65% decrease. Notably, when 4% Re/TiO_2 was tested alone in the absence of Pt, low acetic acid conversion of about 40% and low ethyl acetate selectivity of about 3% were observed (Figure 4.15). This reaffirms that the presence of Pt exerts much influence on the catalyst activity as observed by increased conversion (H_2 dissociation), and the promotion of the esterification reaction leading to ethyl acetate formation (Figures 4.15, 5.1 and 5.13).

5.7 Conclusions

The hydrogenation of C_2-C_4 carboxylic acids favoured the formation of liquid products (≥ 98%) which were mainly their corresponding alcohols and esters. 4% Pt/TiO_2 and 4% Pt-4%Re/TiO_2 catalysts were also evaluated in terms of temperature and time for the hydrogenation of C_2-C_4 carboxylic acids, which showed that 4% Pt/TiO_2 was selective towards ester production while 4% Pt-4%Re/TiO_2 mostly favoured alcohol formation. Hydrogenation of butanoic acid was found to be more selective toward alcohol than lower molecular weight acids. In all cases, alcohol selectivity was observed to decrease with increased temperature. The order of increasing rate of hydrogenation is the same for single feed and multi-component feed systems as: acetic acid > propanoic acid > butanoic acid. When acetic acid was reacted with either propanoic or butanoic acids in a mixed feed system, a greater number of acetic acid esters were observed and the selectivity towards alcohol was found to be ≥ 72%. The mixture of propanoic acid and butanoic acid was found to favour 95% alcohol selectivity as against 57% and 80% selectivity towards propanol and butanol respectively, in a single feed. When a mix feed of acetic, propanoic and butanoic acids was investigated, the selectivity toward alcohols was significant (96%). The investigation of catalyst reusability for 4% Pt/TiO_2 and 4% Pt-4%Re/TiO_2 showed a minimal drop in performance over fresh and two reuse cycles, which was

attributed to agglomeration. 4% Pt-4%Re/TiO_2 showed a better catalyst performance upon reuse which can be linked to the presence of Re and its interaction with Pt. The effect of Re addition to 4% Pt/TiO_2 was investigated using hydrogenation of acetic acid and showed that acetic acid conversion and ethanol yield were linearly improved on increasing Re from 1 to 4 wt %.

Chapter 6. **Kinetic Study of Acetic Acid Hydrogenation**

6.1 Chapter Overview

This chapter describes the hydrogenation of acetic acid under the regime of kinetics using 4% Pt/TiO_2 catalyst. All experiments were carried out using optimum conditions as established from Chapter four of this study. Firstly, the minimum stirring speed required to achieve thorough particle suspension was calculated. Subsequently, the influence of stirring speed on reaction rates was investigated to determine the extent of external mass transfer. Intra-particle diffusion was investigated as a function of acetic acid conversion and product selectivity. The effect of initial concentration, H_2 pressure, temperature, and catalyst loading were investigated, and kinetic parameters such as activation energy and order of reaction were calculated. Langmuir-Hinshelwood model was fitted to the experimental data based on different model assumptions.

6.2 Mass Transfer Considerations

Catalytic hydrogenation of acetic acid is a three-phase reaction involving hydrogen (gas), reactant medium (liquid) and heterogeneous catalyst (solid). For a chemical reaction to occur, hydrogen has to diffuse from the gas phase into the bulk liquid phase through the gas-liquid boundary layer and subsequently onto the external surface of the catalyst. At the same time, acetic acid is transferred from the bulk liquid phase into the external surface of the catalyst before reaction can occur. Therefore, it is imperative to eliminate external and internal mass transfer limitation as well as intra particle diffusion, to ensure reaction rates were evaluated under kinetic control.

6.2.1 External Mass Transfer

During reactions involving identical temperature and hydrogen pressure, the rate of hydrogen mass transfer in the gas-liquid boundary is determined by k_La, and is mainly influenced by various factors such as the reactor impeller, internal diameter, speed of agitation and type of solid/liquid. For example, Zhang et al., (2002) reported an increase in k_La from of 0.005 s^{-1} to 0.09 s^{-1} as the stirring speed increases from 200 min^{-1} to 1200 min^{-1} during the hydrogenation of lactic acid over ruthenium on carbon catalyst. The extent of agitation speed for a given reaction system and reactor configuration appears to be significant towards the k_La value (Bindwal and Vaidya, 2014; Jain and Vaidya, 2015). Therefore, a minimum stirring speed (N_m) required to ensure complete suspension of 4% Pt/TiO_2 catalyst particles for the present batch system was calculated using the Zwietering correlation (Equation 2.19) and was found to be 588 min^{-1} (Table 6.1). Subsequently, a set of experiments were carried out at varied stirring speeds in the range of 600 min^{-1} to 1400 min^{-1} (all above N_m = 588 min^{-1}) to investigate the effect of agitation on mass transfer rate.

Table 6.1: *Parameters used for the calculation of the minimum speed for the complete suspension of 4% Pt/TiO_2 during the hydrogenation of acetic acid in an autoclave batch reactor.*

Parameter	Value	Description
System geometries:		
$\boldsymbol{d_T}$	3.30 cm	internal diameter of reactor
$\boldsymbol{d_I}$	2.06 cm	diameter of stirrer
β	3.74	constant
Catalyst properties:		
w'	0.874 g (catalyst).100 g (solution)$^{-1}$	% catalyst loading
$\boldsymbol{d_P}$	6.2×10^{-3} cm	average diameter of catalyst particles
$\boldsymbol{\rho_P}$	2.392 $g.cm^{-3}$	catalyst density
Hexane properties:		
$\boldsymbol{\mu_P}$	0.0031 $g.cm^{-1}.s^{-1}$	viscosity
$\boldsymbol{\rho_L}$	0.65 $g.cm^{-3}$	density
Others:		
g	981 $cm.s^{-2}$	gravitational acceleration

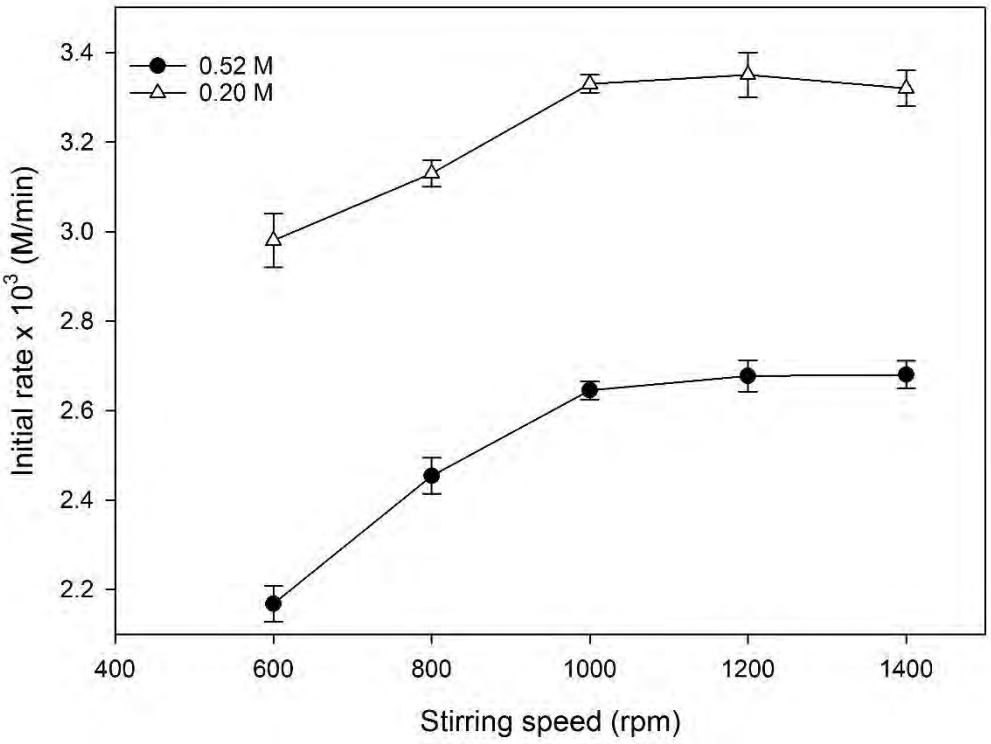

Figure 6.1: *Effect of stirring speed on reaction rates (H_2 pressure, 40 bar; catalyst loading, 0.3 g; temperature, 200 °C and reaction time, 2 h, respectively).*

Figure 6.1 shows the influence of stirring speed on rate of acetic acid hydrogenation at different initial concentrations. As seen in Figure 6.1, it is clear that the reaction rates were strongly dependant on stirring speed between 600-1000 min^{-1}, at which the rates increased from 0.0022 ± 0.04 $M.min^{-1}$ to 0.0026 ± 0.02 $M.min^{-1}$ and 0.0029 ± 0.06 $M.min^{-1}$ to 0.0033 ± 0.02 $M.min^{-1}$ for 0.52 M and 0.20 M respectively. The observed low reaction rates between 600 to 800 min^{-1} indicates the occurrence of gas-liquid mass transfer resistance since the lowest stirring speed of 600 min^{-1} investigated was greater than the calculated minimum speed (N_m = 588 min^{-1}) to ascertain uniform dispersion of the catalyst particles. At stirring speed exceeding 1000 min^{-1}, it was observed that the reaction rates were invariant within experimental error. Therefore, the system was considered free from gas-liquid mass transfer regime at a minimum stirring speed of 1000 min^{-1}. The three phase reactor model in terms of mass transfer resistances can be expressed by:

$$\frac{C_i}{R_A} = \frac{1}{k_{GL}a_B} + \frac{1}{w}\left(\frac{1}{k_{SL}a_P} + \frac{1}{k\eta}\right) \quad 6.1$$

Given:

$\frac{1}{k_{GL}a_B}$ = resistance to gas adsorption

$\frac{1}{k_{SL}a_P} + \frac{1}{k\eta}$ = resistance to liquid-solid mass transfer and internal diffusion with surface reaction.

Mass transfer resistances across the gas-liquid boundary ($1/k_{GL}a_b$) and solid-liquid boundary ($1/k_{SL}a$) at 1000 min^{-1} were estimated experimentally using equation 6.1 and presented in Table 6.2 as demonstrated by Sipos et al., (2014). It is worth noting that equation 6.1 is only valid for reactions with first order reaction kinetics. For non-first order reaction kinetics, the fitted parameters from equation 6.1 can be assumed to be an approximate estimation of the presence or absence of mass transfer limitations, but not for scale-up calculations.

Figure 6.2 shows a plot of the ratio of hydrogen concentration to reaction rate against the inverse of catalyst mass density in a range of 4 – 8 $dm^{-3}.g$. The intercept of the plot represents $1/k_{GL}a_b$, which is the resistance due to gas absorption across the gas-liquid interface and passes through the origin. On the other hand, the slope of the plot $1/k_{SL}a_p + 1/k$ represents the resistance of the solid-liquid interface and surface reaction, and was found to be 499.8 $dm^3.g^{-1}$. Since the gas-liquid mass transfer resistance passes through the origin, it suggests that the mass transfer effect across the gas-liquid interface in the present autoclave system was insignificant. Therefore, a stirring speed of 1000 min^{-1} was used in further hydrogenation experiments.

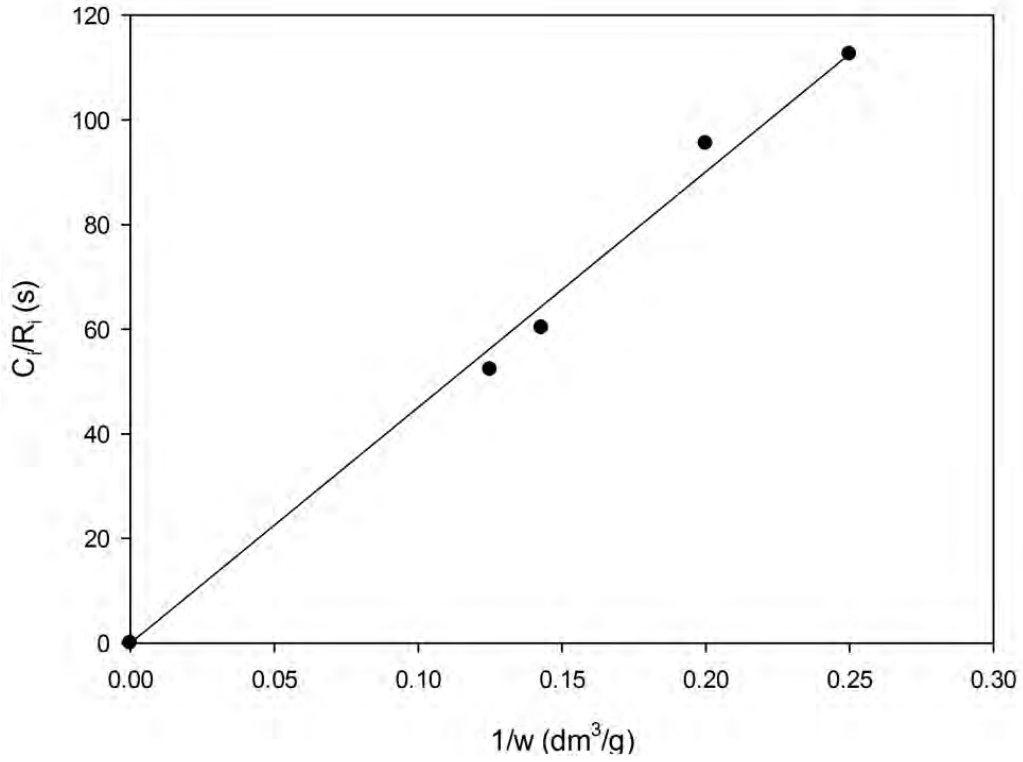

Figure 6.2: *Mass transfer resistances for hydrogen across Gas-Liquid and Solid-Liquid boundaries (reaction conditions: initial concentration, 0.23 M; Stirring speed, 1000 min^{-1}; H_2 pressure, 40 bar; catalyst loading, 0.3 g; temperature, 200 °C and reaction time, 2 h respectively).*

6.2.2 Internal Mass Transfer

The presence of catalytically active sites confined in the pores of spherical catalyst provides the platform for adsorption and reaction to occur. During reactions, the extent of hydrogen and acetic acid diffusion inside the pore network plays a significant role on the rate of reaction which necessitates the investigation of intra particle diffusional resistance. It has been reported in several studies, that the significance of internal diffusion can be evaluated by investigating the particle size influence on reaction rates (Bindwal and Vaidya, 2013; Tike and Mahajani, 2007). Hence, the prepared 4% Pt/TiO_2 was sieved into the following particle size ranges < 63, 63-106, 106-160 and 160-250 μm and used for experiment under the same reaction

conditions. Figure 6.3 shows the conversion of acetic acid and selectivity toward ethanol and ethylacetate as a function of catalyst particle size. While the selectivities of ethanol and ethylacetate are 23.2% and 76.8% respectively, within observed experimental error for the different catalyst size range tested, the conversion of acetic acid narrowly decreases as the catalyst size increases. It can be concluded that the range of catalyst particle sizes investigated show a marginal variation on the hydrogenation activity, thus confirming that pore diffusion limitation can be neglected using the smallest particle size (Akpa et al., 2012; McManus et al., 2015). Therefore, the catalyst with particle size less than 63 μm was chosen for this study because a smaller particle size allows rapid diffusion of reactant and product molecules in and out of the catalyst, since the diffusion path length has been shortened, exposure to active sites enhanced and kinetic control rate enhanced (Singh and Vannice, 2001). Since both inter particle mass transfer and intra particle diffusional resistances have been eliminated under experimental conditions such as agitation speed of 1000 min^{-1} and catalyst particle size ≤63 μm, the reactions are considered to be performed in a kinetically controlled regime. Table 6.2 displays the values of the mass transfer and kinetics parameters obtained.

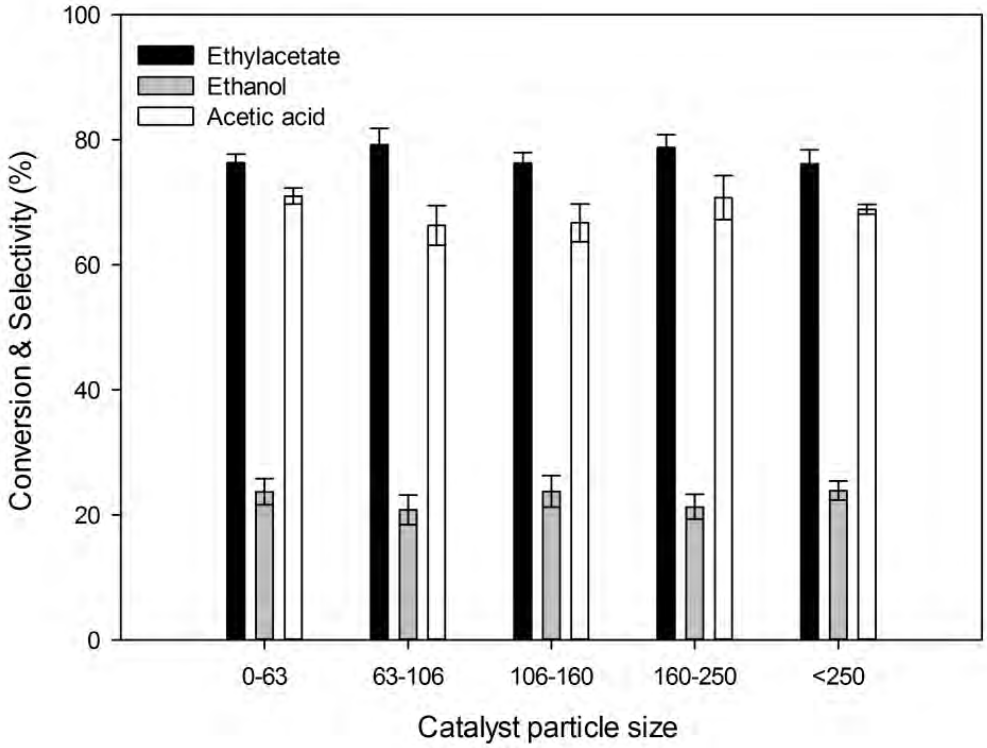

Figure 6.3: *Investigation of internal diffusion using different catalyst particle size (reaction conditions: initial concentration, 0.521 M; H2 pressure, 40 bar; catalyst loading, 0.3 g; temperature, 200 °C; stirring speed, 1000 min^{-1} and reaction time, 2 h, respectively).*

The absence of intra-particle diffusion was further validated by using the Weisz-Prater criterion as shown in equation 6.2 (Bindwal et al., 2012; Jain and Vaidya, 2015). This criterion utilizes the catalyst geometry and verifies the absence of internal diffusion if the measured value is less than 0.3 for reaction orders of ≤ 2 (Singh and Vannice, 2001).

$$\eta\varphi^2 = \frac{r\omega L^2}{C_i D_{e_i}} \qquad 6.2$$

where r is the initial rate, ω is the catalyst loading, L is the characteristic length of spherical particle, C_i is the reactant concentration and D_{ei} is the effective diffusivity. The particle characteristic length and reactants effective diffusivities (D_{ei}) were estimated using $L = \frac{D_p}{6}$ and Wilke-Chang correlations respectively (Wilke and Chang, 1955; Sitaraman et al., 1963; Sporka et al., 1971). The observable modulus $\eta\varphi^2$, which is the ratio of the reaction rate to the effective

diffusion inside the catalyst pores, was found to be much less than 0.3 for both hydrogen and acetic acid (Table 6.2). Therefore, the rate of diffusion within the catalyst pore is greater than the reaction rate; hence, the influence of intra-particle diffusion can be neglected, as the reaction is found to be surface rate limited. The solubility of hydrogen and acetic acid in hexane at various temperatures have been reported elsewhere (Sporka et al., 1971; Wilke and Chang, 1955). Because equilibrium exists between dissolved hydrogen and hydrogen pressure, the concentration of dissolved hydrogen in hexane solvent was estimated by using the Henry's Law correlation as shown in Appendix D (Katayama and Nitta, 1976).

$$C = kP_{H_2} \qquad 6.3$$

where P_{H_2} and k depend on the solubility of H_2 at a given temperature (Brunner, 1985; Katayama and Nitta, 1976). The rate of hydrogen pressure build up in the reaction system increases with temperature which subsequently drops over reaction time as a result of increased hydrogen solubility in the solvent and saturation of catalyst active sites (Appendix D).

Table 6.2: *Values of Weisz-Prater Modulus and parameters used to verify the absence of intra particle diffusion.*

ω (Kg.m^{-3})	6
C_{acetic} (mM)	312
C_{H_2} (mM)	0.75
r ×10^4 (kmol/(kgcat.min))	1.77
L (m)	1.05×10^{-5}
$D_{e,acetic} \times 10^9$ (m^2.s^{-1})	1.49
$D_{e,H_2} \times 10^8$ (m^2.s^{-1})	6.24
$\eta\varphi^2{}_{acetic}$	2.56×10^{-7}
$\eta\varphi^2{}_{H_2}$	2.55×10^{-6}

6.3 Kinetic Study

This study was carried out to examine the effect of reaction variables and estimate kinetic parameters such as reaction order, rate constants and activation energy under isothermal conditions. The method of initial rate (r_0) was used to describe the kinetic data due to the complex reactions involving multiple reaction steps where secondary reactions and products of reaction may influence the rate. During the heat up phase, ≤ 2% conversion of acetic acid was observed under the reaction temperatures investigated. A third order polynomial regression was used to fit the concentration-time data obtained from the experimental mixture at time intervals of 40 mins for 6 h. The reaction rates were calculated by using linearized expressions of the resulting polynomial equation, and the reaction rates at time t=0 were considered as the initial reaction rates (r_0). Furthermore, the reaction order and rate constant values were calculated by plotting the log-log of initial reaction rates versus their corresponding initial concentrations (See equation 6.4). All experiments were performed at a stirring speed of 1000 min^{-1} and catalyst particle size of ≤ 63 μm as established from the mass transfer analysis, to ensure the absence of internal and external mass transfer limitations. As evident from the experimental results, ethanol and ethylacetate were predominantly formed as a result of hydrogenation and esterification reactions. A detailed reaction mechanism will follow describing the reaction pathways.

6.3.1 Initial Concentration

The dependence of reaction rate on the concentrations of reactant species is determined by experimental observation and is described by the linearized expression of power law;

$$\ln r = \ln k + n \ln C_A \qquad 6.4$$

Figure 6.4 shows the concentration-time profile at different initial acetic acid concentration in the range of 0.16 – 0.5 M at 185 °C. Subsequently, rate dependence on initial

acetic acid concentration was investigated at T = 185, 200 and 210 °C in the concentration range 0.16 – 0.5 M. A non-linear reaction rate dependence on initial concentration was established at different temperatures which suggest the reaction exhibited fractional order kinetics as shown in Figure 6.5 (Bindwal et al., 2012). The reaction order from a plot of log r against log C_{AA} at 185, 200 and 200 °C was found to be 0.78, 0.86 and 0.92 (Figure 6.6). In a similar study, Rachmady and Vannice, (2000) reported a lower fractional order in the range of 0.2-0.4 for acetic acid hydrogenation at temperature range 147 °C– 192 °C in a fixed bed reactor.

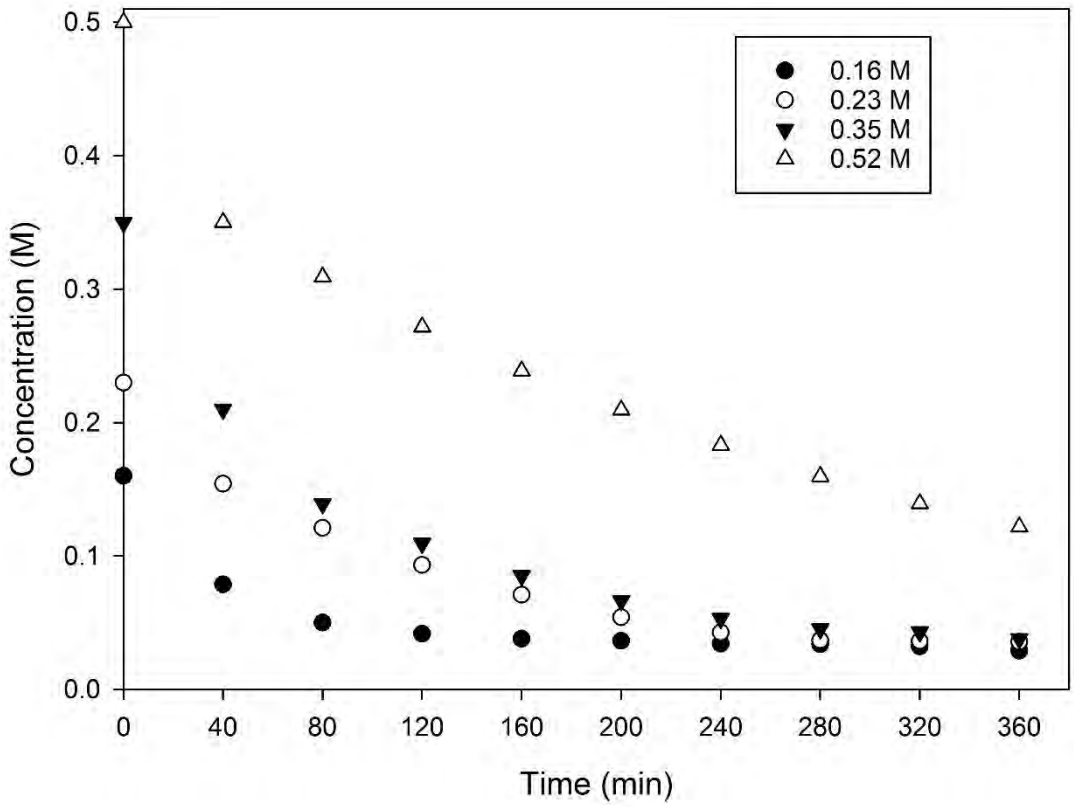

Figure 6.4: *Concentration-Time profile at different concentration (Reaction conditions: catalyst 0.3 g, stirring speed 1000 min^{-1}, temperature 185 °C, pressure 40 bar, hexane 50 ml).*

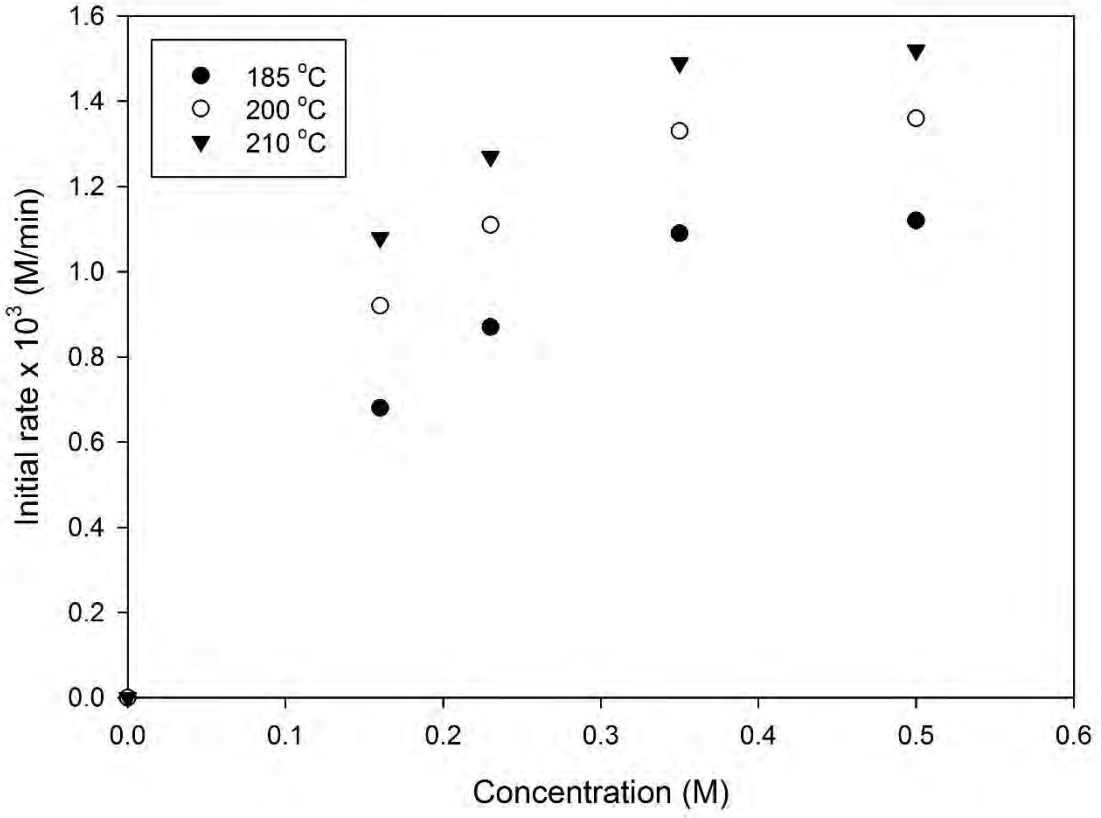

Figure 6.5: *Concentration dependence on rate of disappearance at T = 185, 200 and 210 °C (reaction conditions: H_2 pressure, 40 bar; catalyst loading, 0.3 g).*

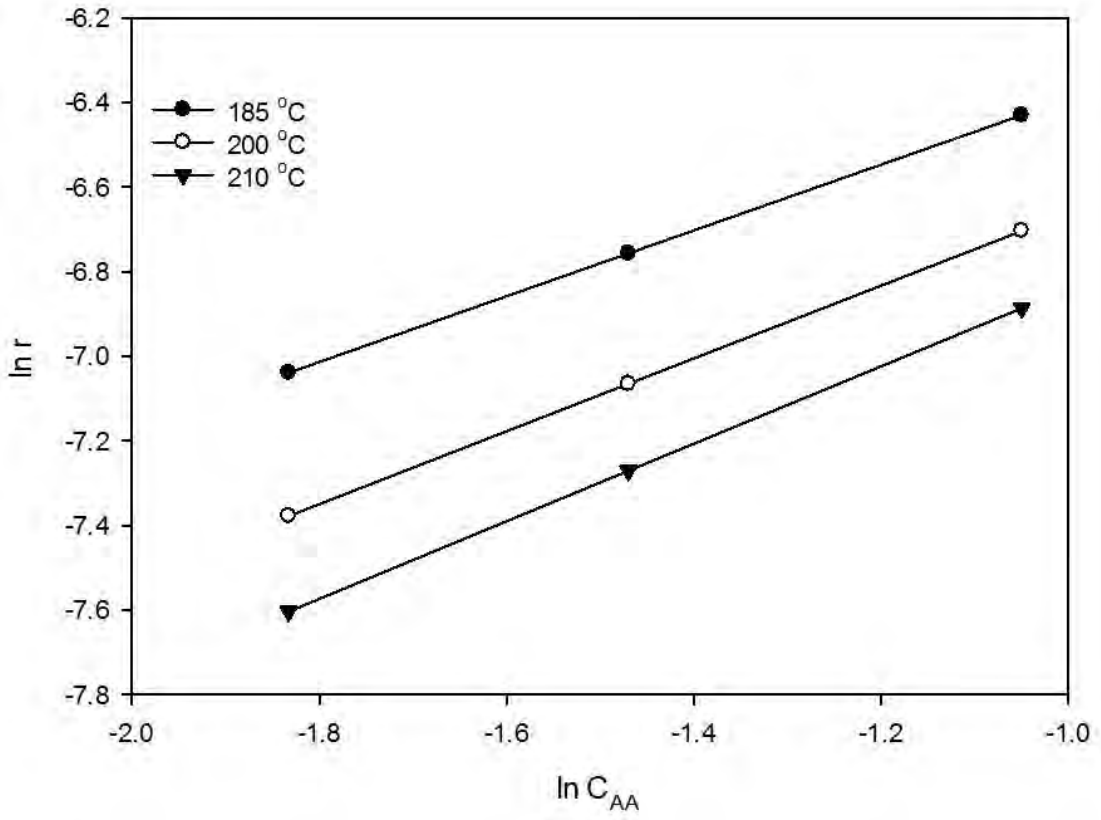

Figure 6.6: *Plots of log r vs log C_{AA} at T = 185, 200 and 210 °C (Reaction conditions: catalyst 0.3 g, pressure 40 bar, hexane 50 ml).*

6.3.2 Temperature

The investigation of activation energy was performed over a temperature range of 185 – 210 °C at 0.35 M of acetic acid, in order to describe temperature dependence on the reaction rate constant. Figure 6.7 shows the Arrhenius plot obtained from the rate constant values estimated at different temperatures from experimental data. Using the Arrhenius equation (see equation 6.5), the activation energy was calculated from the plot to be 48.1 kJ.mol^{-1}. A similar value has been reported in previous studies (Rachmady and Vannice, 2000; Shih and Lee, 1985), which is in agreement to within 4 kJ mol^{-1} obtained in this study. In contrast, Zhou et al., (2017a) studied hydrogenation of acetic acid using Pt-Sn catalyst supported on alumina and reported a value of 19 kJ.mol^{-1}, which might be influenced by mass transfer. Since the

investigation of mass transfer in earlier section of this study confirms the absence of diffusional resistances, the experimental activation energy reported here is the true activation energy and thus the reaction can be considered to be under kinetic control.

$$lnk = ln\, A + \frac{E_A}{RT} \tag{6.5}$$

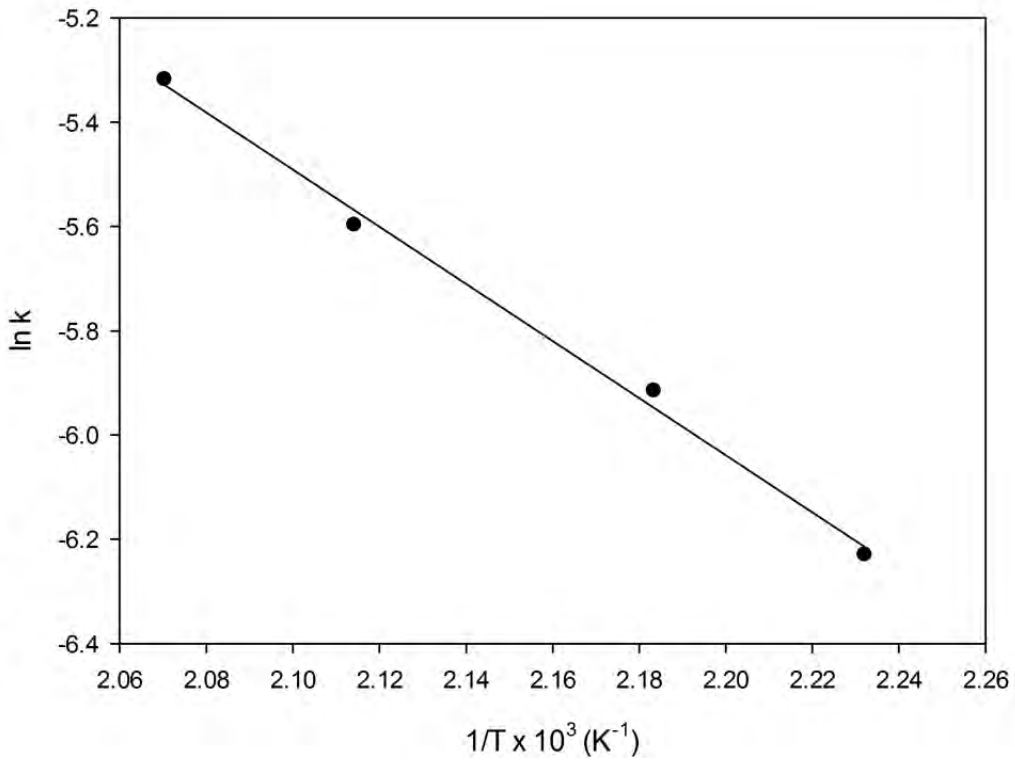

Figure 6.7: *Arrhenius plot for activation energy of acetic acid HDO (reaction conditions: H_2 pressure, 40 bar; catalyst loading, 0.3 g; initial concentration, 0.35M; and reaction time, 6 h respectively).*

6.3.3 Pressure

The effect of hydrogen pressure on the hydrogenation rates was studied in the range of 20-50 bar at a temperature of 200 °C and acetic acid concentration of 0.35 M as shown in Figure 6.8. The dependence of reaction rates on hydrogen pressure shows a non-linear trend which suggests that the reaction order with respect to hydrogen pressure is a fractional order (<1). From the log-log plot of initial rate against hydrogen pressure shown in Figure 6.9, the reaction

order was found to be 0.41, which is characteristic of strongly adsorbed hydrogen on the catalyst surface (Bindwal et al., 2012).

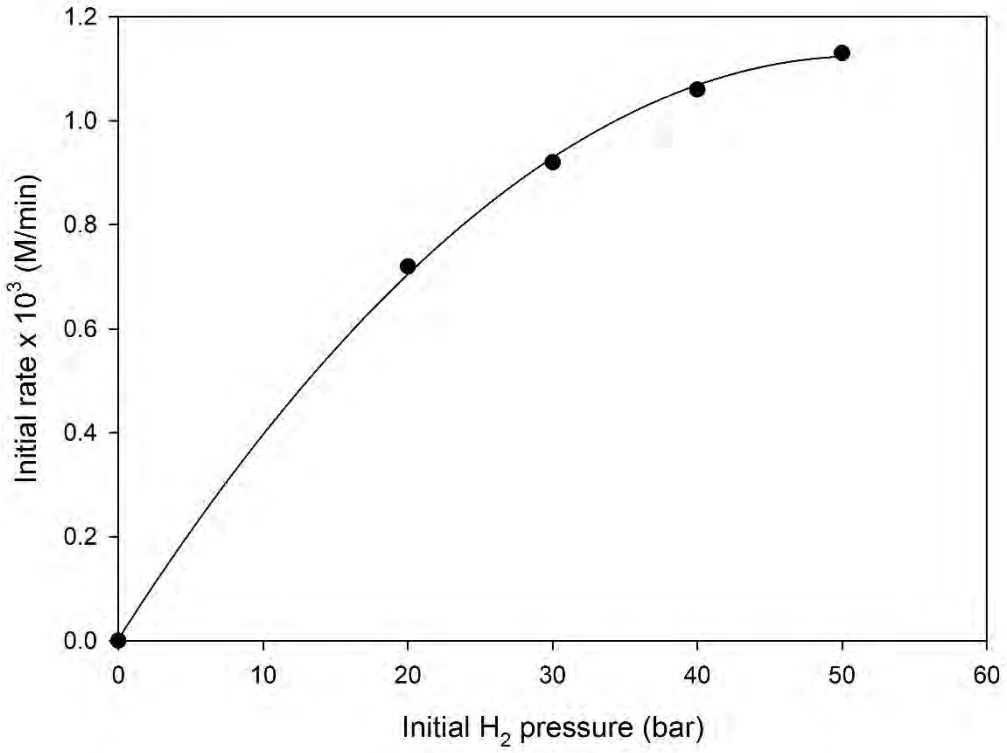

Figure 6.8: *Pressure dependence on reaction rate (reaction conditions: initial concentration, 0.35 M, temperature, 185 °C; catalyst loading, 0.3 g; and reaction time, 6 h respectively).*

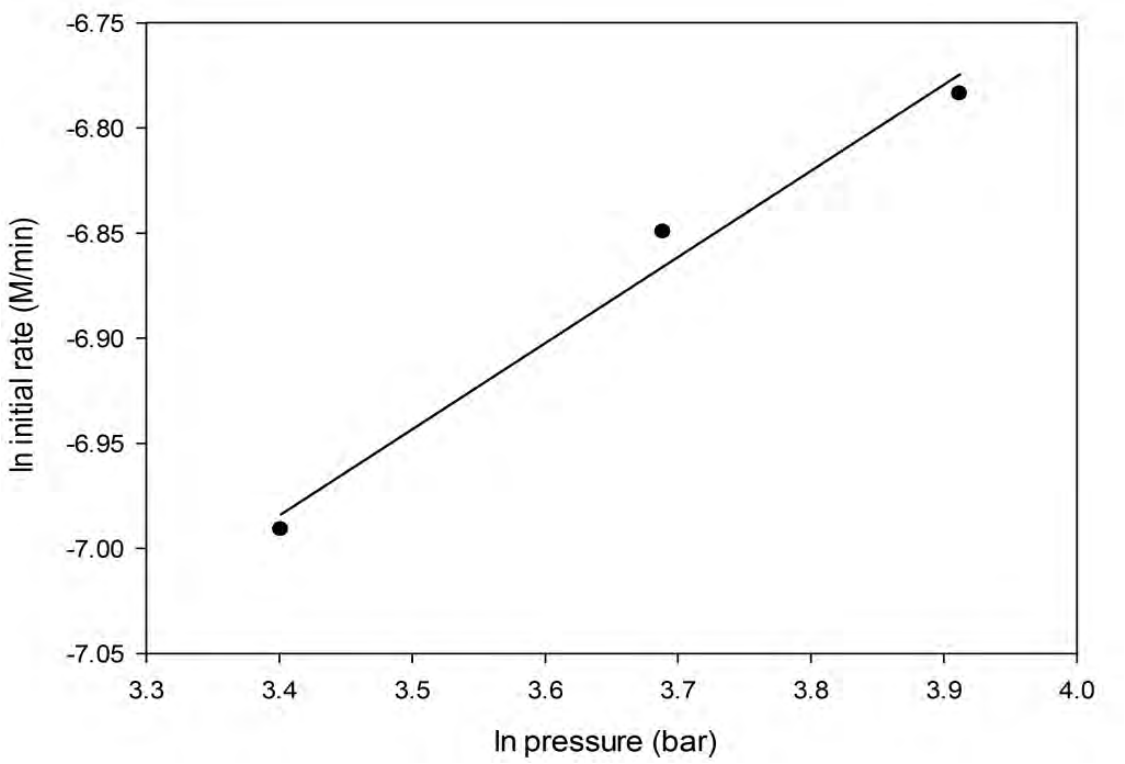

Figure 6.9: *Log-Log plot of initial rate against hydrogen pressure (reaction conditions: initial concentration, 0.35M; catalyst loading, 0.3 g; temperature, 185 ºC and reaction time, 6 h respectively).*

Figure 6.10 shows the influence of hydrogen pressure on acetic acid conversion and the selectivity of ethanol and ethyl acetate production. While acetic acid conversion increased from 75 to 93% as initial hydrogen pressure increased from 30 to 50 bar, the selectivity of ethanol increased and that of ethyl acetate decreased accordingly. This observed increase in acetic acid conversion and ethanol selectivity with increased hydrogen pressure was remarkable and can be attributed to increased adsorption and dissociation of hydrogen by platinum metals. Therefore, increasing hydrogen pressure improves the hydrogenation rate of acetic acid and formation of ethanol. It can also be seen that the production of ethyl acetate appears to be significant at low pressure which indicates that production of ethanol at higher pressure may be associated with increased hydrogen spill over to attack the adsorbed carbonyl group of acetic

acid thereby suppressing the esterification pathway (Kawamoto et al., 2016). To understand the interaction of acetic acid, ethanol and ethyl acetate with the catalyst surface, an adsorption study was carried out to describe the extent of adsorption on the catalyst surface (Appendix B). It is clear that ethanol adsorbs stronger than acetic acid and ethyl acetate to the catalyst, which can be summarised as thus; ethanol > acetic acid > ethyl acetate. Hence, during the HDO reaction of acetic acid, the unreacted acetic acid would have been competing for active sites by reacting with formed ethanol on the catalyst surface. This shows a product inhibitory effect, explaining the higher selectivity of ethyl acetate than that of ethanol at low pressure. At higher pressure, the effect of increased hydrogen spill over from the platinum sites accelerates the rate of hydrogenation which results in higher ethanol production. Several studies have described the kinetics of hydrogenation of acetic acid and proposed that the primary products generated were acetaldehyde, ethanol and ethane via hydrogenation and HDO reactions (Rachmady and Vannice, 2000; Shih and Lee, 1985). In contrast, this study has shown the possibility of esterification, which is a reaction between the formed ethanol and unreacted acetic acid (Figure 6.10).

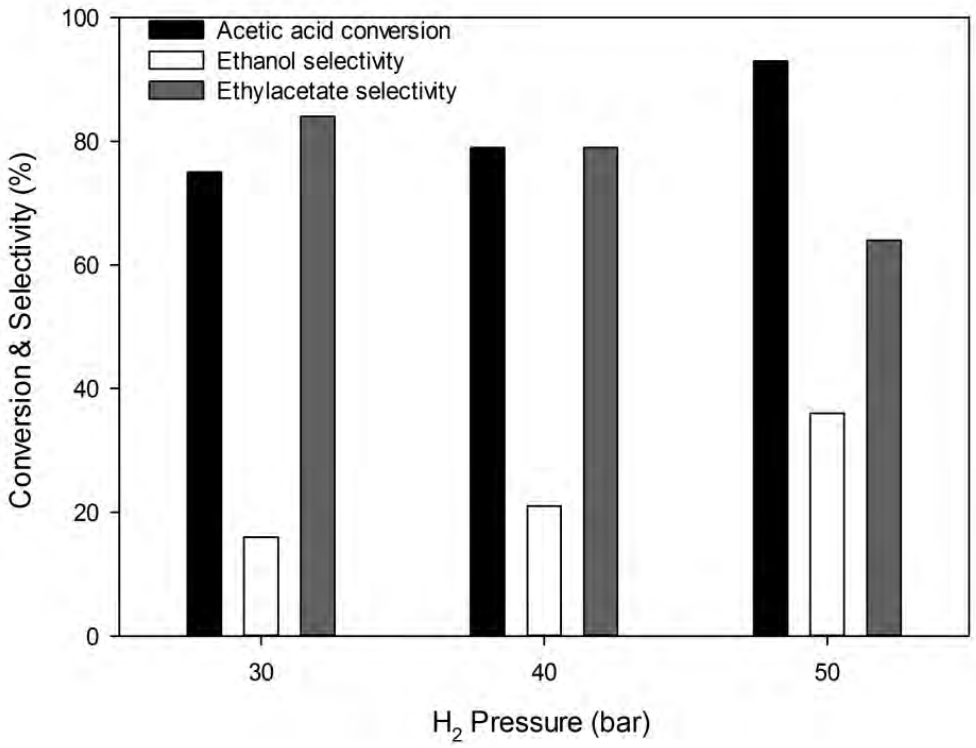

Figure 6.10: *Effect of hydrogen pressure on product distribution (reaction conditions: initial concentration, 0.521 M, temperature, 185 °C; catalyst loading, 0.3 g; and reaction time, 2 h respectively).*

6.3.4 Catalyst Loading

The influence of catalyst on the hydrogenation of acetic acid was studied over 4% Pt/TiO_2 in the range of 0.20 – 0.40 g catalyst loading. Figure 6.11 shows the influence of catalyst loading on initial reaction rate under the conditions employed during hydrogenation. The initial hydrogenation rates increased linearly with increasing catalyst loading through the origin, which further confirms the absence of gas-liquid mass transfer limitation as established from earlier section of this chapter. While increasing the catalyst loading affected the rate of acetic acid hydrogenation by increasing the conversion of acetic acid over the studied range of catalyst loading, selectivity to ethanol increased remarkably from 28 - 58 % while that of ethyl acetate drastically decreased from 71- 41 % (Figure 6.12). This is expected as the esterification is likely

to be a solution phase reaction and therefore its rate is not significantly affected by the catalyst mass.

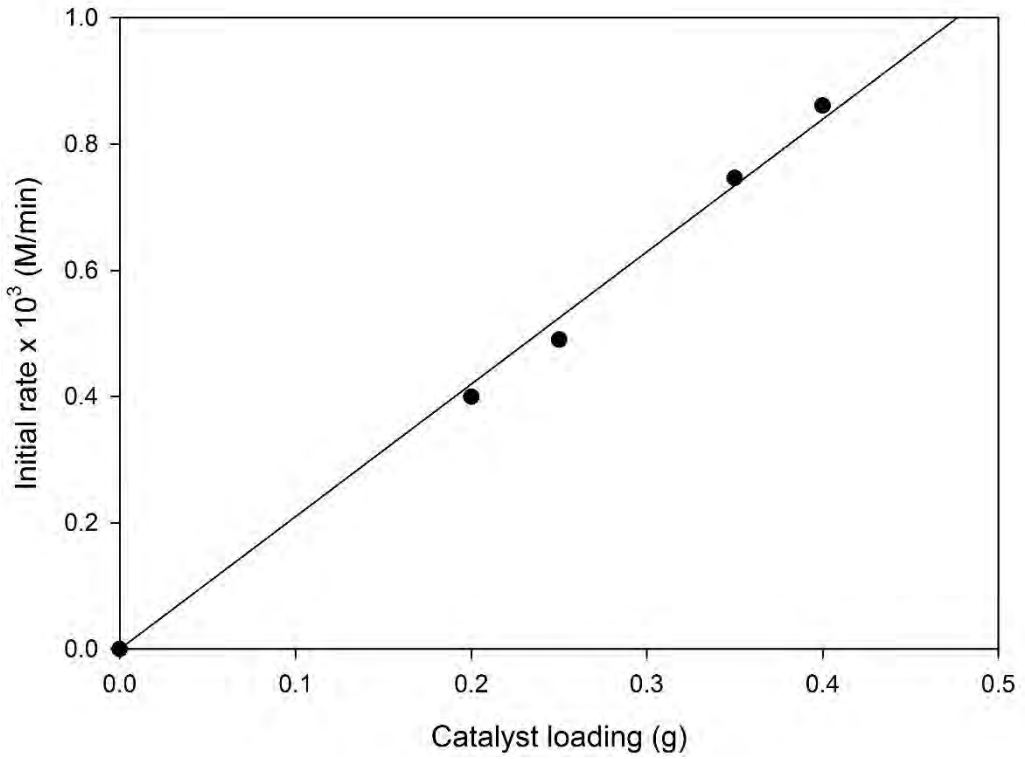

Figure 6.11: *Effect of catalyst loading on initial hydrogenation rates (reaction conditions: initial concentration, 0.350 M, temperature, 185 °C; and H_2 pressure, 40 bar respectively).*

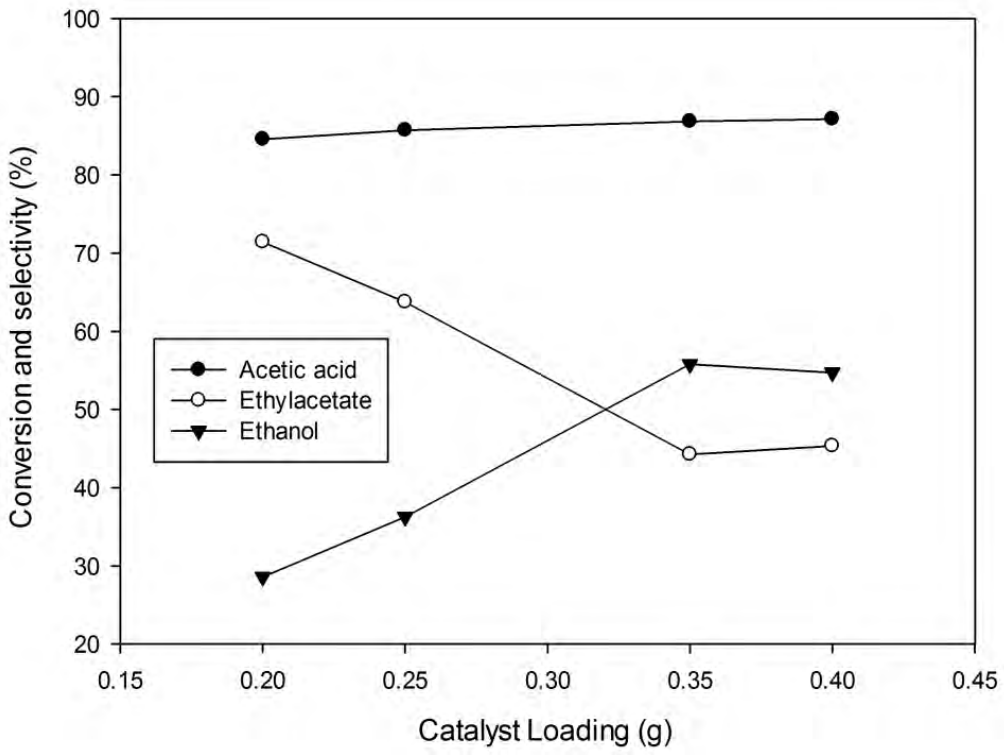

Figure 6.12: *Effect of catalyst loading on product selectivity and acetic acid conversion.*

6.4 Reaction Mechanism and Kinetic Modelling

In this study, Langmuir-Hinshelwood-Hougen-Watson (LHHW) models were used to describe and model the initial rates of acetic acid hydrogenation based on the mechanistic steps presented by Equations 6.6-6.14. Other studies have proposed that the reaction mechanism for acetic acid hydrogenation follows adsorption of acetic acid on the support surface to generate acetyl species which are subsequently hydrogenated to form acetaldehyde and then ethanol (Pallassana and Neurock, 2002; Pestman et al., 1997b). In this study, the production of acetaldehyde was not apparent from the hydrogenation reaction which suggests that acetyl species reacted extremely fast as free radicals with adsorbed hydrogen species to form ethanol (Zhou et al., 2017a). This was further confirmed under GC-MS analysis. The two major products were ethanol as the sole hydrogenation product and ethylacetate as a secondary

product. The significant amount of ethylacetate suggests that the esterification reaction reduced the selectivity to ethanol through its subsequent reaction, with hydrogenation and esterification being consecutive reaction pathways over the catalyst. A catalyst reusability test was carried out to distinguish kinetics from deactivation before interpreting and modelling the kinetic data from batch experiments as reported in Chapter 5. Figure 5.11 shows a clear evolution of catalyst activity as a function of time upon reuse over three cycles which indicates that the C-T profile and reaction rates from kinetic study were not influenced by catalyst deactivation.

Equations 6.6 and 6.7 show the two main reaction observed in this study. Several models have been reported for different mechanisms involving hydrogenation reactions (Bindwal and Vaidya, 2013; Jain and Vaidya, 2015). A model assuming a non-dissociative adsorption of hydrogen was evaluated and was found not to be good as expected with a low activation energy of 30.8 kJ/mol (Appendix C). Therefore, a model assuming dissociative adsorption of hydrogen was considered (equation 6.11). The mechanism and kinetic model was only developed for hydrogenation reaction based on equations 6.6, 6.8-6.10, since only initial reaction rate experimental data was used. In addition, the fitted model is actually a simplification of the model obtained from the mechanism, without considering ethanol adsorption term in the summation of the denominator. This term cannot be fitted using the initial reaction rate experiments because at time t=0, the concentration of ethanol is 0. Thus, the K term represents an apparent constant for the adsorption equilibrium, which is defined differently for other models where hydrogen adsorption is non-dissociative.

Hydrogenation reaction: $CH_3COOH + 2H_2 \rightarrow C_2H_5OH + H_2O$ (6.6)

Esterification reaction: $CH_3COOH + C_2H_5OH \rightarrow CH_3COOC_2H_5 + H_2O$ (6.7)

$H_{2_{(g)}} + 2^* \overset{K_H}{\leftrightarrow} 2H^*$ (6.8)

$$CH_3COOH_{(g)} + {}^{**} \overset{K_{CH_3COOH}}{\longleftrightarrow} CH_3COOH^{**} \quad (6.9)$$

The surface reaction is represented as

$$2H^* + CH_3COOH^{**} \overset{k}{\leftrightarrow} C_2H_5OH \quad (6.10)$$

where ethanol is the main product.

Kinetic model: Competitive adsorption, dissociatively adsorbed H_2;

$$r = \frac{kC_{AA}C_{H_2}^{1/2}}{\left(1+K_{AA}C_{AA}+K_{H_2}C_{H_2}^{1/2}\right)^2} \quad (6.11)$$

The surface reaction is considered to be the rate-determining step as represented in equation 6.10.

The kinetic model was evaluated by using the Excel solver optimization program, minimum values of residual sum of squares (RSS) and coefficient of determination (R^2). The values of RSS were minimized as defined by equation 6.11 where r^{EXP} and r^{CAL} are the experimental and calculated reaction rates respectively (Bindwal and Vaidya, 2013; Jain and Vaidya, 2015).

$$RSS = \sum_i \left(r_{exp} - r_{cal}\right)^2 \quad (6.12)$$

The model fit was considered for 21 points and the resulting correlation based on the R^2 value was calculated by using the relation

$$R^2 = 1 - \frac{RSS}{\sum\left(r^{EXP}-r^{MEAN}\right)^2} \quad (6.13)$$

where r^{MEAN} is the average experimental rates obtained from data analysis. The applicability of the model depends on the significance of R^2 value. Models with negative estimated parameters were considered thermodynamically inconsistent and thus rejected.

Table 6.3: *Values of estimated parameters for kinetic modelling.*

T (°C)	k (kmol/(kgcatmin))	K_{H_2} (m^3/kmol)	K_{AA} (m^3/kmol)	Variance	RSS	R^2
185	1.7 ± 0.02	0.80 ± 0.01	3.94 ± 0.01	5.57×10^{-7}	1.66×10^{-8}	0.970
200	3.7 ± 0.01	0.53 ± 0.06	2.40 ± 0.01	1.19×10^{-7}	3.26×10^{-9}	0.973
210	5.0 ± 0.02	0.21 ± 0.03	1.50 ± 0.01	4.44×10^{-7}	3.35×10^{-9}	0.992

Table 6.3 presents the calculated parameters for adsorption constants, rate constants, RSS, variance and R^2 for the kinetic model. The model adequately described the kinetic data based on the estimated parameters and R^2 values which indicates there is a good agreement between the experimental and predicted rates. Further investigation of temperature dependence on the equilibrium constant and reaction rate constant was carried out using the Van't Hoff expression as shown in equation 6.14.

$$\ln K_{ads} = \left(\frac{-\Delta H_{ads}}{RT}\right) + \left(\frac{\Delta S}{R}\right) \qquad (6.14)$$

where $-\Delta H_{ads}$ is the enthalpy of adsorption, ΔS is the entropy for the molecules, K_{ads} is equilibrium constant, R is gas constant and T is temperature. From Table 6.4, the entropy values for the molecules were negative for the model results which suggest that the reaction is thermodynamically consistent and feasible for adsorption to occur (Rachmady and Vannice, 2000; Vannice et al., 1979). The estimated activation energy based on the predicted rate constants was found to be 80.6 kJ/mol. Thus, the model was deemed to be suitable from the significant R^2 values and high activation energy.

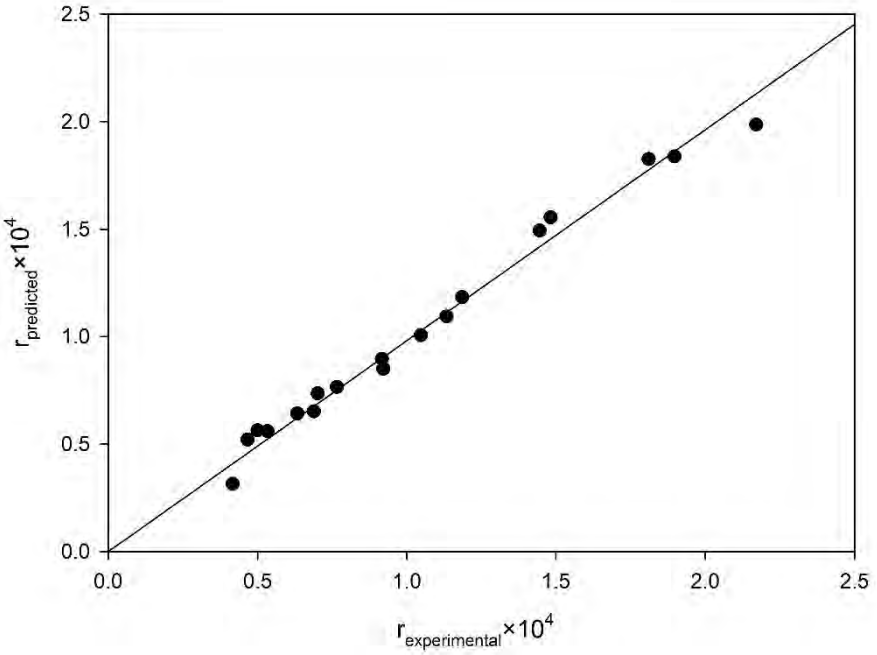

Figure 6.14. *Parity plot for kinetic model assuming competitive adsorption (r^2 = 0.986).*

Table 6.4: *Values of Activation Energy and Heats of Adsorption.*

Parameter	**Value**	**Temperature dependence**
A_1 (kmol.kg$_{cat}^{-1}$.min^{-1})	4.6 ×10^8	k= 4.6 ×10^8 $exp\left(\frac{-9.70}{T}\right)$
E_{act} (kJ.mol^{-1})	80.6	
A_2 (m^3.kmol^{-1})	3.99 ×10^{-8}	K_{AA}= 3.99 ×10^{-8} $exp\left(\frac{8.44}{T}\right)$
ΔH_{AA} (kJ.mol^{-1})	-70.20	
ΔS (kJ.mol^{-1}K^{-1})	-0.142	

6.5 Conclusions

In this study, the reaction kinetics of acetic acid hydrogenation in a 100 mL batch reactor using 4% Pt/TiO_2 catalyst were investigated. The investigated reaction conditions are in the following ranges temperature (185-210 °C), initial concentration (0.16-521 M), initial H_2

pressure (20-50 bar) and catalyst loading (0.20-0.40 g) at which the system belongs to the kinetically controlled regime. A concentration dependence on reaction rate was found to be non-linear with a fractional order of 0.7-0.85. The catalytic hydrogenation of acetic acid follows consecutive reactions which results in the formation of ethanol and ethylacetate via hydrogenation and esterification reaction, respectively with no gas phase products detected. The experimental activation energy was found to be 48.1 $kJ.mol^{-1}$ for the catalytic hydrogenation of acetic acid. It was found that model and the experimental data for the model are positively correlated with $R^2 \geq 0.97$ for all temperatures investigated. The model seemed to be feasible due to the high activation energy and dissociative adsorption of H_2.

Chapter 7. **Conclusions and Future Work**

7.1 Conclusions

The hydrogenation of short chain carboxylic acids mainly acetic, propanoic and butanoic acids was investigated in single and mixed feed systems towards the formation of alcohols. The reactions were carried out in a 100 mL stirred reactor under optimum reaction conditions. The preparation and screening of 4% Pt/TiO_2 and 4% Pt-4%Re/TiO_2 catalysts and comparison against their commercial counterparts was carried out. The kinetics of acetic acid hydrogenation using Langmuir-Hinshelwood model was described. The current study has demonstrated some key findings and limitations, which are listed as follows:

Catalyst Characterization, Catalyst Screening and Process Optimization

This chapter described the results obtained for the characterization of prepared and commercial catalysts used in this study. The prepared catalysts are 4% Pt/TiO_2 and 4% Pt-4%Re/TiO_2, while the commercial catalysts are 5% Pt/SiO_2, 5% Pt/graphite 5% Pt/C and 5% Pt/Al_2O_3. BET results showed that 4% Pt/TiO_2, 4% Pt-4%Re/TiO_2, 4% Pt/SiO_2 and 5% Pt/graphite exhibited a Type IV isotherm with Type 3 hysteresis, while 5% Pt/C and 5% Pt/Al_2O_3 exhibited Type 2 hysteresis. The catalysts with Type 3 hysteresis were found to have a bimodal distribution with peaks in the mesoporous region. The presence of rutile and anatase phases of TiO_2 were the only peaks observed for 4% Pt/TiO_2 and 4% Pt-4%Re/TiO_2 under XRD analysis. The presence of Pt and Re in 4% Pt/TiO_2 and 4% Pt-4%Re/TiO_2 were found to occupy more rutile than anatase phases. The surface morphology of spent 4% Pt/TiO_2 and 4% Pt-4%Re/TiO_2 was distinct from the fresh counterpart due to agglomeration and formation of compact mass. The reduction temperature for 4% Pt/TiO_2 and 4% Pt-4%Re/TiO_2 was found to

be 200 °C according to the H_2-TPR analysis. Catalyst acidity was evaluated using NH_3-TPD analysis which revealed that 4% Pt/TiO_2 contained the highest number of acidic sites (0.48 mmol g^{-1}). The presence of Re in 4% Pt-4%Re/TiO_2 showed decreased acidity compared to 4% Pt/TiO_2 which favours the production of ethanol and suppresses ethyl acetate formation. Catalyst screening test revealed that 4% Pt/TiO_2 and 4% Pt-4%Re/TiO_2 outperformed the commercial catalysts for acetic acid hydrogenation and were found to be more selective towards ethyl acetate and ethanol respectively. The presence of broad bimodal pore size distribution in TiO_2 showed enhanced transfer of reactants into actives sites and product diffusion over 4% Pt/TiO_2 and 4% Pt-4%Re/TiO_2. The application of Taguchi method of optimization revealed that 160 °C, 40 bar H_2, 0.4 g catalyst loading, 1000 min^{-1}, and 4 h were the optimum conditions for ethanol yield. For the conversion of acetic acid, 200 °C, 40 bar H_2, 0.4 g catalyst loading, 1000 min^{-1} and 4 h were found to be the optimum conditions.

Catalytic Hydrogenation of Short Chain Carboxylic Acids

The hydrogenation of C_2-C_4 carboxylic acids was investigated as single feed and multi feed components in terms of product selectivity and acid conversion under identical reaction conditions. This study was carried out over 4% Pt/TiO_2 and 4% Pt-4%Re/TiO_2 catalysts.

For the hydrogenation of C_2-C_4 carboxylic acids as single feed systems, the formation of liquid products was ≥ 98% with 4% Pt/TiO_2 favouring ester formation while 4% Pt-4%Re/TiO_2 favoured alcohol production. These reactions proceeded via a consecutive reaction pathway of hydrogenation followed by esterification to form alcohols and subsequently esters. The effect of reaction temperature over 4% Pt/TiO_2 showed that conversion of C_2-C_4 carboxylic acids and ester selectivity increased with temperature, the conversion of acetic acid increasing from 53 to 100 % over the temperature range 145 to 200 °C. Notably, the conversion of acetic

acid was faster than propanoic and butanoic acids due to the dominant esterification reaction, resulting in higher formation of ethyl acetate compared to propyl propionate and butyl butyrate as respective esters of propanoic and butanoic acids. As the temperature increased, the alcohol selectivity decreased with the hydrogenation of butanoic acid found to give the highest selectivity to alcohol at all temperatures compared to propanoic and acetic acids. The selectivity to butanol and ethanol decreased from 99 to 77% and 52 to 48 % respectively as the temperature increased from 145 to 200 °C. Accordingly, propanol selectivity decreased from 73.4 to 44.9 %. A trend for alcohol selectivity is summarized as: butanol > propanol > ethanol. The hydrogenation reactions over 4% Pt-4%Re/TiO_2 showed improved conversion and alcohol selectivity compared to 4% Pt/TiO_2 for the single feed system. The conversion of C_2-C_4 acids over 4% Pt-4%Re/TiO_2 required only 185 °C to reach completion. Even at 200 °C, the alcohol selectivities were 73% (ethanol), 76.4% (propanol) and 94.3% (butanol) which were significantly higher than for the 4% Pt/TiO_2 catalyst for reaction at 200 °C. The enhanced alcohol selectivity and suppressed ester selectivity is attributed to the promoting effect of Re. After the complete conversion of acetic acid in 2h, de-esterification of ethyl acetate was observed at longer reaction times (2 to 4 h) which gave rise to increased ethanol selectivity from 46 to 67%.

The hydrogenation of a mixed feed system was investigated over 4% Pt/TiO_2 and compared with results from the single feed system under identical reaction conditions. The reaction involving acetic acid with propanoic acid/butanoic acid resulted in improved alcohol selectivity. However, additional esters were formed. When acetic acid reacted with propanoic acid, complete conversion of both acids was observed and selectivity toward alcohols improved to 72% compared to 46% (ethanol) and 57% (propanol) in single feed system. The formation of propyl acetate and ethyl propionate in addition to ethyl acetate and propyl propionate was

observed. Despite additional ester products in the mixed feed, the selectivity to alcohol products (72%) was still significantly higher than that of esters (28%). Similarly, the mixture of propanoic and butanoic acids showed improved alcohol selectivity (96%) as against 57% and 80% selectivity towards propanol and butanol respectively, in a single feed. The mixed feed involving the three acids showed that propanoic and butanoic acids conversion dropped from 94 to 77% and 88.2 to 70% respectively, while acetic acid conversion maintained 100% conversion when compared with single feed. The observation showed that the presence of acetic acid in the mixture led to a competitive effect which inhibited the higher formation of propanol and butanol. However, alcohol selectivity remained dominant (96%) with selectivity of 50% selectivity towards butanol, while propanol and ethanol were 37% and 19% respectively. The suitability and stability of 4% Pt/TiO_2 and 4% $Pt\text{-}4\%Re/TiO_2$ towards the hydrogenation of acetic acid was investigated which showed that catalyst reuse can be carried out over three cycles for 4 hours.

Kinetics of Acetic acid hydrogenation

The kinetics of acetic acid hydrogenation using the formulated 4% Pt/TiO_2 in a batch reactor was investigated. External mass transfer and diffusional resistance were examined to ensure the system was in the kinetically controlled regime under the investigated reaction conditions. It was found that a stirring speed of 1000 min^{-1} and catalyst particle size of < 65 µm were sufficient to overcome external and internal mass transfer limitations respectively. The Weisz-Prater modulus for hydrogen and acetic acid were found to be 2.56×10^{-7} and 2.55×10^{-6} respectively, which verified the absence of internal mass transfer limitation. A non-linear trend of concentration (0.160-0.521 M) against reaction rates was established, while the reaction order was found to be 0.7-0.85. The experimental rate constants at the investigated reaction temperatures were 0.0318 $mol^{0.2}.L^{0.8}.kgcat^{-1}.min^{-1}$ (175 °C), 0.0423 $mol^{0.2}.L^{0.8}.kgcat^{-1}.min^{-1}$

(185 °C), 0.0622 $mol^{0.2}.L^{0.8}.kgcat^{-1}.min^{-1}$ (200 °C) and 0.0817 $mol^{0.2}.L^{0.8}.kgcat^{-1}.min^{-1}$ (210 °C), respectively, with a resulting activation energy of 48.1 kJ mol^{-1}. The effect of hydrogen pressure (20-50 bar) on initial reaction rate was examined and was found to have a fractional order < 1, which indicates a strong adsorption of hydrogen on the catalyst surface. At elevated pressures from 20-50 bar, the reaction rate favoured the selective formation of ethanol from 18% at 20 bar to 40 % at 50 bar, while ethyl acetate diminished as a result of suppressed esterification. The effect of catalyst mass (0.2-0.4 g) on the initial reaction rates increased linearly through the origin, thus, confirming the absence of gas-liquid mass transfer limitation. A Langmuir-Hinshelwood kinetic model assuming dissociative adsorption of hydrogen was used to describe the experimental data. The model parameters were estimated by using a Solver function of MS Excel software. A strong fit ($R^2 \geq 0.97$) between experimental and predicted reaction rates was obtained for all the temperatures investigated. The predicted values of the activation energy and pre exponential factors for acetic acid were found to be 80.6 kJ mol^{-1} and 4.6×10^{-7} $kmol.kgcat^{-1}.min^{-1}$, respectively.

7.2 Future Works and Recommendations

Due to constraints several experiments and analysis could not be performed within the scope of this work and thus recommended for future work as follows:

- To study the kinetics of propanoic and butanoic acids under conditions reported for acetic acid in this study.
- To perform the hydrogenation of acetic, propanoic and butanoic acids using a continuous flow reactor and compare kinetic parameters with those of batch system.

- To study the HDO of mixed feed system involving short chain carboxylic acids and other model compounds typically found in bio-oil using 4% Pt/TiO_2 and 4% Pt-4%Re/TiO_2.
- To investigate the degree of deoxygenation in real bio-oil using the reaction conditions reported for carboxylic acids in this study.
- To investigate the stability of 4% Pt/TiO_2 and 4% Pt-4%Re/TiO_2 over more than 3 reaction cycles reported in this study.
- To perform Thermo Gravimetric Analysis (TGA) on spent 4% Pt/TiO_2 and 4% Pt-4%Re/TiO_2, in order to identify potential deposition of materials on the catalyst surface.
- To perform Inductively Coupled Plasma Mass Spectrometry (ICP-MS) analysis of the product mixture, in order to investigate leaching of metals present in 4% Pt/TiO_2 and 4% Pt-4%Re/TiO_2 after reactions.

List of Publications and Conferences

Journal Publications

Lawal, A.M., Hart, A., Daly, H., Hardacre, C., Wood, J., 2019. Catalytic Hydrogenation of Short Chain Carboxylic Acids Typical of Model Compound Found in Bio-Oils. Ind. Eng. Chem. Res. 58, 7998–8008.

Lawal, A.M., Hart, A., Daly, H., Hardacre, C., Wood, J., 2019. Kinetics of Hydrogenation of Acetic Acid over Supported Platinum Catalyst. Energy Fuels 33, 5551–5560.

Conferences

Catalytic Hydrogenation of Short Chain Carboxylic Acids Typical of Model Compounds Found in Bio-oils. NASCRE 4: 4th North American Symposium on Chemical Reaction Engineering. Houston Texas, 2019. (Poster)

Kinetic Study of Hydrodeoxygenation of Acetic Acid. ChemEngDayUK 2018: Molecules to Manufacturing. Leeds, 2018. (Poster)

Catalytic Upgrading of Bio-oil via Hydrodeoxygenation. IChemE Catalysis and Reaction Engineering Symposium. Sheffield, 2017. (Poster)

References

Abida, B., Chirchi, L., Baranton, S., Napporn, T.W., Kochkar, H., Léger, J.-M., Ghorbel, A., 2011. Preparation and characterization of Pt/TiO2 nanotubes catalyst for methanol electro-oxidation. Appl. Catal. B Environ. 106, 609–615.

Akpa, B.S., D'Agostino, C., Gladden, L.F., Hindle, K., Manyar, H., McGregor, J., Li, R., Neurock, M., Sinha, N., Stitt, E.H., Weber, D., Zeitler, J.A., Rooney, D.W., 2012. Solvent effects in the hydrogenation of 2-butanone. J. Catal. 289, 30–41.

Akpa, B. S., D'Agostino, C., Gladden, L.F., Hindle, K., Manyar, H., McGregor, J., Li, R., Neurock, M., Sinha, N., Stitt, E.H., Weber, D., Zeitler, J.A., Rooney, D.W., 2012. Solvent effects in the hydrogenation of 2-butanone. J. Catal. 289, 30–41.

Alcala, R., Shabaker, J.W., Huber, G.W., Sanchez-Castillo, M.A., Dumesic, J.A., 2005. Experimental and DFT Studies of the Conversion of Ethanol and Acetic Acid on PtSn-Based Catalysts. J. Phys. Chem. B 109, 2074–2085.

Ali, S.H., Al-Rashed, O., Azeez, F.A., Merchant, S.Q., 2011. Potential biofuel additive from renewable sources – Kinetic study of formation of butyl acetate by heterogeneously catalyzed transesterification of ethyl acetate with butanol. Bioresour. Technol. 102, 10094–10103.

Ardiyanti, A.R., Gutierrez, A., Honkela, M.L., Krause, A.O.I., Heeres, H.J., 2011. Hydrotreatment of wood-based pyrolysis oil using zirconia-supported mono- and bimetallic (Pt, Pd, Rh) catalysts. Appl. Catal. Gen. 407, 56–66.

Athreya, S., Venkatesh, D.Y.D., 2012. Application of Taguchi Method for Optimization of Process Parameters in Improving the Surface Roughness of Lathe Facing Operation. IRJES 1, 13–19.

Averill, B., Eldredge, P., 2007. Principles of General Chemistry. McGrawHill.

Bahruji, H., Bowker, M., Brookes, C., Davies, P.R., Wawata, I., 2013. The adsorption and reaction of alcohols on TiO2 and Pd/TiO2 catalysts. Appl. Catal. Gen. 454, 66–73.

Bamwenda, G.R., Tsubota, S., Nakamura, T., Haruta, M., 1997. The influence of the preparation methods on the catalytic activity of platinum and gold supported on TiO2 for CO oxidation. Catal. Lett. 44, 83-87.

Barbara, L.D., Christine, M.C., 2019. X-ray Powder Diffraction (XRD). Retrieved from https://serc.carleton.edu/research_education/geochemsheets/techniques/XRD.html.

Bartholomew, C.H., 2001. Mechanisms of catalyst deactivation. Appl. Catal. Gen. 212, 17–60.

Basagiannis, A.C., Verykios, X.E., 2008. Influence of the carrier on steam reforming of acetic acid over Ru-based catalysts. Appl. Catal. B Environ. 82, 77–88.

Baskar, C., Baskar, S., Dhillon, R.S., 2012. Biomass Conversion: The Interface of Biotechnology, Chemistry and Materials Science. Springer Science & Business Media.

Beamson, G., Papworth, A.J., Philipps, C., Smith, A.M., Whyman, R., 2011. Selective hydrogenation of amides using bimetallic Ru/Re and Rh/Re catalysts. J. Catal. 278, 228–238.

Bergem, H., Xu, R., Brown, R.C., Huber, G.W., 2017. Low temperature aqueous phase hydrogenation of the light oxygenate fraction of bio-oil over supported ruthenium catalysts. Green Chem. 19, 3252–3262.

Betizeau, C., Leclercq, G., Maurel, R., Bolivar, C., Charcosset, H., Frety, R., Tournayan, L., 1976. Platinum-rhenium-alumina catalysts: III. Catalytic properties. J. Catal. 45, 179–188.

Bindwal, A.B., Bari, A.H., Vaidya, P.D., 2012. Kinetics of low temperature aqueous-phase hydrogenation of model bio-oil compounds. Chem. Eng. J. 207–208, 725–733.

Bindwal, A.B., Vaidya, P.D., 2014. Reaction kinetics of vanillin hydrogenation in aqueous solutions using a Ru/C catalyst. Energy Fuels 28, 3357-3362.

Bindwal, A.B., Vaidya, P.D., 2013. Kinetics of Aqueous-Phase Hydrogenation of Levoglucosan over Ru / C Catalyst. Ind. Eng. Chem. Res. 52, 17781−17789.

Bockrath, R.E., Campos, D., Schwartz, J.-A.T., Stimek, R.T., 1999. United States Patent: 6008384 - Method and Ru,Re,Sn/carbon catalyst for hydrogenation in aqueous solution. 6008384.

Boffa, A., 1993. Vanadium Oxide Deposited on an Rh Foil: CO and CO2 Hydrogenation Reactivity. J. Catal. 139, 602–610.

Bridgwater, A.V., 2012. Review of fast pyrolysis of biomass and product upgrading. Biomass Bioenergy 38, 68–94.

Bridgwater, A.V., 2011. Upgrading Fast Pyrolysis Liquids, in: Brown, R.C. (Ed.), Thermochemical Processing of Biomass. John Wiley & Sons, Ltd, pp. 157–199. https://doi.org/10.1002/9781119990840.ch6

Bridgwater, A.V., 2010. Chapter 7: Fast Pyrolysis of Biomass for Energy and Fuels, in: Thermochemical Conversion of Biomass to Liquid Fuels and Chemicals. pp. 146–191.

Broadbent, H.S., CAMPBELL, G.C., BARTLEY, W.J., JOHNSON, J.H., 1959. Rhenium and Its Compounds as Hydrogenation Catalysts. III. Rhenium Heptoxide1,2,3. J. Org. Chem. 24, 1847–1854.

Broadbent, H.S., Whittle, C.W., 1959. Rhenium and Its Compounds as Hydrogenation Catalysts. II. Rhenium Heptaselenide1,2. J. Am. Chem. Soc. 81, 3587–3589.

Brunner, E., 1985. Solubility of Hydrogen in 10 Organic Solvents at 298.15, 323.15, and 373.15 K. J. Chem. Eng. Data 30, 269–273.

Bu, Q., Lei, H., Zacher, A.H., Wang, L., Ren, S., Liang, J., Wei, Y., Liu, Y., Tang, J., Zhang, Q., Ruan, R., 2012. A review of catalytic hydrodeoxygenation of lignin-derived phenols from biomass pyrolysis. Bioresour. Technol. 124, 470–477.

Bui, V.N., Laurenti, D., Delichère, P., Geantet, C., 2011. Hydrodeoxygenation of guaiacol: Part II: Support effect for CoMoS catalysts on HDO activity and selectivity. Appl. Catal. B Environ. 101, 246–255.

Campanati, M., Fornasari, G., Vaccari, A., 2003. Fundamentals in the preparation of heterogeneous catalysts. Catal. Today 77, 299–314.

Campos, D., Ernst, R.E., Michel, J.B., 2003. United States Patent: 6566539 - Catalyst regeneration by treatment with an oxidizing agent. 6566539.

Centeno, A., Laurent, E., Delmon, B., 1995. Influence of the Support of CoMo Sulfide Catalysts and of the Addition of Potassium and Platinum on the Catalytic Performances for the Hydrodeoxygenation of Carbonyl, Carboxyl, and Guaiacol-Type Molecules. J. Catal. 154, 288–298.

Centeno, A., Maggi, R., Delmon, Bernard, 1999. Use of noble metals in hydrodeoxygenation reactions, in: Delmon, B., Froment, G.F., Grange, P. (Eds.), Studies in Surface Science and Catalysis, Hydrotreatment and Hydrocracking of Oil Fractions. Elsevier, pp. 77–84.

Cha, J.S., Brown, H.C., 1993. Reaction of sodium aluminum hydride with selected organic compounds containing representative functional groups. Comparison of the reducing characteristics of lithium and sodium aluminum hydrides. J. Org. Chem. 58, 4727–4731.

Chakraborty, S., Dai, H., Bhattacharya, P., Fairweather, N.T., Gibson, M.S., Krause, J.A., Guan, H., 2014. Iron-based catalysts for the hydrogenation of esters to alcohols. J. Am. Chem. Soc. 136, 7869–7872.

Chen, L., Zhu, Y., Zheng, H., Zhang, C., Zhang, B., Li, Y., 2011. Aqueous-phase hydrodeoxygenation of carboxylic acids to alcohols or alkanes over supported Ru catalysts. J. Mol. Catal. Chem. 351, 217–227.

Chen, Y., Miller, D.J., Jackson, J.E., 2007. Kinetics of Aqueous-Phase Hydrogenation of Organic Acids and Their Mixtures over Carbon Supported Ruthenium Catalyst. Ind. Eng. Chem. Res. 46, 3334–3340.

Cheng, D., Hou, C., Chen, F., Zhan, X., 2009. Effect of manganese and potassium addition on CeO2-Al2O3 catalyst for hydrogenation of benzoic acid to benzaldehyde. J. Rare Earths 27, 723–727.

Cheng, J., Hu, P., 2008. Utilization of the Three-Dimensional Volcano Surface to Understand the Chemistry of Multiphase Systems in Heterogeneous Catalysis. J. Am. Chem. Soc. 130, 10868–10869.

Chiaramonti, D., Bonini, M., Fratini, E., Tondi, G., Gartner, K., Bridgwater, A.V., Grimm, H.P., Soldaini, I., Webster, A., Baglioni, P., 2003. Development of emulsions from biomass pyrolysis liquid and diesel and their use in engines—Part 2: tests in diesel engines. Biomass Bioenergy 25, 101–111.

Ciftci, A., Ligthart, D.A.J.M., Hensen, E.J.M., 2014a. Aqueous phase reforming of glycerol over Re-promoted Pt and Rh catalysts. Green Chem 16, 853–863.

Ciftci, A., Ligthart, D.A.J.M., Sen, A.O., van Hoof, A.J.F., Friedrich, H., Hensen, E.J.M., 2014b. Pt-Re synergy in aqueous-phase reforming of glycerol and the water–gas shift reaction. J. Catal. 311, 88–101.

Condon, J.B., 2006. Chapter 1 - An Overview of Physisorption, in: Surface Area and Porosity Determinations by Physisorption. Elsevier Science, Amsterdam, pp. 1–27.

Corma, A., Serna, P., 2006. Chemoselective Hydrogenation of Nitro Compounds with Supported Gold Catalysts. Science 313, 332–334.

Cychosz, K.A., Thommes, M., 2018. Progress in the Physisorption Characterization of Nanoporous Gas Storage Materials. Engineering 4, 559–566.

Czernik, S., Bridgwater, A.V., 2004. Overview of Applications of Biomass Fast Pyrolysis Oil. Energy Fuels 18, 590–598.

Puente, G.D., Gil, A., Pis, J.J., Grange, P., 1999. Effects of Support Surface Chemistry in Hydrodeoxygenation Reactions over CoMo/Activated Carbon Sulfided Catalysts. Langmuir 15, 5800–5806.

Demirbas, A., 2008. Biofuels sources, biofuel policy, biofuel economy and global biofuel projections. Energy Convers. Manag. 49, 2106–2116.

Deutschmann, O., Knözinger, H., Kochloefl, K., Turek, T., 2009. Heterogeneous Catalysis and Solid Catalysts, in: Ullmann's Encyclopedia of Industrial Chemistry. American Cancer Society.

Diepen, A.E., Moulijn, J.A., 2008. Reactors, in: Fine Chemicals through Heterogeneous Catalysis. John Wiley & Sons, pp. 45–60.

Dimitratos, N., Villa, A., Wang, D., Porta, F., Su, D., Prati, L., 2006. Pd and Pt catalysts modified by alloying with Au in the selective oxidation of alcohols. J. Catal. 244, 113–121.

Doraiswamy, L.K., Sharma, M.M., 1984. Heterogeneous reactions: Analysis examples and reactor design. Gas solid and solid-solid reactions. John Wiley and Sons, New York.

Duan, J., Han, J., Sun, H., Chen, P., Lou, H., Zheng, X., 2012. Diesel-like hydrocarbons obtained by direct hydrodeoxygenation of sunflower oil over Pd/Al-SBA-15 catalysts. Catal. Commun. 17, 76–80.

Duchet, J.C., van Oers, E.M., de Beer, V.H.J., Prins, R., 1983. Carbon-supported sulfide catalysts. J. Catal. 80, 386–402.

Eisentraut, A., 2010. Sustainable production of second-generation biofuels.

Elliott, D.C., 2007. Historical Developments in Hydroprocessing Bio-oils. Energy Fuels 21, 1792–1815.

Ertl, G., Kniizinger, H., Weitkamp, J., 2008a. Promoters and poisons, in: Handbook of Heterogenous Catalysis. pp. 1593–1624.

Ertl, G., Kniizinger, H., Weitkamp, J., 2008b. Reactions during catalyst activation, in: Handbook of Heterogenous Catalysis. pp. 655–676.

Ertl, G., Kniizinger, H., Weitkamp, J., 2008c. Ion exchange and impregnation, in: Handbook of Heterogenous Catalysis. pp. 467–484.

Ertl, G., Kniizinger, H., Weitkamp, J., 2008d. Preparation of supported catalysts by deposition-precipitationPromoters and poisons, in: Handbook of Heterogenous Catalysis. pp. 428–467.

Erwin, B., 1985. Solubility of Hydrogen in 10 Organic Solvents at 298.15, 323.15, and 373.15 K. J. Chem. Eng. Data. 30, 269-273.

Fernández, M.B., Tonetto, G.M., Crapiste, G.H., Damiani, D.E., 2007. Revisiting the hydrogenation of sunflower oil over a Ni catalyst. J. Food Eng. 82, 199–208.

Ferrari, M., Delmon, B., Grange, P., 2002. Influence of the active phase loading in carbon supported molybdenum–cobalt catalysts for hydrodeoxygenation reactions. Microporous Mesoporous Mater. 56, 279–290.

Fillion, B., Morsi, B.I., Heier, K.R., Machado, R.M., 2002. Kinetics, Gas−Liquid Mass Transfer, and Modeling of the Soybean Oil Hydrogenation Process. Ind. Eng. Chem. Res. 41, 697–709.

Fogler, H.S., 2010. Essentials of Chemical Reaction Engineering.

Forni, L., 1999. Mass and heat transfer in catalytic reactions. Catal. Today 52, 147–152.

Frey, D.D., Engelhardt, F., Greitzer, E.M., 2003. A role for "one-factor-at-a-time" experimentation in parameter design. Res. Eng. Des. 14, 65–74.

Froment, G.F., Bischoff, K.B., Wilde, J.D., 2010. Chemical Reactor Analysis and Design, 3rd ed. John Wiley & Sons.

Furimsky, E., 2000. Catalytic hydrodeoxygenation. Appl. Catal. Gen. 199, 147–190.

Furimsky, E., Massoth, F.E., 1999. Deactivation of hydroprocessing catalysts. Catal. Today 115.

Gervasini, A., 2013. Temperature Programmed Reduction/Oxidation (TPR/TPO) Methods, in: Auroux, A. (Ed.), Calorimetry and Thermal Methods in Catalysis, Springer Series in Materials Science. Springer Berlin Heidelberg, Berlin, Heidelberg, pp. 175–195.

Ghani, J.A., Choudhury, I.A., Hassan, H.H., 2004. Application of Taguchi method in the optimization of end milling parameters. J. Mater. Process. Technol. 145, 84–92.

Gollakota, A., Kilshore, N., Gu, S., 2018. A review on hydrothermal liquefaction of biomass. Renew. Sust. Energ. Rev. 81, 1378-1392.

Gunanathan, C., Milstein, D., 2014. Bond Activation and Catalysis by Ruthenium Pincer Complexes. Chem. Rev. 114, 12024–12087.

Gutierrez, A., Kaila, R.K., Honkela, M.L., Slioor, R., Krause, A.O.I., 2009. Hydrodeoxygenation of guaiacol on noble metal catalysts. Catal. Today 147, 239–246.

Gutierrez-Ortiz, M.A., Castano, A., Gonzalez-Marcos, M.P., Gutierrez-Ortiz, J.I., Gonzalez-Velasco, J.R., 1994. Influence of Operational Variables on the Catalytic Behavior of Pt/Alumina in the Slurry-Phase Hydrogenation of Phenol. Ind. Eng. Chem. Res. 33, 2571–2577.

Hart, A., Shah, A., Leeke, G., Greaves, M., Wood, J., 2013. Optimization of the CAPRI Process for Heavy Oil Upgrading: Effect of Hydrogen and Guard Bed. Ind. Eng. Chem. Res. 52, 15394–15406.

Haruo, K., Tomoya, F., Yuto, I., Shiro, S., 2016. Effects of Different Solvents on Hydrogenation of Acetic Acid over Pt/TiO2 for Bioethanol Production. Jpn. Inst. Energy 95, 162–166.

He, D.H., Wakasa, N., Fuchikami, T., 1995. Hydrogenation of carboxylic acids using bimetallic catalysts consisting of group 8 to 10, and group 6 or 7 metals. Tetrahedron Lett. 36, 1059–1062.

He, Z., Wang, X., 2014. Highly selective catalytic hydrodeoxygenation of guaiacol to cyclohexane over Pt/TiO2 and NiMo/Al2O3 catalysts. Front. Chem. Sci. Eng. 8, 369–377.

He, Z., Wang, X., 2013. Required catalytic properties for alkane production from carboxylic acids: Hydrodeoxygenation of acetic acid. J. Energy Chem. 22, 883–894.

He, Z., Wang, X., 2012. Hydrodeoxygenation of model compounds and catalytic systems for pyrolysis bio-oils upgrading. Catal. Sustain. Energy Versita 1, 28–52.

Honkela, M.L., Viljava, T.-R., Gutierrez, A., Krause, A.O.I., 2010. Chapter 11: Hydrotreating for Bio-Oil Upgrading, in: Thermochemical Conversion of Biomass to Liquid Fuels and Chemicals. pp. 288–306.

Huber, G.W., Iborra, S., Corma, A., 2006. Synthesis of Transportation Fuels from Biomass: Chemistry, Catalysts, and Engineering. Chem. Rev. 106, 4044–4098.

Hutchings, G.J., 2001. Promotion in Heterogeneous Catalysis: A Topic Requiring a New Approach? 1–12.

Ibrahim, S., Jasnin, S.N., Wong, S.D., Baker, I.F., 2012. Zwietering's Equation for the Suspension of Porous Particles and the Use of Curved Blade Impellers. Int. J. Chem. Eng. 2012, 1–13.

IEA, 2019. Transport biofuels. Int. Energy Agency. Retrieved from https://www.iea.org/tcep/transport/biofuels.

Ikura, M., Stanciulescu, M., Hogan, E., 2003. Emulsification of pyrolysis derived bio-oil in diesel fuel. Biomass Bioenergy 24, 221–232.

Jacobson, K., Maheria, K.C., Kumar Dalai, A., 2013. Bio-oil valorization: A review. Renew. Sustain. Energy Rev. 23, 91–106.

Jafari, R., Tanguy, P.A., Chaouki, J., 2012. Characterization of Minimum Impeller Speed for Suspension of Solids in Liquid at High Solid Concentration, Using Gamma-Ray Densitometry. Int. J. Chem. Eng. 2012, 1–15.

Jain, A.B., Vaidya, P.D., 2015. Kinetics of aqueous-phase hydrogenation of model bio-oil compounds over a Ru/C catalyst. Energy Fuels 29, 361–368.

Jaita, S., Kaewkum, P., Duangkamol, C., Phakhodee, W., Pattarawarapan, M., 2014. Solvent-free reduction of carboxylic acids to alcohols with NaBH4 promoted by 2,4,6-trichloro1,3,5-triazine and PPh3 in the presence of K2CO3. RSC Adv 4, 46947–46950.

Jasik, A., Wojcieszak, R., Monteverdi, S., Ziolek, M., Bettahar, M.M., 2005. Study of nickel catalysts supported on Al2O3, SiO2 or Nb2O5 oxides. J. Mol. Catal. Chem. 242, 81–90.

Joshi, N., Lawal, A., 2012. Hydrodeoxygenation of acetic acid in a microreactor. Chem. Eng. Sci. 84, 761–771.

Joyner, L.G., Barrett, E.P., Skold, R., 1951. The Determination of Pore Volume and Area Distributions in Porous Substances. II. Comparison between Nitrogen Isotherm and Mercury Porosimeter Methods. J. Am. Chem. Soc. 73, 3155–3158.

Kapteijn, F., Moulijn, J.A., 2008. Laboratory Catalytic Reactors: Aspects of Catalyst Testing 1: Handbook of Heterogeneous Catalysis. American Cancer Society, pp. 2019–2045.

Katayama, T., Nitta, T., 1976. Solubilities of Hydrogen and Nitrogen in Alcohols and n-Hexane. J. Chem. Eng. Data 21, 194–196.

Kawamoto, Haruo, Fujii, T., Ito, Y., Saka, S., 2016. Effects of Different Solvents on Hydrogenation of Acetic Acid over Pt/TiO2 for Bioethanol Production. J. Jpn. Inst. Energy 95, 162–166.

Klaewkla, R., Arend, M., F., W., 2011. A Review of Mass Transfer Controlling the Reaction Rate in Heterogeneous Catalytic Systems, in: Nakajima, H. (Ed.), Mass Transfer - Advanced Aspects. InTech.

Kluytmans, J.H.J., Markusse, A.P., Kuster, B.F.M., Marin, G.B., Schouten, J.C., 2000. Engineering aspects of the aqueous noble metal catalysed alcohol oxidation. Catal. Today 57, 143–155.

Knözinger, H., 2008. Temperature-Programmed Reduction and Oxidation, in: Handbook of Heterogeneous Catalysis. American Cancer Society, pp. 1080–1096.

Kowalczyk, M., 2014. Application of Taguchi and Anova Methods in Selection of Process Parameters for Surface Roughness in Precision Turning of Titanium. Adv. Manuf. Sci. Technol. 38.

Kubička, D., Horáček, J., 2011. Deactivation of HDS catalysts in deoxygenation of vegetable oils. Appl. Catal. Gen. 394, 9–17.

Kushalkar, K.B., Pangarkar, V.G., 1995. Particle-Liquid Mass Transfer in Three-Phase Mechanically Agitated Contactors: Power Law Fluids. Ind. Eng. Chem. Res. 34, 2485–2492.

Laurent, E., Delmon, B., 1994. Study of the Hydrodeoxygenation of Carbonyl, Carboxylic and Guaiacyl Groups Over Sulfided Como/gamma-al2o3 and Nimo/gamma-al2o3 Catalyst .2. Influence of Water, Ammonia and Hydrogen-sulfide. Appl. Catal. Gen. 109, 97.

Lawal, A.M., Hart, A., Daly, H., Hardacre, C., Wood, J., 2019. Kinetics of Hydrogenation of Acetic Acid over Supported Platinum Catalyst. Energy Fuels 33, 5551–5560.

Lee, C.R., Yoon, J.S., Suh, Y.-W., Choi, J.-W., Ha, J.-M., Suh, D.J., Park, Y.-K., 2012a. Catalytic roles of metals and supports on hydrodeoxygenation of lignin monomer guaiacol. Catal. Commun. 17, 54–58.

Lee, J.-M., Upare, P.P., Chang, J.-S., Hwang, Y.K., Lee, J.H., Hwang, D.W., Hong, D.-Y., Lee, S.H., Jeong, M.-G., Kim, Y.D., Kwon, Y.-U., 2014. Direct Hydrogenation of Biomass-Derived Butyric Acid to n -Butanol over a Ruthenium-Tin Bimetallic Catalyst. ChemSusChem 7, 2998–3001.

Li, N., Huber, G.W., 2010. Aqueous-phase hydrodeoxygenation of sorbitol with Pt/SiO2–Al2O3: Identification of reaction intermediates. J. Catal. 270, 48–59.

Li, W., Pan, C., Zhang, Q., Liu, Z., Peng, J., Chen, P., Lou, H., Zheng, X., 2011. Upgrading of low-boiling fraction of bio-oil in supercritical methanol and reaction network. Bioresour. Technol. 102, 4884–4889.

Li, Y., Xu, B., Fan, Y., Feng, N., Qiu, A., He, J.M.J., Yang, H., Chen, Y., 2004. The effect of titania polymorph on the strong metal-support interaction of Pd/TiO2 catalysts and their application in the liquid phase selective hydrogenation of long chain alkadienes. J. Mol. Catal. Chem. 216, 107–114.

Lin, Y.-C., Li, C.-L., Wan, H.-P., Lee, H.-T., Liu, C.-F., 2011. Catalytic Hydrodeoxygenation of Guaiacol on Rh-Based and Sulfided CoMo and NiMo Catalysts. Energy Fuels 25, 890–896.

Liu, J., Lyu, H., Chen, Y., Li, G., Jiang, H., Zhang, M., 2017. Insights into the mechanism of ethanol synthesis and ethyl acetate inhibition from acetic acid hydrogenation over Cu 2 In(100): a DFT study. Phys Chem Chem Phys 19, 28083–28097.

Lu, Q., Song, J., Zhang, M., Wei, J., Li, C., 2018. A theoretical study on the mechanism of hydrogenation of carboxylic acids catalyzed by the Saito catalyst. Dalton Trans. 47, 2460–2469.

Lugo-José, Y.K., Monnier, J.R., Williams, C.T., 2014. Gas-phase, catalytic hydrodeoxygenation of propanoic acid, over supported group VIII noble metals: Metal and support effects. Appl. Catal. Gen. 469, 410–418.

Ly, B.K., Minh, D.P., Pinel, C., Besson, M., Tapin, B., Epron, F., Especel, C., 2012. Effect of Addition Mode of Re in Bimetallic Pd–Re/TiO2 Catalysts Upon the Selective Aqueous-Phase Hydrogenation of Succinic Acid to 1,4-Butanediol. Top. Catal. 55, 466–473.

Ma'amor, A. Bin, Hamid, S., 2006. Combinatorial Technology in Heterogenous Copper-Based Catalysis, in: International Conference on Natural Resources Engineering & Technology. Putrajaya, pp. 255–261.

Magano, J., Dunetz, J.R., 2012. Large-Scale Carbonyl Reductions in the Pharmaceutical Industry. Org. Process Res. Dev. 16, 1156–1184.

Manyar, H.G., Paun, C., Pilus, R., Rooney, D.W., Thompson, J.M., Hardacre, C., 2010. Highly selective and efficient hydrogenation of carboxylic acids to alcohols using titania supported Pt catalysts. Chem. Commun. 46, 6279–6281.

McManus, I., Daly, H., Thompson, J.M., Connor, E., Hardacre, C., Wilkinson, S.K., Sedaie Bonab, N., ten Dam, J., Simmons, M.J.H., Stitt, E.H., D'Agostino, C., McGregor, J., Gladden, L.F., Delgado, J.J., 2015. Effect of solvent on the hydrogenation of 4-phenyl-2-butanone over Pt based catalysts. J. Catal. 330, 344–353.

Mendes, M.J., Santos, O.A.A., Jordao, E., Silva, A.M., 2001. Hydrogenation of oleic acid over ruthenium catalysts. Appl. Catal. Gen. 217, 253–262.

Mercader, F. de M., Groeneveld, M.J., Kersten, S.R.A., Venderbosch, R.H., Hogendoorn, J.A., 2010. Pyrolysis oil upgrading by high pressure thermal treatment. Fuel 89, 2829–2837.

Minh, D.P., Besson, M., Pinel, C., Fuertes, P., Petitjean, C., 2010. Aqueous-Phase Hydrogenation of Biomass-Based Succinic Acid to 1,4-Butanediol Over Supported Bimetallic Catalysts. Top. Catal. 53, 1270–1273.

Moberg, D.R., Thibodeau, T.J., Amar, F.G., Frederick, B.G., 2010. Mechanism of Hydrodeoxygenation of Acrolein on a Cluster Model of MoO3. J. Phys. Chem. C 114, 13782–13795.

Mortensen, P.M., Grunwaldt, J.-D., Jensen, P.A., Knudsen, K.G., Jensen, A.D., 2011. A review of catalytic upgrading of bio-oil to engine fuels. Appl. Catal. Gen. 407, 1–19.

Mukherjee, I., Kumar, R., 2006. A review of optimization techniques in metal cutting processes. Comput. Ind. Eng. 50, 15–34.

Mullen, C.A., Boateng, A.A., 2008. Chemical Composition of Bio - oils Produced by Fast Pyrolysis of Two Energy Crops. Energy Fuels 22, 2104–2109.

Murata, K., Liu, Y., Watanabe, M.M., Inaba, M., Takahara, I., 2014. Hydrocracking of Algae Oil into Aviation Fuel-Range Hydrocarbons Using a Pt–Re Catalyst. Energy Fuels 28, 6999–7006.

Nagendra, G., Madhu, C., Vishwanatha, T.M., Sureshbabu, V.V., 2012. An expedient route for the reduction of carboxylic acids to alcohols employing 1-propanephosphonic acid cyclic anhydride as acid activator. Tetrahedron Lett. 53, 5059–5063.

Nienow, A.W., 1975. Agitated vessel particle-liquid mass transfer: A comparison between theories and data. Chem. Eng. J. 9, 153–160.

Nienow, A.W., 1968. Suspension of solid particles in turbine agitated baffled vessels. Chem. Eng. Sci. 23, 1453–1459.

Oasmaa, A., Sipilä, K., Solantausta, Y., Kuoppala, E., 2005. Quality improvement of pyrolysis liquid: Effect of light volatiles on the stability of pyrolysis liquids. Energy Fuels 19, 2556–2561.

Olcay, H., Xu, L., Xu, Y., Huber, G.W., 2010. Aqueous-Phase Hydrogenation of Acetic Acid over Transition Metal Catalysts. ChemCatChem 2, 1420–1424.

Olcese, R.N., Bettahar, M., Petitjean, D., Malaman, B., Giovanella, F., Dufour, A., 2012. Gas-phase hydrodeoxygenation of guaiacol over Fe/SiO2 catalyst. Appl. Catal. B Environ. 115–116, 63–73.

Pallassana, V., Neurock, M., 2002. Reaction Paths in the Hydrogenolysis of Acetic Acid to Ethanol over Pd(111), Re(0001), and PdRe Alloys. J. Catal. 209, 289–305.

Pan, Y., Shen, X., Yao, L., Bentalib, A., Peng, Z., 2018. Active Sites in Heterogeneous Catalytic Reaction on Metal and Metal Oxide: Theory and Practice. Catalysts 8, 478.

Panpranot, J., Kontapakdee, K., Praserthdam, P., 2006. Effect of TiO2 Crystalline Phase Composition on the Physicochemical and Catalytic Properties of Pd/TiO2 in Selective Acetylene Hydrogenation. J. Phys. Chem. B 110, 8019–8024.

Park, Y.-C., Tokiwa, H., Kakinuma, K., Watanabe, M., Uchida, M., 2016. Effects of carbon supports on Pt distribution, ionomer coverage and cathode performance for polymer electrolyte fuel cells. J. Power Sources 315, 179–191.

Perego, C., Villa, P., 1997. Catalyst preparation methods. Catal. Today 34, 281–305.

Pestman, R., Koster, R.M., Pieterse, J.A.Z., Ponec, V., 1997a. Reactions of Carboxylic Acids on Oxides: 1. Selective Hydrogenation of Acetic Acid to Acetaldehyde. J. Catal. 168, 255–264.

Pestman, R., Koster, R.M., van Duijne, A., Pieterse, J.A.Z., Ponec, V., 1997b. Reactions of Carboxylic Acids on Oxides. J. Catal. 168, 265–272.

Ponec, V., 1997. On the role of promoters in hydrogenations on metals; et, [3-unsaturated aldehydes and ketones 149, 22–48.

Popov, A., Kondratieva, E., Gilson, J.-P., Mariey, L., Travert, A., Maugé, F., 2011. IR study of the interaction of phenol with oxides and sulfided CoMo catalysts for bio-fuel hydrodeoxygenation. Catal. Today 172, 132–135.

Popov, A., Kondratieva, E., Goupil, J.M., Mariey, L., Bazin, P., Gilson, J.-P., Travert, A., Maugé, F., 2010. Bio-oils Hydrodeoxygenation: Adsorption of Phenolic Molecules on Oxidic Catalyst Supports. J. Phys. Chem. C 114, 15661–15670.

Prati, L., Villa, A., Campione, C., Spontoni, P., 2007. Effect of gold addition on Pt and Pd catalysts in liquid phase oxidations. Top. Catal. 44, 319–324.

Pritchard, J., Ciftci, A., Verhoeven, M.W.G.M. (Tiny), Hensen, E.J.M., Pidko, E.A., 2017. Supported Pt-Re catalysts for the selective hydrogenation of methyl and ethyl esters to alcohols. Catal. Today 279, 10–18.

Pritchard, J., Filonenko, G.A., Putten, R. van, Hensen, E.J.M., Pidko, E.A., 2015. Heterogeneous and homogeneous catalysis for the hydrogenation of carboxylic acid derivatives: history, advances and future directions. Chem. Soc. Rev. 44, 3808–3833.

Rachmady, W., Vannice, M.A., 2002a. Acetic Acid Reduction to Acetaldehyde over Iron Catalysts. J. Catal. 208, 158–169.

Rachmady, W., Vannice, M.A., 2002b. Acetic Acid Reduction by H2 over Supported Pt Catalysts: A DRIFTS and TPD/TPR Study. J. Catal. 207, 317–330.

Rachmady, W., Vannice, M.A., 2000. Acetic Acid Hydrogenation over Supported Platinum Catalysts. J. Catal. 192, 322–334.

Rakshit, P.K., Voolapalli, R.K., Upadhyayula, S., 2018. Acetic acid hydrogenation to ethanol over supported Pt-Sn catalyst: Effect of Bronsted acidity on product selectivity. Mol. Catal. 448, 78–90.

Ramachandran, P.A., Chaudhari, R.V., 1983. Three-phase catalytic reactors. Gordon and Breach Science Publishers.

Rase, H.F., 2016. Handbook of Commercial Catalysts: Heterogeneous Catalysts. CRC Press.

Rasu, L., John, J.M., Stephenson, E., Endean, R., Kalapugama, S., Clément, R., Bergens, S.H., 2017. Highly Enantioselective Hydrogenation of Amides via Dynamic Kinetic Resolution Under Low Pressure and Room Temperature. J. Am. Chem. Soc. 139, 3065–3071.

Rawase, Y., Araki, T., Shimzu, K., Miura, H., 1997. Gas—liauid mass transfer in three-phase stirred tank reagors: Newtonian and non-newtonian fluids. Can. J. Chem. Eng. 75, 1159–1164.

Regalbuto, J.R., 2007. Catalyst preparation: science and engineering. Taylor & Francis, Boca Raton.

Reiche, M.A., Maciejewski, M., Baiker, A., 2000. Characterization by temperature programmed reduction. Catal. Today 56, 347–355.

Resende, N.S., Eon, J.-G., Schmal, M., 1999. I. Dispersion of Platinum on Alumina-Grafted Titanium Oxide. Catalysis 183, 6–13.

Richardson, J.T., 1989. Principles of Catalyst Development. Plenum Press, New York.

Ruddy, D.A., Schaidle, J.A., Iii, J.R.F., Wang, J., Moens, L., Hensley, J.E., 2014. Recent advances in heterogeneous catalysts for bio-oil upgrading via “ex situ catalytic fast pyrolysis”: catalyst development through the study of model compounds. Green Chem. 16, 454–490.

Sá, J., Kartusch, C., Makosch, M., Paun, C., van Bokhoven, J.A., Kleymenov, E., Szlachetko, J., Nachtegaal, M., Manyar, H.G., Hardacre, C., 2011. Evaluation of Pt and Re oxidation state in a pressurized reactor: difference in reduction between gas and liquid phase. Chem. Commun. 47, 6590-6592.

Sanna, A., Vispute, T.P., Huber, G.W., 2015. Hydrodeoxygenation of the aqueous fraction of bio-oil with Ru/C and Pt/C catalysts. Appl. Catal. B Environ. 165, 446–456.

Santacesaria, E., Parrella, P., Di Serio, M. snm, Borrelli, G., 1994. Role of mass transfer and kinetics in the hydrogenation of rapeseed oil on a supported palladium catalyst. Appl. Catal. Gen. 116, 269–294.

Saudan, L.A., 2007. Hydrogenation processes in the synthesis of perfumery ingredients. Acc. Chem. Res. 40, 1309–1319.

Shafaghat, H., Rezaei, P.S., Ashri Wan Daud, W.M., 2015. Effective parameters on selective catalytic hydrodeoxygenation of phenolic compounds of pyrolysis bio-oil to high-value hydrocarbons. RSC Adv. 5, 103999–104042.

Shakya, R., Adhikari, S., Mahadevan, R., Hassan, E., Dempster, T., 2018. Catalytic upgrading of bio-oil produced from hydrothermal liquefaction of Nannocloropsis sp. Bioresour. Technol. 252, 28-36.

Sheldon, R.A., Bekkum, H. van, 2008. Fine Chemicals through Heterogeneous Catalysis. John Wiley & Sons.

Sheu, Y.-H.E., Anthony, R.G., Soltes, E.J., 1988. Kinetic studies of upgrading pine pyrolytic oil by hydrotreatment. Fuel Process. Technol. 19, 31–50.

Shih, Y.-S., Lee, C.-K., 1985. Kinetics of the Ruthenium Catalyzed Hydrogenation of Acetic Acid to Ethanol. J. Chin. Chem. Soc. 32, 29–34.

Si, Z., Zhang, X., Wang, C., Ma, L., Dong, R., 2017. An Overview on Catalytic Hydrodeoxygenation of Pyrolysis Oil and Its Model Compounds. Catalysts 7, 169.

Simonetti, D., Kunkes, E., Dumesic, J., 2007. Gas-phase conversion of glycerol to synthesis gas over carbon-supported platinum and platinum–rhenium catalysts. J. Catal. 247, 298–306.

Singh, Utpal K., Vannice, M.A., 2001. Kinetics of liquid-phase hydrogenation reactions over supported metal catalysts — a review. Appl. Catal. Gen. 213, 1–24.

Sipilaè, K., Kuoppala, E., 1998. CHARACTERIZATION OF BIOMASS-BASED FLASH PYROLYSIS OILS 14, 103–113.

Sipos, O., Nagy, K., Galajda, P., 2014. Kinetics and Mass Transfer in the Hydrogenation of 2-((1-benzyl-1,2,3,6-tetrahydropyridin-4-yl)methylene)-5,6-dimethoxy- -2,3-dihydroinden-1-one hydrochloride over Pt/C Catalyst. Chem. Biochem. Eng. Q. J. 28, 233–240.

Sitaraman, R., Ibrahim, S.H., Kuloor, N.R., 1963. A Generalized Equation for Diffusion in Liquids. J. Chem. Eng. Data 8, 198–201.

Sitthisa, S., Pham, T., Prasomsri, T., Sooknoi, T., Mallinson, R.G., Resasco, D.E., 2011. Conversion of furfural and 2-methylpentanal on Pd/SiO2 and Pd–Cu/SiO2 catalysts. J. Catal. 280, 17–27.

Sjöblom, M., Matsakas, L., Christakopoulos, P., Rova, U., 2016. Catalytic upgrading of butyric acid towards fine chemicals and biofuels. FEMS Microbiol. Lett. 363, fnw064.

Smith, W.L., 1977. Selective solubility: “Like dissolves like.” J. Chem. Educ. 54, 228.

Spasyuk, D., Smith, S., Gusev, D.G., 2012. From Esters to Alcohols and Back with Ruthenium and Osmium Catalysts. Angew. Chem. Int. Ed. 51, 2772–2775.

Sporka, K., Hanika, J., Růžička, V., Halousek, M., 1971. Diffusion of gases in liquids. III. Diffusion coefficients of hydrogen in organic solvents. Collect. Czechoslov. Chem. Commun. 36, 2130–2136.

Srivastava, S., Jadeja, G.C., Parikh, J., 2018. Copper-cobalt catalyzed liquid phase hydrogenation of furfural to 2-methylfuran: An optimization, kinetics and reaction mechanism study. Chem. Eng. Res. Des. 132, 313–324.

Sundaramurthy, V., Dalai, A.K., Adjaye, J., 2008. The effect of phosphorus on hydrotreating property of NiMo/γ-Al2O3 nitride catalyst. Appl. Catal. Gen. 335, 204–210.

Takashi, K., Tomishige, N., 1976. Solubilities of Hydrogen and Nitrogen in Alcohols and n-Hexane. J. Chem. Eng. Data. 21, 194-196.

Takeda, Y., Nakagawa, Y., Tomishige, K., 2012. Selective hydrogenation of higher saturated carboxylic acids to alcohols using a ReOx–Pd/SiO2 catalyst. Catal. Sci. Technol. 2, 2221-2223.

Tansel, I.N., Gülmez, S., Demetgul, M., Aykut, Ş., 2011. Taguchi Method–GONNS integration: Complete procedure covering from experimental design to complex optimization. Expert Syst. Appl. 38, 4780–4789.

Tao, T., Glushenkov, A.M., Chen, Q., Hu, H., Zhou, D., Zhang, H., Boese, M., Liu, S., Amal, R., Chen, Y., 2011. Porous TiO2 with a controllable bimodal pore size distribution from natural ilmenite. CrystEngComm 13, 1322–1327.

Thommes, M., Cychosz, K.A., 2014. Physical adsorption characterization of nanoporous materials: progress and challenges. Adsorption 20, 233–250.

Thommes, M., Kaneko, K., Neimark, A.V., Olivier, J.P., Rodriguez-Reinoso, F., Rouquerol, J., Sing, K.S.W., 2015. Physisorption of gases, with special reference to the evaluation of surface area and pore size distribution (IUPAC Technical Report). Pure Appl. Chem. 87, 1051–1069.

Tike, M.A., Mahajani, V. V., 2007. Kinetics of liquid-phase hydrogenation of furfuryl alcohol to tetrahydroftirfuryl alcohol over a Ru/TiO2 Catalyst. Ind. Eng. Chem. Res. 46, 3275–3282.

Toyao, T., Siddiki, S.M.A.H., Touchy, A.S., Onodera, W., Kon, K., Morita, Y., Kamachi, T., Yoshizawa, K., Shimizu, K., 2017. TiO2 -Supported Re as a General and Chemoselective Heterogeneous Catalyst for Hydrogenation of Carboxylic Acids to Alcohols. Chem. - Eur. J. 23, 1001–1006.

US Energy Information Administration (EIA), 2017. Global Transportation Energy Consumption : Examination of Scenarios to 2040 using ITEDD. Retrieved from https://www.eia.gov/analysis/studies/transportation/scenarios/pdf/globaltransportation.pdf

van Ruijven, B., van Vuuren, D.P., 2009. Oil and natural gas prices and greenhouse gas emission mitigation. Energy Policy 37, 4797–4808.

Vannice, M.A., Hyun, S.H., Kalpakci, B., Liauh, W.C., 1979. Entropies of adsorption in heterogeneous catalytic reactions. J. Catal. 56, 358–362.

Vargas, A., Bürgi, T., Baiker, A., 2004. Adsorption of activated ketones on platinum and their reactivity to hydrogenation: a DFT study. J. Catal. 222, 439–449.

Vargas, A., Reimann, S., Diezi, S., Mallat, T., Baiker, A., 2008. Adsorption modes of aromatic ketones on platinum and their reactivity towards hydrogenation. J. Mol. Catal. Chem. 282, 1–8.

Venderbosch, R. h., Ardiyanti, A. r., Wildschut, J., Oasmaa, A., Heeres, H. j., 2010. Stabilization of biomass-derived pyrolysis oils. J. Chem. Technol. Biotechnol. 85, 674–686.

Vissers, J.P.R., Scheffer, B., V. H.J. Beer, D., Moulijn, J.A., Prins, R., 1987. Effect of the support on the structure of Mo-based hydrodesulfurization catalysts : activated carbon versus alumina. J. Catal. 105, 277–284. 3

vom Stein, T., Meuresch, M., Limper, D., Schmitz, M., Hölscher, M., Coetzee, J., Cole-Hamilton, D.J., Klankermayer, J., Leitner, W., 2014. Highly Versatile Catalytic Hydrogenation of Carboxylic and Carbonic Acid Derivatives using a Ru-Triphos Complex: Molecular Control over Selectivity and Substrate Scope. J. Am. Chem. Soc. 136, 13217–13225.

Wan, H., Chaudhari, R.V., Subramaniam, B., 2013. Aqueous Phase Hydrogenation of Acetic Acid and Its Promotional Effect on p -Cresol Hydrodeoxygenation. Energy Fuels 27, 487–493.

Wang, H., Male, J., Wang, Y., 2013. Recent Advances in Hydrotreating of Pyrolysis Bio-Oil and Its Oxygen-Containing Model Compounds. ACS Catal. 3, 1047–1070.

Wang, J., Luo, Z., Zhang, J., Dang, Q., Chen, W., 2011. Reactions of furfural and acetic acid as model compounds for bio-oil upgrading in supercritical ethanol, in: Electronics, Communications and Control (ICECC), 2011 International Conference On. IEEE, pp. 1587–1592.

Wang, K., Dayton, D., Peters, J., Mante, O., 2017. Reactive catalytic fast pyrolysis of biomass to produce high-quality bio-crude. Green Chem. 19, 3243-3251.

Wang, L., Zhang, J., Wang, H., Shao, Y., Liu, X., Wang, Y.-Q., Lewis, J.P., Xiao, F.-S., 2016. Activity and Selectivity in Nitroarene Hydrogenation over Au Nanoparticles on the Edge/Corner of Anatase. ACS Catal. 6, 4110–4116.

Wang, X., Sun, T., Teja, A.S., 2016. Density, Viscosity, and Thermal Conductivity of Eight Carboxylic Acids from (290.3 to 473.4) K. J. Chem. Eng. Data 61, 2651–2658.

Wang, Y., Fang, Y., He, T., Hu, H., Wu, J., 2011. Hydrodeoxygenation of dibenzofuran over noble metal supported on mesoporous zeolite. Catal. Commun. 12, 1201–1205.

Westerhaus, F.A., Jagadeesh, R.V., Wienhöfer, G., Pohl, M.-M., Radnik, J., Surkus, A.-E., Rabeah, J., Junge, K., Junge, H., Nielsen, M., Brückner, A., Beller, M., 2013. Heterogenized cobalt oxide catalysts for nitroarene reduction by pyrolysis of molecularly defined complexes. Nat. Chem. 5, 537–543.

Wienhöfer, G., Westerhaus, F.A., Junge, K., Ludwig, R., Beller, M., 2013. A Molecularly Defined Iron-Catalyst for the Selective Hydrogenation of α,β-Unsaturated Aldehydes. Chem. – Eur. J. 19, 7701–7707.

Wildschut, J., Iqbal, M., Mahfud, F.H., Cabrera, I.M., Venderbosch, R.H., Heeres, H.J., 2010. Insights in the hydrotreatment of fast pyrolysis oil using a ruthenium on carbon catalyst. Energy Environ. Sci. 3, 962–970.

Wildschut, J., Mahfud, F.H., Venderbosch, R.H., Heeres, H., 2009. Hydrotreatment of Fast Pyrolysis Oil Using Heterogeneous Noble-Metal Catalysts. Ind. Eng. Chem. Res. 48, 10324–10334.

WIlke, C.R., Chang, P., 1955. Correlation of diffusion coefficients in dilute solutions. AIChE J. 1, 264–270.

Xiaoyuan, J., Guanghui, D., Liping, L., Yingxu, C., Xiaoming, Z., 2004. Catalytic activities of CuO/TiO2 and CuO-ZrO2/TiO2 in NO + CO reaction. J. Mol. Catal. Chem. 218, 187–195.

Xu, Y., Wang, T., Ma, L., Zhang, Q., Wang, L., 2009. Upgrading of liquid fuel from the vacuum pyrolysis of biomass over the Mo–Ni/γ-Al2O3 catalysts. Biomass Bioenergy 33, 1030–1036.

Yang, Y., Gilbert, A., Xu, C. (Charles), 2009. Hydrodeoxygenation of bio-crude in supercritical hexane with sulfided CoMo and CoMoP catalysts supported on MgO: A model compound study using phenol. Appl. Catal. Gen. 360, 242–249.

Yildiz, Y.Ş., 2008. Optimization of Bomaplex Red CR-L dye removal from aqueous solution by electrocoagulation using aluminum electrodes. J. Hazard. Mater. 153, 194–200.

Yuan, M.L., Xie, J.H., Zhu, S.F., Zhou, Q.L., 2016. Deoxygenative Hydrogenation of Amides Catalyzed by a Well-Defined Iridium Pincer Complex. ACS Catal. 6, 3665–3669.

Zacher, A.H., Olarte, M.V., Santosa, D.M., Elliott, D.C., Jones, S.B., 2014. A review and perspective of recent bio-oil hydrotreating research. Green Chem. 16, 491–515.

Zaera, F., 2017. The Surface Chemistry of Metal-Based Hydrogenation Catalysis. ACS Catal. 7, 4947–4967.

Zanuttini, M.S., Dalla Costa, B.O., Querini, C.A., Peralta, M.A., 2014. Hydrodeoxygenation of m-cresol with Pt supported over mild acid materials. Appl. Catal. Gen. 482, 352–361.

Zhang, C., He, H., Tanaka, K., 2006. Catalytic performance and mechanism of a Pt/TiO2 catalyst for the oxidation of formaldehyde at room temperature. Appl. Catal. B Environ. 65, 37–43.

Zhang, K., Zhang, H., Ma, H., Ying, W., Fang, D., 2014. Effect of Sn addition in gas phase hydrogenation of acetic acid on alumina supported PtSn catalysts. Catal. Lett. 144, 691–701.

Zhang, Q., Chang, J., Wang, T., Xu, Y., 2007. Review of biomass pyrolysis oil properties and upgrading research. Energy Convers. Manag. 48, 87–92.

Zhang, X., Zhang, Q., Wang, T., Ma, L., Yu, Y., Chen, L., 2013. Hydrodeoxygenation of lignin-derived phenolic compounds to hydrocarbons over Ni/SiO2–ZrO2 catalysts. Bioresour. Technol. 134, 73–80.

Zhang, Y., Shinoda, M., Tsubaki, N., 20014. Development of bimodal cobalt catalyst for Fischer-Tropsch synthesis. Catal. Today. 93, 55-63.

Zhang, S., Yang, X., Zhang, H., Chu, C., Zheng, K., Ju, M., Liu, L., 2019. Liquefaction of Biomass and Upgrading of Bio-Oil: A Review. Molecules. 24, 2250-2279.

Zhang, Z., Jackson, J.E., Miller, D.J., 2002. Kinetics of Aqueous-Phase Hydrogenation of Lactic Acid to Propylene Glycol. Ind. Eng. Chem. Res. 41, 691–696.

Zhao, C., He, J., Lemonidou, A.A., Li, X., Lercher, J.A., 2011. Aqueous-phase hydrodeoxygenation of bio-derived phenols to cycloalkanes. J. Catal. 280, 8–16.

Zhao, H.Y., Li, D., Bui, P., Oyama, S.T., 2011. Hydrodeoxygenation of guaiacol as model compound for pyrolysis oil on transition metal phosphide hydroprocessing catalysts. Appl. Catal. Gen. 391, 305–310.

Zhou, L., Lawal, A., 2017. Kinetic study of hydrodeoxygenation of palmitic acid as a model compound for microalgae oil over Pt/γ-Al2O3. Appl. Catal. Gen. 532, 40–49.

Zhou, M., Zhang, H., Ma, H., Ying, W., 2017a. Kinetic Modeling of Acetic Acid Hydrogenation to Ethanol over K-Modified PtSn Catalyst Supported on Alumina. Ind. Eng. Chem. Res. 56, 8833–8842.

Zhu, J., 2014. PhD Thesis titled Synthesis of precious metal nanoparticles supported on bacterial biomass for catalytic applications in chemical transformations. Submitted to the University of Birmingham, UK.

Zhu, X., Lobban, L.L., Mallinson, R.G., Resasco, D.E., 2011. Bifunctional transalkylation and hydrodeoxygenation of anisole over a Pt/HBeta catalyst. J. Catal. 281, 21–29. https://doi.org/10.1016/j.jcat.2011.03.030

Zwietering, T.N., 1958. Suspending of solid particles in liquid by agitators. Chem. Eng. Sci. 8, 244–253.

Appendices

Appendix A: GC Calibration Curves

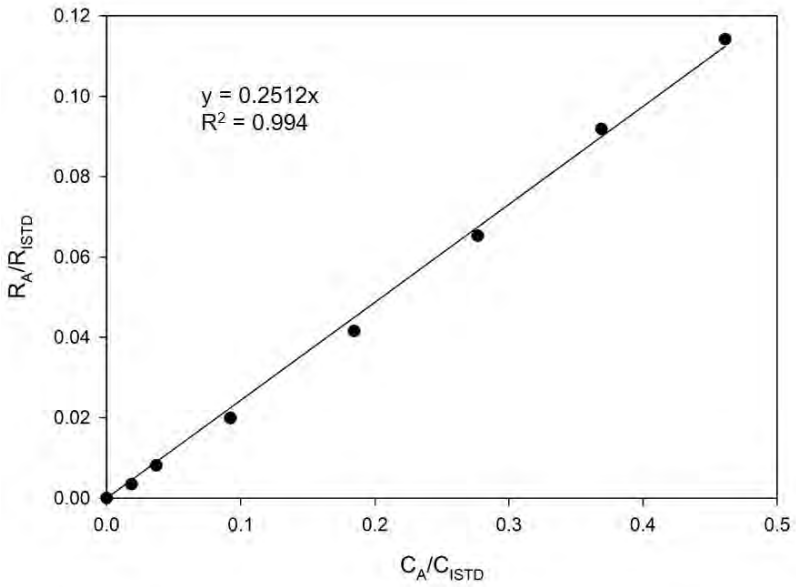

Figure A1: *Acetic acid calibration curve. (Concentration range: 0.04 – 0.6 M)*

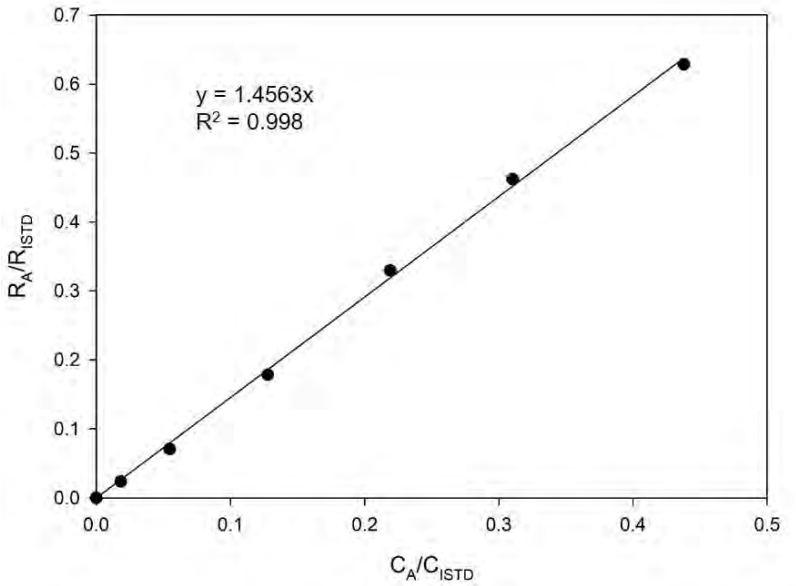

Figure A2: *Propanoic acid calibration curve. (Concentration range: 0.01 – 0.24 M)*

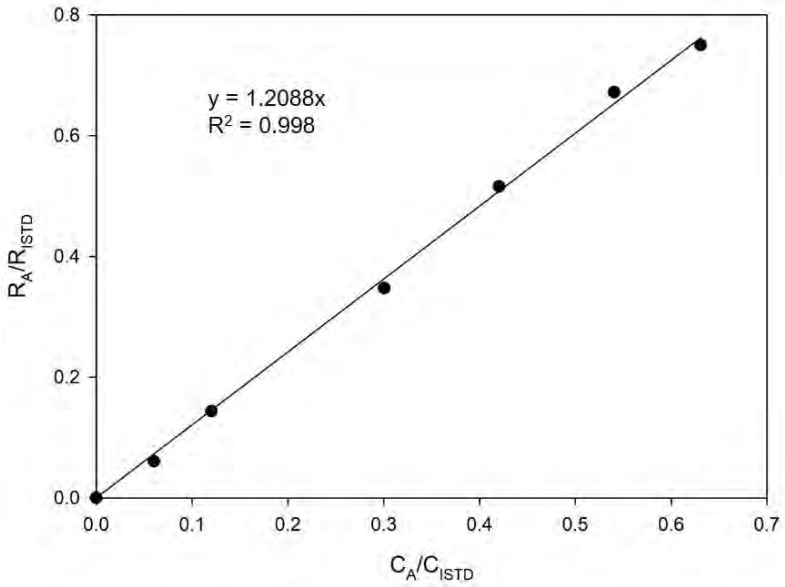

Figure A3: *Butanoic acid calibration curve. (Concentration range: 0.02 – 0.21 M)*

Appendix B: Investigation of Inhibitory Effects Due to Competitive Adsorption.

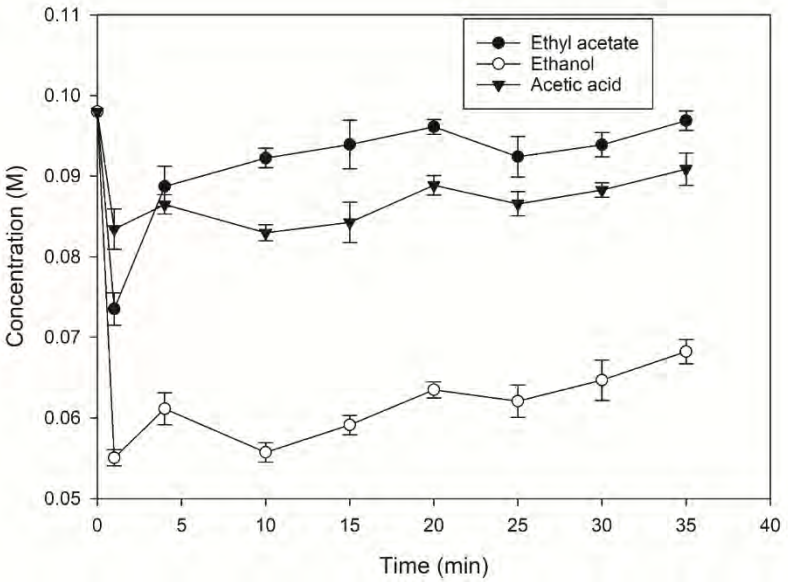

Figure B1: *Adsorption study for mixture acetic acid, ethanol and ethylacetate (experimental conditions: initial concentration, 0.09 M; catalyst loading, 0.3 g; and reaction time, 35 min respectively).*

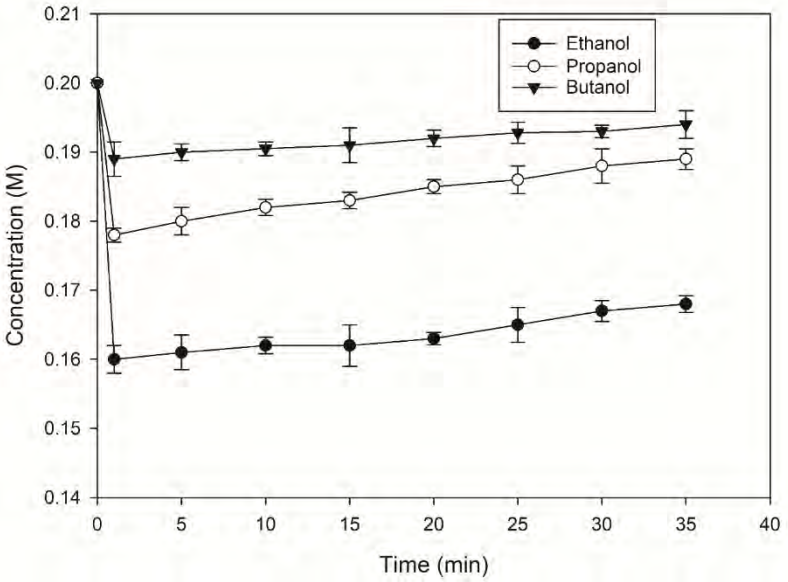

Figure B2: *Adsorption study for mixture of ethanol, propanol and butanol (experimental conditions: initial concentration, 0.2 M; catalyst loading, 0.3 g; and reaction time, 35 min respectively).*

Appendix C: Kinetic Modelling Assuming Non-Dissociative Adsorption of Hydrogen

Competitive adsorption, non-dissociative adsorbed H_2;

$$r = \frac{kK_{AA}K_{H_2}C_{AA}C_{H_2}}{\left(1+K_{AA}C_{AA}+K_{H_2}C_{H_2}\right)^2} \quad \text{(B.1)}$$

Non-dissociative adsorption of hydrogen

$$H_{2_{(g)}} + * \overset{K_H}{\leftrightarrow} H_2{}^* \quad \text{(B.2)}$$

Surface reaction

$$H_2{}^* + CH_3COOH^{**} \overset{K_{CH_3COOH}}{\longleftrightarrow} C_2H_5OH \quad \text{(B.3)}$$

Table C1: *Values of estimated parameters for kinetic model assuming non-dissociative adsorption of H_2.*

T (°C)	k (kmol/(kgcatmin))	K_{H_2} (m^3/kmol)	K_{AA} (m^3/kmol)	Variance	RSS	R^2
185	0.7 ± 0.03	0.07 ± 0.04	0.35 ± 0.01	7.89×10^{-7}	1.59×10^{-8}	0.980
200	0.9 ± 0.05	0.05 ± 0.03	0.21 ± 0.01	5.63×10^{-7}	1.77×10^{-9}	0.969s
210	1.1 ± 0.02	0.03 ± 0.02	0.14 ± 0.01	1.2×10^{-7}	3.72×10^{-8}	0.969

Table C2. *Values of Activation Energy and Heats of Adsorption.*

	Model II	
Parameter	Value	Temperature dependence
A_1 ($kmol.kg_{cat}^{-1}.min^{-1}$)	3.85×10^2	$k = 3.85\times10^2 exp\left(\frac{-9.70}{T}\right)$
E_{act} ($kJ.mol^{-1}$)	30.8	
A_2 ($m^3.kmol^{-1}$)	8.4×10^{-9}	$K_{AA} = 8.4\times10^{-9}\, exp\left(\frac{8.04}{T}\right)$
ΔH_{AA} ($kJ.mol^{-1}$)	-66.86	
ΔS ($kJ.mol^{-1}K^{-1}$)	-0.155	

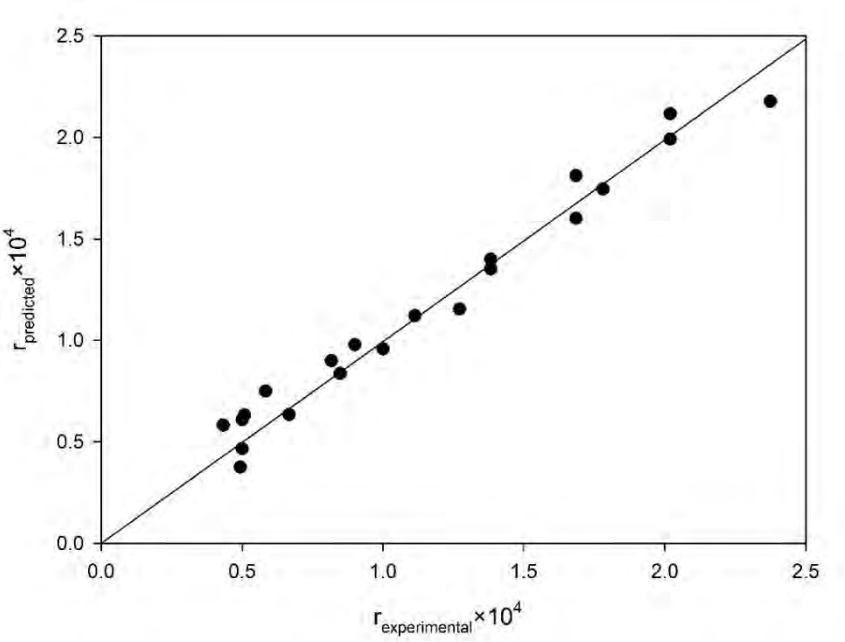

Figure C1. *Parity plot for kinetic model assuming non-dissociative adsorption of H_2.*

Appendix D: Calculation of Thiele Modulus

Effective diffusivities of hydrogen and acetic acid in hexane:

D_{e,H_2} = 6.24 × 10^{-8} $m^2.s^{-1}$ (Sporka et al., 1971)

$D_{e,acetic}$ = 1.49 × 10^{-9} $m^2.s^{-1}$ (Wilke and Chang, 1955)

Length of catalyst particle:

$$L = \frac{D_P}{6}$$

where D_p = 63 μm

L = 1.05 × 10^{-5} m

Concentration of hydrogen:

Using the Henry's Law, $C = kP_{H_2}$

where k is Henry's constant and P_{H2} is partial pressure.

k = 1430 atm for hydrogen solubility in hexane at 25 °C (Takashi and Tomoshige, 1976).

Mole fraction solubility of hydrogen in hexane at 25 °C is 0.0275 (Erwin, 1985).

Hydrogen concentration (C_{H_2}) = 0.00075 M (0.75 mM)

Thiele Modulus:

$$\eta\varphi^2 = \frac{r\omega L^2}{C_i D_{e_i}}$$

where r is the initial rate, ω is the catalyst loading, L is the characteristic length of spherical particle, C_i is the reactant concentration and D_{ei} is the effective diffusivity (See Table 6.2).

$$\eta\varphi^2{}_{acetic} = \frac{1.77 \times 10^{-4} \times 6 \times (1.05 \times 10^{-5})^2}{312 \times 1.49 \times 10^{-9}}$$

$$= 2.56 \times 10^{-7}$$

$$\eta\varphi^2{}_{H_2} = \frac{1.77 \times 10^{-4} \times 6 \times (1.05 \times 10^{-5})^2}{0.75 \times 6.24 \times 10^{-8}}$$

$$= 2.55 \times 10^{-6}$$

Rate of hydrogen solubility in hexane solvent:

Figure D1 shows the evolution of pressure during heating in a reaction system. It is very clear that pressure build up occurs which subsequently drops as hydrogen solubility enhances until saturation is achieved. At the different temperatures investigated, the rate of hydrogen solubility is faster in the early stages of the reaction which subsequently drops over time.

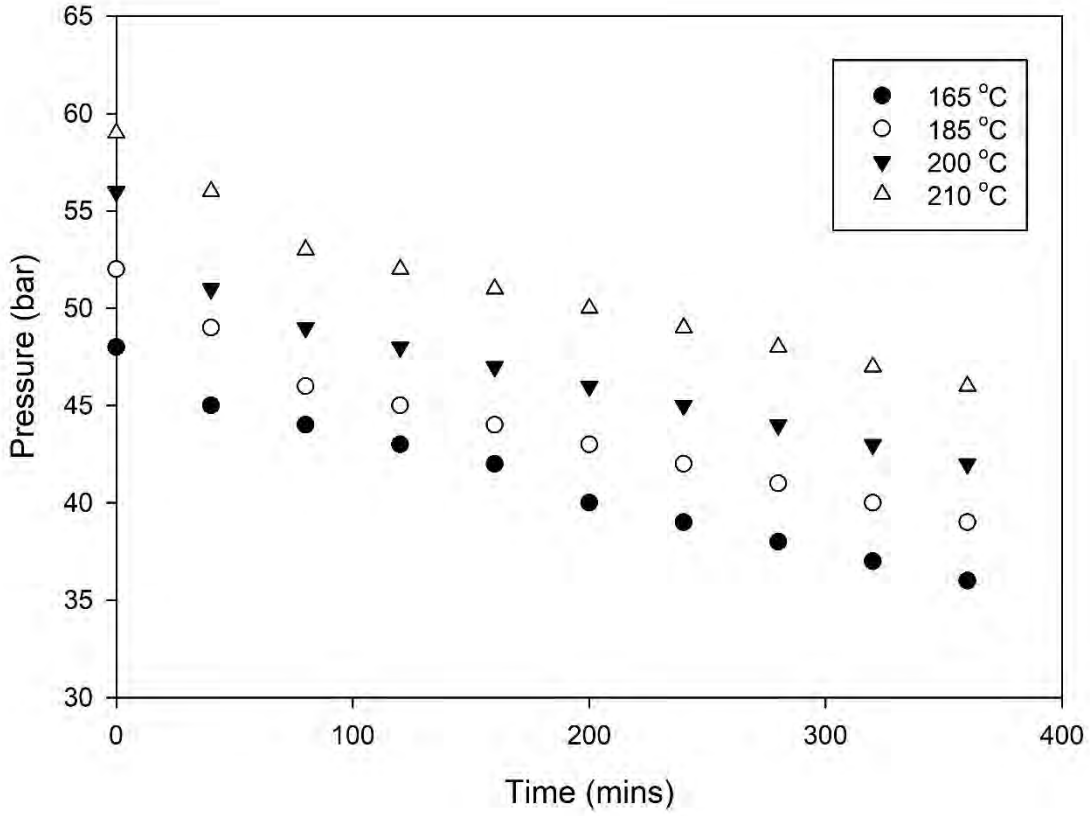

Figure D1. *Effect of temperature on hydrogen solubility over reaction time (experimental conditions: initial concentration, 0.350 M; initial pressure, 40 bar; reaction time, 6 h; and catalyst loading, 0.3 g respectively).*